

The magnetic behavior of diluted magnetic semiconductors

Citation for published version (APA):

Swagten, H. J. M. (1990). *The magnetic behavior of diluted magnetic semiconductors*. [Phd Thesis 1 (Research TU/e / Graduation TU/e), Applied Physics and Science Education]. Technische Universiteit Eindhoven.
<https://doi.org/10.6100/IR340473>

DOI:

[10.6100/IR340473](https://doi.org/10.6100/IR340473)

Document status and date:

Published: 01/01/1990

Document Version:

Publisher's PDF, also known as Version of Record (includes final page, issue and volume numbers)

Please check the document version of this publication:

- A submitted manuscript is the version of the article upon submission and before peer-review. There can be important differences between the submitted version and the official published version of record. People interested in the research are advised to contact the author for the final version of the publication, or visit the DOI to the publisher's website.
- The final author version and the galley proof are versions of the publication after peer review.
- The final published version features the final layout of the paper including the volume, issue and page numbers.

[Link to publication](#)

General rights

Copyright and moral rights for the publications made accessible in the public portal are retained by the authors and/or other copyright owners and it is a condition of accessing publications that users recognise and abide by the legal requirements associated with these rights.

- Users may download and print one copy of any publication from the public portal for the purpose of private study or research.
- You may not further distribute the material or use it for any profit-making activity or commercial gain
- You may freely distribute the URL identifying the publication in the public portal.

If the publication is distributed under the terms of Article 25fa of the Dutch Copyright Act, indicated by the "Taverne" license above, please follow below link for the End User Agreement:

www.tue.nl/taverne

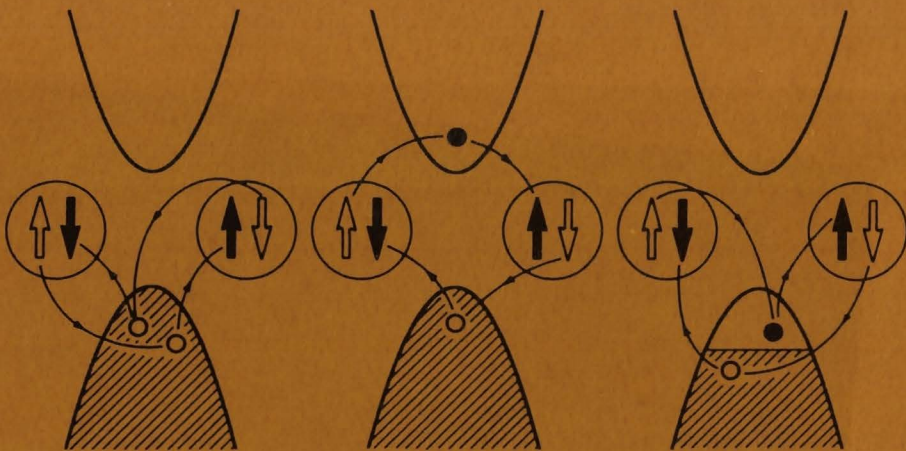
Take down policy

If you believe that this document breaches copyright please contact us at:

openaccess@tue.nl

providing details and we will investigate your claim.

THE MAGNETIC BEHAVIOR OF DILUTED MAGNETIC SEMICONDUCTORS



H.J.M. Swagten

THE MAGNETIC BEHAVIOR OF DILUTED MAGNETIC SEMICONDUCTORS

PROEFSCHRIFT

ter verkrijging van de graad van doctor aan de Technische Universiteit
Eindhoven, op gezag van de Rector Magnificus, prof. ir. M. Tels, voor
een commissie aangewezen door het College van Dekanen in het
openbaar te verdedigen op dinsdag 20 november 1990 te 16.00 uur

door

HENRICUS JOHANNES MARIA SWAGTEN

geboren te Roermond

Dit proefschrift is goedgekeurd door de promotor:

prof. dr. ir. W.J.M. de Jonge.

The work described in this thesis was part of the research program of the Solid State Division, group Cooperative Phenomena, of the Department of Physics at the Eindhoven University of Technology, and was supported financially by the Foundation for Fundamental Research on Matter (FOM).

TABLE OF CONTENTS

CHAPTER I. INTRODUCTION	1
CHAPTER II. MAGNETIC BEHAVIOR OF II-VI GROUP DILUTED MAGNETIC SEMICONDUCTORS, BASED ON Mn	23
1. Magnetic behavior of the diluted magnetic semiconductor $Zn_{1-x}Mn_xSe$, p. 24	
2. Magnetic properties of $Zn_{1-x}Mn_xS$, p. 39	
CHAPTER III. MAGNETIC BEHAVIOR OF II-VI GROUP DILUTED MAGNETIC SEMICONDUCTORS, BASED ON Fe	45
1. Magnetic properties of the diluted magnetic semiconductor $Zn_{1-x}Fe_xSe$, p. 46	
2. Low-temperature specific heat of the diluted magnetic semiconductor $Hg_{1-x-y}Cd_yFe_xSe$, p. 60	
3. Magnetic susceptibility of iron-based semimagnetic semiconductors: high-temperature regime, p. 74	
4. Magnetization steps in iron-based diluted magnetic semiconductors, p. 83	
CHAPTER IV. CARRIER-CONCENTRATION-DEPENDENT MAGNETIC BEHAVIOR IN IV-VI GROUP DILUTED MAGNETIC SEMICONDUCTORS	89
1. Preparation and carrier concentrations of $Pb_{1-x-y}Sn_yMn_xTe$ and $Sn_{1-x}Mn_xTe$, p. 90	
2. Hole density and composition dependence of ferromagnetic ordering in $Pb_{1-x-y}Sn_yMn_xTe$, p. 96	
3. Carrier-concentration dependence of the magnetic interactions in $Sn_{1-x}Mn_xTe$, p. 101	
SAMENVATTING	105
LIST OF PUBLICATIONS	106

Introduction

In this chapter the diluted magnetic semiconductors (DMS) are introduced. First, the general physical properties, such as the composition range and band structure are briefly reviewed. Subsequently, some attention is paid to the $sp-d$ exchange, which is the background of all the phenomena specific for DMS.

The major part of this chapter, however, deals with the magnetic properties of DMS, and serves as an introduction to the other parts of this thesis. With respect to the Mn-containing DMS we will focus on the $d-d$ exchange (J) between Mn ions. In particular, the strength of J , as well as the relevance of long-range interactions, are emphasized. The possible origin of these interactions is analyzed on the basis of existing exchange models. Next, a new family of DMS, containing Fe instead of Mn, is introduced. In Fe-based materials new physical effects are observed, arising from Fe levels located above the valence bands, which are not populated in the Mn case. More importantly, we will discuss the possible influence of this on the magnetic properties. Finally, we will introduce the IV-VI group DMS. In comparison with II-VI and II-V materials, the carrier concentration in these systems is very high, leading, in some cases, to ferromagnetic RKKY interactions. Moreover, it has been shown that the ferromagnetic interactions in $\text{Pb}_{1-x-y}\text{Sn}_y\text{Mn}_x\text{Te}$ and $\text{Sn}_{1-x}\text{Mn}_x\text{Te}$ strongly depend on the carrier density. This phenomenon, the so-called carrier-induced ferromagnetism, is introduced, and also some recent developments are reported.

I. GENERAL

Diluted magnetic semiconductors (DMS) — or semimagnetic semiconductors (SMSC) — are ternary or quaternary semiconductors whose cations are partially replaced by a controlled amount of divalent transition-metal ions and recently, also rare-earth ions. A canonical example of such system is $\text{Cd}_{1-x}\text{Mn}_x\text{Te}$, belonging to the most extensively studied II–VI group alloys. Most of the effort has been devoted to the substitution of Mn^{2+} , partially because physical properties are not complicated by nonvanishing orbital momenta ($S = 5/2$, $L = 0$) but, more importantly, because of the technological ease of Mn^{2+} implantation in the semiconducting host (in striking contrast with other ions such as Fe^{2+} and Co^{2+}).

The scientific interest for DMS materials has been triggered by the observation of a variety of exciting effects, in the field of semiconductor physics, as well as on physics of magnetism of solids. As for the semiconducting effects, they all stem from the interaction between d electrons (the spins) and the s - and p -like orbitals of the band electrons, the so-called sp - d exchange (J_{sp-d}). This interaction amplifies so to say the Zeeman splitting of electronic levels, and, consequently, interesting effects are observed, such as a giant Faraday rotation, an extremely large negative magneto-resistance, and field-dependent metal-insulator transitions.

The magnetic properties of DMS are intimately related to the indirect spin-spin interaction between the random distributed magnetic ions (J_{d-d}). The interaction J_{d-d} originates from indirect electron processes between two localized moments and their intermediating band electrons and as a result, J_{d-d} is strongly coupled to J_{sp-d} . The experimental contributions to unravel these underlying physical mechanisms are mainly dealing with the strength, character and radial dependence of J_{d-d} , and the magnetic phase diagram in which temperature and concentration of magnetic ions trigger the magnetic

state (paramagnetic, spin-glass, antiferromagnetic, ferromagnetic).

The flexibility with which the lattice constants and band gaps can be varied within the wide range of magnetic-ion concentration in, mostly, Mn^{2+} -containing DMS, as well as the unique tunability of the electronic levels with magnetic field and temperature, make DMS materials good candidates for applications in, for example, field-tunable far-infrared sensors and lasers, and optical devices based on the large Faraday rotation. Finally, one of the most spectacular developments concerns the MBE growth of heterostructures, superlattices and thin films based on DMS. Besides the promising preparation of new, hitherto nonexistent structures such as $\text{Ga}_{1-x}\text{Mn}_x\text{As}$ and MnTe it is with MBE possible to bring the physics of DMS, and especially the characteristics known as band-gap engineering, into the rich and exciting phenomena of the Quantum Well.

This first part of the thesis presents a physically oriented introduction to the present status in this new class of materials. As for the structural and electronic properties of DMS, we will, however, confine ourselves to a rather brief overview, since a review by J.K. Furdyna¹ and a recent issue of *Metals and Semiconductors*², as well as more dated reviews³, are providing excellent insights in the physical properties of DMS. In these recent reviews¹⁻², the magnetism of DMS, which is the content of this thesis, is focused merely on II–VI group materials containing the conventionally Mn^{2+} . A broader introduction to this subject will therefore be presented here, emphasizing current topics in this field: the relevance of long-range interactions, the substitution of Fe^{2+} instead of Mn^{2+} , and the observation of carrier-concentration-dependent magnetic interactions in IV–VI group materials. Furthermore, this part will offer the reader an introductory guideline to the forthcoming chapters of the thesis, in which these subjects will be treated in detail.

II. CRYSTAL STRUCTURE, COMPOSITION AND BAND STRUCTURE

In Table I, see page 4, the crystal structure and the composition range of all known Mn- and Fe-containing DMS are tabulated. In most cases DMS crystals of high quality and large dimensions can be synthesized² by using the Bridgman (-Stockbarger) method or, to a lesser extent, chemical transport. The incorporation of Fe, and very recently also Co in the semiconductors is not so straightforward as in the Mn case, which, tentatively, has been ascribed¹ to the resemblance

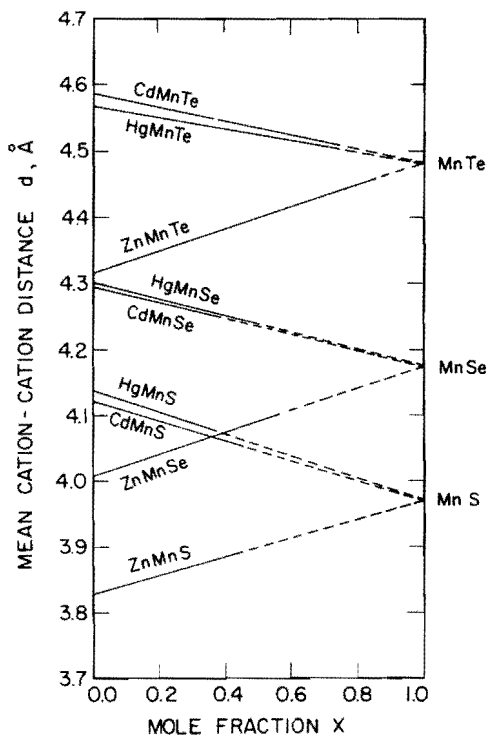


FIG. 1. Mean cation-cation distances d as a function of the Mn mole fraction x for $A_{1-x}Mn_xB$ alloys originating from the II-VI group. The lattice parameters can be obtained from d as follows, zinc blende: $a = d\sqrt{2}$, wurtzite: $a = d$ and $c = (8/3)^{1/2}d$; analytic expressions corresponding to the figure are given in Ref. 1 and Ref. 14.

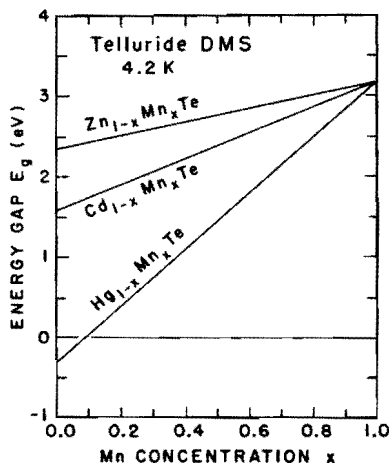


FIG. 2. Energy gap E_g vs. Mn concentration x for telluride DMS at low temperatures. A linear extrapolation of E_g to $x = 1$ gives an energy gap of 3.18 eV for zinc blende MnTe (after Ref. 1).

between the electronic configuration of Mn and the cations (both half or completely filled in contrast to Fe or Co).

The available structural investigations for the systems in Table I reveal a Vegard-type linear dependence of the lattice constant with the concentration of magnetic ions. This linear behavior has been used for the determination of the Mn concentration, besides other more direct methods like electron probe micro analysis (EPMA). For II-VI compounds on the basis of Mn^{2+} the lattice parameters have been established by Furdyna and co-workers¹⁴, and are shown in Fig. 1. The Vegard-type departure of the lattice parameter from that of the semiconducting host is, for all substances, clearly illustrated. One should, however, realize that standard x-ray diffraction only probes the average bond lengths and not the microscopic features of the structure. Very recently^{1,15}, extended x-ray absorption fine structures (EXAFS) studies on $Zn_{1-x}Mn_xSe$ convincingly demonstrated that on microscopic scale strong distortions from the zinc blende phase are visible. Moreover, both the Zn-Se and Mn-Se

TABLE I. Crystal structure and composition range for Mn- and Fe-based diluted magnetic semiconductors.

Material	Type / Ref.	Crystal structure	Composition range
$Zn_{1-x}Mn_xS$	II-VI	zinc blende	$0 < x \leq 0.10$
	Ref. 1-2	wurtzite	$0.10 < x \leq 0.45$
$Zn_{1-x}Mn_xSe$		zinc blende	$0 < x \leq 0.30$
		wurtzite	$0.30 < x \leq 0.57$
$Zn_{1-x}Mn_xTe$		zinc blende	$0 < x \leq 0.86$
$Cd_{1-x}Mn_xS$		wurtzite	$0 < x \leq 0.45$
$Cd_{1-x}Mn_xSe$		wurtzite	$0 < x \leq 0.77$
$Hg_{1-x}Mn_xS$		zinc blende	$0 < x \leq 0.37$
$Hg_{1-x}Mn_xSe$		zinc blende	$0 < x \leq 0.38$
$Hg_{1-x}Mn_xTe$		zinc blende	$0 < x \leq 0.75$
$(Cd_{1-x}Mn_x)_3As_2$	II-V	Ref. 4-6	$0 < x \leq 0.12$
$(Zn_{1-x}Mn_x)_3As_2$	Ref. 4-6	Ref. 4-6	$0 < x \leq 0.15$
$Pb_{1-x}Mn_xS$	IV-VI	rocksalt	$0 < x \leq 0.05$
$Pb_{1-x}Mn_xSe$	Ref. 7-9	rocksalt	$0 < x \leq 0.17$
$Pb_{1-x}Mn_xTe$		rocksalt	$0 < x \leq 0.12$
$Sn_{1-x}Mn_xTe$		rocksalt	$0 < x \leq 0.40$
$Ge_{1-x}Mn_xTe$		rhombohedral	$0 < x \leq 0.18$
		rocksalt	$0.18 < x \leq 0.50$
$Zn_{1-x}Fe_xS$	II-VI	zinc blende	$0 < x \leq 0.26$
$Zn_{1-x}Fe_xSe$	Ref. 10-13	zinc blende	$0 < x \leq 0.21$
$Zn_{1-x}Fe_xTe$		zinc blende	$0 < x \leq 0.01$
$Cd_{1-x}Fe_xSe$		wurtzite	$0 < x \leq 0.20$
$Cd_{1-x}Fe_xTe$		zinc blende	$0 < x \leq 0.03$
$Hg_{1-x}Fe_xSe$		zinc blende	$0 < x \leq 0.20$

bond length remain constant over the entire concentration regime, which is of great importance for the Mn^{2+} - Mn^{2+} exchange constants in DMS. We will return to this in Sec. IV on d - d exchange.

As we quoted before, one of the attractive features in DMS is the tunability of band parameters upon substitution. The most well-known example for this is the proportionality of the energy gap with composition, which for almost all DMS has been established. For Te-containing II-VI compounds the tunability of the gap by composition is plotted in Fig. 2, illustrating the "opening" of the gap in $\text{Hg}_{1-x}\text{Mn}_x\text{Te}$.

The sp - d exchange, which as we pointed out before, is the driving mechanism behind

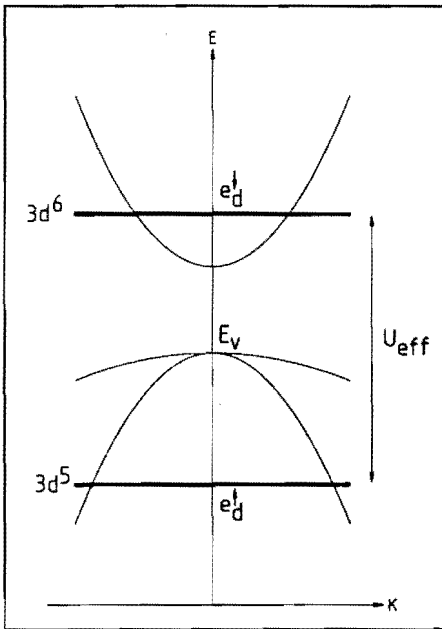


FIG. 3. Schematic band structure for a DMS with the direct gap at the Γ point. The Mn levels $e_d\uparrow$ (occupied) and $e_d\downarrow$ (unoccupied) are split by the energy U_{eff} (≈ 7 eV). The effect of p - d hybridization and crystal field on the Mn levels is neglected in this schematic representation, since the effect is small on the scale of the figure.

the anomalous field-dependent physical behavior of DMS, involves the band structure as well as the local magnetic ion $3d^5$ levels, which are superimposed on the band structure. Fig. 3 shows a schematic illustration of these levels in an idealistic zinc blende band structure, which is a representative example for II-VI DMS having the direct gap at the Γ point. The majority (spin up) and minority (spin down) Mn levels are in reality narrow bands due to mixing or hybridization with s and p orbitals of the semiconductor. According to Larson *et al.*¹⁶, the location and degree of hybridization of these levels are extremely important for the strength of the exchange integrals in DMS, which we will discuss in some detail further on. U_{eff} in Fig. 3 is the energy necessary to add one electron to a Mn^{2+} ($3d^5 \rightarrow 3d^6$) and amounts to ≈ 3.4 eV in $\text{Cd}_{1-x}\text{Mn}_x\text{Te}$, and it should be distinguished from intra-ion transitions involving spin-flip processes. For example, the flipping of one spin ($\uparrow\uparrow\uparrow\uparrow\uparrow$ to $\uparrow\uparrow\uparrow\uparrow\downarrow$) requires approximately 2.2 eV and is the dominating mechanism in optical processes¹.

III. sp - d EXCHANGE

All phenomena in DMS arise from the sp - d exchange between the spins (d electrons) and the band electrons (s or p electrons). For the description of the effect of the interaction on the electronic system one exploits the extension of the electron wave functions — the mobile electron interacts simultaneously with a large number of spins — in order to transform the Heisenberg-exchange Hamiltonian as follows

$$\sum_{\mathbf{R}_i} J_{sp-d}(\mathbf{r}-\mathbf{R}_i) \mathbf{S}_i \cdot \sigma \quad (1)$$

→

$$\sigma_z \langle S_z \rangle_x \sum_{\mathbf{R}} J_{sp-d}(\mathbf{r}-\mathbf{R}) ,$$

where σ and \mathbf{S} are the spin operators for band electron and $3d^5$ electron, respectively, J_{sp-d} is the electron-ion exchange constant, and \mathbf{r} and \mathbf{R}_i the coordinates of band electron and

Mn^{2+} , respectively. Two approximations are made in this transformation, (i) the spin operator S has been replaced by its thermal average in the z direction $\langle S_z \rangle$, using the molecular-field approximation for paramagnetic ions experiencing a field B along the z axis, and (ii) the summation no longer runs over the exact (random) position of the spins (R_i) but over all cation sites (R) weighted by the concentration magnetic ions x . Now, the exchange integral follows the periodicity of the semiconducting lattice (the Virtual Crystal Approximation) and provides the possibility to solve the Landau-energy levels of the DMS system. Just as an illustration for a parabolic conduction band, the following effective g -factor can be derived:

$$\begin{aligned} g_{\text{eff}} &= g^* - N_0 \alpha x \langle S_z \rangle / (\mu_0 H) \\ &= g^* + \alpha M / (g_{Mn} \mu_B^2 H) \end{aligned} \quad (2)$$

where

g^*	: band g -factor
N_0	: number of cations
α	: exchange integral for s -like conduction electrons
M	: magnetization
H	: magnetic field
g_{Mn}	: Landé-factor for Mn^{2+} .

Similar expressions can be found for the valence bands; the exchange integral now denoted as β instead of α . The principal difference between α and β stems from the symmetry of the electron wave functions within the band structure. In II-VI group semiconductors s -like electrons (e.g., of Γ_6 symmetry in $Cd_{1-x}Mn_xTe$) are associated with the conduction band and determine α . On the other hand, β is the exchange integral for p -like holes in the valence bands of these alloys (e.g., of Γ_8 symmetry in $Cd_{1-x}Mn_xTe$).

The right-hand side of the effective g -factor in Eq. 2 is only present in nonzero external magnetic fields and includes the macroscopic magnetization of the system, and, consequently, the magnetic field, temperature and composition enter in the electronic properties of a DMS. Due to this, the electronic

g -factors in DMS can become extremely large, in some cases exceeding 100, which is unique for semiconductors. Some examples of the physical effects arising from the large spin splitting of the electronic levels are (i) excessive exchange splitting of exciton transitions in open-gap semiconductors; (ii) a giant Faraday rotation, containing promising features for applications in, for example, optical devices or very precise magnetic field sensors; (iii) anomalous temperature and field dependence of Shubnikov-de-Haas oscillations in narrow-gap semiconductors [such as $Hg_{1-x}Mn_xSe$ and $(Cd_{1-x}Mn_x)_3As_2$]; and (iv) bound magnetic polarons due to the polarization of Mn^{2+} spins around a electron trapped in an impurity potential. All the available quantitative information on the exchange integrals α and β has been derived from the study of these physical phenomena, since in the magnitude of the effects the exchange constants (or a combination of them) are comprised. It is also worthwhile mentioning that through the study of magneto-optical properties (Faraday rotation, exciton splitting) it is possible to investigate the magnetization of the system; see Eq. 2.

The sp - d exchange J_{sp-d} , quantified in the exchange integrals between conduction band electrons and $3d^5$ electrons, α , and similar for the valence bands, β , have attracted a considerable part of all research activity in recent years, similar to the interest for the indirect d - d exchange between two spins (J_{d-d}). Both the sp - d and d - d exchange are of great fundamental importance, since their sign, strength and, in the case of J_{d-d} , its spherical extension are intimately related to theoretically developed interaction mechanisms such as superexchange. A close examination of these fundamental aspects will be given in the forthcoming section.

IV. d - d EXCHANGE AND MAGNETIC PROPERTIES

In the following subsections we will concentrate on three different subjects, which are closely related to the investigations re-

ported in this thesis. First of all, we will consider the Mn-containing DMS originating from the II-VI group. In these compounds antiferromagnetic (AF) long-range interactions between Mn^{2+} ions have been observed in all existing compounds, irrespective of the wide variety of intrinsic properties, such as band gap, lattice constant, covalency and carrier concentration. Apart from the character and strength of the interaction we will pay much attention to the spherical extension of the interaction, and the relation with the underlying physical mechanism. Subsequently, we will introduce a relatively new class of DMS materials on the basis of Fe. Through the $3d^6$ configuration of Fe^{2+} the magnetism of these alloys is different from Mn-type DMS, and, moreover, in the context of exchange mechanisms, the Fe^{2+} can alter the phenomena we observed in the Mn case. Finally, we will present an introduction to the IV-VI compounds containing Mn^{2+} . The carrier concentration in these systems is so high that the so-called RKKY interaction (i.e., a spin polarization of the carriers) can become effective and induces ferromagnetic interactions. Moreover, it will be shown that in some of these compounds the ferromagnetic behavior of the system can be switched on or off, just by variation of the carrier concentration, the so-called carrier-induced ferromagnetism.

A. Mn-containing DMS

The research on the magnetism of DMS is also almost exclusively restricted to the Mn case. Apart from the relative ease to obtain high-quality crystals with a wide range of Mn concentrations, the $3d^5$ electrons of Mn^{2+} add up to a simple, theoretically attractive spin-only ${}^6S_{5/2}$ ground state. Though crystal-field effects might affect this state by mixing with higher levels, it is generally affirmed [e.g. by electron paramagnetic resonance (EPR) of Mn^{2+} in semiconductors²] that these effects are very small leaving the ground state six-fold degenerate with $S = 5/2$ and $L = 0$.

In a DMS, the magnetic behavior should, obviously, be interpreted as arising from the interaction between Mn^{2+} . Originally, so-called cluster models have been developed to describe the behavior. In these models the interaction is essentially restricted to Mn^{2+} ions at neighboring lattice sites. However, on the basis of the cluster models it was not possible to describe all the available data without the questionable need to adjust the random distribution of the Mn ions. These inconsistencies could only be clarified by allowing a long-range tail for the $d-d$ interactions. The observation of spin-glass freezing for Mn concentrations well below the percolation limit for nearest-neighbor (NN) interaction (≈ 0.195 for an fcc lattice) ultimately proved the existence of an interaction extending over many lattice sites.

Besides the complication of the spherical extension of J_{d-d} , it is in the random diluted system rather difficult to extract the interac-

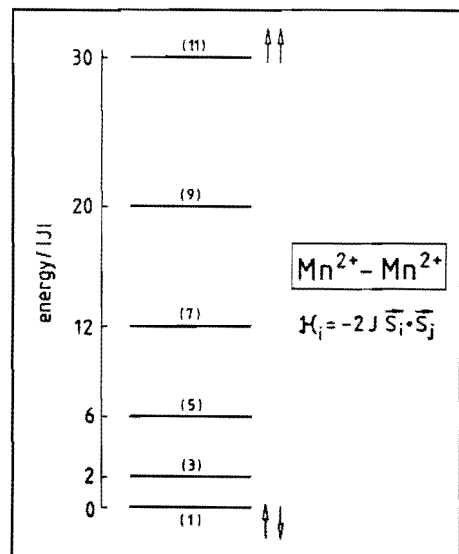


FIG. 4. Energy levels for a pair of Mn^{2+} ions with an antiferromagnetic coupling J and $S = 5/2$. For each level the degeneracy is indicated between brackets.

tion from experimental data, since a variety of cluster types (pairs, triples, quartets, ...) are present on the basis of random statistics, each exhibiting its own energetical structure. By allowing a long-range J_{d-d} even every spin is coupled with any other spin! Nevertheless, for sufficiently small Mn concentrations, typically below 10%, the number of pairs become large enough to dominate the magnetic properties and to trace the character and strength of the Mn-Mn exchange. The energy-level scheme for such a Mn-Mn pair, coupled antiferromagnetically, is shown in Fig. 4. Fortunately, and due to the spin-only state of Mn^{2+} , the exchange-induced splittings directly correspond to the coupling constant $|J|$. Accurate determination of the interaction strength between adjacent Mn^{2+} ions, the so-called nearest-neighbor interaction J_{NN} , can be obtained from probing the gap between the singlet ground state and the first excited state ($2|J|$, see Fig. 4), e.g., by inelastic neutron diffraction¹⁹, Raman scattering² and, somewhat less directly, by the high-field magnetization²⁰, see Fig. 5. Other techniques, such as the high-temperature susceptibility, specific heat and EPR, extract J_{NN} indirectly in the sense that other clusters (triples, quartets and long-range coupled ions) interfere with the phenomena characteristic for J_{NN} , and serious errors are to be expected. In Table II all investigations on J_{NN} are gathered.

We already argued that it is by now commonly accepted that, in general, the exchange integral is not restricted to Mn ions at neighboring cation sites only, but extends also to more distant neighbors. From a scaling analysis of the concentration dependence of the spin-glass freezing temperatures, it was possible to derive how J_{d-d} decays with distance between the Mn ions. It was pointed out that the interaction beyond the nearest neighbors (NN) is rapidly decreasing in strength, and, from the experimental point of view, hard to extract quantitatively. So far, reliable data, though very scarce, could only be obtained on J_{NN} , the next-nearest-neighbor exchange constant, see Table II.

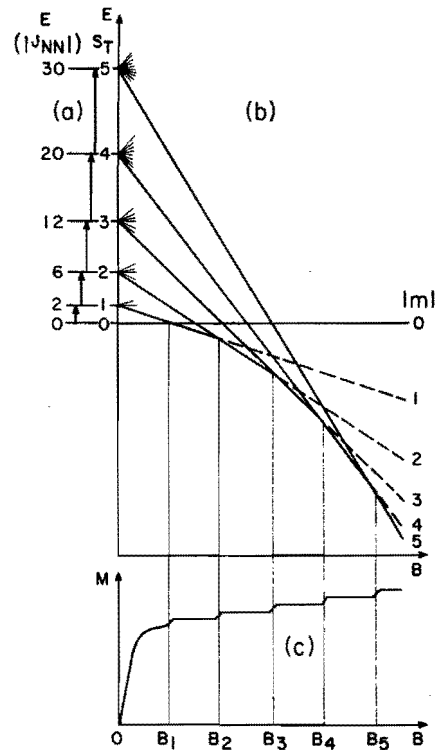


FIG. 5. (a) Energy level diagram, in units $|J_{NN}|$, for a pair of NN Mn^{2+} ions at $B = 0$. (b) Zeeman splitting of the energy levels in a magnetic field B ; note the level crossings at B_n . (c) Illustration of the magnetization curve at low temperatures, showing the apparent saturation ($M = M_s$), followed by the magnetization steps due to pairs. The magnetization steps due to triples or other clusters, as well as long-ranged coupled ions are not shown (after Ref. 20).

To explain the magnitudes of J and the observed tendencies — such as the increasing $|J_{NN}|$ on going from Te via Se to S and from Cd to Zn — we should consider theoretical exchange models. Basically, for the spin-spin interaction in semiconductors three mechanisms are available, i.e., superexchange⁵⁹, Bloembergen-Rowland (BR)⁶⁰ and Ruderman-Kasuya-Kittel-Yosida (RKKY)⁶¹. All mechanisms can be expressed in terms of vir-

TABLE II. Nearest-neighbor and next-nearest-neighbor exchange constants (J_{NN} , J_{NNN}) for Mn- and Fe-based diluted magnetic semiconductors.

Material	$-J_{NN}$ (K)	Techn.	Ref.	$-J_{NNN}$ (K)	Techn.	Ref.
$Zn_{1-x}Mn_xS$	≈ 10 16.9 \pm 0.6	MAGN	21,22	0.6	MAGN	22
	16.1 \pm 0.2	NEUT	23	4.8 \pm 0.1	SUSC	24
	13.0 \pm 1.5	EPR	25	≈ 0.7	$T_F(x)$	26
$Zn_{1-x}Mn_xSe$	≈ 13 9.9 \pm 0.9	MAGN	21,27	2.4 3 \pm 2.4	SUSC	29,30
	≈ 12.6 12.2 \pm 0.3		28,20	≈ 0.7	$T_F(x)$	31
	12.3 \pm 0.2	NEUT	23			
$Zn_{1-x}Mn_xTe$	18 13.5 \pm 0.95	SUSC	21,29			
	10.0 \pm 0.8 10.1 \pm 0.4	MAGN	32,33	0.6	MAGN	35
	9.25 \pm 0.3 8.8 \pm 0.1		34,27	4.6 \pm 0.9 3.6 \pm 2	SUSC	30
$Cd_{1-x}Mn_xS$	9.0 \pm 0.2		20			
	9.52 \pm 0.05 7.9 \pm 0.2	NEUT	36,31			
	12 11.85 \pm 0.25	SUSC	32,37			
$Cd_{1-x}Mn_xSe$	>4 8.6 \pm 0.9	MAGN	21,38	5.2 \pm 0.3	MAGN	39
	10.5 \pm 0.3 10.6 \pm 0.2		28,39			
	9.65 \pm 0.2 11.0 \pm 0.2		22			
$Cd_{1-x}Mn_xTe$	8.3 \pm 0.7 7.9 \pm 0.5	MAGN	21,40	1.6 \pm 1.5	MAGN	40
	8.1 \pm 0.2		39	4.6 \pm 2 5.4 \pm 1.5	SUSC	30
	9 10.6 \pm 0.2	SUSC	21,37			
$Hg_{1-x}Mn_xTe$	7.7 \pm 0.3	RAM	41			
	≈ 10 6.3 \pm 0.3	MAGN	21,40	1.9 \pm 1.1 1.1 \pm 0.2	MAGN	40,42
	6.1 \pm 0.3 6.2 \pm 0.2		28,20	0.67	NEUT	43
$Hg_{1-x}Mn_xSe$	≈ 7.5 6.7	NEUT	44,43	1.2 \pm 1	SUSC	30
	6.9 \pm 0.15	SUSC	37	0.9	LARS	16
	7.7 \pm 0.3	EXCI	46	0.55 \pm 0.05	SPEC	46
$Hg_{1-x}Mn_xTe$	6.1 \pm 0.2	RAM	41			
	8	LARS	16			
	6 \pm 0.5 5.3 \pm 0.5	MAGN	47,35			
$(Zn_{1-x}Mn_x)_3As_2$	10.9 \pm 0.7	SUSC	37			
	0.1	EPR	48			
	5.1 \pm 0.5 4.3 \pm 0.5	MAGN	47,35	1	SUSC	49
$(Cd_{1-x}Mn_x)_3As_2$	15 15.7 7.15 \pm 0.25	SUSC	50,49,37	0.7 \pm 0.3	SPEC	51
	≈ 100	$T_F(x)$	5,51	≈ 2	$T_F(x)$	5,51
	≈ 30	$T_F(x)$	5,52	≈ 5	$T_F(x)$	5,52
$Pb_{1-x}Mn_xS$	0.537	MAGN*	53	0.0537	MAGN	53
	1.28	SUSC	54			
	≈ 1	MAGN*	55			
$Pb_{1-x}Mn_xSe$	1.67	SUSC	54			
	≈ 1	MAGN*	55			
	0.84	SUSC	54			
$Zn_{1-x}Fe_xSe$	22 \pm 2	SUSC	56			
$Cd_{1-x}Fe_xSe$	11.25 \pm 1.5 18.8 \pm 2	SUSC	57,56			
$Hg_{1-x}Fe_xSe$	15 \pm 1 18 \pm 2	SUSC	57,58			

EPR = electron paramagnetic resonance; EXCI = high-field exciton splitting;
LARS = Larson's superexchange model; MAGN = steps in the high-field magnetization;
MAGN* = high-field magnetization, fitted with pair approximations;
NEUT = inelastic neutron scattering; RAM = Raman scattering;
SPEC = low-temperature magnetic specific heat; SUSC = high-temperature susceptibility;
 $T_F(x)$ = spin-glass freezing temperatures, combined with thermodynamic properties.

tual electron transitions (described by exchange and/or hybridization) between band electron or hole, and the d^5 electrons. In Figure 6 it is schematically illustrated that in superexchange 2-electron (or hole) processes take place, the so-called interband transitions. In BR on the other hand, only intra-band transitions are allowed, and finally, RKKY accounts for an interband process at the Fermi level. As a consequence, we may state, roughly speaking, that the only principle difference between them is that superexchange applies for open-gap materials (isolators, semiconductors), BR for small-gap materials (semiconductors) and RKKY for partially filled bands (metals, semimetals).

By a quantitative analysis¹⁶ Larson *et al.* were able to demonstrate that in open-gap DMS [(Zn,Cd)_{1-x}Mn_x(S,Se,Te)] the major contribution comes from the antiferromagnetic superexchange (> 95%), in which only 2-hole processes in the valence band are allowed, see Fig. 6. Furthermore, they established the inferior role of the BR mechanism and the absence of RKKY. In addition, with a simplified so-called three-level superexchange model they could predict the observed chemical trends encountered in Table II. In this model the valence band energy E_v , the difference between the minority and majority Mn level (U_{eff}) and the Mn majority level

(E_d), see Fig. 3, together with the hybridization parameter V_{dp} , completely determine J_{NN} :

$$J_{\text{NN}} = -8.8 V_{\text{dp}}^4 [(E_d + U_{\text{eff}} - E_v)^{-2} U_{\text{eff}}^{-1} + (E_d + U_{\text{eff}} - E_v)^{-3}] \quad (3)$$

Since in this 3-level model J_{NN} is determined by hybridization of d levels with the valence band states only, one would expect that β , the exchange parameter for the valence bands, exhibits the same chemical trends as J_{NN} . This is indeed corroborated by experimental data, although one should realize that β is composed not only of the p - d hybridization term but also of a much smaller term of opposite sign, representing the $1/r$ exchange which tend to align the d -electron spin with the band-electron spin. The absence of hybridization with conduction band states therefore explains why α , the integral for the conduction bands, is small compared to β and of opposite sign.

The extension of the exchange beyond the NN in Larson's model is expressed¹⁶ by a material-independent Gaussian form $f(R)$, yielding

$$J(R) \sim \exp(-\alpha R^2) \quad (4)$$

Material-independent means independent of electronic details, in our case applicable for the wide-gap Mn compounds. In Chapter II we will illustrate on the basis of an experimental study that for those systems, with emphasis on $\text{Zn}_{1-x}\text{Mn}_x\text{Se}$ and $\text{Zn}_{1-x}\text{Mn}_x\text{S}$, a long-range tail of J should be present. From an analysis of the paramagnetic to spin-glass transition temperatures a power-law decay of $J(R)$ will be suggested,

$$J(R) \sim R^{-n}, \quad \text{with } n \approx 7. \quad (5)$$

It will be shown experimentally that, quite remarkably (see the Discussion in Chapter II.1), this R^{-7} decay is also material-insensitive for all wide-gap DMS. However, the power-law decay in Eq. 5 is, particularly at

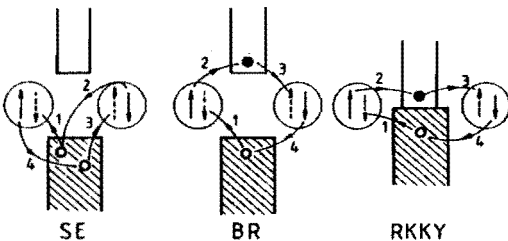


FIG. 6. Schematic representation of the exchange processes superexchange (SE), Bloembergen-Rowland (BR) and Rudermann-Kittel-Kasuya-Yosida (RKKY). The filled valence bands, empty conduction bands, Mn spin states and transitions are shown (based on Ref. 62).

larger distances, essentially different from Larson's approach. Nevertheless, for the first few neighbors (NN, next NN, next-next NN) the difference is rather small, and, moreover, by comparing Eq. 4 and 5 with existing data on J_{NN} , J_{NNN} and J_{NNNN} , see Fig. 7, strong evidence is found for the usefulness of both the approximations in this regime.

More support for the extension of J beyond the NN will be given in Chapter II, where we will closely examine the thermodynamic properties (susceptibility, magnetization, specific heat) of DMS, exemplified for $Zn_{1-x}Mn_x(Se,S)$. It will be convincingly demonstrated that the overall behavior of the properties cannot be understood on the basis of short-range interactions and therefore the long-range character of the interaction should be taken into account. The so-called extended nearest-neighbor pair approximation (ENNPA), developed by Denissen *et al.*⁵ for long-range coupled random diluted spins, is capable to describe all the magnetic properties simultaneously.

Finally, there exists some very recent results on the $d-d$ exchange which, in principle, should be included in our current understanding and modeling methods for DMS. First, it was pointed out on page 3 that strong distortions of the Mn^{2+} - anion - Mn^{2+} bond angles are observed by EXAFS, capable to influence to strength of the interaction by varying the Mn concentration. A thorough examination of $\Theta(x)$ ³⁷, this is the concentration dependence of the Curie-Weiss constant probing interaction strengths, and also neutron diffraction studies probing J_{NN} ¹⁹, seem to substantiate these tendencies. In the latter case, even a linear variation of J_{NN} with concentration has been suggested. Despite all this, the calculations for DMS systems are commonly confined to low concentrations, typically below 10%, where no drastic effects can be expected.

Recently, some investigations were dealing with the the anisotropic part of the exchange. Larson *et al.*¹⁶ were able to relate the observed tendencies of the EPR linewidth to their superexchange model, yielding evidence

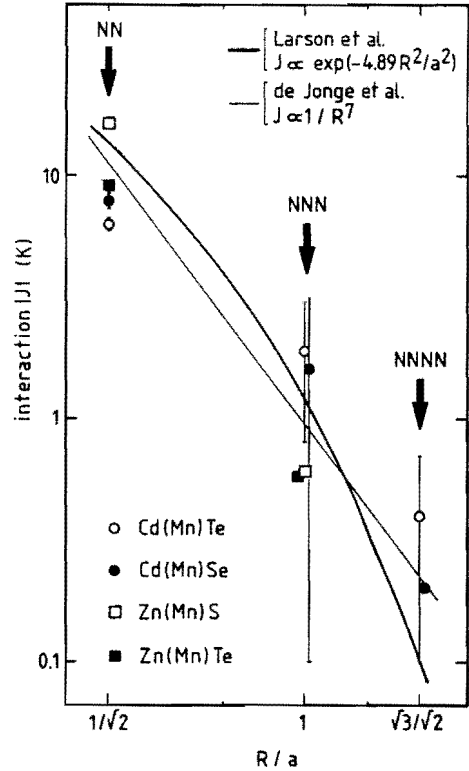


FIG. 7. Radial dependence of the exchange interaction $|J|$ based on (i) Larson's three-level superexchange model¹⁶ (Eq. 3), and (ii) based on a scaling analysis of the spin-glass freezing temperature $T_F(z)$ (Eq. 5) by de Jonge and co-workers (Ref. 5,31,63), compared with experimental data (Ref. 20,22,40 and Table II).

for a Dzyaloshinsky-Moriya anisotropic exchange

$$\mathcal{H}_{DM} = - \sum_{i \neq j} D(\mathbf{R}_{ij}) \cdot \mathbf{S}_i \times \mathbf{S}_j, \quad (6)$$

$|D_{NN}/J_{NN}|$ being roughly between 10^{-3} and 10^{-1} depending on the specific system. Though relatively small compared with the isotropic part of the interaction, this anisotropy can become of vital significance for the magnetic properties at low temperatures

where effects due to J_{NN} can be safely ignored. Moreover, the characteristic upturn of the magnetic specific heat at temperatures below 1 K (see Chapter II and Ref. 26,31) strongly suggest the existence of DM anisotropy, which therefore should be included in future calculations.

In this section we did not pay much attention to small gap DMS materials such as $(\text{Cd}_{1-x}\text{Mn}_x)_3\text{As}_2$ and $\text{Hg}_{1-x}\text{Mn}_x\text{Se}$. Existing data on these compounds^{5,51,52,63,64} pointed to a much slower decay of the interaction (between R^{-3} and R^{-5} instead of R^{-7}), which, tentatively, indicates an increasing role of the BR mechanism and can be described in terms of a small or vanishing fundamental energy gap. There is, however, actually no conclusive theoretical support to explain the observed tendencies, neither for the strength of J_{NN} (being very large for II-V DMS and not accurately known for small gap II-VI's, see Table II) nor for the more extended tail of the interaction. In the Discussion of Chapter II.1 some additional comments will be put forward to bring this subject into a broader context.

B. Fe-based DMS

As we quoted earlier, the majority of experimental studies so far have been devoted on the semiconductors containing Mn^{2+} . Recently, however, new systems based on Fe^{2+} have been investigated¹¹. Apart from the relative short history of this class of DMS — the first papers⁶⁵ on magnetic properties appeared in 1985 —, this is also due to the crystal growing process. Up to now II-VI compounds with Fe concentrations in bulk crystals never exceed 26%; see Table I. In the case of $\text{Zn}_{1-x}\text{Fe}_x\text{Se}$, however, it was by means of MBE growth of thin layers possible to cover the entire range of Fe concentrations, from $x = 0$ (ZnSe) to $x = 1$ (FeSe), containing promising perspectives for future research^{66,67}.

One of the new and challenging opportunities in Fe DMS is created by the surplus of one electron compared to Mn ($3d^6$ instead

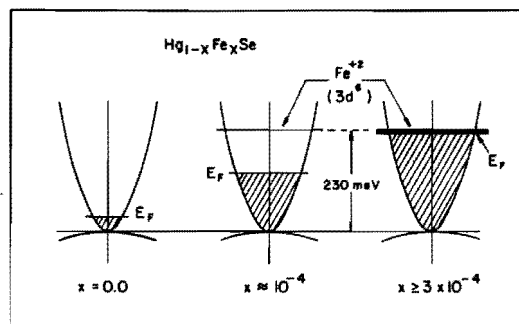


FIG. 8. A schematic picture of the band structure of $\text{Hg}_{1-x}\text{Fe}_x\text{Se}$ near the Γ point for several values of x . The Fe^{2+} level is shown as a resonant donor. There are approximately $5 \cdot 10^{18} \text{ cm}^{-3}$ conduction band states available below the Fe^{2+} -level. For $x > 3 \cdot 10^{-4}$, all these levels are filled by ionization of Fe^{2+} ions to Fe^{3+} ions. This provides a natural limit for the Fermi level (after Ref. 1).

of $3d^5$), forming an occupied Fe level above the valence band. For zero-gap $\text{Hg}_{1-x}\text{Fe}_x\text{Se}$ this implies the level is lying within the conduction band ($\pm 230 \text{ meV}$ from the bottom¹⁰) providing conduction band states by ionization of Fe^{2+} ($\text{Fe}^{2+} \rightarrow \text{Fe}^{3+} + e^-$). The concentration of these so-called resonant donors thus determines the Fermi level, and, by increasing the number of Fe^{2+} ions, the Fermi level will shift to higher energies until, at a dopant level of 10^{18} cm^{-3} ($\equiv x \approx 0.0005$) the level is pinned to the Fe d level. This phenomenon is depicted in Fig. 8 and has attracted much attention, also because the ionized Fe^{3+} donors are believed, according to Mycielski¹¹, to form a so-called perfectly "charge-superlattice".

Also from the magnetic point of view the interest for the Fe compounds is created by the specific $3d$ levels of Fe^{2+} . From the previous subsection we learned that these levels play, for instance in Larson's superexchange model, a decisive role in the magnetic d - d interaction. Any alteration within these levels, such as provided by the Fe^{2+} compared with Mn^{2+} , can therefore be of great

influence on the exchange mechanism in DMS. In particular, the Fe level located above the valence band might affect the magnetic properties, since this implicitly means for zero-gap DMS (e.g. $\text{Hg}_{1-x}\text{Fe}_x\text{Se}$) a level in the conduction band whereas for open-gap systems (e.g. $\text{Cd}_{1-x}\text{Fe}_x\text{Se}$ and $\text{Zn}_{1-x}\text{Fe}_x\text{Se}$) it is located between conduction and valence band.

In that context, some experimental studies indicating striking differences between zero- and open-gap systems appeared in recent years^{11,57,68}. In the study of the specific heat⁶⁹ presented in Chapter III.2 we will, however, report an analogous low-temperature magnetic behavior for *all* Fe-based II-VI group DMS. Therefore, the magnetic properties seem to be predominantly determined by mainly Fe levels below the valence band, which, similar to Mn, hybridize much stronger with the band electrons than Fe levels above the valence band. Moreover, to strengthen this claim we will not only consider the boundary materials $\text{Hg}_{1-x}\text{Fe}_x\text{Se}$ and $\text{Cd}_{1-x}\text{Fe}_x\text{Se}$, but also its quaternary alloy $\text{Hg}_{1-x-y}\text{Cd}_y\text{Fe}_x\text{Se}$. These alloys represent an ideal testcase to unravel the role of the high-

lying Fe levels, since it is known^{10,57,70} that for $y = 0.35 - 0.40$ the Fe level is located just at the bottom of the conduction band; see Fig. 9.

On the whole, the magnetic properties of Fe-based DMS, probed by standard techniques such as magnetization, susceptibility, and specific heat, display other characteristics than we observed for Mn^{2+} , stemming from the nonzero orbital momentum of Fe^{2+} , since, according to Hund's rules, the $3d^6$ configuration of Fe^{2+} implies $S = 2$ and $L = 2$. The crystal field and spin-orbit coupling induce a magnetically inactive ground state, separated from higher-lying levels with energies typically 10 - 30 K, see Fig. 10, exhibiting Van Vleck-type paramagnetism (at low temperatures, the susceptibility is constant). Only in the presence of an external magnetic field, mixing with other states induces a nonzero magnetic moment (in other words, a magnetic-field-induced paramagnetism). For fields strong enough to overcome the cubic symmetry of the wave functions, magnetic anisotropy is observed in the magnetization. These phenomena can be understood on the basis of an existing crystal-field model first developed by Low and Weger⁷¹, and later adjusted⁷² by Slack *et al.*, and several others. The validity of this model in the presence of relatively high Fe-concentrations we encounter in DMS materials was unambiguously verified by recent far-infrared (FIR) absorption data on some representative systems⁷³⁻⁷⁵. As an illustration, the FIR transmission of $\text{Zn}_{1-x}\text{Fe}_x\text{Se}$ is presented in Fig. 11.

In Chapter III.1 and Ref. 76 a thorough analysis of the thermodynamic properties of $\text{Zn}_{1-x}\text{Fe}_x\text{Se}$ will be presented, and, apart from the phenomena characteristic for isolated Fe ions listed above, conclusive evidence for an antiferromagnetic interaction between Fe^{2+} ions, similar to the Mn DMS, will be found. In distinction to Mn, the interaction is masked by the Van-Vleck behavior of non-interacting or weakly coupled ions, and unfortunately, the strength as well as the possible tail of J is therefore extremely hard to

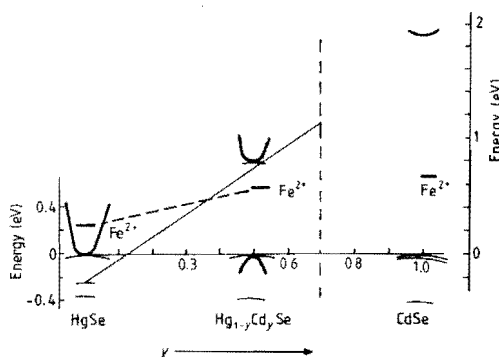


FIG. 9. The schematic band structure of $\text{Hg}_{1-x-y}\text{Cd}_y\text{Fe}_x\text{Se}$ solid solutions ranging from HgSe to CdSe. The position of the $3d^6$ level of Fe^{2+} ions in crystals of different compositions is taken from the paper of Mycielski (Ref. 70). The picture is valid for all accessible concentrations x , i.e., for $0 < x < 0.15$.

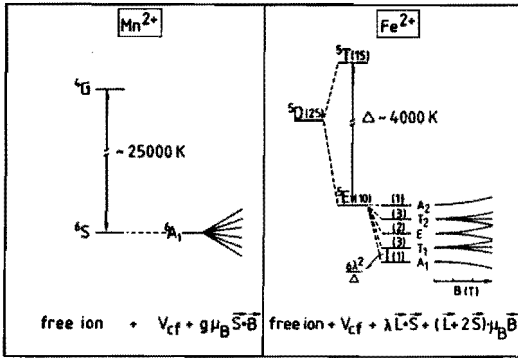


FIG. 10. Energy level diagram for isolated Mn^{2+} and Fe^{2+} ions. Effects of crystal field, spin-orbit interaction and magnetic field are shown (not to scale). The energy distances marked in the figure correspond to a ZnSe host lattice (after Ref. 12).

extract from these data. However, a theoretical study of the high-temperature susceptibility⁵⁶, see Chapter III.3, offers the possibility to extract J_{NN} by comparing data with theoretical expressions for the Curie-Weiss temperature. We recall that for the simple spin-only case J is extracted from the well-known Curie-Weiss law:

$$\chi = C/(T-\Theta),$$

$$\Theta = 2xS(S+1) \sum_i z_i J_i / 3k_B, \quad (7)$$

with $J_i = J_{\text{NN}}$, for $i = 1$,
 J_{NN} for $i = 2$, etc.
 $z_i =$ number of ions coupled by J_i .

In the Fe case similar expressions can be found, although supplemented with additional terms originating from the crystal-field effects, yielding exchange constants approximately two times larger than for Mn; see Table II. Unfortunately, these expressions include some model-dependent parameters which can possibly obscure this approximation.

Finally, a numerical study⁷⁷ presented in

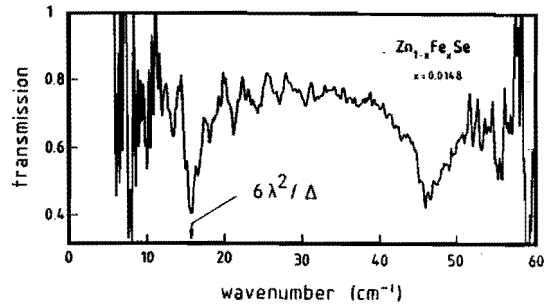


FIG. 11. The transmission of $\text{Zn}_{1-x}\text{Fe}_x\text{Se}$, $x = 0.0148$, at $T = 1.5$ K; the $A_1 \rightarrow T_1$ transition is indicated by the arrow, whereas the broad dip at higher wave numbers can be associated with the $A_1 \rightarrow T_2$ transition (see Fig. 10).

Chapter III.4 predicts the existence of steps in the low-temperature magnetization of Fe compounds, analogously to the Mn case (Fig. 5) and almost insensitive of crystal-field and spin-orbit parameters ($6\lambda^2/\Delta$, see Fig. 10). Though experimental evidence for this is still lacking, these calculations might offer the opportunity to obtain reliable quantitative data on J_{NN} .

C. IV-VI compounds

The number of papers devoted to IV-VI group DMS is completely outnumbered by those on the Mn-containing II-VI group materials and only since very recently a rapidly growing scientific interest can be observed⁹. Among the IV-VI DMS most of the attention has been focused on the Pb-containing compounds^{9,53-55,79-82}, e.g. $\text{Pb}_{1-x}\text{Mn}_x\text{Te}$. The magnetic properties of these alloys closely resemble the behavior of the II-VI Mn-containing DMS described in one of the previous sections, i.e., the interactions are antiferromagnetic, spin-glass phases have been detected, and, in a first order approximation, the thermodynamic properties can be fairly well described by pair approximations.

However, the strength of the AF interaction in $\text{Pb}_{1-x}\text{Mn}_x\text{Te}$ is much weaker than in

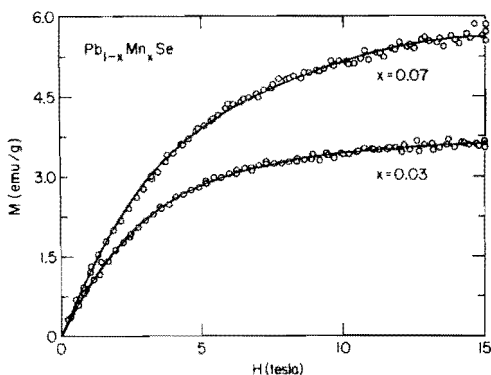


FIG. 12. Magnetization of $\text{Pb}_{1-x}\text{Mn}_x\text{Te}$ at $T = 4.2$ K. The circles represent the data and the solid lines were obtained from three-parameter fits (after Ref. 54).

the II–VI's, leading, as an example, to very small negative Curie–Weiss temperatures and a stepless, quickly saturating magnetization (see Fig. 12). This can be seen also in Table II, where $|J_{\text{NN}}|$ is for all cases below 2 K. Gorska *et al.*⁵⁵ ascribed this strong reduction compared to the II–VI's primarily to the separation ($d_{\text{Mn-a}}$) between Mn and an adjacent anion (in this case Te). Within existing models on superexchange^{16,59} the interaction is very sensitive for this separation through the $d_{\text{Mn-a}}^{-4}$ or $d_{\text{Mn-a}}^{-7/2}$ dependence of the hybridization parameter V_{dp} , yielding

$$J \sim d_{\text{Mn-a}}^{-14} - d_{\text{Mn-a}}^{-16} . \quad (8)$$

We should, however, not exclude that the observed differences are above all induced by the Mn – anion – Mn bond angle. According to a quantum mechanical treatment of an idealized three-site molecule^{37,59}, the NN interaction varies with $\cos^2\phi$ being minimal for the $\pi/2$ angle in the rocksalt structure of $\text{Pb}_{1-x}\text{Mn}_x\text{Te}$. On the other hand, Ginter *et al.*⁸³ indicated that exchange constants at the L point, where the direct gap is located in IV–VI DMS, are substantially diminished compared to the Γ point in the II–VI's.

In the context of exchange mechanisms

we already argued that for the II–VI compounds considered earlier, the small concentration of charge carriers rules out the indirect RKKY mechanism between the Mn^{2+} ions, leaving the antiferromagnetic superexchange dominant in the exchange processes. In contrast to this, the interactions observed in the IV–VI compounds $\text{Sn}_{1-x}\text{Mn}_x\text{Te}$ ^{84–88}, $\text{Pb}_{1-x-y}\text{Ge}_y\text{Mn}_x\text{Te}$ ⁸⁹ and $\text{Ge}_{1-x}\text{Mn}_x\text{Te}$ ⁹⁰ are ferromagnetic, and should be explained by assuming a RKKY-type of interaction. The oscillating RKKY interaction, brought about by the high carrier concentrations in these systems, of the order 10^{21} cm^{-3} , is indeed ferromagnetic, at least for the first few neighbors (see Fig. 13). Moreover, the R^{-3} decay of J_{RKKY} implies, on the basis of scaling arguments, that T_c should be proportional with x , since

$$k_B T_c \sim J_{\text{RKKY}} \sim R_{\text{mean}}^{-3} \sim x , \quad (7)$$

which is indeed experimentally observed⁸⁷.

The carrier concentrations for all DMS are schematically shown in Fig. 14, where we see that for the II–VI compounds the concentrations are so small that the ferromagnetic RKKY interactions can be neglected and only AF coupling is observed. On the right

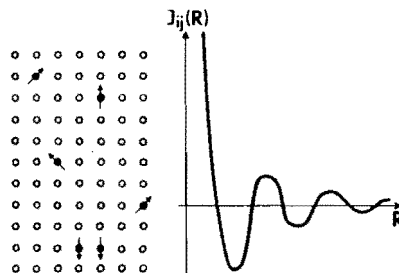


FIG. 13. Schematic sketch of magnetic moments randomly distributed in a matrix, and the resulting RKKY exchange integral plotted as a function of the distance. For the carrier concentrations we usually encounter in $\text{Pb}_{1-x-y}\text{Sn}_y\text{Mn}_x\text{Te}$ and $\text{Sn}_{1-x}\text{Mn}_x\text{Te}$ several positions for magnetic ions are available in the first strong ferromagnetic regime.

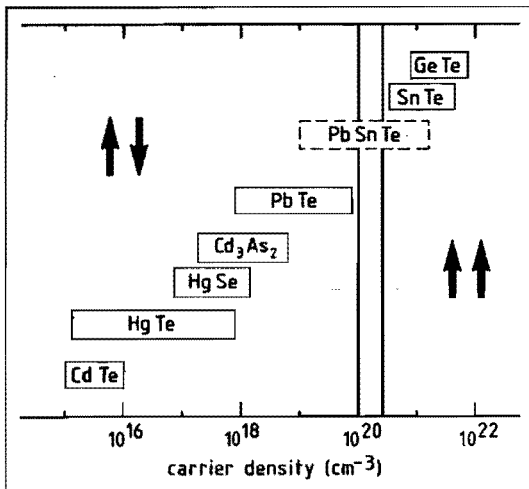


FIG. 14. Schematic representation of carrier concentrations in DMS based on Mn^{2+} . The antiparallel and parallel arrows indicate the observed antiferromagnetic and ferromagnetic interactions in those regimes, respectively. In $\text{Pb}_{1-x-y}\text{Sn}_y\text{Mn}_x\text{Te}$, carrier concentrations in both regimes are covered.

hand side of Fig. 14, at the highest possible carrier densities, the ferromagnetic IV–VI compounds are gathered. Consequently, one can see that in between $\text{Pb}_{1-x}\text{Mn}_x\text{Te}$ and $\text{Sn}_{1-x}\text{Mn}_x\text{Te}$ a natural boundary exists at carrier concentrations of roughly 10^{20} cm^{-3} , dividing the Mn-containing DMS into an antiferromagnetic and ferromagnetic interaction regime.

In 1986 Story *et al.*^{91,92} shed new light on the role of the carrier density by the discovery of the so-called carrier-concentration-induced ferromagnetism in $\text{Pb}_{0.25}\text{Sn}_{0.72}\text{Mn}_{0.03}\text{Te}$, a quaternary blend between $\text{Pb}_{1-x}\text{Mn}_x\text{Te}$ and $\text{Sn}_{1-x}\text{Mn}_x\text{Te}$. In these compounds it is possible to cover a wide range of carrier concentrations, from 10^{19} cm^{-3} up to at least 10^{21} cm^{-3} . At a critical carrier concentration ($p_{\text{crit}} \approx 3 \cdot 10^{20} \text{ cm}^{-3}$) a steplike increase to ferromagnetic interactions was observed, whereas below p_{crit} the interactions become very small and weakly antiferromagnetic, as reported in more recent investigations⁹⁴; see

Fig. 15. It is clear that this effect provides the link between the antiferromagnetic and ferromagnetic regimes, depicted in Fig. 14. The modified RKKY model^{95,94} — modified in the sense that the conventional RKKY is supplemented with a realistic band structure of $\text{Pb}_{1-y}\text{Sn}_y\text{Te}$ — enabled us in 1988 to understand the existence of p_{crit} , as well as the strong ferromagnetic coupling above p_{crit} . In fact, the strong ferromagnetic coupling is provided by the shift of the Fermi level with charge density, which, at p_{crit} , enters a second set of valence bands, located along the Σ direction in the Brillouin zone. This model will be treated in Chapter IV.2. Some recent improvements on this model⁹⁶, taking into account the degeneracy of the Σ bands, alter the calculations presented in Chapter IV.2 to some extent, and, therefore, the most up to date experimental data and calculations in the modified RKKY model are shown in Fig. 15.

Referring once more to the plot of the carrier concentrations in DMS (Fig. 14), and given the fact that $\text{Pb}_{1-x-y}\text{Sn}_y\text{Mn}_x\text{Te}$ sharply separates the ferro- and antiferromagnetic regime by p_{crit} , one would expect for $\text{Pb}_{1-x}\text{Mn}_x\text{Te}$ and $\text{Sn}_{1-x}\text{Mn}_x\text{Te}$, both situated in the vicinity of p_{crit} , the same effect as in $\text{Pb}_{1-x-y}\text{Sn}_y\text{Mn}_x\text{Te}$ if the carrier density can be changed in that amount that p_{crit} is included. For $\text{Pb}_{1-x}\text{Mn}_x\text{Te}$ it is extremely complicated by standard annealing procedures to raise the density to p_{crit} or even higher. For $\text{Sn}_{1-x}\text{Mn}_x\text{Te}$, however, it is possible to decrease the carrier density in such amount that p_{crit} can be reached⁹⁷. As a consequence, it could be shown by us⁹⁸ that the interactions rapidly vanish in the vicinity of the critical carrier concentration. This result does not only generalize the occurrence of a carrier phase line in DMS, but it also provides support on the validity of the modified two-band RKKY model. These results on the ternary $\text{Sn}_{1-x}\text{Mn}_x\text{Te}$ will be presented in Chapter IV.3. In this part we will not only consider the carrier-concentration-dependent magnetic interactions. Also a close examination of the low-temperature magnetic phases will be

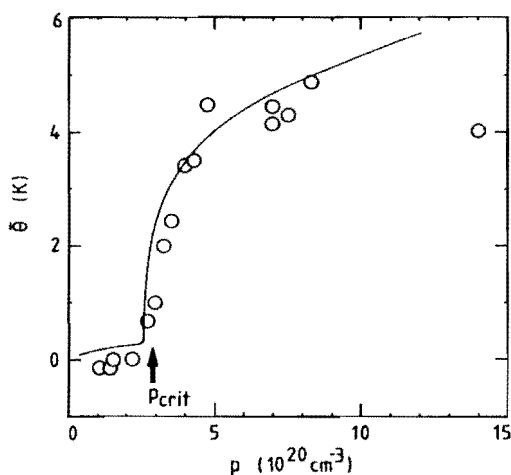


FIG. 15. Curie-Weiss temperature [$\Theta \times (0.03/x)$, used for small variations in Mn concentration] as a function of the carrier concentration p of $\text{Pb}_{0.25}\text{Sn}_{0.72}\text{Mn}_{0.03}\text{Te}$; data are taken from Ref. 91,94 and 95. The calculations are performed within the two-band RKKY model (Ref. 95), supplemented with the multi valley character of the relevant band structure⁹⁶ (parameters $m_1^* = 0.05$, $m_2^* = 1.00$, $J_{\text{sp-d}} = 0.32$ eV).

made, since, somewhat mysteriously, reports by Mauger *et al.*⁸⁵ claimed for $p > p_{\text{crit}}$ and x between 0.03 and 0.06 the existence of ferromagnetic phases mixed with spin-glass features, a so-called reentrant spin-glass. From our data on $\text{Sn}_{1-x}\text{Mn}_x\text{Te}$ in this regime we will show that it is extremely hard to discriminate between the magnetic phase transition, ferromagnetic or reentrant spin-glass. By means of neutron-scattering experiments performed very recently by Vennix *et al.*⁹⁹, it was for the first time possible to rule out spin-glass phenomena in $\text{Sn}_{0.97}\text{Mn}_{0.03}\text{Te}$ and $\text{Sn}_{0.94}\text{Mn}_{0.06}\text{Te}$, and to prove the genuine ferromagnetic character of the phase transition.

Finally, we would like to point out that the current understanding of the magnetism of IV-VI DMS, in particular when the carrier density is involved, is still rather poor.

Though several studies succeeded the initial report of Story *et al.*⁹¹ — extensions have been made to $\text{Pb}_{0.25}\text{Sn}_{0.72}\text{Mn}_{0.03}\text{Te}$ ¹⁰⁰ and $\text{Pb}_{0.52}\text{Sn}_{0.45}\text{Mn}_{0.03}\text{Te}$ ¹⁰¹, and spin-glass-like phases have been detected¹⁰¹ for $p < p_{\text{crit}}$ — the three-dimensional (T, x, p) phase diagram for these compounds is far from complete and hardly any quantitative information on exchange constant (e.g., α , β , J_{NN} , J_{NNN}) is yet available⁸. Magneto-optical investigations employed in II-VI and II-V group DMS to determine α and β , cannot be applied for $\text{Pb}_{1-x-y}\text{Sn}_y\text{Mn}_x\text{Te}$ and $\text{Sn}_{1-x}\text{Mn}_x\text{Te}$ due to the strong carrier absorption, and therefore other techniques, such as EPR¹⁰² or nuclear magnetic resonance, will be indispensable in future investigations. As for the d - d exchange parameters, up to now no adequate tool has been found to correlate experimental phenomena (such as the magnetization steps in the II-VI's) directly to the coupling constants (J_{NN} , J_{NNN} , and so on).

Besides the unique phenomenon of p_{crit} , new effects of fundamental interest may be expected from the delicate interplay of RKKY interaction, magnetic ion concentration and carrier concentration. For example, very preliminary data on $\text{Pb}_{0.26}\text{Sn}_{0.72}\text{Mn}_{0.02}\text{Te}$ and $\text{Sn}_{0.98}\text{Mn}_{0.02}\text{Te}$ by de Jonge *et al.*¹⁰³ indicate a carrier-induced ferromagnetic to spin-glass transition at carrier densities well above p_{crit} , at a fixed concentration of Mn^{2+} . On the basis of the RKKY interaction, this intriguing phenomenon can, tentatively, be brought about by an increasing competition between ferro- and antiferromagnetic coupled ions by increasing the charge density.

- 1 J.K. Furdyna, *J. Appl. Phys.* **64**, R29 (1988).
- 2 *Semiconductors and Semimetals: Diluted Magnetic Semiconductors*, edited by J.K. Furdyna and J. Kossut (Academic, New York, 1988), Vol. 25.
- 3 R.R. Galazka, in *Proceedings on the 14th International Conference on the Physics of Semiconductors, Edinburgh, 1978*, IOP Conference Series, edited by B.L.H. Wilson (IOP, London,

- 1978), Vol. 43., p. 133; J.A. Gaj, *J. Phys. Soc. Japan* **49**, 797 (1980); J.K. Furdyna, *J. Vac. Sci. Technol.* **21**, 220 (1982); J.K. Furdyna, *J. Appl. Phys.* **53**, 7637 (1982); N.B. Brandt and V.V. Moshchalkov, *Adv. Phys.* **33**, 193 (1984); I.I. Lyapilin and I.M. Tsidil'kovskii, *Sov. Phys. Usp.* **28**, 349 (1985); R.R. Galazka, *J. Crystal Growth* **72**, 364 (1985); R.R. Galazka, in *Proceedings on the 18th International Conference on the Physics of Semiconductors*, edited by O. Engstrom (World Scientific Press, Singapore, 1987), p. 1727; J.K. Furdyna, *J. Vac. Sci. Technol.* **A4**, 2002 (1986); J. Stankiewicz, in *Third Brazilian School of Semiconductor Physics*, edited by C.E.T. Goncalves da Silva, L.E. Oliveira and J.R. Leite (World Scientific Press, Singapore, 1987), p. 281; J.K. Furdyna and N. Samarth, *J. Appl. Phys.* **61**, 3526 (1987); A. Twardowski, *Acta Phys. Polon. A* **75**, 327 (1989).
- 4 W. Zdanowicz, K. Kloc, A. Burian, B. Rzepa and E. Zdanowicz, *Crystall. Res. Technol.* **18**, K25 (1983).
- 5 C.J.M. Denissen, Ph. D. thesis, Eindhoven 1986.
- 6 A. Pietrazko, K. Lukaszewics, *Phys. Status Solidi (a)* **18**, 723 (1979).
- 7 *Landolt-Bornstein: Technology of III-V, II-VI and non-tetrahedrally bound compounds*, edited by M. Schultz and H. Weiss (Springer, Berlin, 1984), Vol. 17, Pt. d.
- 8 *Landolt-Bornstein: Physics of II-VI and I-VII compounds, semimagnetic semiconductors*, edited by O. Madelung (Springer, Berlin, 1982), Vol. 17, Pt. b.
- 9 G. Bauer, in *Diluted Magnetic Semiconductors*, edited by R.L. Aggarwal, J.K. Furdyna and S. von Molnar (Materials Research Society, Pittsburgh, 1987), Vol. 89, p. 107.
- 10 H.J.M. Swagten, A. Twardowski, E.H.H. Brentjens, W.J.M. de Jonge, M. Demianiuk and J.A. Gaj, in *Proceedings on the 20th International Conference on the Physics of Semiconductors, Thessaloniki, 1990*, to be published.
- 11 A. Mycielski, *J. Appl. Phys.* **63**, 3279 (1988).
- 12 A. Twardowski, *J. Appl. Phys.* **67**, 5108 (1990).
- 13 A. Twardowski, in *Diluted Magnetic Semiconductors*, (World Scientific Press, Singapore, 1990), edited by M. Jain.
- 14 D.R. Yoder-Short, U. Debska and J.K. Furdyna, *J. Appl. Phys.* **58**, 4056 (1985).
- 15 W.F. Pong, R.A. Mayanovic, B.A. Bunker, J.K. Furdyna and U. Debska, *Phys. Rev. B* **41**, 8440 (1990).
- 16 B.E. Larson, K.C. Hass, H. Ehrenreich and A.E. Carlsson, *Phys. Rev. B* **37**, 4137 (1988); B.E. Larson and H. Ehrenreich, *Phys. Rev. B* **39**, 1747 (1989).
- 17 See for example, J.K. Furdyna and N. Samarth, in *Growth, characterization and properties of ultrathin magnetic films and multilayers*, edited by B.T. Jonker, J.P. Heremans and E.L. Marinaro (Materials Research Society, Pittsburgh, 1989), Vol. 151, p. 129.
- 18 H. Munekata, H. Ohno, S. von Molnar, A. Segmüller, L.L. Chang and L. Esaki, *Phys. Rev. Lett.* **63**, 1849 (1989).
- 19 z.M. Giebultowicz, J.J. Rhyne, J.K. Furdyna, *J. Appl. Phys.* **67**, 5096 (1990).
- 20 S. Foner, Y. Shapira, D. Heiman, P. Becla, R. Kershaw, K. Dwight and A. Wold, *Phys. Rev. B* **39**, 11793 (1989); Y. Shapira, *J. Appl. Phys.* **67**, 5090 (1990).
- 21 Y. Shapira, S. Foner, D.H. Ridgley, K. Dwight and A. Wold, *Phys. Rev. B* **30**, 4021 (1984).
- 22 Y. Shapira, S. Foner, D. Heiman, P.A. Wolff and C.R. McIntyre, *Solid State Commun.* **70**, 355 (1989).
- 23 T.M. Giebultowicz, J.J. Rhyne and J.K. Furdyna, *J. Appl. Phys.* **61**, 3537 (1987).
- 24 V. Spasojevic, A. Bajorek, A. Szytula and W. Giriat, *J. Magn. Magn. Mater.* **80**, 183 (1989).
- 25 W.H. Brumage, C.R. Yarger and C.C. Lin, *Phys. Rev.* **133**, A765 (1964).
- 26 H.J.M. Swagten, A. Twardowski, W.J.M. de Jonge, M. Demianiuk and J.K. Furdyna, *Solid State Commun.* **66**, 791 (1988).
- 27 J.P. Lascaray, M. Nawrocki, J.M. Broto, M. Rakoto and M. Demianiuk, *Solid State Commun.* **61**, 401 (1987).
- 28 Y. Shapira, N.F. Oliveira Jr., *Phys. Rev. B* **35**, 6888 (1987).
- 29 J.K. Furdyna, N. Samarth, R.B. Frankel, J. Spalek, *Phys. Rev.* **37**, 3707 (1988).
- 30 A. Lewicky, J. Spalek, J.K. Furdyna, R.R. Galazka, *Phys. Rev. B* **37**, 1806 (1988).

- 31 A. Twardowski, H.J.M. Swagten, W.J.M. de Jonge and M. Demianiuk, *Phys. Rev. B* **36**, 7013 (1987).
- 32 Y. Shapira, S. Foner, P. Becla, D.N. Domingues, M.J. Naughton and J.S. Brooks, *Phys. Rev. B* **33**, 356 (1986).
- 33 R.L. Aggarwal, S.N. Jasperson, P. Becla and J.K. Furdyna, *Phys. Rev. B* **34**, 5894 (1986).
- 34 G. Barilero, C. Rigaux and N.H. Hau, J.C. Picoche and W. Giritat, *Solid State Commun.* **62**, 345 (1987).
- 35 J.P. Lascaray, A. Bruno, J.C. Ousset, H. Rakoto, J.M. Broto and S. Askenazy, *Physica B* **155**, 353 (1989).
- 36 L.M. Corliss, J.M. Hastings, S.M. Shapiro, Y. Shapira and P. Becla, *Phys. Rev. B* **33**, 608 (1986).
- 37 J. Spalek, A. Lewicky, Z. Tarnawski, J.K. Furdyna, R.R. Galazka, Z. Obuszko, *Phys. Rev. B* **33**, 3407 (1986).
- 38 J.P. Lascaray, M. Nawrocki, J.M. Broto, M. Rakoto and M. Demianiuk, *Solid State Commun.* **61**, 401 (1987).
- 39 D.U. Bartholomew, E.K. Suh, S. Rodriguez, A.K. Ramdas, R.L. Aggarwal, *Solid State Commun.* **62**, 235 (1987).
- 40 B.E. Larson, K.C. Hass and R.L. Aggarwal, *Phys. Rev.* **33**, 1789 (1986).
- 41 E.D. Isaacs, D. Heiman, P. Becla, Y. Shapira, R. Kershaw, K. Dwight and A. Wold, *Phys. Rev. B* **38**, 8412 (1988).
- 42 X. Wang, D. Heiman, S. Foner and P. Becla, *Phys. Rev. B* **41**, 1135 (1990).
- 43 T.M. Giebultowicz, J.J. Rhyne, W.Y. Ching, D.L. Huber, J.K. Furdyna, B. Lebech and R.R. Galazka, *Phys. Rev. B* **39**, 6857 (1987).
- 44 T. Giebultowicz, B. Lebech, B. Buras, W. Minor, H. Kepa, R.R. Galazka, *J. Appl. Phys.* **55**, 2305 (1984).
- 45 R.L. Aggarwal, S.N. Jasperson, P. Becla and R.R. Galazka, *Phys. Rev. B* **32**, 5132 (1985).
- 46 R.R. Galazka, S. Nagata and P.H. Keesom, *Phys. Rev. B* **22**, 3344 (1980).
- 47 R.R. Galazka, W. Dobrowolski, J.P. Lascaray, M. Nawrocki, A. Bruno, J.M. Broto, J.C. Ousset, *J. Magn. Magn. Mater.* **72**, 174 (1988).
- 48 B.B. Stojic, M. Stojic and B. Stosic, *J. Phys.: Condens. Matter* **1**, 7651 (1989).
- 49 A.B. Davydov, L.M. Noskova, B.B. Ponikarov and L.A. Ugodnikova, *Sov. Phys. Semicond.* **14**, 869 (1980).
- 50 H. Savage, J.J. Rhyne, R. Holm, J.R. Cullen, C.E. Carroll and E.P. Wohlfarth, *Phys. Status Solidi (b)* **58**, 685 (1973).
- 51 C.J.M. Denissen, S. Dakun, K. Kopinga, W.J.M. de Jonge, H. Nishihara, T. Sakakibara and T. Goto, *Phys. Rev. B* **36**, 5316 (1987).
- 52 C.J.M. Denissen, H. Nishihara, J.C. van Gool and W.J.M. de Jonge, *Phys. Rev. B* **33**, 7637 (1986).
- 53 G. Karczewski, M. von Ortenberg, Z. Wilamowski, W. Dobrowolski and J. Niewodnizanska-Zawadzka, *Solid State Commun.* **55**, 249 (1985).
- 54 J.R. Anderson, G. Kido, Y. Nishina, M. Gorska, L. Kowalczyk and Z. Golacki, *Phys. Rev. B* **41**, 1014 (1990).
- 55 M. Gorska and J.R. Anderson, *Phys. Rev. B* **38**, 9120 (1988).
- 56 A. Twardowski, A. Lewicky, M. Arciszewski, W.J.M. de Jonge, H.J.M. Swagten and M. Demianiuk, *Phys. Rev. B* **38**, 10749 (1988).
- 57 A. Lewicky, J. Spalek and A. Mycielski, *J. Phys. C* **20**, 2005 (1987).
- 58 A. Twardowski, H.J.M. Swagten and W.J.M. de Jonge, *Phys. Rev. B* **42**, 2455 (1990).
- 59 P.W. Anderson, *Phys. Rev.* **155**, 1 (1959); P.W. Anderson, in *Solid State Physics*, edited by F. Seitz and F. Turnbull (Academic, New York, 1963), Vol. 14, p. 99; W. Geertsma, C. Hass, G.A. Sawatzky and G. Vertogen, *Physica* **86-88A**, 1039 (1977); G.A. Sawatzky, W. Geertsma and C. Hass, *J. Magn. Magn. Mater.* **3**, 37 (1976).
- 60 N. Bloembergen and T.J. Rowland, *Phys. Rev.* **97**, 1679 (1955).
- 61 M. Rudermann and C. Kittel, *Phys. Rev.* **96**, 99 (1954); T. Kasuya, *Prog. Theor. Phys.* **16**, 45 (1956); K. Yoshida, *Phys. Rev.* **106**, 893 (1957).
- 62 B.E. Larson, K.C. Hass, H. Ehrenreich and A.E. Carlsson, *Solid State Commun.* **56**, 347 (1985).
- 63 W.J.M. de Jonge, A. Twardowski and C.J.M. Denissen, in *Diluted Magnetic Semiconductors*, edited by R.L. Aggarwal, J.K. Furdyna and S. von Molnar (Materials Research Society, Pittsburgh, 1987), Vol. 89, p. 153.

- 64 R.R. Galazka, W.J.M. de Jonge, A.T.A.M. de Waele and J. Zeegers, *Solid State Commun.* **68**, 1047 (1988).
- 65 A. Twardowski, M. von Ortenberg and M. Demianiuk, *J. Cryst. Growth* **72**, 401 (1985).
- 66 B.T. Jonker, J.J. Krebs, S.B. Qadri and G.A. Prinz, *Appl. Phys. Lett.* **50**, 848 (1986).
- 67 B.T. Jonker, J.J. Krebs, G.A. Prinz, X. Liu, A. Petrou and L. Salamanca-Young, in *Growth, characterization and properties of ultrathin magnetic films and multilayers*, edited by B.T. Jonker, J.P. Heremans and E.L. Marinaro (Materials Research Society, Pittsburgh, 1989), Vol. 151, p. 151.
- 68 H.J.M. Swagten, F.A. Arnouts, A. Twardowski, W.J.M. de Jonge and A. Mycielski, *Solid State Commun.* **69**, 1047 (1989).
- 69 W.J.M. de Jonge, H.J.M. Swagten, C.E.P. Gerrits and A. Twardowski, *Semicond. Sci. Technol.* **5**, S270 (1990); A. Twardowski, H.J.M. Swagten and W.J.M. de Jonge, *Phys. Rev. B* **42**, 2455 (1990).
- 70 A. Mycielski, P. Dzwonkowski, B. Kowalski, B.A. Orlowski, M. Dobrowolska, M. Arciszewska, W. Dobrowolski and J.M. Baranowski, *J. Phys. C* **19**, 3605 (1986).
- 71 W. Low and M. Weger, *Phys. Rev.* **118**, 1119 (1960).
- 72 G.A. Slack, S. Roberts and J.T. Wallin, *Phys. Rev.* **187**, 511 (1969); J.P. Mahoney, C.C. Lin, W.H. Brumage and F. Dorman, *J. Chem. Phys.* **53**, 4286 (1970).
- 73 A. Twardowski, P. Glod, W.J.M. de Jonge and M. Demianiuk, *Solid State Commun.* **64**, 63 (1987).
- 74 M. Hausenblas, L.M. Claessen, A. Wittlin, A. Twardowski, M. von Ortenberg, W.J.M. de Jonge and P. Wyder, *Solid State Commun.* **72**, 253 (1990).
- 75 A.M. Witowski, A. Twardowski, M. Pohlman, W.J.M. de Jonge, A. Wieck, A. Mycielski and M. Demianiuk, *Solid State Commun.* **70**, 27 (1989).
- 76 A. Twardowski, H.J.M. Swagten, T.F.H. van de Wetering and W.J.M. de Jonge, *Solid State Commun.* **65**, 235 (1988); H.J.M. Swagten, A. Twardowski, W.J.M. de Jonge and M. Demianiuk, *Phys. Rev. B* **39**, 2568 (1989); H.J.M. Swagten, A. Twardowski, F.A. Arnouts, and W.J.M. de Jonge, *J. Physique C* **8**, 873 (1988); A. Twardowski, H.J.M. Swagten and W.J.M. de Jonge, in *Proceedings of the 19th International Conference on Physics of Semiconductors*, edited by W. Zawadski (Warsaw, 1988), p. 1543.
- 77 H.J.M. Swagten, C.E.P. Gerrits, A. Twardowski and W.J.M. de Jonge, *Phys. Rev. B* **41**, 7330 (1990); W.J.M. de Jonge, H.J.M. Swagten and A. Twardowski, in *Properties of II-VI semiconductors: Bulk crystals, epitaxial films, quantum well structures, and dilute magnetic systems*, edited by F.J. Bartoli, H.F. Schaaek and J.F. Schetzina (Materials Research Society, Pittsburgh, 1990), Vol. 161, p. 485.
- 78 M. Taniguchi, Y. Ueda, I. Morisada, Y. Mura-shita, T. Ohta, I. Souma and Y. Oka, *Phys. Rev. B* **41** 3069 (1990).
- 79 Z. Korczak and M. Subotowicz, *Phys. Status Solidi (a)* **77**, 497 (1983).
- 80 M. Escorne, A. Mauger, J.L. Tholence and R. Triboulet, *Phys. Rev. B* **29**, 6306 (1984).
- 81 V.C. Lee, *Phys. Rev. B* **34**, 5430 (1986).
- 82 H. Pascher, P. Rothlein, G. Bauer and M. von Ortenberg, *Phys. Rev. B* **40**, 10469 (1989).
- 83 J. Ginter, J.A. Gay, and Le Si Dang, *Solid State Commun.* **48**, 849 (1983).
- 84 R.W. Cochrane, F.T. Hedgcock and J.O. Strom-Olsen, *Phys. Rev. B* **8**, 4262 (1973).
- 85 M. Escorne, A. Ghazalli and P. Leroux-Hugon, in *Proceedings of the 12th International Conference on Physics of Semiconductors*, edited by M.H. Pilkuhn (Teubner, Stuttgart, 1974), p. 915; A. Mauger and M. Escorne, *Phys. Rev. B* **35**, 1902 (1987).
- 86 M. Mathur, D. Deis, C. Jones, A. Patterson, W. Carr and R. Miller, *J. Appl. Phys.* **41**, 1005 (1970).
- 87 U. Sondermann, *J. Magn. Magn. Mater.* **2**, 216 (1976).
- 88 M. Inoue, H.K. Fun and H. Yagi, *J. Phys. Soc. Jpn.* **49**, 835 (1980).
- 89 T. Hamasaki, *Solid State Commun.* **32**, 1069 (1979).
- 90 R.W. Cochrane, F.T. Hedgcock and J.O. Strom-Olsen, *Phys. Rev. B* **9**, 3013 (1974).
- 91 T. Story, R.R. Galazka, R.B. Frankel and P.A. Wolff, *Phys. Rev. Lett.* **56**, 777 (1986).
- 92 In fact, the investigations reported in Ref. 89

- and 93 already demonstrated, though somewhat obscured, the carrier-induced ferromagnetism; however, these authors did not pay attention to the decisive role of the carrier density
- 93 F.T. Hedgcock, P.C. Sullivan, K. Kadowaki and S.B. Woods, *J. Magn. Magn. Mater.* **54-57**, 1293 (1986); A.V. Brodovoi, G.V. Lashkarev, M.V. Radchanko, E.I. Slyn'ko and K.D. Tovstyuk, *Sov. Phys. Semicond.* **18**, 970 (1984).
- 94 W.J.M. de Jonge, H.J.M. Swagten, R.R. Galazka, P. Warmenbol and J.T. Devreese, *IEEE Trans. on Magn.* **24**, 2542 (1988).
- 95 H.J.M. Swagten, W.J.M. de Jonge, R.R. Galazka, P. Warmenbol and J.T. Devreese, *Phys. Rev. B* **37**, 9907 (1988).
- 96 T. Story, L. Swierkowski, G. Karczewski, W. Staguhn and R.R. Galazka, in *Proceedings of the 19th International Conference on Physics of Semiconductors*, edited by W. Zawadski (Warsaw, 1988), p. 1567.
- 97 M. Inoue, M. Tanabe, H. Yagi, T. Tatsakuwa, *J. Phys. Soc. Jpn.* **47**, 1879 (1979).
- 98 H.J.M. Swagten, S.J.E.A. Eltink and W.J.M. de Jonge, in *Growth, characterization and properties of ultrathin magnetic films and multilayers*, edited by B.T. Jonker, J.P. Heremans and E.L. Marinaro (Materials Research Society, Pittsburgh, 1989), Vol. 151, p. 171; W.J.M. de Jonge, H.J.M. Swagten, S.J.E.A. Eltink and N.M.J. Stoffels, *Semicond. Sci. Technol.* **5**, S131 (1990); S.J.E.A. Eltink, H.J.M. Swagten, N.M.J. Stoffels and W.J.M. de Jonge, *J. Magn. Magn. Mater.* **83**, 483 (1990).
- 99 C.W.H.M. Vennix, E. Frikkee, H.J.M. Swagten, K. Kopinga and W.J.M. de Jonge, in *Proceedings of the MMM Fall Meeting, San Diego, 1990*, to be published in *J. Magn. Magn. Mater.* (1991).
- 100 G. Karczewski, A. Wisniewski, T. Story, M. Baran and R.R. Galazka, in *Proceedings of the 19th International Conference on Physics of Semiconductors*, edited by W. Zawadski (Warsaw, 1988), p. 1555.
- 101 H.J.M. Swagten, H. v.d. Hoek, W.J.M. de Jonge, R.R. Galazka, P. Warmenbol and J.T. Devreese, in *Proceedings of the 19th International Conference on Physics of Semiconductors*, edited by W. Zawadski (Warsaw, 1988), p. 1559.
- 102 T. Story, C.H.W. Swuste, H.J.M. Swagten, R.J.T. van Kempen and W.J.M. de Jonge, in *Proceedings of the MMM Fall Meeting, San Diego, 1990*, to be published in *J. Magn. Magn. Mater.* (1991).
- 103 W.J.M. de Jonge and H.J.M. Swagten, in *Proceedings of the NATO Institute on the Science and Technology of Nanostructured Materials, Greece 1990*, to be published.

SCOPE OF THE THESIS

In this thesis the results of experimental studies on diluted magnetic semiconductors are presented. In Chapter II the low-temperature magnetic properties of both $\text{Zn}_{1-x}\text{Mn}_x\text{Se}$ and $\text{Zn}_{1-x}\text{Mn}_x\text{S}$ will be analyzed. The relevance of long-range interactions and how to incorporate them into model calculations, and the underlying physical mechanisms for the Mn-Mn interaction, will be the central items in this chapter. Subsequently, an analogous treatment will be made in Chapter III of the low-temperature behavior of DMS on the basis of Fe^{2+} instead of Mn^{2+} . The electronic configuration of Fe^{2+} necessitates a more complicated treatment, and the Fe interaction, though observable, will be hard to extract from the available data. The high-temperature susceptibility and high-field magnetization will be analyzed in order to obtain *quantitative* information on the Fe^{2+} - Fe^{2+} interaction. Finally, Chapter IV will deal with carrier-concentration-dependent interactions observed in the low-temperature magnetic behavior of $\text{Pb}_{1-x-y}\text{Sn}_y\text{Mn}_x\text{Te}$ and $\text{Sn}_{1-x}\text{Mn}_x\text{Te}$. A model will be presented in which these phenomena are related to the exchange mechanism in combination with the band structure of the host semiconductor.

The contents of Chapters II, III and IV have already been published elsewhere. We have chosen to embody the corresponding texts in this thesis in essentially the same form as they have been published. As a consequence, some parts of these chapters may seem somewhat superfluous for the reader of this thesis. On the other hand, this choice has the advantage that these parts can be read rather independently.

Magnetic behavior of II-VI group diluted magnetic semiconductors, based on Mn

The magnetic susceptibility and specific heat of the diluted magnetic semiconductor $\text{Zn}_{1-x}\text{Mn}_x\text{Se}$ (paragraph 1) and $\text{Zn}_{1-x}\text{Mn}_x\text{S}$ (paragraph 2) have been measured in the temperature range $10 \text{ mK} < T < 40 \text{ K}$ for $0.01 < x < 0.53$. A paramagnetic-spin-glass transition was observed in the whole concentration range. The concentration dependence of the freezing temperature T_f was found to be compatible with a radial dependence of the exchange interaction between manganese ions of the type $J(R) \sim R^{-6.8}$ for $\text{Zn}_{1-x}\text{Mn}_x\text{Se}$ and $J(R) \sim R^{-7.6}$ for $\text{Zn}_{1-x}\text{Mn}_x\text{S}$. Based on this observation we calculated thermodynamic properties with the extended nearest-neighbor pair approximation. It appears that this approximation provides a good simultaneous description of the specific heat, high-field magnetization as well as the high-temperature susceptibility with parameters $J_0/k_B = -13 \text{ K}$ (nearest-neighbors interaction) and $J_i(R)/k_B = -7/R^{6.8} \text{ K}$ (distant-neighbors interaction) for $\text{Zn}_{1-x}\text{Mn}_x\text{Se}$, and parameters $J_0/k_B = -16 \text{ K}$ and $J_i(R)/k_B = -10/R^{7.6} \text{ K}$ for $\text{Zn}_{1-x}\text{Mn}_x\text{S}$. A comparison is made with other diluted magnetic semiconductors and the possible origin of the exchange mechanism is then discussed.

Chapter II, paragraph 1

Magnetic behavior of the diluted magnetic semiconductor $Zn_{1-x}Mn_xSe$

[published in Phys. Rev. B **36**, 7013 (1987)]

I. INTRODUCTION

During the past years extensive investigations have been performed on the magnetic behavior of diluted magnetic semiconductors (DMS) (i.e., II-VI or II-V compounds containing controlled quantities of randomly substituted magnetic ions)¹. So far data have been obtained almost exclusively on systems of the type $A_{1-x}Mn_xB$, such as $Hg_{1-x}Mn_xTe$, $Cd_{1-x}Mn_xTe$, $Cd_{1-x}Mn_xSe$, $Zn_{1-x}Mn_xTe$ and $(Cd_{1-x}Mn_x)_3As_2$, $(Zn_{1-x}Mn_x)_3As_2$ ^{2,3}. From these data, as far as available, a rather typical behavior is observed. This behavior can be characterized as follows.

(1) Curie-Weiss behavior of the magnetic susceptibility χ at high temperatures indicating antiferromagnetic (AF) Mn-Mn interactions.

(2) A cusp or kink in the low-temperature χ indicating a spin-glass-like transition at a temperature depending on the Mn concentration x .

(3) A magnetic contribution to the specific heat C_m with a broad maximum shifting to higher T with x .

(4) A field dependence of the magnetization M indicating AF interactions, usually accompanied with steps in high fields.

Originally this magnetic behavior was interpreted as arising from interactions between Mn ions situated at the nearest-neighbor (NN) sites in the host lattice^{4,5}. This conjecture was strongly supported by the original

observation of the spin-glass (SG) transition only *above* the percolation limit (x_c) of the host lattice^{4,5}. It was suggested then that the SG transition was brought about by short-range [nearest-neighbor (NN)] AF interaction causing topological frustration effects due to the high symmetry of the host lattice. Recent results, however, for low Mn concentrations in $Hg_{1-x}Mn_xTe$ ¹, $(Cd_{1-x}Mn_x)_3As_2$ ², $(Zn_{1-x}Mn_x)_3As_2$ ³, $Cd_{1-x}Mn_xTe$ ⁶, $Cd_{1-x}Mn_xSe$ ⁷ and very recently $Zn_{1-x}Mn_xTe$, $Zn_{1-x}Mn_xSe$ ⁸ reveal the existence of SG phase also *below* x_c . The situation for $(Cd_{1-x}Mn_x)_3As_2$ is even more pronounced since in this case for $x > x_c$ the NN frustration mechanism is also excluded due to the simple cubic symmetry of the host lattice². Moreover, subsequent calculations on the basis of NN interactions only, gave rise to a wide spread of exchange parameters deduced from various sets of data and the need to adjust the random distribution of the magnetic ions. To our knowledge no consistent set of parameters explaining all the data simultaneously has been obtained on this basis.

It is our claim that these discrepancies are mainly due to the fact that the long-range character of the interactions is not taken into account as we have shown recently for $(Cd_{1-x}Mn_x)_3As_2$ ² and, though less extensive, for some other systems as well⁹. Moreover, as we argued before¹⁰, detailed knowledge about the range or radial dependence of this long-range interaction might yield valuable information about the driving physical mechanisms behind the Mn-Mn interaction in DMS.

In view of this we thought it worthwhile to study the magnetic properties of $\text{Zn}_{1-x}\text{Mn}_x\text{Se}$ in some detail. Preliminary results have been reported recently⁸. We will report susceptibility and specific-heat results in a wide composition range ($0.01 < x < 0.53$) and we will try to interpret these data (together with magnetization¹¹ data and high-temperature susceptibility¹²) simultaneously on the basis of one model incorporating short-range as well as long-range interaction in a random array.

II. EXPERIMENTAL RESULTS

The samples of $\text{Zn}_{1-x}\text{Mn}_x\text{Se}$ were grown by the modified Bridgman method under the pressure of a neutral gas. The crystalline structure of this material was reported¹³ to be cubic for $x \leq 0.06$, polytypic for $0.06 \leq x \leq 0.12$ and hexagonal for $x > 0.12$. In a previous magneto-optical investigation¹⁴ of this material no essential influence of polytypism was found although some scattering of energy gap for $x \geq 0.2$ was reported¹⁵.

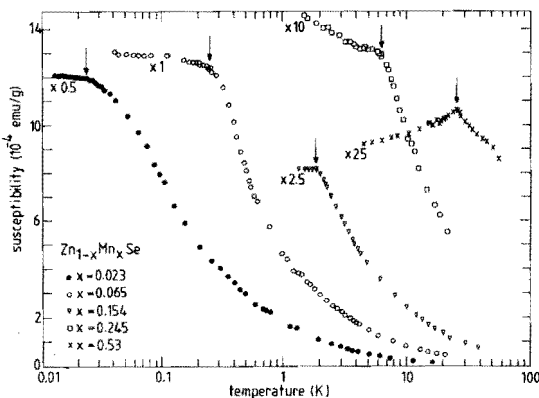


FIG. 1. ac susceptibility of $\text{Zn}_{1-x}\text{Mn}_x\text{Se}$ [$x = 0.023$ (●), 0.064 (○), 0.154 (▽), 0.245 (□) and 0.53 (×)] as a function of temperature for different Mn compositions. The arrows indicate the freezing temperatures T_f . Note the different vertical scales; the data are multiplied by the factor indicated in the figure.

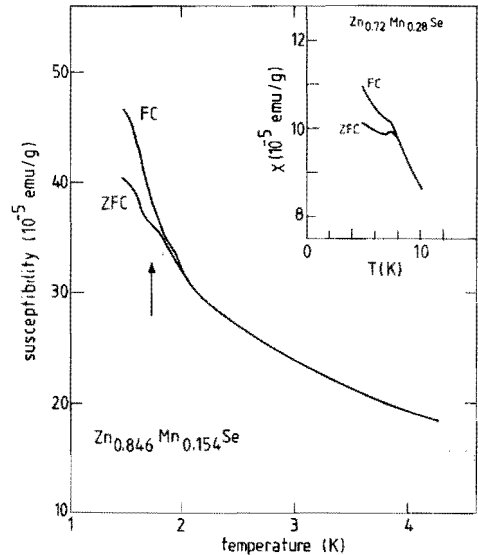


FIG. 2. dc susceptibility of $\text{Zn}_{0.846}\text{Mn}_{0.154}\text{Se}$ measured after zero-field cooling (ZFC, $H < 1$ G) and field cooling (FC, $H = 20$ G) as a function of temperature. The arrow indicates freezing temperature T_f as obtained from ac susceptibility. Inset: similar data for $\text{Zn}_{0.72}\text{Mn}_{0.28}\text{Se}$ (Ref. 12).

The Mn concentrations x of the investigated samples as measured by microprobe analysis were: $x = 0.014 \pm 0.001$, 0.023 ± 0.002 , 0.056 ± 0.002 , 0.064 ± 0.006 , 0.103 ± 0.005 , 0.154 ± 0.004 , 0.254 ± 0.003 and 0.53 ± 0.02 . Generally these actual concentrations were considerably larger (typically 50%) than the nominal concentrations of the starting materials.

A. Low-temperature susceptibility

The ac susceptibility was measured with a conventional mutual inductance bridge operating in the region $100 < f < 2000$ Hz and fields less than 1 G. Some representative susceptibility data for various x are shown in Fig. 1. The results below 1.5 K were obtained in a dilution refrigerator for which no adequate absolute calibration of χ was available, which may result in some deviation of

TABLE I. The freezing temperatures T_f for $Zn_{1-x}Mn_xSe$.

$T_f(x)$	x
0.022	0.023
0.225	0.064
0.55	0.103
1.7	0.154
5.7	0.245
24	0.53

the data at low temperatures. Figure 1 clearly shows an anomalous behavior of the susceptibility at a certain temperature T_f (freezing temperature) depending on the concentration of Mn ions (see Table I). The anomalies are cusplike for high concentra-

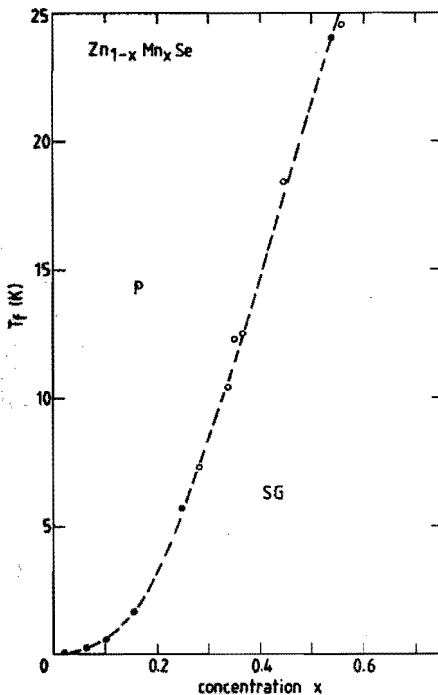


FIG. 3. Phase diagram for $Zn_{1-x}Mn_xSe$ (● our data; ○ Ref. 12). The dashed line is a guide to the eye only.

tions and kinklike for low concentrations. A similar situation was reported for $Cd_{1-x}Mn_xTe$ where a well-pronounced cusp for $x > 0.3$ (Ref. 4) and a kink for $x < 0.15$ (Ref. 6) was observed. In contrast to the susceptibility, as we will see later on, no anomalous behavior can be detected in the specific heat.

dc susceptibility data, field-cooled as well as zero-field-cooled, are shown in Fig. 2 for concentrations above and below the percolation limit. This characteristic behavior supports the interpretation of the anomaly in the susceptibility as a transition to a spin-glass state. The resulting phase diagram, $T_f - x$, in the range $0.023 \leq x \leq 0.53$ is shown in Fig. 3. Inspection of this phase diagram shows that $T_f \rightarrow 0$ when $x \rightarrow 0$. From this experimental observation one may already conjecture that the interactions inducing this spin-glass transition are relatively long ranged, since otherwise no freezing should have been observed for x below the percolation limit, which amounts to $x_c = 0.18$ in this case.

B. Specific heat

Specific-heat data were obtained with a conventional adiabatic heat-pulse calorimeter in the temperature range $0.4 < T < 20$ K. The magnetic contribution C_m to the specific heat was obtained by subtraction of the lattice contribution of pure ZnSe and the nuclear hyperfine contribution of the Mn ions.

The results for C_m in zero external magnetic field are shown in Fig. 4. As quoted above, no anomaly was observed at the temperature T_f , indicated by arrows in the figure. The overall behavior of C_m is similar to that observed for the other DMS: a broad maximum shifting to higher temperatures with increasing x . In our case this maximum is not observed for $x \leq 0.06$ since it is located at temperatures lower than 0.4 K. In the presence of a magnetic field the specific-heat data show a shift of the maximum to higher temperatures with increasing field, as shown in Fig. 5 for $Zn_{0.986}Mn_{0.014}Se$. These data look very similar to earlier results¹⁶ in the

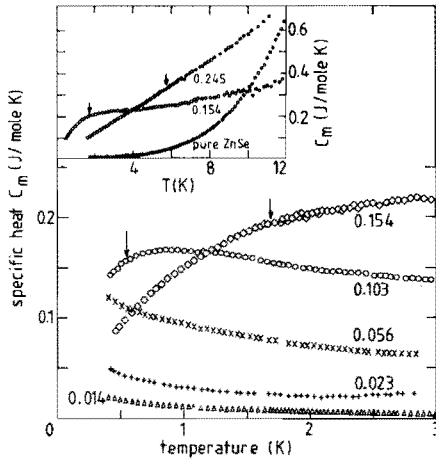


FIG. 4. Magnetic specific heat of $Zn_{1-x}Mn_xSe$ [$x = 0.014$ (Δ), 0.023 ($+$), 0.056 (\times), 0.103 (\circ) and 0.154 (\diamond)]. Inset: magnetic specific heat of $Zn_{1-x}Mn_xSe$ ($x = 0.154$ and 0.245) as well as specific heat of pure ZnSe). The arrows indicate the freezing temperatures T_f .

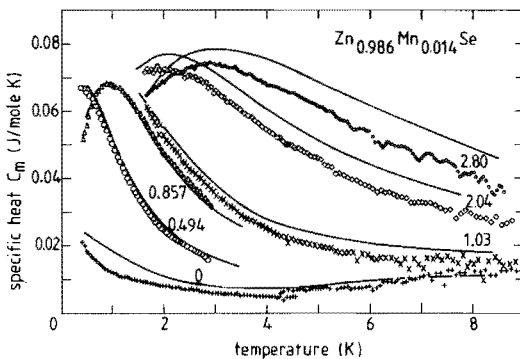


FIG. 5. Magnetic-field dependence of the magnetic specific heat of $Zn_{0.986}Mn_{0.014}Se$ for $B = 0.00, 0.494, 0.857, 1.03, 2.04$ and 2.80 T. The solid lines are obtained from the ENNPA using $J_0/k_B = -13$ K and $J_1/k_B = -7/R^{6.8}$ K.

temperature range $0.3 \leq T \leq 3.5$ K on $Zn_{1-x}Mn_xSe$ with a *nominal* Mn concentration of 0.01. Quantitative comparison is, however, difficult since the actual Mn concentration is not known.

C. High-temperature susceptibility and magnetization

The magnetization has been measured up to 15 kOe and was reported earlier by one of the present authors¹¹. For comparison some selected results will be shown later on. The high-temperature susceptibility results¹² show a Curie-Weiss behavior with $\Theta = -45$ K for $x = 0.05$ at high temperatures, indicating AF interactions between the Mn^{2+} ions. Moreover, Θ was found to be a linear function of the concentration¹² suggesting a random distribution of Mn^{2+} ions.

III. INTERPRETATION

A. The spin-glass transition

Among the data reported above, the existence of a spin-glass transition for vanishingly small concentrations of x is the most obvious indication of the existence of long-range interactions between the Mn^{2+} ions.

As a basis for the interpretation we would like to focus our attention on this freezing transition since the concentration dependence of this transition can be considered as a probe of the radial dependence of the interaction strength between the impurities¹⁰.

In this respect it is relevant to note that the experimental data on the transition strongly support the spin-glass nature of the transition. These data include the cusp or kink in the ac susceptibility, the continuous behavior of the specific heat, and the hysteresis observed in the dc susceptibility. These observations match perfectly the phenomenological characteristics which are commonly applied to define a transition to a canonical spin-glass¹⁷.

If one accepts the nature of the transi-

tion as a spin-glass freezing (which is, however, disputed as we will argue in the discussion), then a scaling analysis should be applicable. Such a scaling analysis generally exploits the fact that for a continuous random distribution it is assumed that $R_{ij}^3 x = \text{const}$, where R_{ij} denotes a typical distance between the ions. Implementation of this expression in a model for spin-glass freezing, given a known functional form for the radial dependence of the exchange interaction, then yields a theoretical prediction for $T_f(x)$ which can be compared with experimental data.

This procedure is elaborated in the Appendix for a continuous as well as a discrete distribution of ions. In the spirit of earlier analyses^{18,19} the spin-glass-freezing condition is based on the existence of a critical fraction of blocked or frozen ions at the freezing temperature. The fraction of these ions is determined by the probability of finding at least one ion within a sphere of radius $R_i(T)$, implicitly given by $J(R_i)S^2 = k_B T$. The results demonstrate the applicability of this approach also outside the limit of the very dilute regime to which it is usually restricted. Given a powerlike or exponential radial dependence of the interaction, the concentration dependence of T_f can be expressed as

$$\ln T_f \sim \frac{1}{3} n \ln x \quad \text{for } J(R) = J_0 R^{-n}$$

or

$$\ln T_f \sim \alpha x^{-1/3} \quad \text{for } J(R) = J_0 \exp(-\alpha R)$$

In Fig. 6 the experimental data $T_f(x)$ for $\text{Zn}_{1-x}\text{Mn}_x\text{Se}$ are plotted in the coordinates suitable for power and exponential dependence, respectively. A comparison between these shows that the simple power dependence $J(R) \sim R^{-n}$ seems to describe the data in the whole concentration range better than the exponential decay [$J(R) \sim \exp(-\alpha R)$]. The exponent n deduced from Fig. 6 is ≈ 6.8 . We would like to stress here that although it is clear that a power law yields a better fit to the experimental data than an exponential decay in the concentration range from far below to far above the percolation limit, one

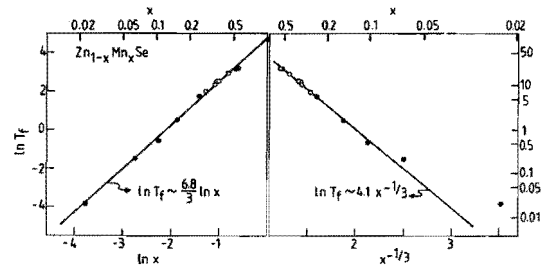


FIG. 6. Natural logarithm of the freezing temperature T_f as a function of (a) $\ln x$ and (b) $x^{-1/3}$ for $\text{Zn}_{1-x}\text{Mn}_x\text{Se}$ (●, our data, ○ Ref. 12). The straight solid lines have slopes of (a) 2.3 and (b) -4.1.

should not exclude the possibility that the x dependence of the freezing temperature T_f can be different above and below the percolation limit. Therefore one should be careful in drawing definite conclusions from Fig. 6.

B. Magnetic properties

It follows from the inspection of the experimental data and the analysis of the spin-glass transition that the Mn-Mn interaction in $\text{Zn}_{1-x}\text{Mn}_x\text{Se}$ is AF and that it is rather long ranged, decaying as $R^{-6.8}$. The relevant thermodynamic properties can be described with the so-called pair-approximation model, which is an approximative calculation method, particularly useful for random arrays with long-range interaction. It has been introduced by Matho²⁰ for canonical metallic SG's and was recently successfully used for DMS as well^{2,3,9}. This approximation is based on the assumption that the partition function of the system can be factorized into contributions of pairs of spins. We will consider two models in some detail: extended nearest-neighbor pair approximation² (ENNPA) and hierarchy pair approximation (HPA) of Rosso²¹. In the ENNPA each spin is considered to be coupled by an exchange interaction J_i only to its nearest magnetic neighbor, which may be located anywhere at a distance R_i from a reference site. The stat-

istical weight of these pair configurations with various R_i (which can only take on discrete values depending on the symmetry of the host lattice) is assumed to be determined by the random distribution of the ions.

The Hamiltonian for a pair is given by

$$\mathcal{H}_i = -2J_i \mathbf{S}_i \cdot \mathbf{S}_j - g\mu_B (S_i^z + S_j^z) B^z, \quad (1)$$

where $J_i = J(R_i)$ and R_i denotes the distance between the sites i and j . If N_i is the number of lattice sites in a shell with radius R_i and using $n_i = \sum_{j=1}^i N_j$ for $j > 0$ and $n_0 = 0$, the probability for a pair formation can be taken as the probability of finding at least one nearest spin in the i th shell (assuming all $j < i$ shells empty) and reads for a random distribution as

$$\begin{aligned} P_i(x) &= (1-x)^{n_{i-1}} [1 - (1-x)^{N_i}] \\ &= (1-x)^{n_{i-1}} - (1-x)^{n_i}. \end{aligned} \quad (2)$$

On the other hand in HPA the spins are arranged in a collection of separate pairs ordered by decreasing interactions²¹. The calculation of the probability distribution for pairs in this case is similar to that used in the ENNPA: $P_i(x)$ is a product of (a) the probability for a spin to have a magnetic neighbor at a distance R_i and (b) the probability that both spins do not belong to a pair with a shorter R_i . We then obtain:

$$P_i(x) = [1 - (1-x)^{N_i}] \left[1 - \prod_{\substack{j=1 \\ (j \in R_i)}}^{n_i} P_j(x) \right]^2 \quad (3)$$

where the summation runs over sites in the sphere R_i ; some sites are skipped in the summation because the probabilities that ion i and ion j do not belong to a pair with shorter R_i are not independent²¹. The principal difference between ENNPA and HPA is shown in Fig. 7 for a system of four ions. The calculated probability distributions for $x = 0.023$

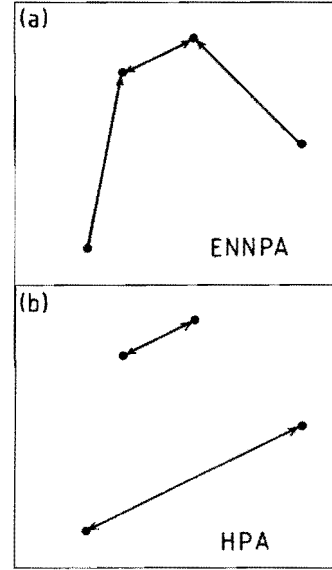


FIG. 7. Pair formation in the (a) ENNPA and (b) HPA. The arrows represent spin-spin interactions.

in both models are shown in Fig. 8. As could be expected, the number of pairs with small R_i ($i \leq 7$) is enhanced in ENNPA, with respect to HPA. This situation is reversed for more distant pairs. Since the probability distributions are known, the thermodynamic properties (A_m) can be obtained by summing the respective pair contributions:

$$A_m = \sum_{i=1}^v \frac{1}{2} A_{mi} P_i(x). \quad (4)$$

Each pair contribution (A_{mi}) contains the exchange parameter J_i . Following the results of previous section we take $J_i = J_0/R_i^{6.8}$, where R_i is in units of the NN distance in the host lattice. The summation over the shells i is carried up to shell i for which $\sum_{i=1}^v P_i \geq 0.995$. For low concentrations ($x < 0.03$) usually $v < 20$, being even less for higher concentrations.

The results of the specific-heat calcula-

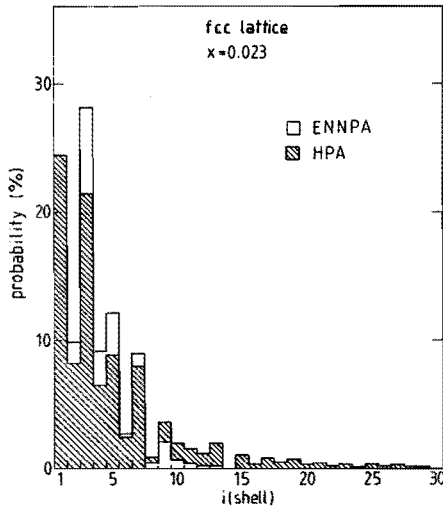


FIG. 8. Probability of finding at least one magnetic neighbor in shell i represented by the blank histogram [Eq. (2)] and probability for a spin to have at least one magnetic neighbor in shell i under the condition that both spins do not belong to a pair with a shorter distance [Eq. (3)] represented by the shaded histogram.

tion for both the ENNPA and HPA are shown in Fig. 9 together with the experimental data. For J_0 (i.e., NN interaction) we have taken -13 K as indicated by high-field magnetization data²². Recent inelastic neutron scattering data²³ yielded a comparable value, although slightly lower. One can notice that at low temperatures ($T \leq 0.2$ K) HPA gives larger values than ENNPA, whereas for higher temperatures the situation is reversed. This results from the discussed difference in probability distributions (Fig. 8). The difference is much more significant for higher concentrations ($x \approx 0.06$) than for lower ($x \approx 0.01$), for which ENNPA and HPA nearly coincide. It should be stressed that the specific-heat curves shown in Fig. 9 were simply calculated with no fitting to the experimental data. Presumably a better agreement will be obtained if J_i values are treated as adjustable parameters. Since the

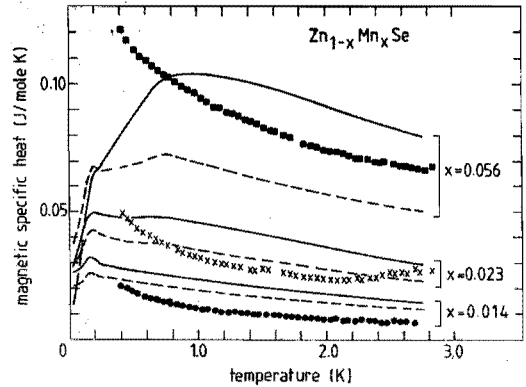


FIG. 9. Zero-field magnetic specific heat calculated in the ENNPA (solid lines) and HPA (dashed lines) together with experimental data.

nearest-neighbor interaction J_0 is inferred from independent experiments and the radial dependence from $T_f(x)$, we inserted J_0 as a constant value ($= -13$ K) and assumed for further neighbors $J_i = J_1/R_i^{6.8}$ ($i > 0$) where J_1 is the only adjustable parameter. J_1 was chosen to obtain the best overall agreement

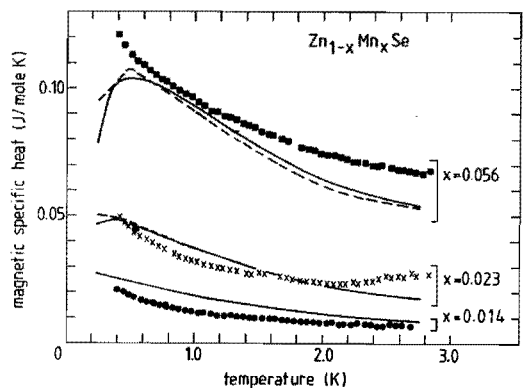


FIG. 10. Magnetic specific heat of $Zn_{1-x}Mn_xSe$. The dashed lines represent calculations with the ENNPA as described in the text using $J_0/k_B = -13$ K and $J_i/k_B = -7/R_i^{6.8}$ K. The solid lines represent the ENNPA with triples included.

for all three experimental quantities: C_m , M and χ . For the final calculations we have extended our ENNPA similarly as it was done for $(\text{Cd}_{1-x}\text{Mn}_x)_3\text{As}_2$ (Ref. 2) and $(\text{Zn}_{1-x}\text{Mn}_x)_3\text{As}_2$ (Ref. 3); we considered not only pairs but also "triples" (i.e., configurations in which two spins are located at the same distance from the reference site).

The results of ENNPA calculations with $J_0 = -13$ K and $J_1 = -7$ K are shown in Figs. 5 and 10 (C_m), 11 and 12 (M). The high-temperature susceptibility calculations for $\text{Zn}_{0.95}\text{Mn}_{0.05}\text{Se}$ yield a Curie-Weiss temperature $\Theta = -45$ K which is in perfect agreement with the experiment¹². The high-field magnetization, shown in Fig. 12, has been recently fitted with a model including a nearest-neighbor interaction $J_0 = -9.9$ K and a mean field²⁴. Our results also show that a satisfactory description can be obtained with the same set of parameters as used for the other thermodynamic quantities.

The ENNPA may be further extended by combining it with a mean-field approximation to account for the average interaction of a spin with the other spins not belonging to a pair (i.e., spins with $i > v$). The results

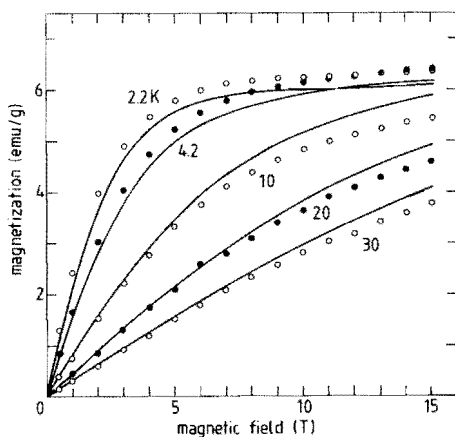


FIG. 11. High-field magnetization of $\text{Zn}_{0.95}\text{Mn}_{0.05}\text{Se}$. The solid lines represent calculations with the ENNPA using $J_0/k_B = -13$ K and $J_1/k_B = -7/R^{6.8}$ K.

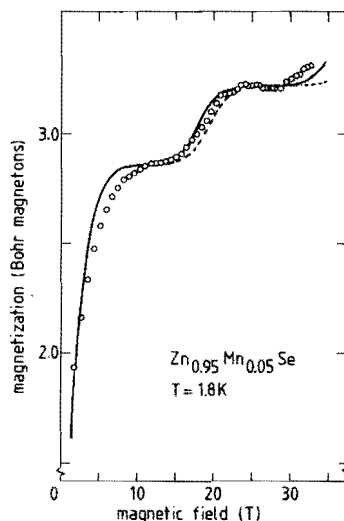


FIG. 12. Steplike magnetization of $\text{Zn}_{0.95}\text{Mn}_{0.05}\text{Se}$ [Ref. 24] together with the ENNPA prediction (solid line, $J_0/k_B = -13$ K and $J_1/k_B = -7/R^{6.8}$ K; dashed line, $J_0/k_B = -12$ K and $J_1/k_B = -7/R^{6.8}$ K). Since no absolute value of magnetization is given in Ref. 24 the magnetization was scaled at 25 T.

generally confirm this conjecture, although the obtained correction is rather small. We conclude that, although these extensions do not significantly improve the results and some systematic deviations remain, the general agreement shows that it is, in principle, possible to explain the behavior of specific heat, magnetization and susceptibility simultaneously, without the need to adjust the random distribution of the Mn ions. As we quoted before, recently some C_m data on $\text{Zn}_{1-x}\text{Mn}_x\text{Se}$ with nominal Mn concentration of $x = 0.01$ were published by Keesom¹⁶. Assuming only contributions from singles, pairs and triples he was able to describe the data rather well. However, since essentially both the total Mn concentration as well as the statistical distribution were used as a fitting parameter, a comparison with these results does not seem very significant.

IV. DISCUSSION

The analysis of the concentration dependence of the freezing temperature, as performed for $\text{Zn}_{1-x}\text{Mn}_x\text{Se}$ in the preceding section, can also be applied to other DMS. The available data on $T_f(x)$ for a number of them are gathered in Fig. 13. In all cases it appears that a description of $T_f(x)$ which is based on a power-law dependence of $J(R) = J_0 R^{-n}$ fits the data in the whole concentration range rather well, in contrast with the description based on an exponential decay of $J(R)$. Whether this is indicative of a specific mechanism remains to be seen, however, since (as was argued before⁸) it is not *a priori* clear whether the same mechanism is responsible for the spin-glass freezing below and above the percolation limit.

The exponents n deduced from Fig. 13 are tabulated in Table II. The various systems in Table II are arranged in the order of decreasing gap. Reviewing the table gives rise to the following comments. The considerable increase of the range ($\sim 1/n$) of the interaction going from wide-band-gap materials to small-band-gap materials is obvious. This fact is not inconsistent with the expectations based on the Bloembergen-Rowland exchange interaction²⁵ as the driving mechanism behind the spin-glass freezing. In this case, however, an exponential decrease [$J(R) \sim \exp(-\alpha R)$] should have been expected and the apparent universal range of the exchange for the II-VI compounds, irrespective of the appreciable variation of the gap magnitude, is somewhat surprising. Moreover, if superexchange would be the driving mechanism as suggested by Larson *et al.*²⁶, at least for the nearest-neighbor interactions, an increasing range of the interaction would be related to an increasing covalent character of the bonding²⁶. Roughly speaking, such an increasing covalency may indeed be expected when the II-VI systems are compared with II-V and IV-VI systems. More detailed information can be obtained from the location of the energy of the Mn d levels with respect to the top of the valence band. Recently

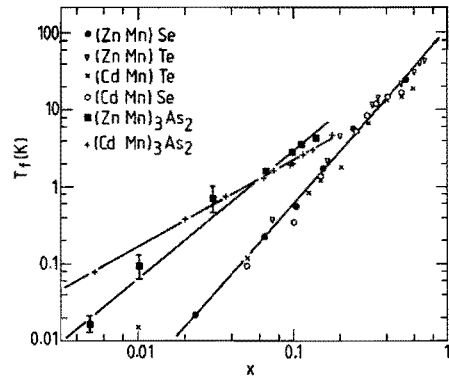


FIG. 13. Freezing temperature T_f as a function of the Mn concentration x for various DMS on logarithmic scale. The straight lines are fitted to the data yielding the power dependence $J(R) \sim R^{-n}$ as tabulated in Table II. References on the origin of the data are given in the text.

Taniguchi *et al.*²⁷ obtained information about the Mn $3d$ density of states and p - d hybridization in the series $\text{Cd}_{1-x}\text{Mn}_x\text{Y}$ ($Y = \text{S}, \text{Se}$ and Te). They concluded that for this series the degree of p - d hybridization increases on going from Te to S . However, the data tabulated in Table II do not reflect the expected systematic change in range of the interaction.

In fact, a most remarkable feature of the data on T_f versus x as shown in Fig. 13 is the surprising universal behavior of the II-VI wide-band-gap materials. Not only is the concentration dependence analogous (and thus the range $1/n$), but the absolute magnitude of the freezing temperature is also the same, taking into account the scattering of the data. In view of the fact that considerable differences exist between the lattice parameters of the II-VI compounds in this series (up to 20%), a variation of the freezing temperature by a factor of 2 or 3 might have been anticipated within the concept of our model, given the pronounced radial dependence of the interaction strength $J(R)$. The data apparently do not support this conjecture. This might be considered as an indication that, besides the interaction strength,

TABLE II. Type, concentration range, band gap, nearest-neighbor distance and exponent n of various DMS.

Material	Type	x range	E_g (eV)	NN distance (\AA)	n	Ref.
$Zn_{1-x}Mn_xS$	II - VI	0.3 - 0.4	≈ 3.8	3.83	≈ 6.8	31
$Zn_{1-x}Mn_xSe$	II - VI	0.02 - 0.5	2.8 - 3	4.00	6.8	This paper, 12
$Zn_{1-x}Mn_xTe$	II - VI	0.07 - 0.6	2.4 - 2.8	4.31	6.8	8,32
$Cd_{1-x}Mn_xSe$	II - VI	0.05 - 0.5	1.8 - 2.6	4.28	≈ 6.8	7,30
$Cd_{1-x}Mn_xTe$	II - VI	0.01 - 0.6	1.6 - 2.5	4.58	≈ 6.8	4,19,6,33
$Hg_{1-x}Mn_xTe$	II - VI	0.02 - 0.5	$\approx 0 - 1.1$	4.55	≈ 5	5,34,35
$Hg_{1-x}Mn_xSe$	II - VI	0.02 - 0.3	≈ 0	4.30	≈ 5.0	37
$(Zn_{1-x}Mn_x)_3As_2$	II - V	0.005 - 0.1	≈ 1	2.94	4.5	3
$(Cd_{1-x}Mn_x)_3As_2$	II - V	0.005 - 0.2	0 - 0.2	3.17	3.5	2
$Pb_{1-x}Mn_xTe$	IV - VI	0.03 - 0.1	0.2 - 0.4	4.56	3	36

the freezing process is also determined by topological criteria.

As we quoted in the Introduction, the overall characteristics of DMS include, among others, AF long-ranged interactions and spin-glass formation for a wide range of concentrations. It has been questioned whether real spin-glass formation is possible in a random diluted array coupled by long-ranged isotropic AF interactions only, since in that case the driving mechanisms of frustration or competition would not be effective¹⁷. To start with, we would like to emphasize that the present experiments on $Zn_{1-x}Mn_xSe$ did yield the observation of typical spin-glass characteristics. These include the cusp in the susceptibility, a continuous specific heat, and a difference in zero-field-cooled and field-cooled magnetizations, both for concentrations above as well as below the percolation limit. We feel that with these data the canonical spin-glass nature of the transition is strongly supported¹⁷.

With respect to the fundamental question about the spin-glass freezing in DMS as such, we would like to point out that anisotropy might play an important role. From Monte Carlo calculations and renormalization group treatments^{28,29}, it has been suggested that, in general, an additional anisotropy in an isotropic system will lower the critical dimension and a small anisotropy is

needed to activate a clearcut transition. More specifically, it was suggested for impurity spins in III-V semiconductors that the random anisotropy of the indirect exchange is the driving force towards a spin-glass state, irrespective of the sign of the exchange integral³⁹.

Experimental evidence of such an additional anisotropy in DMS is scarce, though not completely absent. For the present compound $Zn_{1-x}Mn_xSe$, electron-spin-resonance results were reported for dilute samples, indicating a uniaxial single-ion anisotropy $D = 0.1 \text{ K}$ ³⁹. Moreover, inspection of the specific-heat data as shown in Fig. 4 indicates an increase in C_m at the lowest temperatures, which is not reflected in the calculations. This is by no means unique for $Zn_{1-x}Mn_xSe$ and has been observed in a number of DMS. Earlier attempts have been made in $Cd_{1-x}Mn_xSe$ to explain this behavior in terms of a single-ion anisotropy, although in that case no single-ion splitting was observed in ESR experiments³¹. For $Zn_{1-x}Mn_xSe$, the reported value of $D \approx 0.1 \text{ K}$ can, as calculations of the resulting Schottky anomaly have shown, explain, in principle, the increase of the low-temperature C_m . Further direct evidence on this anisotropy is, however, difficult to obtain. Preliminary experiments on a single crystal with 1 at.% Mn^{2+} in an external field applied along the principal axis showed no

macroscopic preferred direction. This, however, can be understood by assuming random local axes, in agreement with the ESR results³⁹. In order to establish the presence of these anisotropic terms and their influence on the freezing process, further research is necessary.

APPENDIX

In this Appendix we present a simple model which corroborates the usefulness of the scaling analysis relating the freezing temperature to the concentration. This model is based generally on the idea of Smith¹⁷ and Escorne *et al.*¹⁸ defining the SG freezing as the process of cluster blocking.

We consider a particular magnetic ion which may be blocked (frozen) by coupling with its magnetic neighbors if the exchange energy $J(R)S^2$ is larger than the thermal energy $k_B T$. On the other hand, an ion is considered as being "free" (i.e., freely responding to the external magnetic field) if it has no magnetic neighbor inside the sphere of radius R_i defined by

$$J(R_i)S^2 = k_B T . \quad (A1)$$

The probability that a particular ion is free is given by

$$P_{\text{free}} = (1-x)^{n_i} , \quad (A2)$$

where n_i is the total number of lattice sites inside a sphere with volume $4\pi R_i^3/3$.

Equation (A1) relates R_i to the temperature and P_{free} may be calculated directly for a particular lattice, as we will show below. Before that we consider the approximation for a very dilute system which results in analytical solution. For a very dilute system (i.e., semicontinuous distribution of ions) we have

$$n_i = 4\pi R_i^3/(3A) , \quad (A3)$$

where A is volume per one lattice site ($A = a^3$ for a simple-cubic structure and $A = a^3/4$

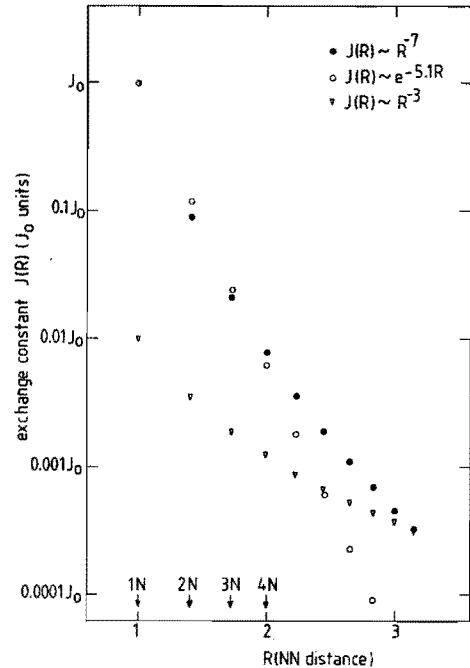


FIG. 14. Exchange constant $J(R)$ and radial dependence for $J(R) \sim R^{-7}$ (●) and $J(R) \sim \exp(-5.1R)$ (○). The prefactors are chosen so that $J(R_{NN}) = J_0$. Arrows indicate nearest neighbors (1N), next-nearest neighbors (2N), and so on. For comparison also $J(R) \sim R^{-3}$, corresponding to dipole-dipole interaction, is also shown. The prefactor for this case was chosen to be $0.01 J_0$, an overestimation of the dipole-dipole interaction in DMS.

for a fcc structure).

For DMS materials the exchange constant is supposed to be relatively long ranged (i.e., extending also for further, not only the nearest, neighbors) and depending on distance as

$$J(R) = J_0 R^{-n} \quad (A4a)$$

or

$$J(R) = J_0' \exp(-\alpha R) . \quad (A4b)$$

In Fig. 14 both relations (A4a) and (A4b) are shown for $n = 7$ and $\alpha = 5.1$ as proposed for

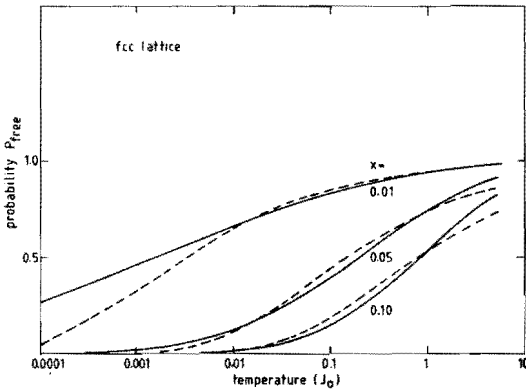


FIG. 15. Probability that a magnetic ion in a fcc lattice is not blocked for $x = 0.01, 0.05$ and 0.10 as a function of temperature for continuous distributions. Solid line, $J(R) \sim \exp(-5.1R)$ [(A5b)]; dashed line, $J(R) \sim R^{-7}$ [(A5a)]. Temperature is in J_0 units, where J_0 is the interaction value for the nearest neighbors.

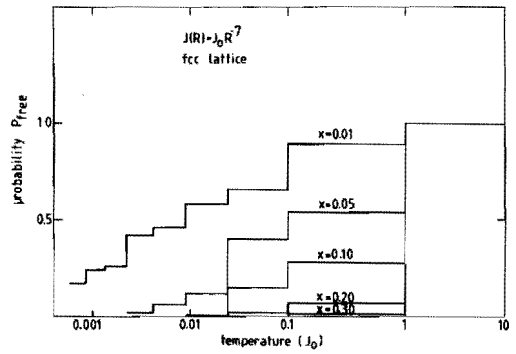


FIG. 17. Probability that a magnetic ion in a fcc lattice is not blocked as a function of temperature for $J(R) \sim R^{-7}$ and $x = 0.01, 0.05, 0.10, 0.20$ and 0.30 . At the nearest-neighbor distance $J(R) = J_0$.

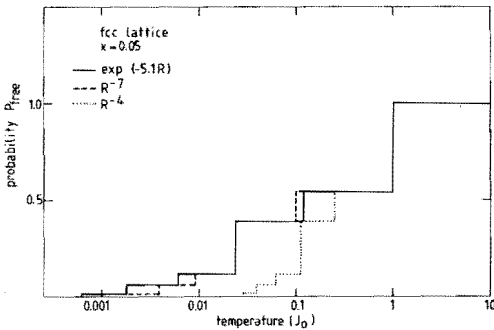


FIG. 16. Probability that a magnetic ion in a fcc lattice is not blocked as a function of temperature for $x = 0.05$. Solid line, $J(R) \sim \exp(-5.1R)$; dashed line, $J(R) \sim R^{-7}$; dotted line, $J(R) \sim R^{-4}$. All interactions are chosen so that all of them have the same value (J_0) at nearest-neighbor distance.

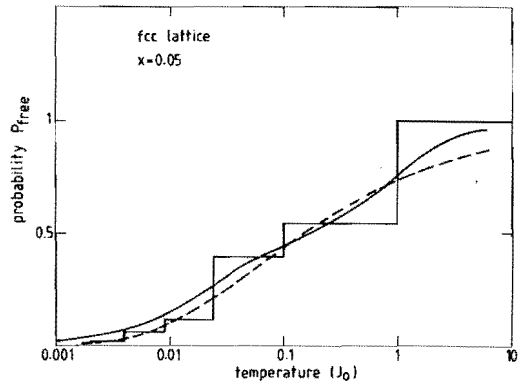


FIG. 18. Probability that a magnetic ion in a fcc lattice is not blocked for $x = 0.05$ and $J(R) \sim R^{-7}$. Solid steplike line, distribution the same as in Fig. 17; solid line, the same distribution but convoluted with exponential function with $\gamma = 0.4 J_0$; dashed line, continuous approximation [Eqs. (A5) and (A6)].

TABLE III. Freezing temperatures T_f (in units of $J_0 S^2$) for various P_f values and concentrations.

$J(R)$	P_{free}	Concentration						
		0.01	0.02	0.05	0.10	0.15	0.20	0.30
$e^{-5.1r}$	0.10	3.77×10^{-4}	1.39×10^{-4}	4.62×10^{-3}	2.45×10^{-2}	0.0773	0.139	0.208
	0.05	8.11×10^{-7}	3.49×10^{-5}	1.58×10^{-3}	1.19×10^{-2}	0.0284	0.0619	0.105
	0.01	3.94×10^{-8}	2.69×10^{-6}	1.95×10^{-4}	2.18×10^{-3}	0.00615	0.119	0.0228
$1/R^7$	0.10	1.31×10^{-4}	6.55×10^{-4}	5.41×10^{-3}	0.0218	0.0657	0.127	0.205
	0.05	5.82×10^{-5}	2.90×10^{-4}	2.38×10^{-3}	0.0106	0.0249	0.0549	0.103
	0.01	1.25×10^{-5}	5.90×10^{-5}	4.88×10^{-4}	0.00225	0.00542	0.0105	0.0221

wide-band-gap DMS^{8,9}. Finally we get from (A1)–(A4),

$$P_{\text{free}} = (1-x)^{4\alpha/3[J_0 S^2/T]^{3/n}}, \quad (\text{A5a})$$

$$P_{\text{free}} = (1-x)^{4\alpha/3[1/\alpha \ln(J_0 S^2/T)]^3}. \quad (\text{A5b})$$

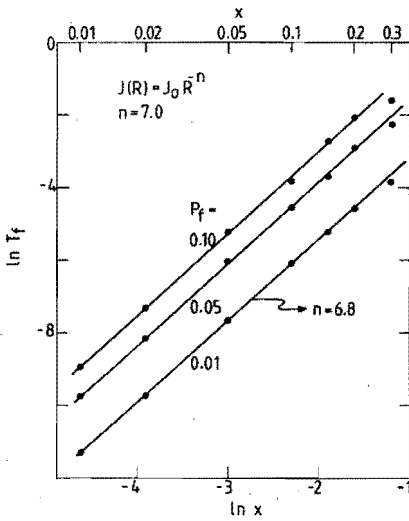


FIG. 19. Logarithm of the freezing temperature resulting from probability distribution (as discussed in the text) as a function of logarithm of concentration for $J(R) = J_0 R^{-n}$, $n = 7$, for different freezing probabilities $P_f = 0.01, 0.05$ and 0.10 . The slope of the lines yields an exponent $n = 6.8$.

The obtained distributions are shown in Fig. 15 for a fcc lattice, showing a gradual decrease of the probability that an ion is not frozen with decreasing temperature. We assume that for a sufficiently small $P_{\text{free}} = P_f$, where P_f is an arbitrary chosen constant depending on the specific mechanism, the ion system may be considered frozen, the temperature at which P_f is reached defined as the freezing temperature T_f [$P_{\text{free}}(T_f) = P_f$]. Then, from (A5), one may obtain the scaling laws:

$$\ln T_f \sim \frac{1}{3} n \ln x \quad \text{for (A4a)}, \quad (\text{A6a})$$

$$\ln T_f \sim \alpha x^{-1/3} \quad \text{for (A4b)}. \quad (\text{A6b})$$

These relations have also been reported by other authors¹⁸ and are applied in this article.

We now abandon the limitation to the very dilute case (continuous distribution assumption) and extend our model to higher x . In Fig. 16 the probability distribution versus temperature is shown for $x = 0.05$ for both interactions (A4a) and (A4b). As can be noticed, there is only slight difference between power (A4a) and exponential decay (A4b), since for $T \geq 0.003 J_0$ (and $\alpha = 5.1$, $n = 7$) both dependencies are practically the same (cf. Fig. 14). It is also evident that for a longer-range interaction (such as R^{-4}) the ion system freezes faster at higher temperatures than for a shorter-range interaction (such as

R^{-7}). The steplike structure of the P_{free} distribution is a consequence of the "sharp" freezing condition (A1). The steps correspond to the passing through consecutive discrete coordination spheres. In Fig. 17 the P_{free} distributions are shown for $0.01 \leq x \leq 0.30$. It follows from this figure that for low concentrations ($x \leq 0.05$) the ion system freezes gradually whereas for higher x ($x \geq 0.10$) rather abrupt freezing may be observed. For $x > 0.3$ (i.e., exceeding the validity of our model) the P_{free} distribution practically does not depend on x , as could be expected. To obtain a more realistic model we may "smooth" the freezing condition (A1) by convoluting the obtained distributions with a Gaussian, Lorentz, or an exponential function. The result for exponential function [$0.5 \times \exp(-|\log T|/\gamma)$ where γ is the full width at half maximum parameter] is shown in Fig. 18 for $x = 0.05$ and arbitrary chosen as $\gamma = 0.4 \times J_0$. Freezing temperatures T_f found from this convoluted distributions are tabulated in Table III for various P_f values. It may be noticed that the T_f values obtained for $P_f = 0.05$ are well comparable with experimental results for $Zn_{1-x}Mn_xSe$ ($J_0 = -13$ K and $S = 5/2$). They also obey formulas (A6) quite well. An example is shown in Fig. 19 for $J(R) = J_0 R^{-7}$ for $P_f = 0.10, 0.05,$ and 0.01 . Good linearity may be observed for $x \leq 0.20$. The n value deduced from the slope is ≈ 6.8 , which compares favorably with the inserted value $n = 7$. We therefore feel confident in using scaling laws in the form (A6) to describe our data, even for a discrete lattice and at somewhat higher concentrations.

pinga, J. Magn. Magn. Mater. **31-34**, 1373 (1983).

- 1 See the following review papers: N.B. Brandt, V.V. Moshchalkov, Adv. Phys. **33**, 193 (1984); J.K. Furdyna, J. Appl. Phys. **53**, 8637 (1982); J.A. Gaj, J. Phys. Soc. Jpn. Suppl. **49**, A797 (1980).
- 2 C.J.M. Denissen, H. Nishihara, J.C. van Gool and W.J.M. de Jonge, Phys. Rev. B **33**, 7637 (1986); W.J.M. de Jonge, M. Otto, C.J.M. Denissen, F.A.P. Blom, C. v.d. Steen, K. Ko-

- 3 C.J.M. Denissen, Sun Dakun, K. Kopinga W.J.M. de Jonge, H. Nishihara, T. Sakakibara and T. Goto, Phys. Rev. B **36**, 5316 (1987).
- 4 R.R. Galazka, S. Nagata and P.H. Keesom, Phys. Rev. B **22**, 3344 (1980).
- 5 S. Nagata, R.R. Galazka, D.P. Mullin, H. Arbarzadeh, G.D. Khattak, J.K. Furdyna and P.H. Keesom, Phys. Rev. B **22**, 3331 (1980).
- 6 M.A. Novak, O.G. Symko, D.J. Zheng and S. Oseroff, J. Appl. Phys. **57**, 3418 (1985).
- 7 M.A. Novak, O.G. Symko, D.G. Zheng and S. Oseroff, Physica **126B**, 469 (1984).
- 8 A. Twardowski, C.J.M. Denissen, W.J.M. de Jonge, A.T.A.M. de Waele, M. Demianiuk and R. Triboulet, Solid State Commun. **59**, 199 (1986).
- 9 C.J.M. Denissen and W.J.M. de Jonge, Solid State Commun. **59**, 503 (1986).
- 10 W.J.M. de Jonge, A. Twardowski and C.J.M. Denissen, in *Diluted Magnetic Semiconductors*, edited by R.L. Aggarwal, J.K. Furdyna and S. von Monar (Materials Research Society, Pittsburgh, 1987), Vol. 89, p. 153.
- 11 A. Twardowski, M. von Ortenberg, M. Demianiuk and R. Pauthenet, Solid State Commun. **51**, 849 (1984).
- 12 J.K. Furdyna, private communications.
- 13 E. Michalski, M. Demianiuk, S. Kaczmarek and J. Zmija, Electron Technology **13**, 4, 9 (1982).
- 14 A. Twardowski, T. Dietl and M. Demianiuk, Solid State Commun. **48**, 345 (1983).
- 15 R.B. Bylisma, W.M. Becker, J. Kossut and U. Debska, Phys. Rev. B **33**, 8207 (1986).
- 16 P.H. Keesom, Phys. Rev. B **33**, 6512 (1986).
- 17 J.A. Mydosh, in *Hyperfine Interactions*, Vol. 31 of *Lecture Notes in Physics* (Springer, New York, 1986), p. 347.
- 18 D.A. Smith, J. Phys. F **5**, 2148 (1975).
- 19 M. Escorne, A. Mauger, R. Triboulet and J.L. Tholence, Physica **107B**, 309 (1981).
- 20 K. Matho, J. Low Temp. Phys. **35**, 165 (1979).
- 21 M. Rosso, Phys. Rev. Lett. **44**, 1541 (1980)
- 22 P.A. Thomas and M. Rosso, Phys. Rev. B **34**, 7936 (1986).
- 23 Y. Shapira, S. Foner, D.H. Ridgley, K. Dwight and A. Wold, Phys. Rev. B **30**, 4021 (1984).

- 23 T.M. Giebultowicz, J.J. Rhyne and J.K. Furdyna, in *Proceedings of the thirty-first annual conference on magnetism and magnetic materials, Baltimore, 1986*, edited by N.C. Coon, J.D. Adam, J.A. Beardsley and D.L. Huber [J. Appl. Phys. **61**, 3537 (1987); **61**, 3540 (1987)].
- 24 J.P. Lascaray, M. Nawrocki, J.M. Broto, M. Rakoto and M. Demianiuk, *Solid State Commun.* **61**, 401 (1987).
- 25 N. Bloembergen and T.J. Rowland, *Phys. Rev.* **97**, 1679 (1955); G. Bastard and C. Lewiner, *ibid.* **20**, 4256 (1979).
- 26 W. Geertsma, C. Hass, G.A. Sawatzky and G. Vertogen, *Physica* **86-88A**, 1039 (1977); G.A. Sawatzky, W. Geertsma and C. Hass, *J. Magn. Magn. Mat.* **3**, 37 (1976); B.E. Larson, K.C. Hass, H. Ehrenreich and A.E. Carlsson, *Solid State Commun.* **56**, 347 (1985).
- 27 M. Taniguchi, M. Fujimori, M. Fujisawa, T. Mori, I. Souma and Y. Oka, *Solid State Commun.* **62**, 431 (1987).
- 28 A.J. Bray, M.A. Moore and A.P. Young, *Phys. Rev. Lett.* **56**, 2641 (1986).
- 29 A. Chakrabarti and Ch. Dasgupta, *Phys. Rev. Lett.* **56**, 1404 (1986).
- 30 C.D. Amarasekara, R.R. Galazka, Y.Q. Yang and P.H. Keesom, *Phys. Rev. B* **27**, 2868 (1983).
- 31 Y.Q. Yang, P.H. Keesom, J.K. Furdyna and W. Giriat, *J. Solid State Chem.* **49**, 20 (1983).
- 32 S.P. McAlister, J.K. Furdyna and W. Giriat, *Phys. Rev. B* **29**, 1310 (1984).
- 33 M. Escorne and A. Mauger, *Phys. Rev. B* **25**, 4674 (1982).
- 34 N.B. Brandt, V.V. Moshchalkov, A.O. Orlov, L. Skrbek, I.M. Tsiril'kovskii and S.M. Chudinov, *Sov. Phys. JETP* **57**, 614 (1983).
- 35 A. Mycielski, C. Rigaux, M. Menaut, T. Dietl and M. Otto, *Solid State Commun.* **50**, 257 (1984).
- 36 M. Escorne, A. Mauger, J.L. Tholence and R. Triboulet, *Phys. Rev. B* **29**, 6306 (1984).
- 37 R.R. Galazka, W.J.M. de Jonge and A.T.A.M. de Waele and J. Zeegers, *Solid State Commun.* **6**, 1047 (1988).
- 38 N.P. Il'in and I.Ya. Korenblit, *Zh. Eksp. Teor. Fiz* **81**, 2070 (1981) [*Sov. Phys. - JETP* **54**, 1100 (1982)].
- 39 J. Kreissl and W. Gehlhoff, *Phys. Status Solidi (a)* **81**, 701 (1984).

Chapter II, paragraph 2

Magnetic properties of $Zn_{1-x}Mn_xS$

[published in Solid State Commun. 66, 791 (1988)]

I. INTRODUCTION

The magnetic properties of diluted magnetic semiconductors (DMS) or semimagnetic semiconductors (SMSC) have attracted considerable attention during the past years. Most of the investigations have been devoted to the class of the II-VI compounds such as $Cd_{1-x}Mn_xTe$, $Zn_{1-x}Mn_xTe$, $Hg_{1-x}Mn_xTe$, and the corresponding selenides. Among others, the phase diagram, including the transition to the spin-glass (SG) phase, the interaction between the Mn^{2+} ions and the carrier system, as well as the nature and strength of the interaction between the Mn^{2+} ions, have been extensively studied¹.

In some recent publications²⁻⁶ we emphasized the relevance of the long-range interactions between the magnetic ions beyond the nearest neighbor. It has been demonstrated that only when the long-range character of the $d-d$ interaction is taken into account, a simultaneous and consistent description of all the thermodynamic properties can be obtained. Moreover, the range and strength of this long-range interaction can be used to relate the interaction to the underlying physical mechanism. In addition, it has been shown⁶ that the freezing temperature T_f which marks the transition to the spin-glass state, can be used as a probe to determine the spatial range of the interaction $J(R)$ in this class of compounds.

In various aspects, $Zn_{1-x}Mn_xS$ represents an extreme case. Not only does it possess the shortest interatomic lattice distance, as com-

pared with the Cd or Zn selenides or tellurides, but also it has been reported that the tendency for hybridization of the Mn d levels increases going from the Te via Se to S; see Taniguchi *et al.*⁷. Both aspects are believed to be of possible importance in determining the strength and range of the Mn-Mn exchange⁸.

Since no data in the low-concentration regime are yet available for $Zn_{1-x}Mn_xS$ we thought it worthwhile to study the magnetic properties of this compound in some detail. To that purpose we have performed ac susceptibility and specific-heat capacity measurements on $Zn_{1-x}Mn_xS$ for concentrations x below 10%. From the concentration dependence of T_f the specific decay of the Mn^{2+} - Mn^{2+} interaction with the interatomic distance will be derived. Subsequently we will try to interpret the specific-heat data, together with earlier magnetization and susceptibility data on the basis of one model incorporating short-range as well as long-range interactions in a random array.

II. RESULTS

The ac susceptibility and specific-heat experiments were performed on $Zn_{1-x}Mn_xS$ with $x = 0.028, 0.047, 0.092$ and 0.097 . All concentrations were checked by microprobe analysis. The susceptibility was measured with a mutual inductance bridge operating at 90 - 9000 Hz and an excitation field of less than 1 G. The low-temperature results are shown in Fig. 1. The well-pronounced cusp

TABLE I. The freezing temperatures T_f for $Zn_{1-x}Mn_xS$.

$T_f(x)$	x
0.023	0.028
0.050	0.047
0.280	0.092
7.97	0.30
11.46	0.35
13.97	0.40

(or kink) in the ac susceptibility is attributed to the paramagnetic to spin-glass transition. In Table I the freezing temperatures as deduced from Fig. 1 are tabulated, including some earlier data for higher concentrations obtained by Yang *et al.*¹⁰

It seems obvious that also in this case a freezing transition extends to very dilute systems, far below the nearest-neighbor (NN)

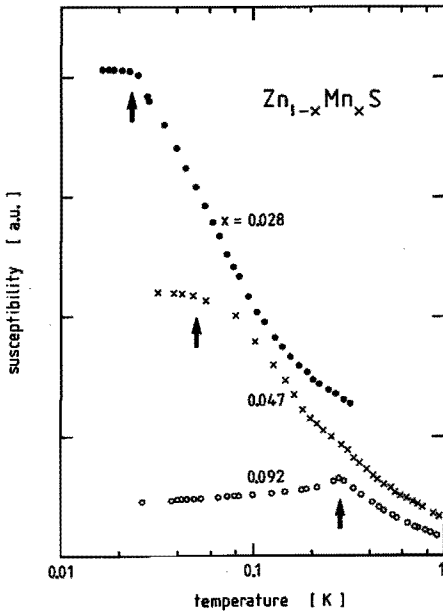


FIG. 1. Low-temperature ac susceptibility of $Zn_{1-x}Mn_xS$; $f = 1000$ Hz, $H_{ac} \approx 0.5$ G. The arrows indicate the freezing temperature T_f .

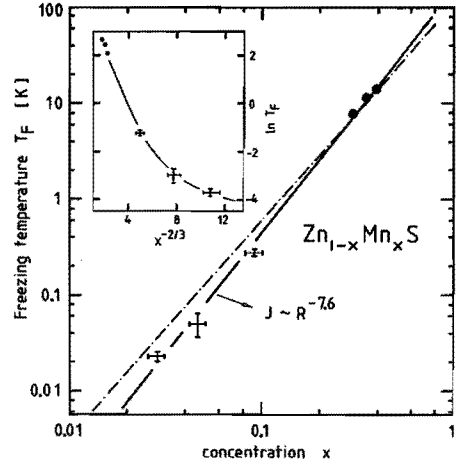


FIG. 2. Freezing temperature T_f of $Zn_{1-x}Mn_xS$ as a function of the Mn concentration x . The full circles are data obtained from Yang *et al.* (Ref. 10). The solid line and the dashed-dotted line represent $n = 7.6$ and $n = 6.8$, respectively, with $\log T_f \sim \frac{1}{3}n \log x$. In the inset $\ln T_f$ is plotted as a function of $x^{-2/3}$ (see the text).

percolation limit. As quoted earlier, the concentration dependence of the freezing temperature $T_f(x)$ can be related to the radial dependence of the exchange interaction triggering the transition. By assuming a power law behavior $J(R) \sim R^{-n}$, $T_f(x)$ can be expressed⁶ as

$$\log T_f(x) \sim \frac{1}{3}n \log x \quad (1)$$

In Fig. 2 we plotted T_f versus x , both on a logarithmic scale. The figure shows indeed a linear dependence between $\log T_f$ and $\log x$ characterized by $n = 7.6$. This result differs slightly from results in related materials like $A_{1-x}Mn_xB$ in which $A = Zn, Cd$ and $B = Se, Te$, where for all the systems $n = 6.8$ has been found (indicated by a dashed-dotted curve in Fig. 2). We will return to this point in the discussion.

The specific heat of $Zn_{1-x}Mn_xS$ has been measured with an adiabatic heat-pulse calorimeter between 0.4 and 15 K. The magnetic

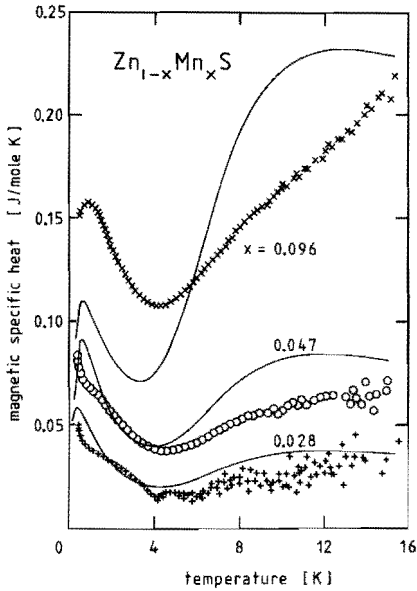


FIG. 3. Magnetic specific heat (C_m) of $\text{Zn}_{1-x}\text{Mn}_x\text{S}$. The solid lines represent the ENNPA calculations with $J_{\text{NN}}/k_B = -16$ K and $J(R)/k_B = -10R^{-7.6}$ K.

contribution C_m , obtained by subtracting the lattice specific heat of ZnS from the total specific heat, is shown in Fig. 3. The scattering of the data points at higher T is brought about by the fact that in that temperature region the magnetic contribution C_m is only a small fraction of the total specific heat, especially for low concentrations x . In contrast to the specific heat measured in related compounds, the structure observed in C_m is rather pronounced. As we will show later on, this is due to the extremely high value of the NN interaction and the fast decay of the interaction as indicated by $n = 7.6$, resulting in well-separated values for the nearest-neighbor (NN), next-nearest-neighbor (NNN) and further magnetic-neighbor interactions.

Magnetization (M) and high-temperature susceptibility (χ) measurements have been reported by Twardowski *et al.*¹¹ and Brumage *et al.*¹², respectively. Both thermo-

dynamic properties reflect the typical behavior for the II-VI wide gap DMS. The magnetization, as exemplified for $\text{Zn}_{0.958}\text{Mn}_{0.042}\text{S}$ in Fig. 4, reveals at low temperatures so-called technical saturation in fields up to 15 T, well below $M_s = (5/2)g\mu_B$ (≈ 12 emu/g in this particular case) for uncoupled paramagnetic ions. This behavior supports strong antiferromagnetic (AF) coupling between the Mn^{2+} ions, which is common for related DMS. In Fig. 5 the susceptibility of $\text{Zn}_{1-x}\text{Mn}_x\text{S}$ is shown. For high temperatures the susceptibility obeys typical Curie-Weiss behavior. The Curie-Weiss temperature is negative, again indicating antiferromagnetic coupling, and scales with x , while χ deviates from Curie-Weiss law at lower temperatures.

It follows from our data that the d - d exchange interaction is antiferromagnetic and rather long ranged, decaying like $R^{-7.6}$. Consequently, the system consists of a random array of Mn^{2+} ions all coupled with an antiferromagnetic interaction whose strength depends on the specific Mn-Mn distance. The behavior of such an extremely complicated

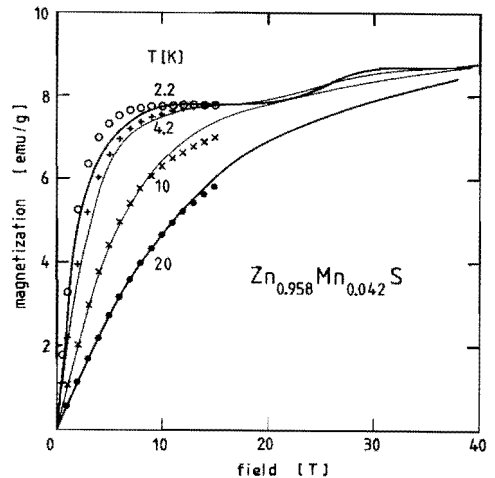


FIG. 4. High-field magnetization (M) of $\text{Zn}_{0.958}\text{Mn}_{0.042}\text{S}$ for several temperatures (Ref. 11). The solid lines represent the ENNPA calculations with $J_{\text{NN}}/k_B = -16$ K and $J(R)/k_B = -10R^{-7.6}$ K.

network can only be solved in an approximate way. In the dilute limit the so-called extended nearest-neighbor pair approximation (ENNPA), introduced by Matho¹³, has been successfully used recently for other DMS²⁻⁶. It is based on the assumption that the partition function of such a system can be factorized into contributions of pairs. In the ENNPA each ion is considered to be coupled by an exchange interaction J_i only to its nearest magnetic neighbor, located anywhere at the distance R_i . This interaction is treated in the conventional isotropic Heisenberg Hamiltonian:

$$\mathcal{H}_i = -2J_i \mathbf{S}_i \cdot \mathbf{S}_j . \quad (2)$$

The statistical weight of the pair configuration is assumed to be determined by the random distribution of the ions. Thus any thermodynamic function of the crystal can be evaluated as

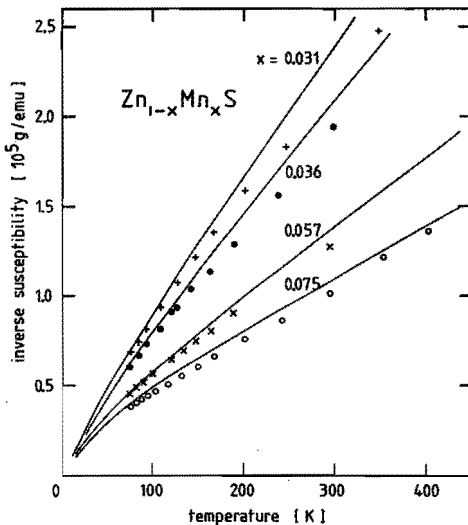


FIG. 5. High-temperature susceptibility (χ) of $\text{Zn}_{1-x}\text{Mn}_x\text{S}$ (Ref. 12). The solid lines represent the ENNPA calculations with $J_{\text{NN}}/k_{\text{B}} = -16$ K and $J(R)/k_{\text{B}} = -10R^{-7.6}$ K.

$$A = \sum_i \frac{1}{2} A_i(J_i) P_i(x) , \quad (3)$$

where $P_i(x)$ is the probability of finding at least one magnetic neighbor at a distance R_i . The summation is performed until 99.5% of the pairs is taken into account. This ENNPA model may be extended by including 3-spin clusters (open triples) in order to account for the increasing probability to find clusters of more than 2 spins, with increasing x .

The only input parameters for our model are the exchange constants J_i for the different possible pairs. For NN we take $J_{\text{NN}}/k_{\text{B}} = -16$ K resulting from recent neutron-diffraction studies¹⁴, whereas the long-range interaction we assumed in the form deduced from SG freezing, $J(R) = J_{\text{LR}}R^{-7.6}$. J_{LR} is not necessarily equal to J_{NN} since one cannot a priori exclude different interaction mechanisms between nearest and further neighbors. In fact J_{LR} was our only adjustable parameter chosen to obtain the best overall agreement with the data and amounts to -10 K, which means $J_{\text{NNN}}/k_{\text{B}} = -0.72$ K, $J_{\text{NNNN}}/k_{\text{B}} = -0.15$ K and so on.

Let us now consider the numerical results for C_m , χ and M of $\text{Zn}_{1-x}\text{Mn}_x\text{S}$. As we quoted above, the NN interaction strength is 20 times as large as the NNN interaction strength. This is convincingly demonstrated by the theoretical as well as the experimental magnetic contribution to the specific heat (Fig. 3), where the contribution of J_{NN} , at higher temperatures, is well separated from the low-temperature contribution of more distant pairs. From the figure it is clear that the specific heat of magnetic neighbors beyond the NN cannot be neglected. At higher concentrations quantitative deviations between experimental data and the ENNPA calculations occur, which is inherent to the pair approximation.

The magnetization of $\text{Zn}_{1-x}\text{Mn}_x\text{S}$ is also well predicted within the concepts of our model, as shown in Fig. 4. In this case we considered each pair to be influenced by the effective field B_{eff} arising from all ions more distant than R_i ,

$$B_{\text{eff}} = \frac{2}{g\mu_B} \langle S_z \rangle \sum_{j>i}^{20} J_j N_j x . \quad (4)$$

It is also illustrated in the figure that the inclusion of triples is highly necessary to obtain a correct magnitude of M . In fact, the ground state of an open triple is degenerate and responds to relatively low fields, whereas the ground state of a pair is nondegenerate and contributes to M only at sufficiently high fields ($B > 2|J|/g\mu_B$), when it becomes magnetically active, leading to the well-known steps in the magnetization. The first step in the magnetization of the NN pairs in $Zn_{1-x}Mn_xS$ is predicted at a field of roughly 25 T, far outside the present experimental data range.

Finally, also the susceptibility agrees fairly with the ENNPA prediction. In Fig. 5 the theoretical curves for χ^{-1} bend from Curie-Weiss law at lower T and the extrapolation from the high-temperature regime to the T axis reflects the AF net interaction. However, quantitative comparison does not seem very significant, since the magnitude of the susceptibility has been fitted to the Mn concentration¹².

III. DISCUSSION AND CONCLUSIONS

Summarizing the results shown before we feel that the magnetic properties of $Zn_{1-x}Mn_xS$, in particular in the dilute limit, can be simultaneously described with a single set of parameters, provided the long-range character as deduced from the concentration dependence of the freezing temperature, is taken into account. In that respect, we would like to emphasize that no fitting procedure has been employed. Although such a procedure certainly would yield a better description of some of the data, it remains to be seen, however, whether such a procedure would give physically meaningful results.

In Table II we have tabulated the exchange parameters of $Zn_{1-x}Mn_xS$ together with the closely related Se and Te. The sys-

tematic decrease of the nearest-neighbor (J_{NN}) and further-neighbor interaction strength ($J_{LR}R^{-n}$) in the series going from sulfides to tellurides is obvious. This trend is in accordance with the systematic decrease of the p - d hybridization in such a series as observed by Taniguchi *et al.*⁷ by synchrotron radiation photoemission. According to Larson *et al.*⁸ in their treatment of superexchange, such a decrease of hybridization (denoted by the parameter V_{dp}) yields a decrease of J since their results indicate that $J \sim V_{dp}^4$. With respect to the R dependence of the interaction Ehrenreich *et al.*¹⁵ state that, on the basis of the same superexchange mechanism within a class of materials, the R dependence is expected to remain largely independent of the actual atomic constituents. Despite the slight increase of n for $Zn_{1-x}Mn_xS$ it seems that the results tabulated in Table II qualitatively confirm this expectation. It should be noted, however, that these authors predict a Gaussian decay of the interaction out to about the fourth NN [$J \sim 0.2 \exp(-4.89 \times R^2/a^2)$ (eV) where a is the lattice constant], instead of the power dependence for all distances ($\sim R^{-n}$) employed in the present analysis. Such a Gaussian decay for all R would yield a proportionality between $\ln T_f$ and $x^{-2/3}$ which is not supported by the data (see the inset in Fig. 2). One might argue, however, that $T_f(x)$ probes specifically the long-range interactions, which is also implicitly assumed when continuous scaling laws are applied.

A final comment concerns the freezing transition. It has been noted before⁶ that the actual observed freezing temperature T_f as a function of the concentration x seems surpris-

TABLE II. Exchange interaction parameters for $Zn_{1-x}Mn_xS$, $Zn_{1-x}Mn_xSe$ and $Zn_{1-x}Mn_xTe$ ^{1,6}.

	J_{NN}/k_B [K]	J_{LR}/k_B [K]	n
$Zn_{1-x}Mn_xS$	-16	-10	7.6
$Zn_{1-x}Mn_xSe$	-13	-7	6.8
$Zn_{1-x}Mn_xTe$	-9	—	6.8

ingly universal for a large class of wide-gap Mn-type DMS $A_{1-x}Mn_xB$ where $A = Cd, Zn$ and $B = Se, Te$. The present results on $Zn_{1-x}Mn_xS$ seem to strengthen this impression. As we quoted in the Introduction, $Zn_{1-x}Mn_xS$ represents an extreme case with respect to hybridization, band gap and lattice constant. The resulting exchange constants, as we saw in Table II, are almost a factor two larger for $Zn_{1-x}Mn_xS$ than for the corresponding $Zn_{1-x}Mn_xTe$. Despite all this, the freezing transition $T_f(x)$ is very close to the other wide-gap materials and in the very dilute limit even lower (see Fig. 2) which seems to be at variance with the common wisdom that the freezing transition should be proportional to the driving interaction. Therefore, it seems that these observations point to alternative triggering mechanisms of the spin-glass transition such as anisotropy, topological effects or system-independent long-range interaction mechanisms, which have not been considered so far.

-
- ¹ See the following review papers: N.B. Brandt and V.V. Moshchalkov, *Adv. Phys.* **33**, 193 (1984); J.K. Furdyna, N. Samarth, *J. Appl. Phys.* **61**, 3526 (1987).
 - ² C.J.M. Denissen and W.J.M. de Jonge, *Solid State Commun.* **59**, 503 (1986).
 - ³ C.J.M. Denissen, H. Nishihara, J.C. van Gool and W.J.M. de Jonge, *Phys. Rev. B* **33**, 7637 (1986).
 - ⁴ C.J.M. Denissen, Sun Dakun, K. Kopinga, W.J.M. de Jonge, H. Nishihara, T. Sakakibara and T. Goto, *Phys. Rev. B* **36**, 5316 (1987).
 - ⁵ W.J.M. de Jonge, A. Twardowski and C.J.M. Denissen, in *Diluted Magnetic Semiconductors*,

- edited by R.L. Aggarwal and J.K. Furdyna and S. von Molnar (*Materials Research Society, Pittsburgh, 1987*), Vol. 89, p. 153.
- ⁶ A. Twardowski, H.J.M. Swagten, W.J.M. de Jonge and M. Demianiuk, *Phys. Rev. B* **36**, 7013 (1987).
- ⁷ M. Taniguchi, M. Fujimori, M. Fujisawa, T. Mori, I. Souma and Y. Oka, *Solid State Commun.* **62**, 431 (1987).
- ⁸ W. Geertsma, C. Hass, G.A. Sawatzky and G. Vertogen, *Physica* **86-88A**, 1039 (1977); G.A. Sawatzky, W. Geertsma and C. Hass, *J. Magn. Magn. Mater.* **3**, 37 (1976); B.E. Larson, K.C. Hass, H. Ehrenreich and A.E. Carlsson, *Solid State Commun.* **56**, 347 (1985).
- ⁹ A. Twardowski, C.J.M. Denissen, W.J.M. de Jonge, A.T.A.M. de Waele, M. Demianiuk and R. Triboulet, *Solid State Commun.* **59**, 199 (1986).
- ¹⁰ Y.Q. Qiang, P.H. Keesom, J.K. Furdyna and W. Giriat, *J. Solid State Chem.* **49**, 20 (1983).
- ¹¹ A. Twardowski, M. von Ortenberg, M. Demianiuk and R. Pauthenet, *Acta Phys. Pol. A* **67**, 339 (1985).
- ¹² W.H. Brumage, C.R. Yarger and C.C. Lin, *Phys. Rev.* **133**, A765 (1964).
- ¹³ K. Matho, *J. Low Temp. Phys.* **35**, 165 (1979).
- ¹⁴ T.M. Giebultowicz, J.J. Rhyne and J.K. Furdyna, in *Proceedings of the Thirty-First Annual Conference on Magnetism and Magnetic Materials, Baltimore, 1986*, edited by N.C. Coon, J.D. Adam, J.A. Beardsley and D.L. Huber [*J. Appl. Phys.* **61**, 3537 (1987); **61**, 3540 (1987)].
- ¹⁵ H. Ehrenreich, K.C. Hass, B.E. Larson and N.F. Johnson, in *Diluted Magnetic Semiconductors*, edited by R.L. Aggarwal and J.K. Furdyna and S. von Molnar (*Materials Research Society, Pittsburgh, 1987*), Vol. 89, p. 187.

CHAPTER THREE

Magnetic behavior of II-VI group diluted magnetic semiconductors, based on Fe

The magnetic specific heat and low-field ac susceptibility of the iron-based diluted magnetic semiconductor (DMS) $\text{Zn}_{1-x}\text{Fe}_x\text{Se}$ in the temperature range 0.4 – 20 K are reported in paragraph 1. Antiferromagnetic $d-d$ interactions and indications of spin-glass freezing are observed. These data, together with high-temperature susceptibility and high-field magnetization, are interpreted in the extended nearest-neighbor pair approximation, with an antiferromagnetic exchange between the Fe^{2+} ions. Fair agreement between theory and experiment is obtained for all the thermodynamic quantities with one set of parameters provided by independent experiments. The strength and range of the interactions, as well as the freezing mechanisms, are compared with DMS containing Mn^{2+} , and the results are discussed in relation with the existing models.

In paragraph 2 the specific heat of the diluted magnetic semiconductors $\text{Hg}_{1-x-y}\text{Cd}_y\text{Fe}_x\text{Se}$ will be presented for temperatures below 25 K. The excess specific heat (C_m) has been extracted by scaling of nonmagnetic lattice contributions. The resulting C_m of these systems reveal a broad maximum at $T \approx 10$ K, whereas for low temperatures a Schottky-type exponential decay of C_m can be observed. These phenomena can be fairly well understood on the basis of a simple crystal-field model and a random distribution of Fe^{2+} . On the other hand, no drastic effect of the energy gap is clearly reflected by our data and therefore, we suggest that only Fe^{2+} states involving the valence bands are dominating the antiferromagnetic $d-d$ interactions, analogously to the Mn^{2+} case.

The high-temperature magnetic susceptibility of random, diluted magnetic systems is discussed in paragraph 3, for magnetic ions having not only spin momentum but also nonvanishing orbital momentum. In particular, the magnetic susceptibility of $\text{Zn}_{1-x}\text{Fe}_x\text{Se}$ (Fe^{2+} , $S = 2$, $L = 2$) is reported in the temperature range 2 – 300 K. The nearest-neighbor exchange Fe-Fe interaction is estimated as: $J_{\text{NN}}/k_B = -22$ K for $\text{Zn}_{1-x}\text{Fe}_x\text{Se}$ and $J_{\text{NN}}/k_B = -17.8$ K for $\text{Cd}_{1-x}\text{Fe}_x\text{Se}$.

In paragraph 4 the high-field magnetization of diluted magnetic semiconductors has been calculated for magnetic ions with spin- and orbital momenta. It is shown that, in addition to the spin-only case (Mn^{2+}), also for Fe-based DMS characteristic steps in the low-temperature magnetization should be detectable. The position of first step in the magnetization, being almost insensitive for crystal-field parameters and sample orientation, can be used to establish the nearest-neighbor interaction (J_{NN}), provided that $|J_{\text{NN}}|$ exceeds a critical value.

Chapter III, paragraph 1

Magnetic properties of the diluted magnetic semiconductor $\text{Zn}_{1-x}\text{Fe}_x\text{Se}$

[published in Phys. Rev. B 39, 2568 (1989)]

I. INTRODUCTION

Diluted magnetic semiconductors (DMS) or semimagnetic semiconductors (SMSC) — i.e., II–VI, II–V, or IV–VI semiconductors with a controlled amount of magnetic ions substituted for nonmagnetic cations — have been extensively studied during the recent years because of their interesting magneto-optical and magnetic properties¹. Since DMS can generally be synthesized with a wide range of concentrations of magnetic ions, they offer an exceptional possibility to study both the very diluted and the concentrated regimes in one material. In fact, the existence of paramagnetic, spin-glass and antiferromagnetic phases was reported in these materials depending on the concentration and temperature range².

So far the research has been devoted mainly to DMS containing Mn ions. The magnetic behavior of these systems show common characteristics which can be understood on the basis of a random array of localized Mn ions coupled by long ranged, isotropic antiferromagnetic exchange interactions^{2,3} which are mediated by the carriers. The underlying microscopic mechanisms in relation to the band structure, as well as the nature of and the driving force behind the observed phase transition and the role of the anisotropy, are, however, still somewhat obscure and object of further investigations¹⁻³.

In that respect, substitutional Mn^{2+} with its degenerate 6A_1 spin-only ground state represents a rather simple, though theoretic-

ally attractive case, since all the phenomena which involve orbital momentum are absent.

In contrast, substitutional iron (Fe^{2+}) can serve as a much more general case, since it possesses both spin and orbital momenta ($S = 2$ and $L = 2$). Fe^{2+} has a d^6 electronic configuration. The ground state of an Fe^{2+} free ion (5D) is split by a tetrahedral crystal field into a 5E orbital doublet and a higher-lying 5T orbital triplet (separated from 5E by $\Delta = 10Dq$, where Dq is the crystal-field parameter). The spin-orbit interaction splits the 5E term into a singlet A_1 , a triplet T_1 , a doublet E , a triplet T_2 and a singlet A_2 (the energy separation between these states is approximately equal to $6\lambda^2/10Dq$, where λ is the spin-orbit parameter)^{4,5}. The ground state is a magnetically inactive singlet A_1 resulting in Van Vleck-type paramagnetism⁴⁻⁶. The properties of Fe-based DMS are, however, relatively unexplored yet⁷, although recently some attempts to understand the magnetic behavior of these compounds were reported⁸⁻¹¹. In view of that, we thought it worthwhile to study the magnetic properties of $\text{Zn}_{1-x}\text{Fe}_x\text{Se}$ in some detail.

In this paper we report the results of magnetic specific heat and low-field susceptibility measurements in the temperature range 0.4 – 20 K. Together with the high-temperature susceptibility obtained by us¹¹ very recently, and high-field magnetization data⁸, we were able — for the first time for Fe-based DMS — to describe all these magnetic properties within one model (extended nearest-neighbor pair approximation) and obtain

a fairly good agreement between experiment and theory.

II. EXPERIMENTAL RESULTS

The samples of $\text{Zn}_{1-x}\text{Fe}_x\text{Se}$ were grown by the modified Bridgman method under the pressure of a neutral gas, in the nominal concentration range $0.001 < x < 0.55$. All the ingots were checked by microprobe analysis and it was found that the iron concentration never exceeded $x = 0.22$. Growing crystals with higher iron content only yielded an increase of precipitations of iron selenide. Crystals with precipitations were not used for further study.

The crystalline structure of this material was studied by x-ray diffraction and was found to be cubic in the whole concentration range. Variation of the resulting lattice constant with x is shown in Fig. 1. Results reported for $\text{Zn}_{1-x}\text{Fe}_x\text{Se}$ thin layers¹¹ are also inserted in this figure.

The electron paramagnetic resonance (EPR) analysis performed on some of our samples revealed the presence of paramagnetic impurities (mainly Mn^{2+}) originating from the source materials used for crystal growing.

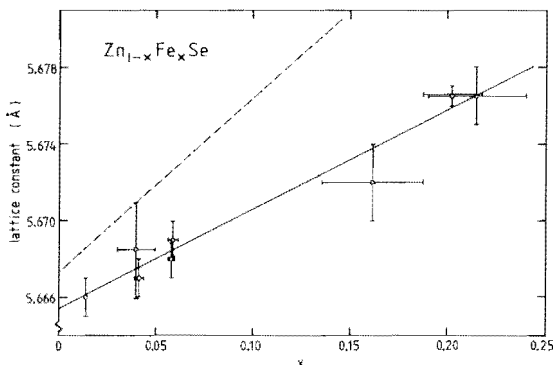


FIG. 1. Lattice constant of $\text{Zn}_{1-x}\text{Fe}_x\text{Se}$ as a function of concentration x . The solid line denoting $a(x) = (5.666 \pm 0.001) + (0.051 \pm 0.01)x$ Å, is obtained from a least-squares fit. The dashed line represents results from Ref. 12.

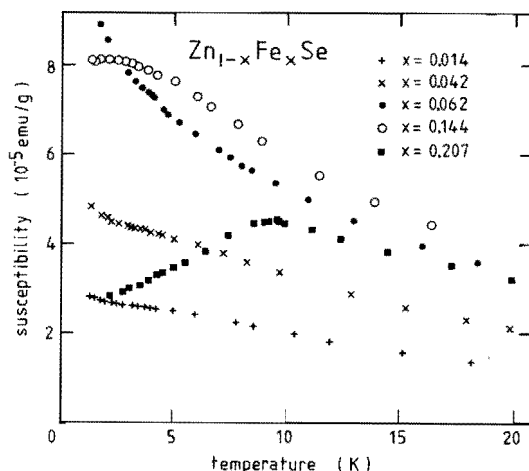


FIG. 2. ac susceptibility of $\text{Zn}_{1-x}\text{Fe}_x\text{Se}$ as a function of temperature.

The concentration of these impurities was typically less than 0.01% of the actual Fe^{2+} content. The Fe concentration of the crystals reported in this paper was $x = 0.014, 0.04, 0.062, 0.14$ and 0.21 .

A. Low-temperature susceptibility

The ac susceptibility χ was measured with a conventional mutual inductance bridge operating in the region $100 < f < 2000$ Hz and fields less than 0.0001 T. Some representative susceptibility data are shown in Fig. 2. The data for low concentrations ($x < 0.07$) differ from susceptibility results previously reported for Fe^{2+} -doped crystals⁶: instead of temperature-independent susceptibility at low temperatures (i.e., typical Van Vleck-type paramagnetism), we observe a monotonous increase of the susceptibility. We believe that such a behavior is due to paramagnetic impurities present in our crystals, as mentioned earlier. We estimated this additional contribution to χ as a difference between the χ value at 4 K and χ measured below 4 K. For $\text{Zn}_{0.958}\text{Fe}_{0.042}\text{Se}$ the Mn^{2+} impurity concentration was estimated this way as $x_{\text{imp}} = 0.0002$, in fair agreement with

EPR data for this crystal.

For the crystals with higher x one can observe a maximum in χ , which is well pronounced for $x = 0.21$ at $T_f = 9$ K, whereas for $x = 0.144$, one can only notice that it appears at roughly 2 K. Since no anomalies occur in the specific heat for these samples at the corresponding temperatures, we tentatively ascribe these maxima to a paramagnetic to spin-glass phase transition, in analogy with the Mn systems. We should stress, however, that this conjecture requires further study. In particular the zero-field-cooled and field-cooled dc susceptibility should be measured, and a wider composition range should be investigated. The latter one depends, however, strongly on improvement in the crystal growing technology.

Nevertheless, if one accepts the nature of the susceptibility anomaly as a spin-glass freezing, then a scaling analysis should be applicable. Such a scaling analysis generally exploits the fact that for a continuous random distribution it is assumed that R_{ij}^3/x is constant, where R_{ij} denotes a typical distance between the ions. Implementation of this expression in a model for spin-glass freezing, given a known functional form for the radial dependence of the exchange interaction, then yields a theoretical prediction for $T_f(x)$ which can be compared with experimental data.

This procedure was successfully used for Mn-based DMS^{2,3,13}, where T_f was found to obey the relation

$$\ln T_f \sim \frac{1}{3}n \ln x .$$

This is compatible with a radial dependence of the exchange interaction between Mn ions of the type: $J(R) \sim R^{-n}$, where $n = 6.8$ for wide-gap materials as $\text{Cd}_{1-x}\text{Mn}_x\text{Te}$ or $\text{Zn}_{1-x}\text{Mn}_x\text{Se}$ and $n = 5$ for lower-gap materials ($\text{Hg}_{1-x}\text{Mn}_x\text{Te}$ and $\text{Hg}_{1-x}\text{Mn}_x\text{Se}$)³. We performed a similar procedure for our data as shown in Fig. 3, where we also inserted all the available data for other Fe-based DMS¹⁰. The exponent n deduced from Fig. 3 is $n \approx 12$, indicating a much shorter range of inter-

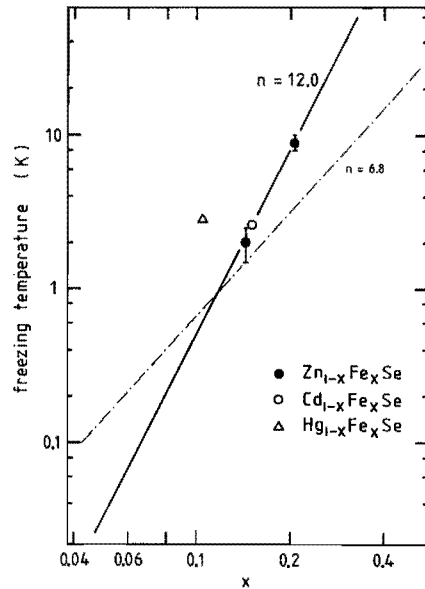


FIG. 3. Freezing temperature as a function of concentration x for $\text{Zn}_{1-x}\text{Fe}_x\text{Se}$, $\text{Cd}_{1-x}\text{Fe}_x\text{Se}$ (Ref. 10) and $\text{Hg}_{1-x}\text{Fe}_x\text{Se}$ (Ref. 10). The solid line indicates a radial decay of the exchange integral $J \sim R^{-n}$ with $n = 12$; for comparison the dashed-dotted line illustrates $n = 6.8$; see Ref. 3.

action between Fe ions than observed in the Mn case. We should stress, however, that this result can be considered only as an indication of the possible difference in interaction range for Fe and Mn ions, since the data available up till now are too limited. We will return to this point in the Discussion.

B. High-temperature susceptibility

The high-temperature susceptibility of $\text{Zn}_{1-x}\text{Fe}_x\text{Se}$ was recently studied by us¹¹ in order to compare the experimental data with a high-temperature series expansion (HTE) derived for Fe^{2+} . The susceptibility was found to obey a Curie-Weiss law in the temperature range 70 – 300 K, with a negative Curie-Weiss temperature indicating antiferromagnetic coupling between Fe^{2+} ions. Based on

these results we evaluated the nearest-neighbor exchange integral $J_{\text{NN}} = -22$ K, which is substantially larger than in $\text{Zn}_{1-x}\text{Mn}_x\text{Se}$ [-12.6 K (Ref. 14)]. Such a strong exchange interaction seems compatible with the freezing temperature $T_f = 9$ K for $\text{Zn}_{0.79}\text{Fe}_{0.21}\text{Se}$ which is twice as large as that observed³ in $\text{Zn}_{1-x}\text{Mn}_x\text{Se}$ with similar concentration x . We will return to the detailed analysis of the susceptibility for both low and high temperatures later on.

C. Specific heat

Specific-heat data were obtained with a conventional adiabatic heat-pulse calorimeter in the temperature range $0.4 - 20$ K. The magnetic contribution C_m to the specific heat was obtained by subtraction of the lattice contribution of pure ZnSe. The results for C_m (per mol Fe) in zero external magnetic field are shown in Fig. 4. As quoted earlier, no anomaly was observed at the temperature T_f as indicated by arrows in the figure. The

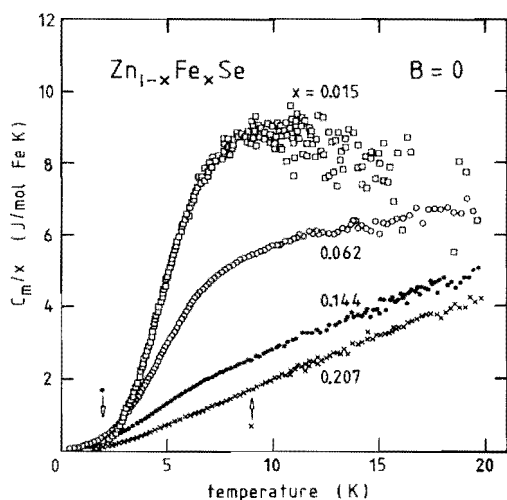


FIG. 4. Magnetic specific heat of $\text{Zn}_{1-x}\text{Fe}_x\text{Se}$ in the absence of magnetic field. The arrows indicate the freezing temperatures T_f .

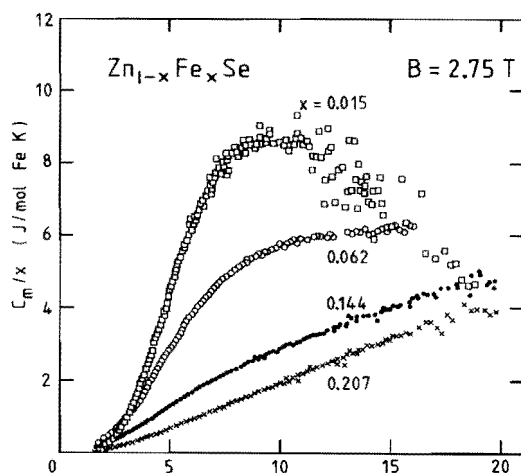


FIG. 5. Magnetic specific heat of $\text{Zn}_{1-x}\text{Fe}_x\text{Se}$ for $B = 2.75$ T.

overall behavior of C_m resembles a Schottky-type anomaly for the lowest concentrations for which a well pronounced, broad maximum is observed at about 10 K. For $x > 0.14$ no maximum is observed and C_m is practically a linear function of the temperature. In distinction to the Mn-based DMS^{15,16,3,17} no structure is observed below 2 K: C_m tends to zero monotonously with decreasing temperature. No additional contribution at lower temperatures is expected since in the measured range already $\approx 87\%$ of the entropy of the ten-level system is recovered for $x = 0.015$ (assuming $C_p \sim T^2$ for $T > 20$ K).

The decrease of C_m/x with x indicates the relevance of the $\text{Fe}^{2+}\text{-Fe}^{2+}$ interaction. If the only contribution to C_m would be from single (isolated) ions, as proposed previously⁸, C_m would scale with x . We found that the specific heat is not appreciably influenced by a magnetic field as shown in Fig. 5: only a very slight shift of C_m to higher temperatures, hardly exceeding the experimental accuracy, can be observed. Such a behavior is again in contrast with results reported for manganese DMS^{3,15}.

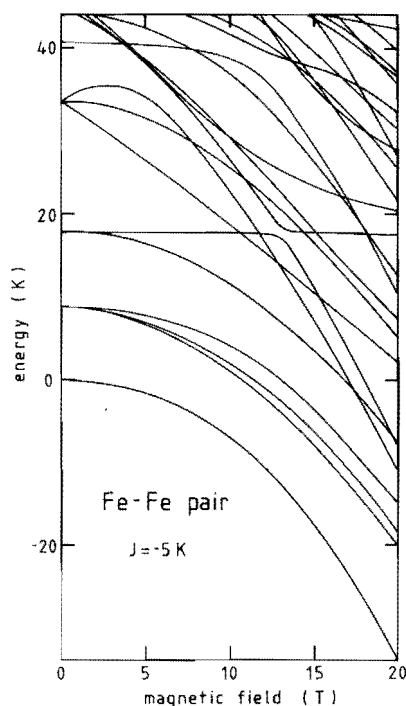


FIG. 7. Splitting of the pair energy levels in magnetic field ($J = -5$ K, $Dq = 293$ cm^{-1} and $\lambda = -85$ cm^{-1}).

Hamiltonian matrix. The resulting energy pair diagram is shown in Fig. 6 for some values of J . For the crystal-field splitting and spin-orbit parameter, we adopted the values reported⁶ for ZnSe:Fe ($Dq = 293$ cm^{-1} , $\lambda = -85$ cm^{-1}). To demonstrate the influence of the spin-orbit coupling, the energy levels for $\lambda = -103$ cm^{-1} (i.e., the free ion value) are also shown in Fig. 6(b). It can be noticed that the exchange interaction does not essentially change the iron energy level structure, in the sense that the ground state is still a singlet one. However, the first excited state approaches the ground state when J increases. In the presence of a magnetic field the degeneracy of the $\text{Fe}^{2+}\text{-Fe}^{2+}$ pair is lifted as shown in Fig. 7 for fields up to 20 T.

The energy level scheme can be used for the calculation of all thermodynamic prop-

erties of an $\text{Fe}^{2+}\text{-Fe}^{2+}$ pair. In Fig. 8 we show the specific heat of a pair for different exchange interactions. For all presented J values, at low temperatures a well pronounced maximum in the specific heat is observed, similarly to a single Fe^{2+} ion ($J = 0$). This maximum shifts to lower temperatures as the exchange interaction increases and slightly changes its shape. Application of moderate magnetic fields influences the specific heat only slightly (less than 5% for $B < 6$ T), which is a consequence of the small changes of the energy level separations with magnetic field (cf. Fig. 7).

In Fig. 9 the calculated magnetization of an $\text{Fe}^{2+}\text{-Fe}^{2+}$ pair is shown for different temperatures. In distinction to the free Fe^{2+} ion magnetization (Fig. 9, inset), the pair magnetization shows no saturation with magnetic field (we checked it up to 60 T). Moreover, no characteristic steps are observed, which occur for $\text{Mn}^{2+}\text{-Mn}^{2+}$ pairs²⁰⁻²² and are due to crossings of excited pair levels with the ground state. In the present case the ground

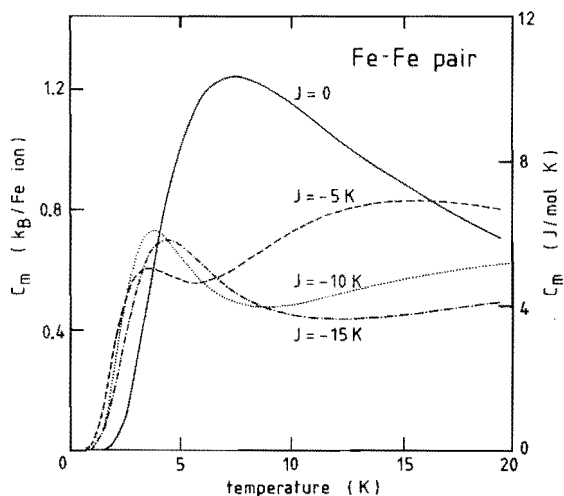


FIG. 8. Specific heat of an $\text{Fe}^{2+}\text{-Fe}^{2+}$ pair as a function of temperature for $J = -5$, -10 K, and -15 K ($Dq = 293$ cm^{-1} , $\lambda = -85$ cm^{-1}) in the absence of a magnetic field. For comparison the behavior for noninteracting ions ($J = 0$) is also shown.

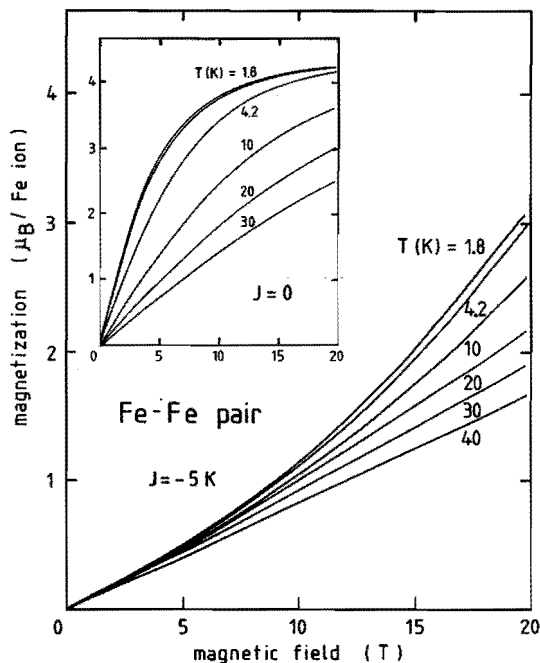


FIG. 9. Magnetization of an $\text{Fe}^{2+}\text{-Fe}^{2+}$ pair coupled by an exchange interaction $J = -5$ K as a function of magnetic field for different temperatures ($Dq = 293$ cm^{-1} , $\lambda = -85$ cm^{-1}). Inset: magnetization of a single, isolated Fe^{2+} ion ($J = 0$) as a function of temperature for the same parameters Dq and λ .

state is coupled to the excited states by the magnetic field and is then pushed down instead of being crossed by excited states (Fig. 7). Therefore no steps are predicted even at very low temperatures.

Finally, in Fig. 10 the susceptibility as a function of temperature is shown. A typical Curie-Weiss behavior [$\chi \sim (T-\Theta)^{-1}$] is predicted for the high-temperature limit when an interaction is present in distinction to the Curie-type behavior ($\chi \sim T^{-1}$) for a single Fe ion in a crystal field.

IV. INTERPRETATION

Using the results of the preceding section, one can now describe the relevant thermo-

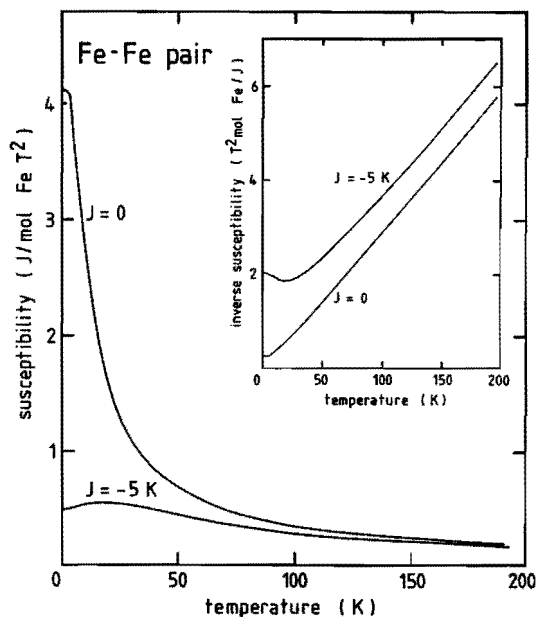


FIG. 10. Susceptibility of an $\text{Fe}^{2+}\text{-Fe}^{2+}$ pair coupled by an exchange interaction $J = -5$ K as a function of temperature ($Dq = 293$ cm^{-1} , $\lambda = 85$ cm^{-1}). For comparison the behavior of noninteracting ions ($J = 0$) is also shown. Inset: inverse susceptibility as a function of temperature.

dynamic properties of a "real" $\text{Zn}_{1-x}\text{Fe}_x\text{Se}$ crystal in the so-called extended nearest-neighbor pair approximation (ENNPA)¹³, which was recently successfully used for description of the magnetic properties of Mn-based DMS^{13,3}.

The ENNPA is an approximative calculation method particularly useful for random, diluted systems with long-ranged interactions. It is based on the assumption that the partition function of the whole crystal can be factorized into contributions of pairs of ions. In this method each ion is considered to be coupled by an exchange interaction J_i only to its nearest magnetic neighbor, which may be located anywhere at a distance R_i . The statistical weight of pair configurations with different R_i is given by random distribution of the magnetic ions, and therefore any thermo-

dynamic quantity can be expressed in the following form

$$A = \sum_i \frac{1}{2} A_i(J_i) P_i(x) , \quad (3)$$

where A_i represents the specific heat, susceptibility or magnetization of a pair and depends on J_i . $P_i(x)$ is the probability of finding at least one nearest Fe ion in the i th shell and corresponds for a random distribution to:

$$P_i(x) = (1-x)^{n_{i-1}} - (1-x)^{n_i} , \quad (4)$$

where n_i is the number of lattice sites inside a shell of radius R_i .

For the actual calculations we have to insert values for the parameters: Dq , λ , J_1 , J_2 , J_3 , For the crystal-field splitting and spin-orbit parameters we have taken the values $\Delta = 2930 \text{ cm}^{-1}$ (or $Dq = 293 \text{ cm}^{-1}$) and $\lambda = -85 \text{ cm}^{-1}$ reported⁶ for ZnSe doped with Fe. These values result from combining spectroscopic data for the ${}^5E \rightarrow {}^5T$ optical transition²⁴ with susceptibility results⁶, assuming Ham's reduction factor²⁵ to equal 1. We notice that the crystal-field parameter obtained in that way is practically determined by the energy of the ${}^5E \rightarrow {}^5T$ transition, since it depends only very weakly on the value of λ (20% variation of λ results in 1% variation of Δ), whereas the spin-orbit parameter results from the fitting procedure. The exchange integral for nearest neighbors is provided by recent high-temperature susceptibility data¹¹: $J_{\text{NN}} = -22 \text{ K}$. The interaction range is suggested to be $J_i = J_{\text{NN}} R^{-12}$ (see Sec. II). This means, in practice, that only the nearest-neighbor interaction is relevant, since more distant neighbors are so weakly coupled that their magnetic properties differ very little from those of single ions. However, as we already discussed in Sec. II, the data concerning the spin-glass freezing in Fe-based DMS are not sufficient to provide reliable information about this interaction range. We will therefore discuss two cases: only nearest neighbor, short-ranged interaction (NN) and a long-range interaction (LR), as-

suming the same interaction range as reported³ for $\text{Zn}_{1-x}\text{Mn}_x\text{Se}$ ($J_i = J_{\text{NN}} R^{-6.8}$).

The ENNPA calculations were performed numerically. The summation over i shells in (3) was carried out up till $i = v$ for which

$$\sum_{i=1}^v P_i(x) > 0.99 . \quad (5)$$

In practice $v = 12$ was quite sufficient for all x .

The calculated specific heat, together with the experimental data, is shown in Fig. 11 for $x = 0.015$, and Fig. 12 for $x = 0.062$. It is obvious that if the exchange interaction between the Fe ions is taken into account, a much better description of the ex-

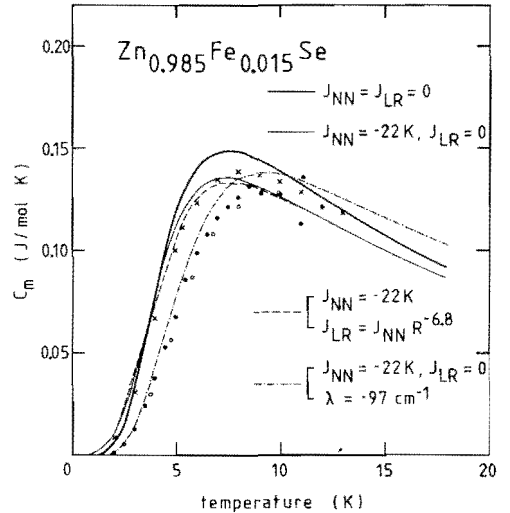


FIG. 11. Specific heat of $\text{Zn}_{0.985}\text{Fe}_{0.015}\text{Se}$ in the ENNPA as a function of temperature without a magnetic field for $Dq = 293 \text{ cm}^{-1}$, $\lambda = -85 \text{ cm}^{-1}$, and various exchange interaction parameters. The crosses show the influence of a magnetic field $B = 2.64 \text{ T}$ for $J_{\text{NN}} = -22 \text{ K}$ and $J_{\text{LR}} = 0$. Also the influence of a different spin-orbit parameter, $\lambda = -97 \text{ cm}^{-1}$, is shown. The points are experimental data: solid circles $B = 0$, open circles $B = 2.75 \text{ T}$.

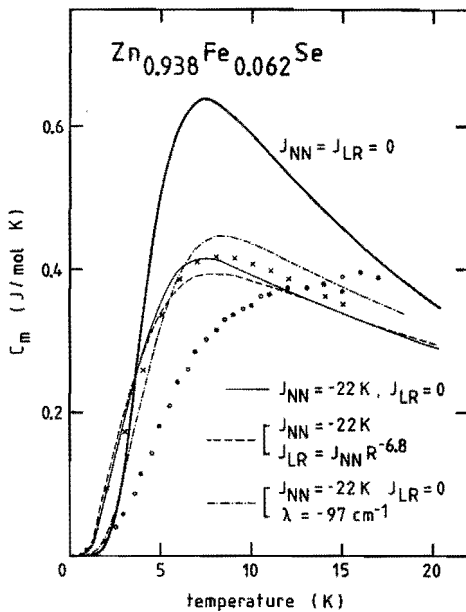


FIG. 12. Specific heat of $Zn_{0.938}Fe_{0.062}Se$ in the ENNPA as a function of temperature without a magnetic field for $Dq = 293 cm^{-1}$, $\lambda = -85 cm^{-1}$, and various exchange interaction parameters. The crosses show the influence of a magnetic field $B = 2.64 T$ for $J_{NN} = -22 K$ and $J_{LR} = 0$. Also the influence of a different spin-orbit parameter, $\lambda = -97 cm^{-1}$, is shown. The points are experimental data: solid circles $B = 0$, open circles $B = 2.75 T$.

perimental data can be obtained than for the noninteracting ion model ($J = 0$ in Figs. 11 and 12). The latter description is reasonable for $x = 0.015$ whereas a substantial discrepancy is found for $x = 0.062$. We should note, however, that the dilute limit which is essential in the ENNPA may not be satisfied for $x = 0.06$. In fact, for Mn-based DMS only crystals containing less than 5% magnetic ions could be properly described by the ENNPA^{13,3}.

In the dilute limit, where the single-ion contribution is dominant, the exponential onset of C_m clearly marks the influence of the energy gap between the ground state and the

first-excited state. The systematic deviation of the calculations from the experimental data in the low-temperature region indicates that the actual lowest energy gap is somewhat larger than resulting from the parameters taken in the present calculation ($\approx 18 K$). An increase of this gap to $\approx 22 K$ is necessary to explain the observed specific heat. Preliminary far-infrared transmission (FIR) experiments²⁶, where we observed the optical transitions $A_1 \rightarrow T_1$ and $A_1 \rightarrow T_2$, have confirmed this suggestion. To explain the experimental $E(T_1) - E(A_1)$ and $E(T_2) - E(A_1)$ energy differences within the framework of Slack's model⁵, one has to adjust the spin-orbit parameter to $-97 cm^{-1}$ keeping Dq unchanged. The resulting specific heat is shown in Figs. 11 and 12. One can notice that this larger value of λ indeed improves the description, although, especially for the higher concentration, significant deviations

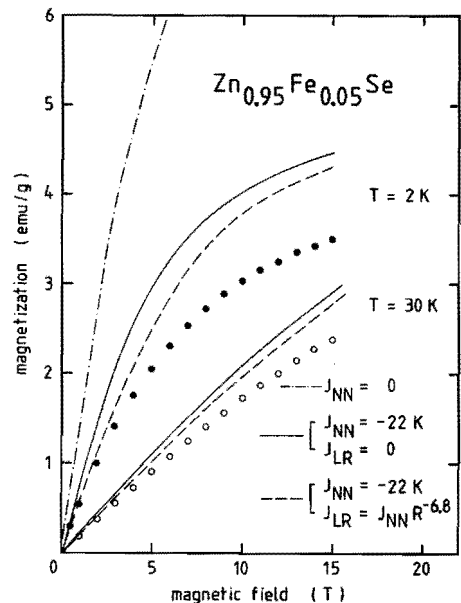


FIG. 13. Magnetization of $Zn_{0.95}Fe_{0.05}Se$ in the ENNPA as a function of magnetic field at $T = 2 K$ and $T = 30 K$ for $Dq = 293 cm^{-1}$, $\lambda = -85 cm^{-1}$, and various exchange interaction parameters. The points represent experimental data (Ref. 8).

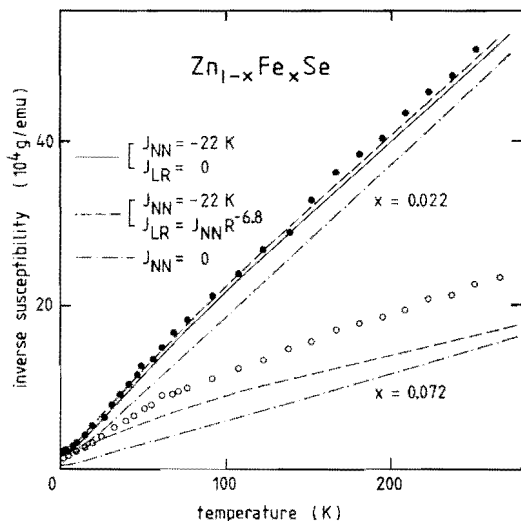


FIG. 14. Inverse susceptibility of $\text{Zn}_{1-x}\text{Fe}_x\text{Se}$ for $x = 0.022$ and $x = 0.072$ in the ENNPA as a function of temperature for $Dq = 293 \text{ cm}^{-1}$, $\lambda = -85 \text{ cm}^{-1}$, and different exchange interaction parameters. The points are experimental data (Ref. 11).

remain.

High-field magnetization results are shown in Fig. 13 for $\text{Zn}_{0.95}\text{Fe}_{0.05}\text{Se}$. Also in this case it is evident that ion-ion interactions have to be taken into account.

The magnetic susceptibility calculations are presented in Fig. 14 for $\text{Zn}_{0.978}\text{Fe}_{0.022}\text{Se}$ and $\text{Zn}_{0.928}\text{Fe}_{0.072}\text{Se}$ (Ref. 11). The typical curvature of the calculated susceptibility, which is also observed in the experimental data, is obviously due to exchange interactions and is neither observed for semi-isolated Fe^{2+} ions⁶, nor reproduced by calculations for isolated ions as shown in Fig. 14 ($J = 0$). Again we observe an increasing discrepancy between calculations and experimental data when the concentration increases.

For all magnetic properties considered here, we observe (cf. Figs. 11–14) that the difference between calculations in which the exchange interaction is implemented by the nearest neighbors alone, or by a long-range

interaction $J(R)$, is not very significant. This results from the fact, as we quoted before⁹, that the further-neighbors exchange interactions are too weak to alter the Fe^{2+} level scheme significantly. Consequently, no pertinent conclusions about the interaction range can be drawn from the present data.

Summarizing the present results we feel that the model presented above provides a reasonable, simultaneous description of all the magnetic properties with a single set of parameters. We believe that the observed deviations at higher Fe concentrations are mainly due to the fact that these concentrations are somewhat outside the diluted limit, to which the ENNPA is specifically applicable.

We would like to emphasize that no fitting parameters are employed in our calculations and comparison with the data. Such a procedure would certainly yield a better description of some of the experimental data, but, in view of the large number of parameters, it would not be necessarily physically meaningful.

V. DISCUSSION AND CONCLUSIONS

As quoted earlier, specific-heat data and preliminary FIR experiments indicated that the energy gap between the ground state and the first-excited states is somewhat larger than the calculated gap resulting from the reported crystal-field and spin-orbit parameters. To describe this splitting within Slack's model, the spin-orbit coupling parameter had to increase from -85 cm^{-1} to -97 cm^{-1} . One has to note, however, that this is just a formal description. Physically, it seems more likely that substitution of magnetic ions results in a local lowering of the cubic symmetry which may lift the orbital degeneracy to start with. However, data to support this conjecture are not available and we therefore refrained from implementing these effects.

Furthermore we would like to point out that our use of an isotropic exchange interaction term of the Heisenberg type must be considered as a first approximation. General-

TABLE I. Nearest-neighbor interaction strength (J_{NN}), radial dependence of the interaction (n with $J \sim R^{-n}$) and p - d exchange parameter (N_0) for several Mn- and Fe-type DMS.

	Mn			Fe		
	$J_{NN}(\text{K})$	n	$N_0(\text{eV})$	$J_{NN}(\text{K})$	n	$N_0(\text{eV})$
CdSe	-10 ^a	6.8 ^c	-1.27 ^e	-18 ^{g,h}		
ZnSe	-12.6 ^a	6.8 ^c	-1.30 ^f	-22 ^h	12	-1.6 ⁱ
ZnS	-16 ^b	7.6 ^d				

a Reference 28
 b Reference 14
 c Reference 3
 d Reference 17
 e Reference 27

f Reference 29
 g Reference 10
 h Reference 11
 i Reference 30

ly speaking, anisotropic terms will be present for Fe^{2+} - Fe^{2+} interactions, specifically when the actual calculations are restricted (as in the present case) to the lower subset of levels.

Finally, we would like to comment on the exchange interaction between Fe^{2+} ions in relation to Mn^{2+} - Mn^{2+} exchange. In Table I we collected the available data concerning Fe and Mn exchange in similar DMS. Inspection of this table shows that no drastic differences are observed between Mn and Fe exchange. An antiferromagnetic, long-range exchange is found in all cases, although the nearest-neighbor interaction is stronger for Fe and seems to be of shorter range than for Mn. Assuming that superexchange is the dominant mechanism, as was rather well established for Mn-type DMS, the simultaneous increase of strength and decrease of range is not completely in accordance with theory. In general an increasing strength is expected to be accompanied with an increasing range³¹ or the range is considered as largely independent of the atomic constituents³². These tendencies, however, mainly refer to comparisons between Mn-type DMS. The substitution of Fe instead of Mn may well result in changes in the band structure and d energy levels, which complicate a meaningful comparison since both the location of the unoccupied d levels with respect to the valence band, as well as the degree of hybridization, determine the strength of J_{NN} , at least for the

first few neighbors^{31,32}. Although calculations of Wei *et al.*³³ seem to indicate an increase of the hybridization for Fe^{2+} (or Mn^{2+}), which would be consistent with the observed increase of J_{NN} as well as the p - d exchange parameter N_0 (cf. Table I), we feel that pertinent conclusions would be rather speculative at the present stage.

With respect to the range of the long-range interaction ($\sim 1/n$), as probed by the freezing temperature as a function of x , a comment must be made. The relation between T_f and concentration x is based on a scaling analysis and the conjecture that T_f is related to the interaction energy at the average distance (R_{av}) between the magnetic ions³, e.g.,

$$k_B T_f \approx J(R_{av})S^2 \quad (6)$$

In the case that we are dealing with a singlet ground state with a quenched magnetic moment, the interaction energy is less effective and should be modified, implementing the fact that the interacting ions have only an induced moment. This situation is somewhat analogous to the case studied by Moriya³⁴ who showed, in a mean-field approximation, that an ensemble of Ni^{2+} ions with singlet ground state cannot sustain spontaneous order unless the exchange interaction is, roughly speaking, strong enough to overcome the ground-state splitting.

We will illustrate this behavior by con-

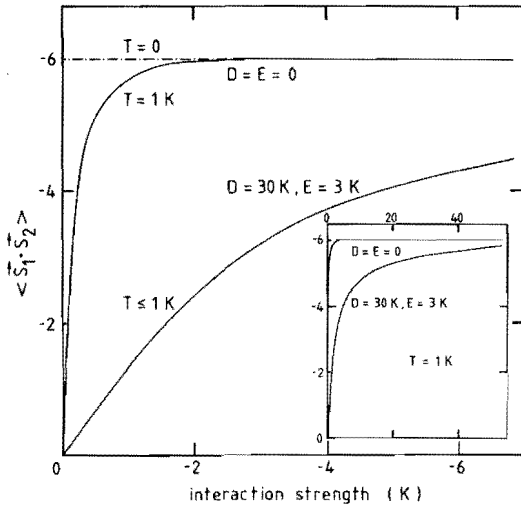


FIG. 15. Calculated low-temperature pair correlation function $\langle \mathbf{S}_1 \cdot \mathbf{S}_2 \rangle$, for Hamiltonian (7) with $S = 2$, as a function of interaction strength J . Two cases are considered, i.e., the degenerate ($D = E = 0$) and the singlet single-ion ground state ($D \neq 0$, $E \neq 0$). In the latter case the energy splitting between ground and first-excited state equals 22 K.

sidering the pair correlation function $\langle \mathbf{S}_1 \cdot \mathbf{S}_2 \rangle$ for $S = 2$ ions both with and without a singlet ground state coupled with an exchange interaction $J\mathbf{S}_1 \cdot \mathbf{S}_2$. The Hamiltonian is written as

$$\begin{aligned} \mathcal{H}_{12} = & -2J\mathbf{S}_1 \cdot \mathbf{S}_1 + D(S_{1z}^2 + S_{2z}^2) \\ & + \frac{1}{2}E(S_{1x}^2 - S_{1y}^2 + S_{2x}^2 - S_{2y}^2). \end{aligned} \quad (7)$$

The singlet ground state of the individual ions is created by allowing D and E to be nonzero. For zero D , E a degenerate ground state of the ions is obtained. Figure 15 shows the calculated pair correlation function $\langle \mathbf{S}_1 \cdot \mathbf{S}_2 \rangle$ for the two cases at low temperatures, as a function of J . D and E are chosen such that an energy-level scheme is obtained with a splitting between ground state and first-excited state similar to that observed in $\text{Zn}_{1-x}\text{Fe}_x\text{Se}$. From Fig. 15 it is clear that the pair correlation for coupled ions with singlet

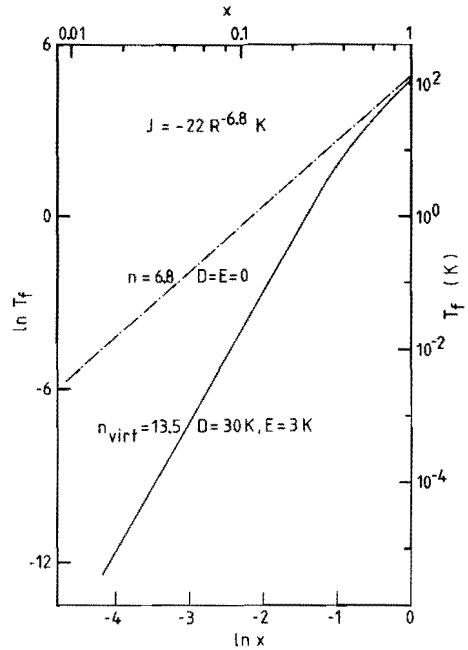


FIG. 16. Calculated freezing temperature T_f as a function of the concentration x on a logarithmic scale, using $k_B T_f = J(R_{av}) \langle \mathbf{S}_0 \cdot \mathbf{S}_{Rav} \rangle$ and $J(R) = -22R^{-6.8} \text{ K}$, $R = R_{av}/R_{NN} = (1/x)^{1/3}$; see Fig. 15 ($T = 0$).

ground states depends on J and is appreciably smaller than the pair correlation for coupled ions with a degenerate ground state, at least for small J . Now we have to realize that actually the interaction energy in Eq. (6) must be written as proportional to $J \langle \mathbf{S}_1 \cdot \mathbf{S}_2 \rangle$, which, as can be seen from Fig. 15, approaches the value $-JS(S+1)$ in the fully aligned limit. If we perform an analysis on the concentration dependence³ of T_f , using the pair exchange energy $J(R_{av}) \langle \mathbf{S}_0 \cdot \mathbf{S}_{Rav} \rangle$ following from the preceding calculations, the resulting $T_f(x)$ does not necessarily reveal the radial dependence of $J(R)$. This is illustrated in Fig. 16 where the calculated results for $T_f(x)$ are shown obtained for the two cases considered in Fig. 15. For both cases the same radial dependence of $J(R_{av})$ is

used: $J \sim R^{-6.8}$. For the pairs with the degenerate ground state, the resulting $T_f(x)$ indeed shows the implemented range of interaction ($1/n$). However, for pairs with a singlet ground state, the range, as probed by $T_f(x)$, is virtually suppressed due to the reduction of $\langle S_1 \cdot S_2 \rangle$ for small J , yielding $n \approx 13.5$ instead of $n = 6.8$. Although the actual energy level scheme of Fe^{2+} in $\text{Zn}_{1-x}\text{Fe}_x\text{Se}$ is much more complicated than considered in this simple illustration, it is surprising to note that this virtual range of interaction ($n \approx 13.5$) is rather close to the range actually observed from the experimental data ($n \approx 12$).

-
- 1 See review papers: *Diluted Magnetic Semiconductors*, edited by R.L. Aggarwal, J.K. Furdyna and S. von Molnar (Materials Research Society, Pittsburgh, 1987), Vol. 89, p. 153; N.B. Brandt and V.V. Moshalkov, *Adv. Phys.* **33**, 193 (1984); J.K. Furdyna, *J. Appl. Phys.* **53**, 8637 (1982); J.A. Gaj, *J. Phys. Soc. Jpn.* **49**, Suppl. A797 (1980).
- 2 W.J.M. de Jonge, A. Twardowski and C.J.M. Denissen, in *Diluted Magnetic Semiconductors*, edited by R.L. Aggarwal, J.K. Furdyna and S. von Molnar (Materials Research Society, Pittsburgh, 1987), Vol. 89, p. 153.
- 3 A. Twardowski, H.J.M. Swagten, W.J.M. de Jonge and M. Demianiuk, *Phys. Rev. B* **36**, 7013 (1987).
- 4 W. Low and M. Weger, *Phys. Rev.* **118**, 1119 (1960).
- 5 G.A. Slack, S. Roberts and J.T. Wallin, *Phys. Rev.* **187**, 511 (1969).
- 6 J.P. Mahoney, C.C. Lin, W.H. Brumage and F. Dorman, *J. Chem. Phys.* **53**, 4286 (1970).
- 7 See the review paper A. Mycielski in *Diluted Magnetic Semiconductors*, edited by R.L. Aggarwal, J.K. Furdyna and S. von Molnar (Materials Research Society, Pittsburgh, 1987), Vol. 89, p. 159.
- 8 A. Twardowski, M. von Ortenberg and M. Demianiuk, *J. Cryst. Growth* **72**, 401 (1985).
- 9 A. Twardowski, H.J.M. Swagten, T.F.H. v.d. Wetering and W.J.M. de Jonge, *Solid State Commun.* **65**, 235 (1988).
- 10 A. Lewicki, J. Spalek and A. Mycielski, *J. Phys. C* **20**, 2005 (1987).
- 11 A. Twardowski, A. Lewicki, M. Arciszewska, W.J.M. de Jonge, H.J.M. Swagten and M. Demianiuk, *Phys. Rev. B* **38**, 10749 (1988).
- 12 B.T. Jonker, J.J. Krebs, S.B. Qadri and G.A. Prinz, *Appl. Phys. Lett.* **50**, 848 (1987).
- 13 C.J.M. Denissen, H. Nishihara, J.C. van Gool and W.J.M. de Jonge, *Phys. Rev. B* **33**, 7637 (1986).
- 14 T.M. Giebultowicz, J.J. Rhyne and J.K. Furdyna, *J. Appl. Phys.* **61**, 3537 (1987); **61**, 3540 (1987).
- 15 R.R. Galazka, S. Nagata and P.H. Keesom, *Phys. Rev. B* **22**, 3344 (1980), S. Nagata, R.R. Galazka, D.P. Mullin, H. Arbarzadeh, G.D. Khattak, J.K. Furdyna and P.H. Keesom, *ibid.* **22**, 3331 (1980).
- 16 C.D. Amarasekara, R.R. Galazka, Y.Q. Yang and P.H. Keesom, *Phys. Rev. B* **27**, 2868 (1983).
- 17 H.J.M. Swagten, A. Twardowski, W.J.M. de Jonge, M. Demianiuk and J.K. Furdyna, *Solid State Commun.* **66**, 791 (1988).
- 18 We neglected here a possible pseudodipolar exchange interaction which was, in general, considered in Ref. 9, since no information is provided about it.
- 19 In our previous paper (Ref. 9) we used a simpler basis, given by Slack *et al.* (Ref. 5) in their Tables VIII and IX. In that way $^5E-^5T$ mixing due to \mathcal{H}_{SO} was treated in second-order perturbation method. It should be stressed, however, that no substantial difference was found between present and the later results.
- 20 R.L. Aggarwal, S.N. Jasperson, Y. Shapira, S. Foner, T. Sakibara, T. Goto, N. Miura, K. Dwight and A. Wold, in *Proceedings of the 17th International Conference on the Physics of Semiconductors, San Francisco, 1984*, edited by J.D. Chadi and W.A. Harrison (Springer, New York, 1985), p. 1419.
- 21 Y. Shapira, S. Foner, D.H. Ridgley, K. Dwight and A. Wold, *Phys. Rev. B* **30**, 4021 (1984).
- 22 J.P. Lascaray, M. Nawrocki, J.M. Broto, M. Rakoto and M. Demianiuk, *Solid State Commun.* **61**, 401 (1987).
- 23 K. Matho, *J. Low Temp. Physics* **35**, 165

- (1979).
- 24 J.M. Baranowski, J.W. Allen and G.L. Pearson, *Phys. Rev.* **160**, 627 (1967).
- 25 F.S. Ham, *Phys. Rev.* **138**, A1727 (1965).
- 26 A. Twardowski, H.J.M. Swagten and W.J.M. de Jonge, in *Proceedings of the 19th International Conference on Physics of Semiconductors*, edited by W. Zawadski (Warsaw, 1988), p. 1543.
- 27 M. Arciszewska and M. Nawrocki, *J. Phys. Chem. Solids* **47**, 309 (1986).
- 28 J. Spalek, A. Lewicki, Z. Tarnawski, J.K. Furdyna, R.R. Galazka and Z. Obuszko, *Phys. Rev. B* **33**, 3407 (1986).
- 29 A. Twardowski, M. von Ortenberg, M. Demianiuk and R. Pauthenet, *Solid State Commun.* **51**, 849 (1984).
- 30 A. Twardowski, P. Glod, W.J.M. de Jonge and M. Demianiuk, *Solid State Commun.* **64**, 63 (1987).
- 31 G.A. Sawatzky, W. Geertsma and C. Hass, *J. Magn. Magn. Mater.* **3**, 37 (1976); C.E.T. Goncalves da Silva and L.M. Falicov, *J. Phys. C* **5**, 63 (1972); A.N. Kocharyan and D.I. Khomskii, *Fiz. Tverd. Tela (Leningrad)* **17**, 462 (1975) [*Sov. Phys. – Solid State* **17**, 290 (1975)].
- 32 H. Ehrenreich, K.C. Hass, B.E. Larson and N.F. Johnson, in *Diluted Magnetic Semiconductors*, edited by R.L. Aggarwal, J.K. Furdyna and S. von Molnar (Materials Research Society, Pittsburgh, 1987), Vol. 89, p. 187; B.E. Larson, K.C. Hass, H. Ehrenreich and A.E. Carlsson, *Solid State Commun.* **56**, 347 (1985).
- 33 Su-Huai Wei and A. Zunger, *Phys. Rev. B* **35**, 2340 (1987).
- 34 T. Moriya, *Phys. Rev.* **117**, 635 (1960).

Chapter III, paragraph 2

Low-temperature specific heat of the diluted magnetic semiconductor $\text{Hg}_{1-x-y}\text{Cd}_y\text{Fe}_x\text{Se}$

[published in Phys. Rev. B 42, 2455 (1990)]

I. INTRODUCTION

Diluted magnetic semiconductors (DMS) or semimagnetic semiconductors are currently attracting considerable attention because of their interesting transport, magneto-optical and magnetic properties¹. So far, research has been focused mainly on DMS containing Mn^{2+} ions. The magnetic behavior of these systems can be understood on the basis of a random array of localized Mn ions coupled by long-ranged isotropic antiferromagnetic exchange interactions¹⁻³ which are mediated by the carriers. It has been shown that the dominant microscopic mechanism causing d - d exchange interaction between the Mn ions is probably superexchange (at least for the nearest neighbors). However, the relation to the band structure, as well as the nature of and the driving force behind, the observed phase transitions and the role of anisotropy are still somewhat obscure, and subject for further investigations^{2,3}.

In a way the substitutional Mn^{2+} with its degenerate 6A_1 spin-only ground state, represents a rather simple, although theoretically attractive case, since all the phenomena which involve the orbital momentum are absent. In contrast, substitutional iron Fe^{2+} (d^6) can serve as a much more general case, since it possesses both spin and orbital momenta ($S = 2$ and $L = 2$). Moreover, the d - d exchange is intimately related to the location of the magnetic ion levels with respect to the band structure¹. Therefore, substitution of Fe instead of Mn might affect the character and

strength of these interactions, since the Fe^{2+} d^6 level may be located far above the valence band in contrast to the Mn^{2+} levels. The properties of Fe-based DMS are, however, still relatively unexplored⁴, although recently some optical and magnetic data were reported for some DMS⁴⁻¹⁰. The optical properties, and in particular the band splitting of Fe-based DMS (which follow macroscopic magnetization⁹) show a similar behavior as the analogous quantities for the Mn-type materials, and, in that sense seem not very sensitive to the orbital momentum.

On the other hand, the magnetic properties are expected to be substantially different from Mn-type DMS. This difference can be ascribed to the different energy scheme of Mn^{2+} and Fe^{2+} ions. Substitutional Fe^{2+} has a d^6 electronic configuration. The ground state of the Fe^{2+} free ion (5D) is split by a tetrahedral crystal field into a 5E orbital doublet and a higher lying 5T orbital triplet (separated from 5E by $10Dq$, where Dq is the crystal-field parameter). Spin-orbit interaction splits the 5E term into a singlet A_1 , a triplet T_1 , a doublet E , a triplet T_2 and a singlet A_2 (the energy separation between these states is approximately equal to $6\lambda^2/10Dq$, where λ is the spin-orbit parameter)^{11,12}. Thus the ground state is magnetically inactive singlet A_1 resulting in Van Vleck-type paramagnetism^{12,13}. Moreover, isolated Fe^{2+} ions contribute to the specific heat even in the absence of a magnetic field, in contrast with isolated Mn^{2+} ions, where only Mn-Mn pairs and larger clusters can contribute to the specific

heat for $B = 0$.

So far some experimental data reported on $\text{Zn}_{1-x}\text{Fe}_x\text{Se}$ ^{6,14}, as well as $\text{Cd}_{1-x}\text{Fe}_x\text{Se}$ ^{10,15}, seem to corroborate this model of Fe-based DMS. Reported data on the zero-gap DMS $\text{Hg}_{1-x}\text{Fe}_x\text{Se}$ ⁸ are, however, at variance with such a model, since the specific heat was reported to be much smaller than for $\text{Zn}_{1-x}\text{Fe}_x\text{Se}$ and the low-temperature susceptibility reveals a rather typical Brillouin-type paramagnetic behavior instead of Van Vleck behavior. It was suggested⁸ that this behavior of $\text{Hg}_{1-x}\text{Fe}_x\text{Se}$ results from the specific location of the Fe d^6 level in relation to the HgSe bands (in this material the Fe level is situated 0.2 eV above the bottom of the conduction band, whereas in wide-gap materials like ZnSe or CdSe it is located in the gap between conduction and valence band⁵).

Very recently it was suggested that some of these discrepancies between wide and zero-gap materials mentioned earlier, might be removed by a more careful analysis of the specific-heat data¹⁶ and by taking into account the contribution of the Fe^{3+} ions, which are always present in $\text{Hg}_{1-x}\text{Fe}_x\text{Se}$ crystals¹⁷, to the susceptibility. In view of this we thought it worthwhile to investigate the magnetic properties of open as well as zero-gap Fe-containing DMS in a more detailed way. As we will see later these results will allow us to estimate the nearest-neighbor interactions between Fe^{2+} ions.

TABLE I. Materials used in experiment.

Material	x (Fe)	y (Cd)	$1-x-y$ (Hg)
$\text{Hg}_{1-x}\text{Fe}_x\text{Se}$	0.015	0	0.985
	0.024	0	0.976
	0.045	0	0.955
$\text{Hg}_{1-x-y}\text{Cd}_y\text{Fe}_x\text{Se}$	0.01	0.43	0.56
	0.044	0.446	0.51
$\text{Cd}_{1-x}\text{Fe}_x\text{Se}$	0.008	0.992	0
	0.034	0.966	0
	0.080	0.920	0

II. EXPERIMENTAL

The samples of $\text{Hg}_{1-x}\text{Fe}_x\text{Se}$, $\text{Hg}_{1-x-y}\text{Cd}_y\text{Fe}_x\text{Se}$ (cubic) and $\text{Cd}_{1-x}\text{Fe}_x\text{Se}$ (hexagonal) investigated in the present paper are listed in Table I. They were grown by a modified Bridgman technique, and their concentration and homogeneity was checked by microprobe analysis. The specific heat (C_p) was measured by a standard heat-pulse method in the temperature range 1.5–25 K and in the absence, as well as in the presence, of a magnetic field (up to $B = 2.75$ T). The specific-heat results for $\text{Hg}_{1-x}\text{Fe}_x\text{Se}$, $\text{Hg}_{1-x-y}\text{Cd}_y\text{Fe}_x\text{Se}$ and $\text{Cd}_{1-x}\text{Fe}_x\text{Se}$ are shown in Figs. 1, 2 and 3, respectively. The magnetic contribution to the total specific heat can be well observed in low temperatures. We notice that C_p for all the compounds is practically field independent (at least for $B < 3$ T), which is exemplified in Fig. 4 for $\text{Hg}_{1-x}\text{Fe}_x\text{Se}$. This suggests a singlet ground state for Fe ions for

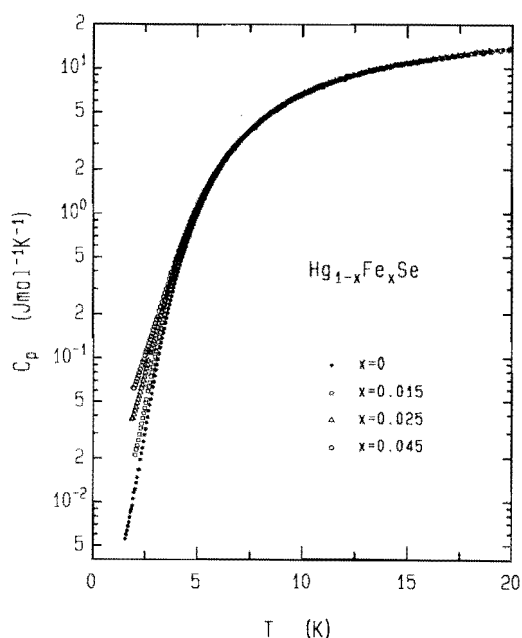


FIG. 1. Specific heat (C_p) of $\text{Hg}_{1-x}\text{Fe}_x\text{Se}$, for several concentrations x .

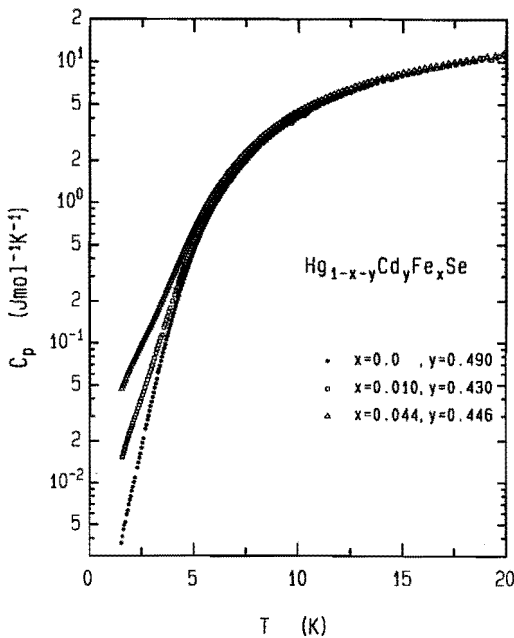


FIG. 2. Specific heat (C_p) of $\text{Hg}_{1-x-y}\text{Cd}_y\text{Fe}_x\text{Se}$, for several concentrations.

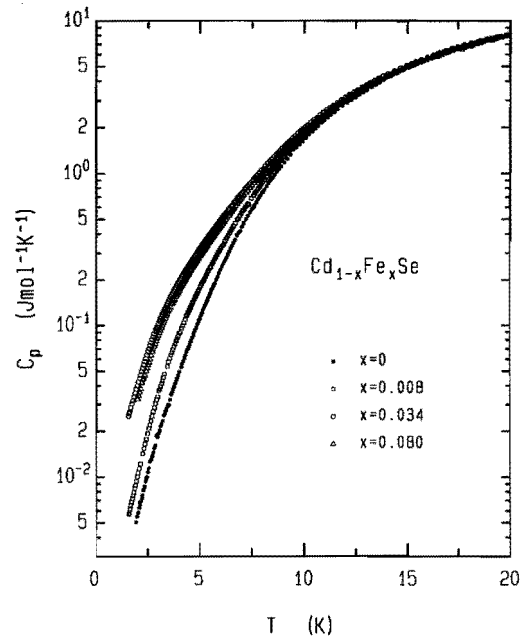


FIG. 3. Specific heat (C_p) of $\text{Cd}_{1-x}\text{Fe}_x\text{Se}$, for several concentrations x .

all the compounds. At higher temperatures, C_p is dominated by the lattice contribution. In the case of $\text{Hg}_{1-x}\text{Fe}_x\text{Se}$, C_p of pure HgSe exceeds C_p for the diluted system with iron for sufficiently high T . Such a situation was observed earlier by us¹⁶ and was also reported for $\text{Hg}_{1-x}\text{Mn}_x\text{Te}$ ¹⁸.

If the magnetic contribution C_m is estimated by subtraction of the undiluted lattice, i.e.,

$$C_m(\text{Hg}_{1-x}\text{Fe}_x\text{Se}) = C_p(\text{Hg}_{1-x}\text{Fe}_x\text{Se}) - C_p(\text{HgSe}), \quad (1)$$

this would lead to the physically unacceptable situation of negative magnetic specific heat at higher temperatures. This situation is extreme for $\text{Hg}_{1-x}\text{Fe}_x\text{Se}$ but not unique. Moreover, for $\text{Cd}_{1-x}\text{Fe}_x\text{Se}$, with 8% of Fe, the magnetic specific heat obtained by Eq. (1) can become negative at high T .

Such a situation results from the fact

that substitution of heavy Hg or Cd atoms by relatively light Fe atoms changes the lattice vibrational modes considerably, and, consequently, the lattice specific heat of the mixed or diluted system differs significantly from that of the nondiluted system. This may be well observed in Fig. 5, where we show the specific heat of pure ZnSe (as a close approximation of FeSe), CdSe, HgSe and a mixed compound $\text{Hg}_{0.51}\text{Cd}_{0.49}\text{Se}$. The increasing difference in atomic mass of Zn, Cd and Hg as compared to Fe, which in the Debye approach yields an increasing difference in Θ_D , is clearly reflected in C_p . It is obvious that for $\text{Hg}_{1-x}\text{Fe}_x\text{Se}$, and to a lesser extent for $\text{Cd}_{1-x}\text{Fe}_x\text{Se}$, a more realistic procedure of extracting the magnetic contribution from the total specific heat should be used.

There are several possible procedures of simulating the lattice heat capacity of an actual crystal. We have tested some of them (based mainly on the Debye approach or lin-

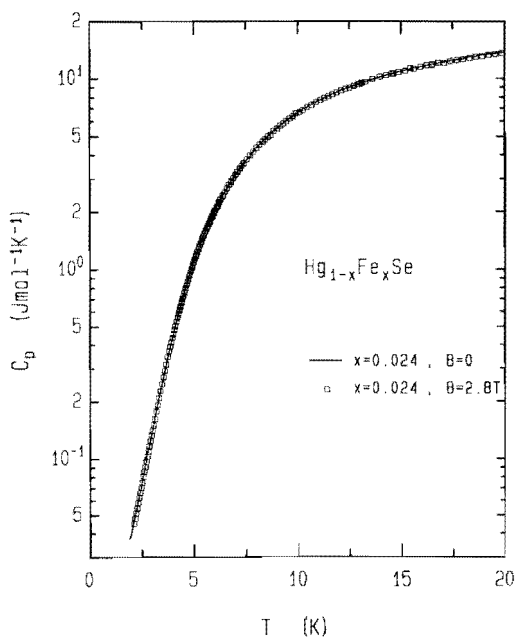


FIG. 4. Specific heat (C_p) of $\text{Hg}_{1-x}\text{Fe}_x\text{Se}$ ($x = 0.024$), for $B = 0$ and $B = 2.8$ T.

ear interpolation of nonmagnetic lattices), and we have found that the validity of all of them is rather limited to the temperature range where the magnetic contribution is somehow comparable to the lattice C_p . At higher temperatures where $C_m \ll C_p$, simulation of lattice C_p requires very accurate information about the crystal composition. Such accuracy can hardly be obtained for the systems like $\text{Hg}_{1-x}\text{Fe}_x\text{Se}$ or $\text{Hg}_{1-x-y}\text{Cd}_y\text{Fe}_x\text{Se}$ with the help of standard microprobe or chemical analysis. Finally, whatever procedure was used, we were not able to obtain so fine high-temperature results as were found for $\text{Zn}_{1-x}\text{Fe}_x\text{Se}$. We should stress that the low-temperature data, which provide the most important physical information, are reliable for all the compounds.

With respect to the remarks given above we decided to use a simple phenomenological interpolation procedure for the lattice simulation (PLS):

$$C_p^{\text{latt}}(\text{Hg}_{1-x-y}\text{Cd}_y\text{Fe}_x\text{Se}, T) \quad (2)$$

$$= AC_p(\text{HgSe}, T) + BC_p(\text{CdSe}, T)$$

$$+ xC_p(\text{ZnSe}, T) ,$$

where the prefactors A , B and x are chosen in accordance to the actual x and y concentration (Table I).

In order to test this procedures we calculated the specific heat of $\text{Hg}_{0.51}\text{Cd}_{0.49}\text{Se}$ using the experimental data on the HgSe and CdSe lattices. The result of these attempts are

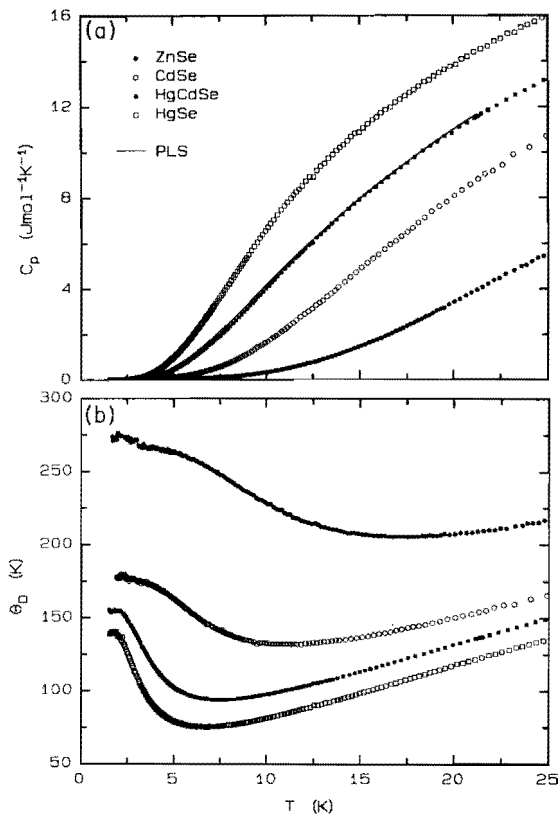


FIG. 5. (a) Specific heat of ZnSe , CdSe , $\text{Hg}_{0.51}\text{Cd}_{0.49}\text{Se}$ and HgSe ; the solid line represents calculations within PLS (see the text). (b) The corresponding Debye-temperatures [$\Theta_D(T)$] of the nonmagnetic lattices.

shown in Fig. 5(a) together with the actual experimental data. Our procedure, although it has no physical background, seems to provide a very reasonable approximation for the lattice specific heat of the mixed crystal.

The results obtained for C_m are given in Figs. 6 ($\text{Hg}_{1-x}\text{Fe}_x\text{Se}$) and 7 ($\text{Cd}_{1-x}\text{Fe}_x\text{Se}$), where C_m/x is displayed as a function of temperature. For completeness, in Fig. 8 the results for $\text{Zn}_{1-x}\text{Fe}_x\text{Se}$ (Ref. 14) are given, obtained by a simple lattice subtraction [Eq. (1)] which is equivalent to PLS for this compound. Due to the delicate dependence of C_p on the actual composition of Hg and Cd for the quaternary compound $\text{Hg}_{1-x-y}\text{Cd}_y\text{Fe}_x\text{Se}$, we could not obtain the reliable C_m data in this case. Therefore, this compound will not be analyzed quantitatively. We only note that the overall behavior of the $\text{Hg}_{1-x-y}\text{Cd}_y\text{Fe}_x\text{Se}$ heat capacity is the same as that of the other systems (cf. Figs. 1–3).

It can be observed that the overall shape of C_m is similar for all Fe-based DMS and the magnetic specific heat calculated per one Fe ion (C_m/x) generally decreases with increasing iron concentration. However, there is

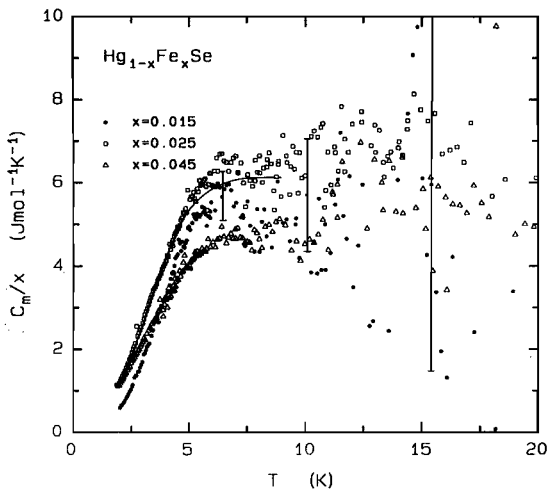


FIG. 6. Magnetic specific heat per mole Fe (C_m/x) of $\text{Hg}_{1-x}\text{Fe}_x\text{Se}$, using PLS [Eq. (2)]. The solid line shows C_m/x for $x = 0.025$ at $B = 2.8$ T.

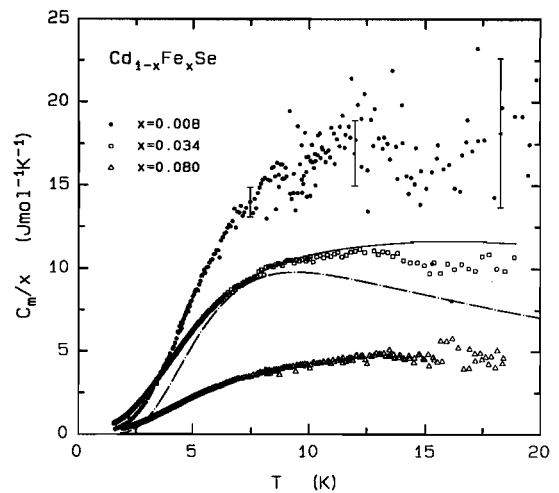


FIG. 7. Magnetic specific heat per mole Fe (C_m/x) of $\text{Cd}_{1-x}\text{Fe}_x\text{Se}$, using PLS [Eq. (2)]. The solid line shows C_m/x for $x = 0.034$ at $B = 2.8$ T. The dashed line displays the calculated C_m/x (Refs. 21–26) assuming no interaction between Fe ions.

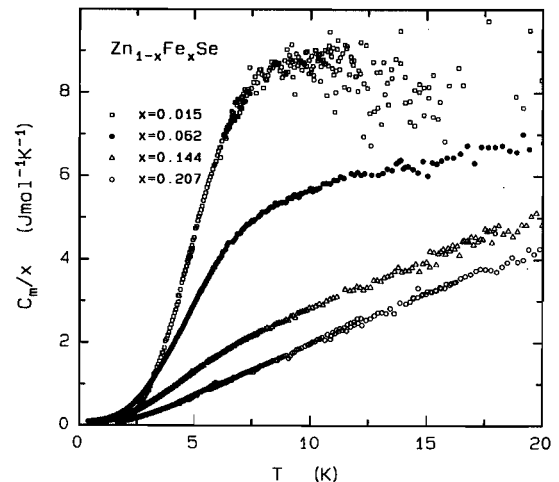


FIG. 8. Magnetic specific heat per mole Fe (C_m/x) of $\text{Zn}_{1-x}\text{Fe}_x\text{Se}$; see Ref. 14.

practically no magnetic-field dependence of C_m for $B < 3$ T (see Figs. 4, 6 and 7). From this behavior one may conclude that the major contribution to C_m originates from Fe^{2+} ions in a singlet ground state as we showed before¹⁴.

In that case one could also expect roughly the same absolute values of C_m at the maximum, which is apparently not observed. These large differences may only partially result from the fact that our procedure of simulating the lattice is not perfect. On the whole, however, it seems rather well established that the absolute value at the maximum of the magnetic specific heat of $\text{Cd}_{1-x}\text{Fe}_x\text{Se}$ is much higher than that of $\text{Zn}_{1-x}\text{Fe}_x\text{Se}$. We return to this point later.

In order to visualize the exponential onset of the magnetic specific heat we plotted the low-temperature data of $\text{Zn}_{1-x}\text{Fe}_x\text{Se}$ (Fig. 9), $\text{Cd}_{1-x}\text{Fe}_x\text{Se}$ (Fig. 10) and $\text{Hg}_{1-x}\text{Fe}_x\text{Se}$ (Fig. 11) as $\ln(C_m T^2)$ versus T^{-1} . The specific ordinates are chosen in accordance to the low-temperature behavior of a Schottky anomaly originating from a singlet ground

state and a threefold degenerate first-excited state at ΔE , which schematically represents the lowest levels of the Fe^{2+} ion in a cubic crystal field with spin-orbit interaction¹²:

$$C_{\text{Sch}}(T) = xR \left[\frac{g_1}{g_0} \right] \left[\frac{\Delta E}{k_B T} \right]^2 \exp(-\Delta E/k_B T) , \quad (3)$$

with $g_1/g_0 = 3$. Within the framework of obtained below the maximum of C_m with a slope determined by ΔE . Extrapolation to $T = \infty$ will yield the value for g_1/g_0 . Detailed calculations for the real energetical structure of an isolated Fe ion (i.e., five levels¹²) reveal a similar linear behavior of $\ln(C_m T^2)$ versus T^{-1} (Fig. 12).

The data for the various compounds indeed show a linear part below $C_{m\text{max}}$ yielding, for low Fe concentrations where Eq. (3) should apply, ΔE in the range 20 – 25 K, in accordance with data from spectroscopic experiments, and g_1/g_0 in the range 2–4. The deviations at extremely low temperatures

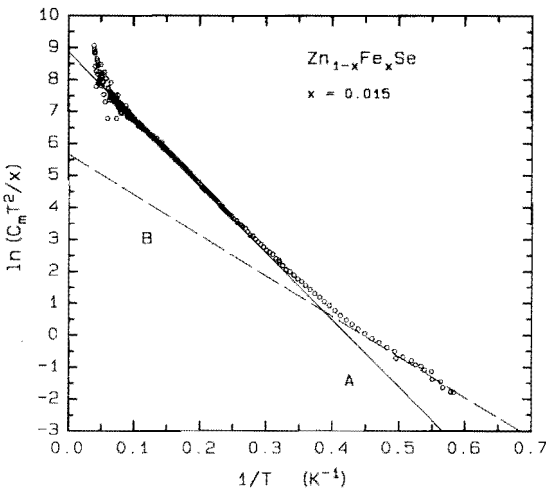


FIG. 9. Magnetic specific heat per mole Fe (C_m/x) of $\text{Zn}_{1-x}\text{Fe}_x\text{Se}$, plotted as $\ln(C_m T^2/x)$ versus $1/T$; the lines are described in the text. Line A yields $\Delta E_{\text{single}} = 21\text{K}$ and line B $\Delta E_{\text{pair}} < 13$ K.

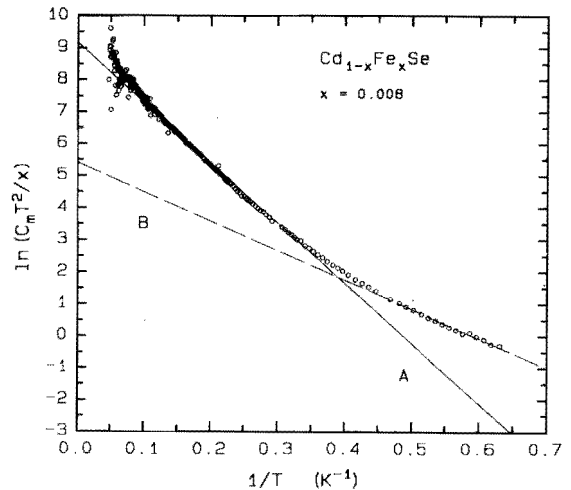


FIG. 10. Magnetic specific heat per mole Fe (C_m/x) of $\text{Cd}_{1-x}\text{Fe}_x\text{Se}$, plotted as $\ln(C_m T^2/x)$ versus $1/T$; the lines are described in the text. Line A yields $\Delta E_{\text{single}} = 19\text{K}$ and line B $\Delta E_{\text{pair}} < 9$ K.

(see Figs. 9–11) result from the fact that in our crystals we are dealing not only with isolated Fe ions [to which Eq. (3) applies], but also with Fe–Fe pairs as well as larger clusters. We recall that for $x = 0.015$ only 83% of the Fe ions can be regarded as isolated in the sense that they have no magnetic nearest neighbor (NN). It was shown^{7,14} that the energetical structure of a Fe–Fe pair, coupled by exchange interaction, yields a situation essentially similar to that of an isolated Fe ion: the pair ground state is a singlet, however, the energy gap between the ground and the first-excited states is strongly reduced [typically by a factor of two (Refs. 7 and 14)]. Therefore, if Fe–Fe pairs are present in the crystal, one may expect an additional contribution to the C_m which will be dominant at low temperatures since only the first excited pair states will be thermally populated. This pair contribution can be observed in Fig. 12, where we plotted the calculated C_m assuming only NN interactions and a statistical distribution of Fe ions in the crystal (for details of the calculations we refer to Refs. 7 and 14). We note that al-

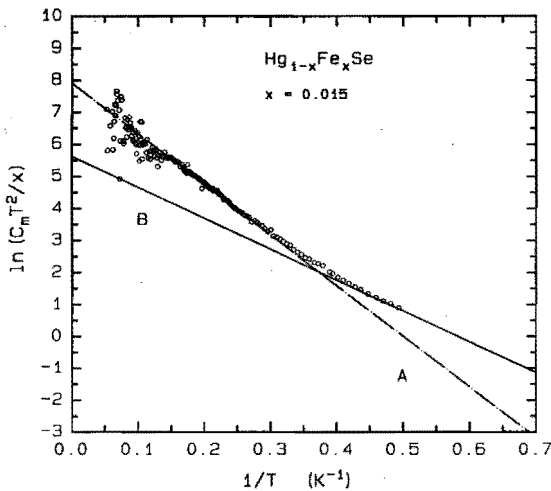


FIG. 11. Magnetic specific heat per mole Fe (C_m/x) of $\text{Hg}_{1-x}\text{Fe}_x\text{Se}$, plotted as $\ln(C_m T^2/x)$ versus $1/T$; the lines are described in the text. Line A yields $\Delta E_{\text{single}} = 16\text{K}$ and line B $\Delta E_{\text{pair}} < 10\text{K}$.

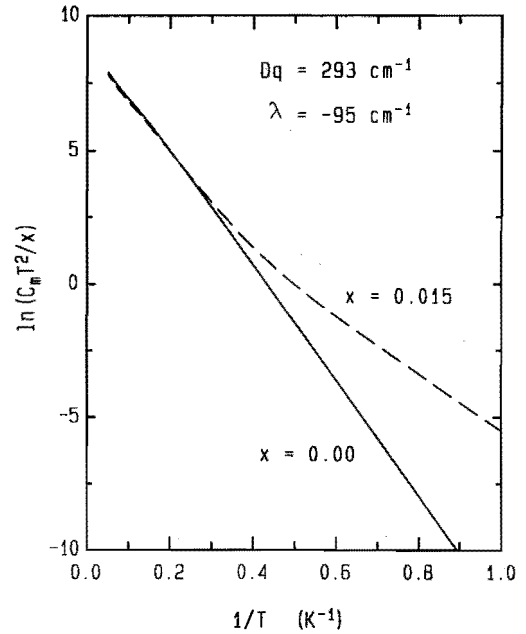


FIG. 12. Calculated magnetic specific heat per mole Fe (C_m/x), plotted as $\ln(C_m T^2/x)$ versus $1/T$ ($Dq = 293\text{ cm}^{-1}$, $\lambda = -95\text{ cm}^{-1}$, $J_{\text{NN}} = -22\text{K}$). The line for $x = 0.00$ corresponds to the case of noninteracting Fe ions.

though our model calculations result from a rather simple Hamiltonian describing Fe–Fe pairs and single ions^{7,14}, the behavior of the real experimental data can be well recovered. It is also apparent that plotting $\ln(C_m T^2/x)$ versus T^{-1} enables one to estimate energy gaps for an isolated Fe ion as well as for the Fe–Fe pair from the appropriate linear parts of the plot. In the present case the temperature is still somewhat too high to restore the linear part in the pair contribution completely. Therefore the "pair" straight lines in Figs. 9–11 give only an estimate of the upper limit for the pair energy gap. Actually, we find a reduction of the pair energy gap by a factor 1.6–2 (in respect to the isolated Fe ion energy gap) instead of 2.44 resulting from the calculations (assuming exchange interaction between nearest neighbors of the order of

-20 K).

For completeness we would like to add that the contributions resulting from nuclear hyperfine interaction, the presence of paramagnetic impurities in our crystals (mainly Mn^{2+} with concentrations $n = 10^{17} - 10^{19} \text{ cm}^{-3}$) and the linear term in C_m brought about by the free carriers ($n < 10^{19} \text{ cm}^{-3}$), are too small to be observed in this specific experiment.

III. DISCUSSION

From the experimental data presented we conclude the following.

(i) The magnetic contribution to the specific heat of our crystals is fairly large at low temperatures, whereas at higher temperatures it is only a small fraction of the lattice contribution. Therefore, the high-temperature C_m of some materials is very sensitive to the extraction method and in some cases ($\text{Hg}_{1-x-y}\text{Cd}_y\text{Fe}_x\text{Se}$) reliable data cannot be obtained (at least not without a separate study of the $\text{Hg}_{1-x-y}\text{Cd}_y\text{Zn}_x\text{Se}$ lattice specific heat). However, the most important physical information results from the low-temperature data, where there are no problems with extracting C_m from the total heat capacity.

(ii) The magnetic contribution to the specific heat shows similar overall behavior for all the Fe-type DMS investigated so far (in spite of some uncertainty in the absolute value).

(iii) The exponential low-temperature increase of C_m clearly indicates an energy gap between the ground state and the excited states, of the order 20 K.

(iv) The very weak field dependence of C_m strongly indicates that the ground state of the Fe ion is a singlet one.

(v) The decrease of the magnetic specific heat per one Fe ion (C_m/x) with increasing concentration, suggests an antiferromagnetic $d-d$ exchange interaction between Fe ions in all cases.

These observations are in agreement with our "crystal-field" model developed recently for Fe-based DMS^{7,14}. We recall

briefly that in this model we factorized the whole magnetic system into pairs coupled by (principally) long-range exchange interaction [so-called extended nearest-neighbors pair approximation (ENNPA)^{19,20,3}]. The basic element in this model is based on the numerical solution of an Fe-Fe pair, where the crystal field (cubic or hexagonal), spin-orbit interaction, magnetic field and the Heisenberg-type exchange interaction are taken into account simultaneously. It was shown⁷ that the ground state of both an isolated Fe ion and an Fe-Fe pair is a singlet with a first (excited) threefold degenerate state at about 10 - 20 K, leading to a Schottky-type specific heat, which is very weakly magnetic field dependent, in accordance with the experimental evidence.

However, this model also predicts a similar maximal absolute value of the specific heat (practically independent of crystal-field and spin-orbit interaction parameters), whereas our experimental maximal values differ largely in magnitude. In Fig. 7 we show the calculated specific heat C_m/x for $\text{Cd}_{1-x}\text{Fe}_x\text{Se}$ assuming no interaction between Fe ions, which is the upper limit for C_m/x^{21-26} . Inspection of Fig. 7 shows that the maximal specific heat of $\text{Cd}_{1-x}\text{Fe}_x\text{Se}$ is apparently consistently too large irrespective of the specific procedure used to estimate the lattice²⁷.

In order to substantiate this fact we calculated the total entropy contained in the experimental specific heat. The data in the temperature range $0 < T < 1.5 \text{ K}$ were approximated by a linear extrapolation, whereas for $T > 20 \text{ K}$ a high temperature T^{-2} approximation was used. The recovered experimental entropy is always 50-60% larger than expected for an Fe^{2+} ten-level system²⁸ $S = R \ln 10$. This suggests that in fact we are dealing with more than the ten levels contained in the 5E multiplet. Since the term structure of Fe is rather well established for both $\text{Cd}_{1-x}\text{Fe}_x\text{Se}$ and $\text{Hg}_{1-x-y}\text{Cd}_y\text{Fe}_x\text{Se}$ from the ${}^5E \rightarrow {}^5T$ optical transition^{5,25}, the only mechanism which can supply additional energy levels seems inclusion of electron-phonon interaction, i.e., Jahn-Teller effect²⁹.

The Jahn–Teller effect on the 5E term of Fe^{2+} has been studied by several authors^{30–32}. Generally speaking, modifications of the 5E energy structure due to electron–phonon interaction depend on the coupling phonon energy. If the phonon interaction is larger than the spin–orbital splitting of the 5E term, the main effect of the Jahn–Teller effect is a reduction of the energy intervals between the 5E term levels³². This reduction, however, can be accounted for by a small change in the crystal–field and spin–orbit parameters and is thus not very apparent. Only if the phonon energy is small enough (in practice smaller than spin–orbital splitting of the 5E term), this electron–phonon coupling modifies the energy levels seriously³⁰. In particular, new energy levels appear in the energy spectrum as a result of coupling of 0,1,2, phonons to the electronic levels³⁰. For crystals like ZnS or ZnSe, phonons which can couple to the electronic states [TA(L)] have sufficiently high energies³⁴ and produce no noticeable effects. The far–infrared spectroscopic data for ZnS:Fe and $\text{Zn}_{1-x}\text{Fe}_x\text{Se}$ can be satisfactorily described by considering only the crystal–field and spin–orbit interaction³⁵. On the other hand, for instance in CdTe, the TA(L) phonon has an energy small enough (35 cm^{-1}) to modify the energetical structure and optical selection rules considerably³⁰. The reported TA phonon energy for CdSe³⁶ is 43 cm^{-1} , which is a considerably smaller value than the total splitting of the 5E term, suggesting that the Jahn–Teller effect should be taken into account for this material. To our knowledge nothing is known about electron–phonon coupling for the 5E term in $\text{Hg}_{1-y}\text{Cd}_y\text{Se}$ or HgSe. Only very recently it was suggested from Mössbauer experiments³⁷ that a Jahn–Teller distortion might be expected for $\text{Hg}_{1-x}\text{Fe}_x\text{Se}$. Since no Jahn–Teller calculations have been reported for CdSe:Fe (in particular, taking into account its hexagonal structure), we performed a simple calculation to demonstrate the influence of "phonon replica" energy levels on the specific heat. We considered five equally spaced Fe electronic levels¹¹, to which up to ten

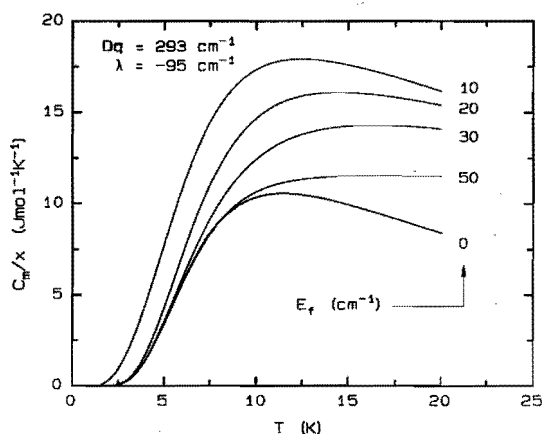


FIG. 13. Influence of additional "phonon-replica" energy levels (simulating the Jahn–Teller effect) on the specific heat in the crystal field model, using $Dq = 293\text{ cm}^{-1}$, $\lambda = -95\text{ cm}^{-1}$.

phonons of energy $h\omega$ can be coupled. For simplicity we assumed no coupling between these vibronic levels, i.e., no true Jahn–Teller effect. The resulting specific heat is shown in Fig. 13 for different phonon energies. As conjectured, the maximal value of the specific heat increases with decreasing phonon energy, i.e., with increasing number of vibronic levels which can be thermally populated. Although the phonon energies, which produce a substantial increase of C_m , are apparently too low as compared to the reported Brillouin–zone–edge TA phonon [43 cm^{-1} (Ref. 36)], one cannot exclude the possibility that phonons over a considerable range inside the entire Brillouin zone contribute to electron–phonon coupling, which may result in smaller "effective phonon" energy. We should stress, however, that these calculations should be regarded only as an illustration suggesting a possible source of the anomalous high specific–heat values. A detailed discussion of this problem requires precise calculations of the Fe^{2+} energy levels with crystal–field, spin–orbit, and Jahn–Teller interactions taken into account. One can, however, expect that for the Fe–Fe pair, such calculations would

lead to rather large Hamiltonian matrices.

Summarizing the remarks listed, we notice that no essential differences are observed for the specific heat for $\text{Hg}_{1-x}\text{Fe}_x\text{Se} - \text{Hg}_{1-x-y}\text{Cd}_y\text{Fe}_x\text{Se} - \text{Cd}_{1-x}\text{Fe}_x\text{Se}$ series. The general behavior of $C_m(\text{Hg}_{1-x-y}\text{Cd}_y\text{Fe}_x\text{Se})$ is also similar to that found for $\text{Zn}_{1-x}\text{Fe}_x\text{Se}^{14}$. Recent analysis of the magnetic susceptibility of $\text{Hg}_{1-x}\text{Fe}_x\text{Se}$ (Ref. 17) shows that the reported Brillouin-type behavior in Ref. 8 is mainly due to the presence of Fe^{3+} ions in all the investigated $\text{Hg}_{1-x}\text{Fe}_x\text{Se}$ crystals: a result of self-ionization of Fe^{2+} ions⁴. Fe^{3+} ions have a d^5 electronic configuration (the same as Mn^{2+} ions) resulting in a Curie-type susceptibility. Although the concentration of Fe^{3+} ions is small [$n = 5 \cdot 10^{18} \text{ cm}^{-3}$, constant for all $x > 0.01$ (Refs. 4 and 5)], their contribution to the total susceptibility may be dominant at low temperatures ($T < 3 \text{ K}$) and may completely mask the Van Vleck-type temperature-independent susceptibility of Fe^{2+} ions. In Ref. 17 it was shown that below 3–4 K, the temperature-dependent susceptibility is independent of the Fe concentration and can be well described as the Curie-type susceptibility of $n = 5 \cdot 10^{18} \text{ cm}^{-3} \text{ Fe}^{3+}$ ions. A similar effect was also reported in $\text{Zn}_{1-x}\text{Fe}_x\text{Se}^9$, although in that case the paramagnetic ions were impurities in the material used for crystal growing (mainly Mn^{2+} as detected by electron paramagnetic resonance⁹).

Summarizing our discussion on the results of specific-heat and susceptibility data so far, we are tempted to conclude that these data do not reveal any anomalous behavior which can be related to the location of the Fe^{2+} energy level relative to the band structure. This does not exclude, in principle, hybridization of the resonant Fe^{2+} level with the conduction band⁸, but the effect of such a hybridization does, in our opinion, not manifest itself in the present data. This weak Fe-level dependence may be understood on the basis of recent calculations of the $\text{Cd}_{1-x}\text{Mn}_x\text{Te}$ energy structure³⁸. In Fig. 14 we reproduce a schematic diagram for the d levels in II–VI semiconductors³⁸. In the case of Mn-

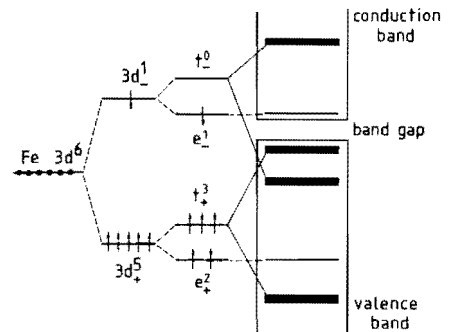


FIG. 14. Schematic representation of the electronic Fe levels within the band structure of a II–VI semiconductor, based on recent calculations on the Mn containing CdTe (Ref. 38).

type DMS (d^5), the five electrons of Mn occupy e , and t , orbitals ($e,^2t,^3$ configuration) located deeply in the valence band. For Fe-type materials (d^6) the additional sixth electron must occupy an e , orbital, yielding a $e,^2t,^3e,^1$ configuration. The reported variation of the Fe-level position with Cd content in $\text{Hg}_{1-x-y}\text{Cd}_y\text{Fe}_x\text{Se}$ (Ref. 5) concerns precisely electrons from the e , orbital. However, e orbitals in tetrahedral crystals hybridize very weakly with p -type bands: they do not form strong σ -type bonds; only weak π -type bonding is formed. Therefore, no first-order effects are expected with variation of the Fe-level position relative to the band structure³⁹. Consequently, we feel confident to assume that the description of the magnetic properties of all the Fe-based DMS investigated so far, can be based in first approximation on a simple "crystal field model"⁷ (eventually augmented by electron-phonon interaction).

In that respect one can now estimate the d - d exchange interaction parameters for the series $\text{Hg}_{1-x-y}\text{Cd}_y\text{Fe}_x\text{Se}$. This can be done using high-temperature series expansion for the magnetic susceptibility developed recently⁴⁰ and based on the "crystal-field model" of Fe-based DMS. In this model the Curie-Weiss temperature determined from high-

temperature susceptibility data, can be expressed as⁴⁰

$$\Theta(x) = \frac{\langle M_z^2 \rangle_\infty \langle E \rangle_\infty - \langle M_z^2 E \rangle_\infty}{\langle M_z^2 \rangle_\infty k_B} (4)$$

$$+ \frac{2 \langle M_z S_z \rangle_\infty^2}{\langle M_z^2 \rangle_\infty} \times \sum_p z_p (J_p / k_B),$$

where $\langle \dots \rangle$ denotes average values of energy (E), magnetic moment (M) and spin (S) operators. J_p is the exchange integral for the p th coordination sphere and z_p is the coordination number. Assuming that the possible electron-phonon interaction does not significantly influence the average values in Eq. 4 and using parameters from Table II, we calculated the nearest-neighbor exchange integrals for the mixed $\text{Hg}_{1-x-y}\text{Cd}_y\text{Fe}_x\text{Se}$ systems from the reported $\Theta(x)$ values^{8,41}. The results are tabulated in Table III.

We should stress that, although crystal field and spin-orbit parameters for $\text{Hg}_{1-x}\text{Fe}_x\text{Se}$ and $\text{Hg}_{1-x-y}\text{Cd}_y\text{Fe}_x\text{Se}$ are not provided by spectroscopic experiments as in the case of $\text{Cd}_{1-x}\text{Fe}_x\text{Se}$ ²¹⁻²⁵, changing these parameter values results only in a very small variation of J_{NN} (significantly smaller than the errors given by the experimental inaccuracy of the Curie-Weiss temperature). Inspection of Table III shows that the d - d exchange interaction for Fe-type DMS is of the same sign (AF) but stronger than the exchange observed in Mn-type materials. The interaction strength is of the same order of magnitude for all the Fe-DMS, although a general trend of increasing interaction while passing from

TABLE II. Parameters for the crystal-field model.

Material	Dq	λ	ν	ν'
$\text{Hg}_{1-x}\text{Fe}_x\text{Se}$	293	-85 .. -95	0	0
$\text{Hg}_{1-x-y}\text{Cd}_y\text{Fe}_x\text{Se}$	280	-80	0	0
$\text{Cd}_{1-x}\text{Fe}_x\text{Se}$	257	-93.8	31	38
$\text{Zn}_{1-x}\text{Fe}_x\text{Se}$	293	-95	0	0 (14)

HgSe to ZnSe is found.

Considering the different possible mechanisms we notice that the dipole-dipole interaction can be effective only at mK temperatures. A Ruderman-Kittel-Kasuya-Yosida interaction⁴⁶ is also ineffective because the concentration of free carriers in Fe-type DMS is too low (similarly as for Mn-type materials). The Bloembergen-Rowland mechanism^{47,48} would yield a strong dependence of exchange on the energy gap of the crystal. In contrast, we observe practically the same strength of exchange in the series $\text{Hg}_{1-x}\text{Fe}_x\text{Se}$ (zero-gap material), $\text{Hg}_{1-x-y}\text{Cd}_y\text{Fe}_x\text{Se}$ (narrow-gap material), $\text{Cd}_{1-x}\text{Fe}_x\text{Se}$, as well as $\text{Zn}_{1-x}\text{Fe}_x\text{Se}$ (both wide-gap crystals) (Table III). Therefore, it seems very likely that also for an Fe-ion system, superexchange^{49,50} is the dominant mechanism of exchange (at least for NN), as was well established in Mn-type DMS^{45,51}. This hypothesis is further supported by the fact that for both Fe- and Mn-ion systems, the major contribution to the exchange comes from the same electrons (Fig. 14).

If superexchange produces the major contribution to the interaction, then the "three-level model" developed for Mn-type

TABLE III. Curie-Weiss temperatures and d - d interaction strength for II-VI Fe-containing DMS; a comparison is made with Mn compounds.

Material	$\Theta(\text{K})$	$J_{\text{NN}}(\text{K})$	$J_{\text{NN}}(\text{Mn})(\text{K})$
$\text{Hg}_{0.99}\text{Fe}_{0.01}\text{Se}$	-9±5 (8)	-18±2	-11 (45), -6 (42)
$\text{Hg}_{0.95}\text{Fe}_{0.05}\text{Se}$	-38±5 (41)	-18±2	-11 (45), -6 (42)
$\text{Hg}_{0.54}\text{Cd}_{0.41}\text{Fe}_{0.05}\text{Se}$	-35±5 (8)	-18±2	
$\text{Cd}_{0.95}\text{Fe}_{0.05}\text{Se}$	-36 (8)	-18.8±2	-9 (43)
$\text{Zn}_{1-x}\text{Fe}_x\text{Se}$		-22±2 (40)	-13 (44)

DMS (Ref. 51) can be also adopted for Fe-type materials giving some insight in chemical trends observed in Table III. The "three-level model" is based on kinetic superexchange^{49,51} and simplifies the actual situation by considering only three levels: the valence band (at energy E_v), the six-electron occupied d level (E_d), and an unoccupied level to which electron from the valence band can be transferred. Such an electron transfer results in an increase of the correlation energy, so a seven-electron configuration has energy $E_d + U$. Thus the analytic expression for J can be written as⁵¹

$$J = -2V_{pd}^4 [(E_d + U - E_v)^{-2}U^{-1} + (E_d + U - E_v)^{-3}] f(R), \quad (5)$$

where V_{pd} is the hybridization parameter describing the probability of a valence band electron hopping to the Fe d level; $f(R)$ describes the dependence on the Fe-Fe distance. The parameter V_{pd} may be related to the s - d exchange constant for the valence band $N_0\beta$ ⁵¹

$$N_0\beta = -2V_{pd}^2[(E_d + U - E_v)^{-1} - (E_d - E_v)^{-1}]. \quad (6)$$

At the moment knowledge about the parameters occurring in Eqs. (5) and (6) is rather poor. In particular, $N_0\beta$ is known only for $\text{Zn}_{1-x}\text{Fe}_x\text{Se}$ (Ref. 9) and $\text{Cd}_{1-x}\text{Fe}_x\text{Se}$ (Ref. 52). For these materials one finds that $N_0\beta$ is larger in $\text{Zn}_{1-x}\text{Fe}_x\text{Se}$ by a factor of 1.3 in respect to $\text{Zn}_{1-x}\text{Mn}_x\text{Se}$ ^{9,53} (1.5 in the case of CdSe). Assuming that this increase of $N_0\beta$ results mainly from a stronger hybridization, one can expect a larger d - d exchange parameter by a factor 1.7 (2.1 for CdSe), which compares favorably with the experimental value for J [$J_{\text{NN}}(\text{Zn}_{1-x}\text{Fe}_x\text{Se}) = -22 \text{ K} \approx 1.7 \times J_{\text{NN}}(\text{Zn}_{1-x}\text{Mn}_x\text{Se})$, $J_{\text{NN}}(\text{Cd}_{1-x}\text{Fe}_x\text{Se}) = -19 \text{ K} \approx 2.1 \times J_{\text{NN}}(\text{Cd}_{1-x}\text{Mn}_x\text{Se})$]. The higher J_{NN} values obtained for HgSe and $\text{Hg}_{1-y}\text{Cd}_y\text{Se}$ with iron suggest a similar situation also for the $\text{Hg}_{1-x-y}\text{Cd}_y\text{Fe}_x\text{Se}$ series. Detailed analysis of the chemical trends in d - d and s - d ex-

change interaction in these materials awaits further study. Magneto-optical experiments providing information about $N_0\beta$ and ultraviolet photoemission studies determining E_d would also be very useful.

IV. CONCLUSIONS

In the present study of the specific heat of $\text{Hg}_{1-x-y}\text{Cd}_y\text{Fe}_x\text{Se}$ DMS we found that all the Fe-type DMS investigated so far demonstrate generally similar magnetic properties, which suggest that the ground state of both the isolated Fe ion and the Fe-Fe pair is a singlet (separated from the excited states by at about 20 cm^{-1} for an isolated ion and 10 cm^{-1} for Fe-Fe pair). Antiferromagnetic coupling between Fe ions is observed. No experimental evidence was found that the magnetic properties of narrow-gap DMS differ from those of wide-gap materials and, consequently, no Fe-level position dependence could be deduced. A simple crystal-field model (eventually complemented by electron-phonon interaction) seems to be sufficient to describe the magnetic properties of all the Fe-type DMS. The d - d exchange parameters for $\text{Hg}_{1-x-y}\text{Cd}_y\text{Fe}_x\text{Se}$ systems are substantially larger than those of $\text{Hg}_{1-x-y}\text{Cd}_y\text{Mn}_x\text{Se}$, in agreement with the situation encountered for $\text{Zn}_{1-x}\text{Fe}_x\text{Se}$ and $\text{Zn}_{1-x}\text{Mn}_x\text{Se}$.

- 1 See, *Diluted Magnetic Semiconductors*, Vol. 25 of *Semiconductors and Semimetals*, edited by J.K. Furdyna and J. Kossut (Academic, New York, 1988); *Diluted Magnetic Semiconductors*, edited by R.L. Aggarwal, J.K. Furdyna and S. von Molnar (Materials Research Society, Pittsburgh, 1987), Vol. 89; J.K. Furdyna, *J. Appl. Phys.* **64**, R29 (1988).
- 2 W.J.M. de Jonge, A. Twardowski and C.J.M. Denissen in *Diluted Magnetic Semiconductors*, edited by R.L. Aggarwal, J.K. Furdyna and S. von Molnar (Materials Research Society, Pittsburgh, 1987), Vol. 89, p.156.
- 3 A. Twardowski, H.J.M. Swagten, W.J.M. de Jonge and M. Demianiuk, *Phys. Rev. B* **36**,

- 7013 (1987).
- 4 See the review papers, A. Mycielski, *J. Appl. Phys.* **63**, 3279 (1988); A. Twardowski, *J. Appl. Phys.* **67**, 5108 (1990).
 - 5 A. Mycielski, P. Dąwionkowski, B. Kowalski, B.A. Orlowski, M. Dobrowolska, M. Arciszewska, W. Dobrowolski and J.M. Baranowski, *J. Phys. C* **19**, 3605 (1986).
 - 6 A. Twardowski, M. von Ortenberg and M. Demianiuk, *J. Cryst. Growth* **72**, 401 (1985).
 - 7 A. Twardowski, H.J.M. Swagten, T.F.H. v.d. Wetering and W.J.M. de Jonge, *Solid State Commun.* **65**, 235 (1988).
 - 8 A. Lewicki, J. Spalek and A. Mycielski, *J. Phys. C* **20**, 2005 (1987).
 - 9 A. Twardowski, P. Glod, W.J.M. de Jonge and M. Demianiuk, *Solid State Commun.* **64**, 63 (1987).
 - 10 D. Heiman, A. Petrou, S.H. Bloom, Y. Shapira, E.D. Isaacs and W. Giriat, *Phys. Rev. Lett.* **60** (18), 1876 (1988).
 - 11 W. Low and M. Weger, *Phys. Rev.* **118**, 1119 (1960).
 - 12 G.A. Slack, S. Roberts and J.T. Wallin, *Phys. Rev.* **187**, 511 (1969).
 - 13 J. Mahoney, C. Lin, W. Brumage and F. Dorman, *J. Chem. Phys.* **53**, 4386 (1970).
 - 14 H.J.M. Swagten, A. Twardowski, W.J.M. de Jonge and M. Demianiuk, *Phys. Rev. B* **39**, 2568 (1989).
 - 15 A. Lewicki and A. Kozłowski, *Acta Phys. Pol. A* **73**, 435 (1988).
 - 16 H.J.M. Swagten, F.A. Arnouts, A. Twardowski, W.J.M. de Jonge and A. Mycielski, *Solid State Commun.* **69**, 1047 (1989).
 - 17 M. Arciszewska A. Lenard T. Dietl, W. Pleśiewicz, T. Skoskiewicz and W. Dobrowolski, *Acta Phys. Pol. A* **77**, 155 (1990).
 - 18 R.R. Galazka, S. Nagata and P.H. Keesom, *Phys. Rev. B* **22**, 3344 (1980).
 - 19 K. Matho, *J. Low Temp. Phys.* **35**, 165 (1979).
 - 20 C.J.M. Denissen, H. Nishihara, J.C. van Gool and W.J.M. de Jonge, *Phys. Rev. B* **33**, 7637 (1986).
 - 21 The "crystal-field" model for hexagonal materials has been recently reported (see Ref. 22) with relatively simple form of the hexagonal term in the Hamiltonian. In this paper we used basically the same model, however, expressing hexagonal distortion in a way more common in the literature (see Ref. 23): $H_1 = -2/3B_4 \times (O_4^0 + 20\sqrt{2}O_4^3) + B_2^0 O_2^0 + B_4^0 O_4^0$, and the z axis was chosen along [111] direction (i.e., parallel to crystal c axis). The presence of trigonal distortion in the Hamiltonian causes splitting of triplets T_1 , T_2 into singlets and doublet ($T_1 - A_2, E$ and $T_2 - A_1, E$) (Ref. 13). Since the Hamiltonian matrix is parametrized by material constants Dq (describing cubic crystal field), ν , ν' (both describing hexagonal distortion), and λ (spin-orbit interaction), the obtained energies can be used for the estimation of these parameters for $\text{Cd}_{1-x}\text{Fe}_x\text{Se}$. We used for that very recent measured energies of optical transition $A_1 \rightarrow A_2$ [13 cm^{-1} (Ref. 24)], $A_1 \rightarrow E$ [17.6 cm^{-1} (Ref. 24)] as well as zero-phonon line energy for ${}^5E \rightarrow {}^5T$ transition [2375 cm^{-1} (Ref. 25)]. The best fit was found for $Dq = 257 \text{ cm}^{-1}$, $\lambda = -93.8 \text{ cm}^{-1}$, $\nu = 31 \text{ cm}^{-1}$ and $\nu' = 38 \text{ cm}^{-1}$.
 - 22 A. Twardowski, *Solid State Commun.* **68**, 1069 (1988).
 - 23 A. Abragam and B. Bleaney, *Electron Paramagnetic Resonance of Transition Metal Ions* (Clarendon, Oxford, 1970).
 - 24 D. Scalbert, J. Cernogora, A. Mauger and C. Benoit a la Guillaume, A. Mycielski, *Solid State Commun.* **69**, 453 (1989).
 - 25 M. Arciszewska and A. Mycielski (private communication).
 - 26 Parameters used for this calculation are tabulated in Table II and were chosen for $\text{Cd}_{1-x}\text{Fe}_x\text{Se}$, to fit spectroscopic data, and for $\text{Hg}_{1-x}\text{Fe}_x\text{Se}$ and $\text{Hg}_{1-x-y}\text{Cd}_y\text{Fe}_x\text{Se}$, to provide reasonable description of the low-temperature C_m .
 - 27 One should not be confused by data for higher Fe concentrations, which compares reasonably with the calculations. The calculated specific heat shown in Figs. 6–8 corresponds to the very dilute limit, in which interactions between Fe ions can be neglected. For higher x , AF interaction between Fe ions results in lowering of C_m/x .
 - 28 We notice that an Fe-Fe pair contributes in the same way: $S_{\text{pair}} = \frac{1}{2}R \ln(10 \times 10) = R \ln 10$.
 - 29 M.D. Sturge in *Solid State Physics*, edited by F. Seitz, D. Turnbull and H. Ehrenreich (Academic, New York, 1967), Vol. 20.

- 30 J.T. Vallin, Phys. Rev. B **2**, 2390 (1970).
- 31 G.A. Slack, S. Roberts and F.S. Ham, Phys. Rev. **155**, 170 (1967).
- 32 G.A. Slack, F.S. Ham and R.M. Chrenko, Phys. Rev. **152**, 376 (1966).
- 33 D. Buhmann, H.J. Schultz and M. Thiede, Phys. Rev. B **24**, 6221 (1981).
- 34 J.C. Irvin and J. LaCombe, Can. J. Phys. **50**, 2596 (1972)
- 35 A.M. Witowski, A. Twardowski, M. Pohlmann, W.J.M. de Jonge, A. Wieck, A. Mycielski and M. Demianiuk, Solid State Commun. **70**, 27 (1989).
- 36 R. Beserman, Solid State Commun. **23**, 323 (1977).
- 37 I. Nowik, E.R. Bauminger, A. Mycielski and H. Szymczak, Physica B **153**, 215 (1988).
- 38 Su-Huai Wei and A. Zunger, Phys. Rev. B **35**, 2340 (1987).
- 39 It is worthwhile to notice then, that in both Mn-type and Fe-type DMS, the same electrons (occupying t_+ orbital) are responsible for $s-d$ interaction.
- 40 A. Twardowski, A. Lewicki, M. Arciszewska, W.J.M. de Jonge, H.J.M. Swagten and M. Demianiuk, Phys. Rev. B **38**, 10749 (1988).
- 41 J. Spalek (private communication).
- 42 R.R. Galazka, W. Dobrowolski, J.P. Lascaray, M. Nawrocki, A. Bruno, J.M. Broto, J.C. Ouset, J. Mag. Mag. Mater. **72**, 174 (1988).
- 43 R.L. Aggarwal, S.N. Jaspersen, Y. Shapira, S. Foner, T. Sakibara, T. Goto, N. Miura, K. Dwight and A. Wold, in *Proceedings of the 17th International Conference of the Physics of Semiconductors*, San Francisco, 1984, edited by J.D. Chadi and W.A. Harrison (Springer, New York, 1985), p. 1419.
- 43 T.M. Giebultowicz, J.J. Rhyne, J.K. Furdyna, J. Appl. Phys. **61**, 3537 (1987); **61**, 3540 (1987).
- 44 J. Spalek, A. Lewicki, Z. Tarnawski, J.K. Furdyna, R.R. Galazka, Z. Obuszko, Phys. Rev. B **33**, 3407 (1986).
- 46 M.A. Ruderman and C. Kittel, Phys. Rev. **96**, 99 (1954); K. Yoshida, Phys. Rev. **106**, 893 (1957); T. Kasuya, Prog. Theor. Phys. **16**, 45 (1956).
- 47 N. Bloembergen and T.J. Rowland, Phys. Rev. **97**, 1679 (1955).
- 48 C. Lewiner and G. Bastard, J. Phys. C **13**, 2347 (1980); C. Lewiner, J.A. Gaj and G. Bastard, J. Phys. (Paris) Colloq. **41**, C5-289 (1980).
- 49 P.W. Anderson in *Solid State Physics* **14**, 99 (1963), edited by F. Seitz and D. Turnbull (Academic, New York, 1963), Vol. 14, p. 99.
- 50 G.A. Sawatzky, W. Geertsma and C. Hass, J. Magn. Magn. Mater. **3**, 37 (1976); C.E.T. Goncalves da Silva and L.M. Falicov, J. Phys. C **5**, 63 (1972).
- 51 B.E. Larson, K.C. Hass, H. Ehrenreich and A.E. Carlsson, Solid State Commun. **56**, 347 (1985); Phys. Rev. B **37**, 4137 (1988).
- 52 A. Twardowski, K. Pakula, M. Arciszewska and A. Mycielski, Solid State Commun. **73**, 601 (1990).
- 53 A. Twardowski, in *Diluted Magnetic Semiconductors*, edited by M. Jain (World Scientific, Singapore, 1990).

Chapter III, paragraph 3

Magnetic susceptibility of iron - based semimagnetic semiconductors: High - temperature regime

[published in Phys. Rev. B 38, 10749 (1988)]

I. INTRODUCTION

Semimagnetic semiconductors (SMSC) or diluted magnetic semiconductors¹ are materials based on the well known II-VI or II-V compounds in which some cations are substituted by magnetic ions. The concentration of magnetic ions can be controlled in a very wide range (from doped to mixed crystals) which allows one to study in one material both the very dilute and highly concentrated regimes. Because of that, these alloys have attracted considerable attention during the last decade and interesting magneto-optical and magnetic properties were reported¹. The strong *s-d* exchange interaction between band electrons and localized *d* electrons of the magnetic ions results in effects like giant free-exciton Zeeman splitting or formation of magnetic polaron. On the other hand, due to the antiferromagnetic *d-d* interaction between magnetic ions, various magnetic phases (paramagnetic, spin-glass and antiferromagnetic) were found, depending on the concentration and temperature range.

So far, most of the studies were devoted to manganese-based SMSC, such as $\text{Cd}_{1-x}\text{Mn}_x\text{Te}$, $\text{Hg}_{1-x}\text{Mn}_x\text{Te}$ or $\text{Zn}_{1-x}\text{Mn}_x\text{Se}$. From a magnetic point of view these materials are particular since Mn^{2+} has a d^5 electronic configuration resulting in a spin-only ground state since the orbital momentum is zero. Only recently, more attention has been focused on iron-based SMSC ($\text{Hg}_{1-x}\text{Fe}_x\text{Se}$, $\text{Zn}_{1-x}\text{Fe}_x\text{Se}$ or $\text{Cd}_{1-x}\text{Fe}_x\text{Se}$)², which can be considered as examples of a more general

magnetic situation, because Fe^{2+} possesses both spin and orbital momenta ($S = 2$ and $L = 2$)³⁻⁵.

Although some attempts to understand the magnetic behavior of these compounds were already reported⁶⁻⁸, crucial information about the Fe-Fe interaction (strength and range) is still lacking. The only estimate for the nearest-neighbors interaction (J_{NN}) is derived from the high-temperature susceptibility⁸ assuming $L = 0$. We therefore thought it worthwhile to study the $L \neq 0$ case more carefully in order to be able to evaluate the *d-d* exchange parameters more reliable. We also report in this paper new results of the magnetic susceptibility of $\text{Zn}_{1-x}\text{Fe}_x\text{Se}$ in the temperature range 2 - 300 K. Finally, we reexamine previous results⁸ for $\text{Cd}_{1-x}\text{Fe}_x\text{Se}$.

II. DERIVATION OF THE HIGH-TEMPERATURE SUSCEPTIBILITY FOR $L \neq 0$

In this section we calculate the high-temperature expansion (HTE) of the static magnetic susceptibility following the method applied in Ref. 9 for the spin-only case ($L = 0$). We obtain a Curie-Weiss law for the general case of magnetic ions with both $S \neq 0$ and $L \neq 0$, resulting in a relationship between macroscopic parameters such as the Curie constant, the Curie-Weiss temperature, the magnetic ion concentration x , and *d-d* exchange integrals. Assuming that magnetic ions interact isotropically with each other via spin momenta, the Hamiltonian for

a random, dilute system can be expressed in the following way:

$$\mathcal{H} = -\frac{1}{2} \sum_{i,j} 2J_{ij} \mathbf{S}_i \cdot \mathbf{S}_j \xi_i \xi_j + \mu_B B_z \sum_i (L_{zi} + gS_{zi}) \xi_i + \sum_i H_{cfi} \xi_i + \sum_i \lambda \mathbf{L}_i \cdot \mathbf{S}_i \xi_i , \quad (1)$$

where sums over i and j run over all lattice sites ($i \neq j$), and ξ_i is 0 or 1, depending on whether the cation site is occupied by a nonmagnetic (Zn, Cd or Hg) or a magnetic ion, respectively. \mathbf{S}_i , \mathbf{L}_i are the atomic-spin and orbital-momenta operators, respectively. The first term in Hamiltonian (1) describes the d - d exchange interaction (J_{ij} is the exchange integral), the second the influence of the magnetic field, the third the crystal-field splitting and the last the spin-orbit interaction. A given sequence $\{\xi_i\}$ determines a specific distribution of magnetic ions on the lattice sites. The static susceptibility per unit volume is defined by:

$$\chi_v = -\frac{1}{V} \left[\frac{\partial^2 F}{\partial B_z^2} \right] T , \quad (2)$$

where V is the volume of the system and F is its free energy, given by

$$F = -k_B T \sum_{\{\xi\}} P(\{\xi_i, \dots, \xi_N\}) \ln \text{Tr} e^{-\beta H} = -k_B T \overline{\ln Z} . \quad (3)$$

In this expression $P(\{\xi_i, \dots, \xi_N\})$ is the probability distribution of a given sequence $(\xi_1, \xi_2, \dots, \xi_N)$, Tr denotes trace, Z is the partition function for a particular configuration $\{\xi_1, \dots, \xi_N\}$, $(\overline{\quad})$ means averaging over configurations and $\beta = 1/k_B T$.

In the high-temperature regime the partition function Z can be expanded as follows:

$$Z = \text{Tr} e^{-\beta H} \approx \text{Tr}(1 - \beta H + \beta^2 H^2/2 - \beta^3 H^3/6) . \quad (4)$$

Performing double derivation of free energy (3), one finds

$$\chi = \frac{k_B T}{V} \left[\frac{1}{Z} \frac{\partial^2 Z}{\partial B_z^2} - \left[\frac{1}{Z} \frac{\partial Z}{\partial B_z} \right]^2 \right] , \text{ and} \quad (5)$$

$$\frac{\partial Z}{\partial B_z} = -\beta \text{Tr} M + \beta^2 \text{Tr}(MH) - \beta^3 \text{Tr}(MH^2)/2 , \quad (6)$$

$$\frac{\partial^2 Z}{\partial B_z^2} = \beta^2 \text{Tr}(M^2) - \beta^3 \text{Tr}(M^2 H) , \quad (7)$$

where we introduced $M \equiv \partial H / \partial B_z$ and used the relation $\text{Tr}(ABC) = \text{Tr}(BCA) = \text{Tr}(CAB)$. Substituting (6) and (7) into (5) yields, to first order in H ,

$$\chi = \frac{\beta}{V} \left[\frac{\text{Tr}(M^2)}{\text{Tr} 1} + \beta \frac{\text{Tr}(M^2) \text{Tr}(H)}{\text{Tr} 1 \text{Tr} 1} - \beta \frac{\text{Tr}(M^2 H)}{\text{Tr} 1} - \frac{[\text{Tr} M]^2}{[\text{Tr} 1]^2} \right. \\ \left. - 2\beta \frac{\text{Tr} M}{\text{Tr} 1} \left[\frac{\text{Tr}(M) \text{Tr}(H)}{\text{Tr} 1 \text{Tr} 1} - \frac{\text{Tr}(MH)}{\text{Tr} 1} \right] \right] \quad (8)$$

$$= (\beta/V) \left(\langle M^2 \rangle_\infty + \beta \langle M^2 \rangle_\infty \langle H \rangle_\infty - \beta \langle M^2 H \rangle_\infty - \langle M \rangle_\infty^2 \right. \\ \left. - 2\beta \langle M \rangle_\infty^2 \langle H \rangle_\infty + 2\beta \langle M \rangle_\infty \langle MH \rangle_\infty \right),$$

where $\langle A \rangle_\infty = \text{Tr}(A)/\text{Tr}1$ means the statistical average taken at infinite temperature. The advantage of using $\langle \dots \rangle_\infty$ is that as $T \rightarrow \infty$ magnetic moments on different sites ($i \neq j$) can be regarded as independent and averages $\langle \dots \rangle_\infty$ in (8) can be expressed by single-ion averages. Noting that $\langle M \rangle \rightarrow 0$ as $B \rightarrow 0$ and $T \rightarrow \infty$, we finally obtain the high-temperature, zero-field susceptibility:

$$\chi = (\beta/V) \left[\langle M^2 \rangle_\infty + \beta \langle M^2 \rangle_\infty \langle H \rangle_\infty - \beta \langle M^2 H \rangle_\infty \right]. \quad (9)$$

One can now evaluate the traces in (9) and get

$$\langle M^2 \rangle = \sum_{i,j} \delta_{ij} \langle M_{zi}^2 \rangle_\infty \xi_i,$$

$$\langle M^2 \rangle \langle H \rangle = \sum_{i,j} \left[\delta_{ij} \langle M_{zi}^2 \rangle_\infty (\langle E_i \rangle_\infty \xi_i + \sum_{k \neq i} \langle E_k \rangle_\infty \xi_k) \right], \quad (10)$$

$$\langle M^2 H \rangle = \sum_{i,j} \left\{ \delta_{ij} \left[\langle M_{zi}^2 E_i \rangle_\infty \xi_i + \langle M_{zi}^2 \rangle_\infty \left(\sum_{k \neq i} \langle E_k \rangle_\infty \xi_k \right) \right] + 2J_{ij} \xi_i \xi_j \langle M_{zi} S_{zj} \rangle_\infty^2 \right\},$$

where $E_i = \lambda L_i S_i + H_{cfi}$ is the single-ion crystal-field and spin-orbit operator, and $M_{zi} = L_{zi} + gS_{zi}$ is the single ion magnetic moment operator. It follows from (10) and (9) that

$$\chi = (\mu_B^2/k_B TV) \sum_{i,j} \left\{ \delta_{ij} \left[\langle M_{zi}^2 \rangle_\infty + \beta (\langle M_{zi}^2 \rangle_\infty \langle E_i \rangle_\infty - \langle M_{zi}^2 E_i \rangle_\infty) \xi_i \right] + \right. \\ \left. 2\beta J_{ij} \xi_i \xi_j \langle M_{zi} S_{zj} \rangle_\infty^2 \right\}. \quad (11)$$

Performing an averaging over configurations yields

$$\chi = (\mu_B^2/k_B TV) xN \left[\langle M_z^2 \rangle_\infty + \beta (\langle M_z^2 \rangle_\infty \langle E \rangle_\infty - \langle M_z^2 E \rangle_\infty) + 2\beta \langle M_z S_z \rangle_\infty^2 x \sum_p J_p z_p \right], \quad (12)$$

where z_p is the number of cations in the p th coordination sphere and we inserted a random arrangement of magnetic ions, yielding

$$\xi_i \xi_j = \begin{cases} \overline{\xi_i^2} = \overline{\xi_i} = x & \text{for } i = j, \\ \overline{\xi_i \xi_j} = x^2 & \text{for } i \neq j. \end{cases} \quad (13)$$

Equation (12) can be expressed as follows:

$$\chi = \frac{\mu_B^2}{k_B TV} xN \langle M_z^2 \rangle_\infty \left[1 + \frac{\langle M_z^2 \rangle_\infty \langle E \rangle_\infty - \langle M_z^2 E \rangle_\infty}{\langle M_z^2 \rangle_\infty} + \frac{2\langle M_z S_z \rangle_\infty^2}{\langle M_z^2 \rangle_\infty} x \sum_p J_p z_p \right] \quad (14)$$

and for high temperatures can be expanded as a Curie–Weiss law $C(x)/[T-\Theta(x)]$ with Curie constant

$$C(x) = \frac{\mu_B^2 N \langle M_z^2 \rangle_\infty}{k_B V} x = C_0 x \quad (15)$$

and a Curie–Weiss temperature

$$\begin{aligned} \Theta(x) &= \frac{\langle M_z^2 \rangle_\infty \langle E \rangle_\infty - \langle M_z^2 E \rangle_\infty}{\langle M_z^2 \rangle_\infty k_B} \\ &+ \frac{2 \langle M_z S_z \rangle_\infty^2}{\langle M_z^2 \rangle_\infty} x \sum_p z_p (J_p/k_B) \\ &= A + \Theta_0 x, \end{aligned} \quad (16)$$

which reduces to a standard HTE (Ref. 9) for $L = 0$. If the distribution of magnetic ions is truly random [Eq. (3)], then both the Curie constant and the Curie–Weiss temperature are a linear function of temperature. However — in distinction from the spin-only case⁹ — the Curie–Weiss temperature may be nonzero even for $x \rightarrow 0$ (noninteracting ions). The values of averages in (12) and (13) can be evaluated for a particular ion in a particular crystal field if the ion eigenfunctions are known. We will return to this point for Fe^{2+} in the Discussion.

III. EXPERIMENTAL RESULTS

We have measured the magnetic susceptibility per unit mass χ_m [related to Eq. (2) by $\chi_m = \chi_v/\rho$, ρ being density of the crystal] of $\text{Zn}_{1-x}\text{Fe}_x\text{Se}$, with $x = 0.022 \pm 0.002$, 0.049 ± 0.003 , 0.057 ± 0.003 , and 0.072 ± 0.005 as checked by microprobe analysis. χ_m was studied in the temperature range 2–300 K, in two stages. Below 77 K we used a standard ac mutual inductance method, whereas above 77 K the Faraday method was applied. In the latter case the magnetization M_m of the samples was measured, which was found to depend linearly on the magnetic field up to 1 T. The susceptibility was obtained from the relation $\chi = M_m/B$. All the data were corrected for the diamagnetic susceptibility of ZnSe ($\chi_d = -0.32 \cdot 10^{-6}$ emu/g)¹⁰.

The results are shown in Fig. 1, where

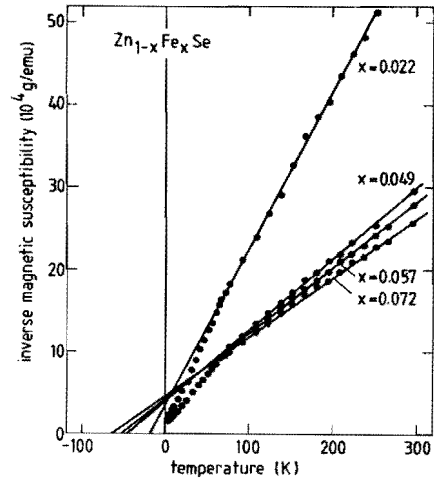


FIG. 1. Inverse magnetic susceptibility of $\text{Zn}_{1-x}\text{Fe}_x\text{Se}$ as a function of temperature. Straight lines show Curie–Weiss law with parameters according to Table I.

the inverse susceptibility is plotted versus temperature. For clarity of the figure the low-temperature part (below 77 K) is shown only for $x = 0.022$ and 0.072 . At high temperatures all the samples reveal a typical Curie–Weiss behavior with a negative Curie–Weiss temperature. These temperatures $\Theta(x)$, as determined from extrapolation of χ_m^{-1} versus T , are tabulated in Table I. Below ≈ 70 K a well-pronounced downward bending of χ_m^{-1} can be observed. This bending — as distinct from Mn-based materials¹¹ — changes its slope as $T \rightarrow 0$, although even at the lowest measured temperatures no temperature-independent χ_m^{-1} is observed (i.e., typical Van Vleck-type behavior is absent). This is in agreement with our previous results¹² and is probably due to paramagnetic impurities present in the source iron material used for crystal growing¹². The deviation from Van Vleck-type behavior in the low-temperature range seems to be proportional to the iron content, which corroborates such an assumption.

IV. DISCUSSION

A. High-temperature susceptibility

The behavior of the experimental data presented above as $\chi_m(T)$ in the range of high temperatures may be compared with the results of HTE as derived in Sec. II. In Fig. 2, $\Theta(x)$ and $C(x)$ are shown as functions of x . Both quantities are proportional with concentration x , in agreement with Eqs. (15) and (16). Moreover, the Curie-Weiss temperature tends to zero (within experimental accuracy) as $x \rightarrow 0$ suggesting that parameter A from Eq. (16) vanishes in our case. The detailed fit of the data presented in Fig. 2 by Eqs. (15) and (16) yields the following values: $C_0 =$

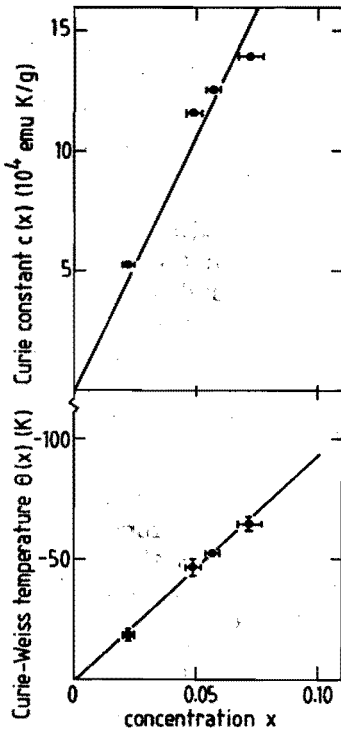


FIG. 2. Concentration dependence of the Curie constant $C(x)$ and the Curie-Weiss temperature $\Theta(x)$ of $\text{Zn}_{1-x}\text{Fe}_x\text{Se}$. Solid lines represent $C_0 = 212 \cdot 10^4$ emuK/g and $\Theta(x) = +(0.85 - 920x)$ K.

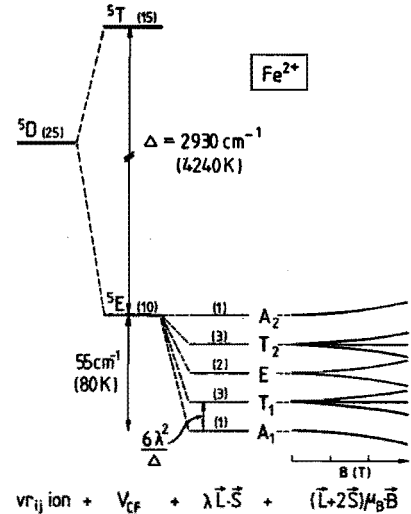


FIG. 3. Energy-level diagram for an isolated Fe^{2+} ion. Effects of crystal field, spin-orbit interaction and magnetic field are shown (not to scale).

$(212 \pm 40) \cdot 10^4$ emuK/g, ($\langle M_z^2 \rangle = 7.6$), $A = +0.85 \pm 2.7$ K and $\Theta_0 = -920 \pm 54$ K. A negative value of Θ_0 indicates a negative $d-d$ exchange integral J , i.e., antiferromagnetic coupling.

In order to obtain more detailed information from the evaluated parameters, one has to calculate averages $\langle \dots \rangle_\infty$ present in Eqs. (15) and (16). We performed these calculations, using the Fe^{2+} single-ion wave functions as proposed by Slack *et al.*⁴ with the parameters obtained⁵ for ZnSe:Fe , crystal-field splitting $10Dq = 2930 \text{ cm}^{-1}$ and spin-orbit coupling $\lambda = -85 \text{ cm}^{-1}$.

The summation in the average $\langle \dots \rangle_\infty$ is performed over all states originating from the ground 5E term. The other states originating from the first-excited term (5T) can be omitted since the separations from the ground state is 4000 K (Fig. 3). The regime we are considering is therefore a high-temperature regime relative to the (split) 5E ground state and, at the same time, a low-temperature regime in respect to crystal-field splitting. We obtained the following values:

TABLE I. Relevant parameters for $\text{Zn}_{1-x}\text{Fe}_x\text{Se}$ and $\text{Cd}_{1-x}\text{Fe}_x\text{Se}$.

Material	x	C (10^4 emuK/g)	Θ (K)	$\langle M_z^2 \rangle$
$\text{Zn}_{1-x}\text{Fe}_x\text{Se}$	0.022	5.25±0.1	-18.5±2.1	9.2
	0.049	11.60±0.1	-46.5±3.5	9.1
	0.057	12.53±0.1	-52.2±1.3	8.4
	0.072	13.93±0.2	-64.5±2.5	7.4
$\text{Cd}_{1-x}\text{Fe}_x\text{Se}$	0.05		-36±6	$\frac{1}{2}g^2 S_{\text{eff}}(S_{\text{eff}}+1)$ 10.6 (Ref. 8)
	0.15		-102±8	10.1 (Ref. 8)

$$\langle M_z^2 \rangle_{\infty} = 10.89 ,$$

$$\langle E \rangle_{\infty} = -11.71 \lambda^2 / 10Dq$$

(is the mean energy of the 5E term) (17)

$$\langle M_z^2 E \rangle_{\infty} = -130.76 \lambda^2 / 10Dq ,$$

$$\langle M_z S_z \rangle_{\infty} = 4.22 .$$

We first notice that the calculated $\langle M_z^2 \rangle_{\infty}$ value is larger than that obtained from the experimental Curie constant. Such an effect is not unique for $\text{Zn}_{1-x}\text{Fe}_x\text{Se}$ and was observed previously also in Mn^{2+} -based SMSC¹³. Although this reduction can be attributed to some physical mechanisms^{13,9} it may also be due to the simplicity of our model. In particular, one should remember that we assumed infinite temperature deriving Eqs. (12)–(16). Although the experimental Curie–Weiss temperatures are smaller than our temperature range, they are not negligible even compared to the highest temperatures at which χ_m was obtained (cf. Table I). One can therefore expect that spins in different lattice sites are not completely independent, which means that the average $\langle M_{z_i} M_{z_j} \rangle_{\infty}$, which defines the Curie constant, is smaller than $\langle M_{z_i}^2 \rangle_{\infty}$. This effect should increase with increasing concentration of magnetic ions. Inspection of Table I seems to reveal such a tendency. The question now arises whether this mismatch also may affect the reliability of the values which can be obtained for J_p and A , in which averages like

$\langle M_z^2 \rangle_{\infty}$ also play a role [see Eqs. (15) and (16)]. One has to recall, however, that J_p and A (through Θ_0) are given by ratios like $\langle M_z^2 E \rangle_{\infty} / \langle M_z^2 \rangle_{\infty}$ or $\langle M_z S_z \rangle_{\infty}^2 / \langle M_z^2 \rangle_{\infty}$. It seems likely that these ratios, since they contain similar expectation values in both nominator and denominator, are less sensitive for these deviations. This is demonstrated by the fact that parameter A resulting from (16) ($A = +1.07$ K) is indeed very small, in agreement with the experimental observation ($A = +0.85 \pm 2.7$ K). Combining now the experimental Curie–Weiss temperature Θ_0 with (16) and (17), one is able to determine the d – d exchange constant:

$$\sum_p z_p J_p / k_B = -281 \pm 17 \text{ K} , \quad (18)$$

which gives the upper estimate of the nearest-neighbors interaction $|J_{NN}/k_B| < 23.5$ K. Assuming the same distance dependence of the interaction as observed in $\text{Zn}_{1-x}\text{Mn}_x\text{Se}$ and related compounds¹⁴: $J_p = J_{NN}/R_p^{5.8}$, where R_p is the radius of p th coordination sphere (in units of R_{NN}), we find that

$$\sum_p z_p J_p / k_B = (z_{NN} J_{NN} / k_B) 1.09 , \quad (19)$$

which results in $J_{NN}/k_B = -22 \pm 1$ K. This is a much higher value than was found¹⁵ for $\text{Zn}_{1-x}\text{Mn}_x\text{Se}$ ($J_{NN}/k_B = -12.6$ K).

A similar analysis can be performed for the other Fe-based SMSC, in particular for $\text{Cd}_{1-x}\text{Fe}_x\text{Se}$, for which susceptibility data are

available⁸ (see Table I). $\text{Cd}_{1-x}\text{Fe}_x\text{Se}$ crystallizes in hcp structure, which results in lowering of the cubic symmetry, and consequently, the threefold degeneracy of T_1 and T_2 levels is removed. In order to account for this effect, we completed single-ion crystal-field Hamiltonian H_{cf} by the trigonal distortion term $C_p(z^2 - \frac{1}{3}r^2)$. Assuming⁵ for $\text{Cd}_{1-x}\text{Fe}_x\text{Se}$ $= -81 \text{ cm}^{-1}$, $10Dq = 2680 \text{ cm}^{-1}$, and²⁷ $C_p = 30 \text{ cm}^{-1}$, we obtain

$$\langle M_z^2 \rangle_{\infty} = 10.95$$

[to be compared with the experimental value $g^2 S_{\text{eff}}(S_{\text{eff}}+1)/3$ from Table I],

$$\langle E \rangle_{\infty} = -11.71 \lambda^2 / 10Dq, \quad (20)$$

$$\langle M_z^2 E \rangle_{\infty} = -132.48 \lambda^2 / 10Dq,$$

$$\langle M_z S_z \rangle_{\infty} = 4.24.$$

In this case the calculated value for $\langle M_z^2 \rangle_{\infty}$ is in perfect agreement with experimental data (cf. Table I). However, we believe this agreement may be rather accidental, especially for $x = 0.15$, for which the reported Curie-Weiss temperature is -102 K , since the experimental temperature range from which the data were obtained cannot be considered as the high-temperature limit.

It follows in this case from (20) that $A = 1.4 \text{ K}$, which results in $\sum_p z_p J_p / k_B = -228 \pm 37 \text{ K}$. Assuming again the relation $J_p = J_{\text{NN}} / R_p^{6,8}$, one obtains $J_{\text{NN}} / k_B = -17.8 \pm 3 \text{ K}$ for $\text{Cd}_{1-x}\text{Fe}_x\text{Se}$, which is also appreciable higher than reported⁹ for $\text{Cd}_{1-x}\text{Mn}_x\text{Se}$ (-10.6 K).

In a previous analysis the value for the integral in $\text{Cd}_{1-x}\text{Fe}_x\text{Se}$ was reported⁸ to be $J_{\text{NN}} / k_B = -11 \text{ K}$. The difference between our result and this value is a direct consequence of using the *spin-only* high-temperature series expansion in the latter case, where it is not applicable. The smaller value for J_{NN} obtained by this procedure may be understood by the following reasoning. While using the spin-only model^{9,8}, one usually rewrites Eq. (15) in the form:

$$C(x) = (\mu_B g)^2 S_{\text{eff}}(S_{\text{eff}}+1) N x / 3k_B V, \quad (21)$$

where S_{eff} is the so-called effective spin and is derived from the experimental value $C(x)$. Thus the factor $\frac{1}{3} g^2 S_{\text{eff}}(S_{\text{eff}}+1)$ plays the same role as $\langle M_z^2 \rangle_{\infty}$, and $g S_{\text{eff}}$ can be regarded as an effective magnetic moment. This magnetic moment, furthermore, is used to determine the exchange integrals [from relation (16) substituting S_{eff} for S and $L = 0$]. Roughly speaking, one implicitly assumes in such a procedure that the magnetic ions interact via the total magnetic momenta and not by the spins only [cf. Eq. (1)]. In that respect the lower value of J produced by the spin-only model can be understood: Since the susceptibility is a response of the magnetic moments to the experiencing magnetic field [Eq. (9)], a weaker interaction is needed between magnetic moments (composed of both spin and orbital momenta) than between spins only to obtain the same effect on the susceptibility (Curie-Weiss temperature).

It should be stressed, however, that although we prefer ion-ion interaction via spin momenta instead of full magnetic momenta, the Heisenberg Hamiltonian used in (1) is one of the simplest possibilities to describe the magnetic interactions. Further experiments are needed to confirm our assumption or to establish a proper Hamiltonian.

B. Low-temperature susceptibility

Having determined the $d-d$ exchange integral, one can describe the high-temperature as well as the low-temperature susceptibility by applying the method proposed recently by us for iron-type SMSC⁷. This method is based on solving numerically the Fe-Fe pair eigenproblem [i.e., Hamiltonian (1) with $i, j = 1, 2$], which allows one to calculate the Fe-Fe pair partition function and the susceptibility. The susceptibility of the whole crystal is calculated in extended nearest-neighbor pair approximation (ENNPA), which is an approximative calculation method, particularly useful for random, diluted alloys with long-ranged interaction¹³.

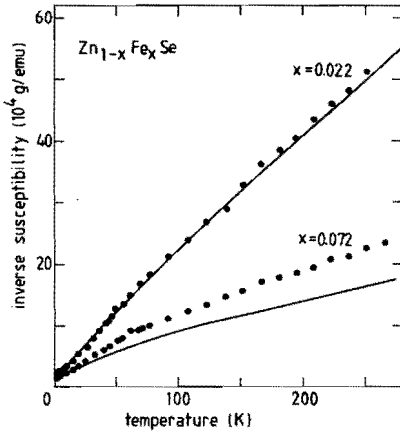


FIG. 4. Inverse magnetic susceptibility of $Zn_{1-x}Fe_xSe$ as a function of temperature. Solid lines represent the ENNPA calculations with parameters $J_{NN} = -22$ K, $J_D = J_{NN}/R_p^{6,8}$, $10Dq = 2930$ cm $^{-1}$ and $\lambda = -85$ cm $^{-1}$.

^{14,17}. This method is based on the assumption that the partition function of the system can be factorized into contributions of pairs of ions. In the ENNPA each ion is considered to be coupled by an exchange interaction J_L only to its nearest magnetic neighbor, which may be located anywhere at the distance R_L from a reference site. The statistical weight $[P_L(x)]$ of pair configurations with various R_L is assumed to be determined by the random distribution of the ions. Knowing the susceptibility of an Fe pair, coupled by an exchange integral J_L , one can evaluate the susceptibility of the whole crystal as

$$\chi = \sum_L \frac{1}{2} \chi_L(J_L) P_L(x) ,$$

where the summation is performed until 98% of the pairs are included. For more details of the calculations we refer to Ref. 7.

Results of our calculations for $Zn_{1-x}Fe_xSe$ ($x = 0.022$ and $x = 0.072$) are shown in Fig. 4. Fairly good agreement between the experimental and calculated susceptibility is

observed for $x = 0.022$, whereas a substantial discrepancy exist for $x = 0.072$. We should stress, however, that for $x = 0.072$, the dilute limit as considered in the ENNPA, may not be approached. In fact, in all the cases when the ENNPA was applied for SMSC, a reasonable description of the experimental data was obtained only for low concentrations ($x < 0.05$)^{13,14}. We therefore find the situation presented in Fig. 4 quite satisfactory.

V. CONCLUSIONS

We generalized the high-temperature expansion of the magnetic susceptibility of SMSC for the case of magnetic ions with non-vanishing orbital momenta. We obtained a Curie-Weiss law with Curie constant and Curie-Weiss temperature linearly dependent on the concentration of the magnetic ions. This result is in agreement with high-temperature experimental data for $Zn_{1-x}Fe_xSe$ and $Cd_{1-x}Fe_xSe$. From the Curie-Weiss temperature we estimated the exchange integrals $J_{NN}/k_B = -22$ K for $Zn_{1-x}Fe_xSe$ and $J_{NN}/k_B = -17.8$ K for $Cd_{1-x}Fe_xSe$, which are both systematically higher than those observed in the corresponding Mn compounds. Using these exchange constants, we were able to fit the susceptibility in the whole temperature range by applying the ENNPA.

- 1 N.B. Brandt and V.V. Moshalkov, *Adv. Phys.* **33**, 193 (1984), J.K. Furdyna, *J. Appl. Phys.* **53**, 8637 (1982), J.A. Gaj, *J. Phys. Soc. Jpn.* **49**, 797 (1980).
- 2 A. Mycielski, in *Diluted Magnetic Semiconductors*, edited by S. von Molnar, R.L. Aggarwal and J.K. Furdyna, (Materials Research Society, Pittsburgh, 1987), Vol. 89, p. 159.
- 3 W. Low and M. Weger, *Phys. Rev.* **118**, 1119 (1960).
- 4 G.A. Slack, S. Roberts and J.T. Wallin, *Phys. Rev.* **187**, 511 (1969).
- 5 J. Mahoney, C. Lin, W. Brumage and F. Dorman, *J. Chem. Phys.*, **53**, 4386 (1970).
- 6 A. Twardowski, M. von Ortenberg and M.

- Demianiuk, J. *Cryst. Growth* **72**, 401 (1985).
- ⁷ A. Twardowski, H.J.M. Swagten, T.F.H. van de Wetering and W.J.M. de Jonge, *Solid State Commun.* **65**, 235 (1988).
- ⁸ A. Lewicki, J. Spalek and A. Mycielski, J. *Phys. C* **20**, 2005 (1987).
- ⁹ J. Spalek, A. Lewicki, Z. Tarnawski, J.K. Furdyna, R.R. Galazka and Z. Obuszko, *Phys. Rev. B* **33**, 3407 (1986).
- ¹⁰ D.J. Chadi, R.M. White and W.A. Harrison, *Phys. Rev. Lett.* **35**, 1372 (1975).
- ¹¹ R.R. Galazka, S. Nagata and P.H. Keesom, *Phys. Rev. B* **22**, 3344 (1980), S. Nagata, R.R. Galazka, D.P. Mullin, H. Arbarzadeh, G.D. Khattak, J.K. Furdyna and P.H. Keesom, *ibid.* **22**, 3331 (1980).
- ¹² A. Twardowski, P. Glod, W.J.M. de Jonge and M. Demianiuk, *Solid State Commun.* **64**, 63 (1987).
- ¹³ C.J.M. Denissen, H. Nishihara, J.C. van Gool and W.J.M. de Jonge, *Phys. Rev. B* **33**, 7637 (1986).
- ¹⁴ A. Twardowski, H.J.M. Swagten, W.J.M. de Jonge and M. Demianiuk, *Phys. Rev. B* **36**, 7013 (1987), W.J.M. de Jonge, A. Twardowski and C.J.M. Denissen, in *Diluted Magnetic Semiconductors*, edited by S. von Molnar, R.L. Aggarwal and J.K. Furdyna, (Materials Research Society, Pittsburgh, 1987), Vol. 89, p. 156.
- ¹⁵ T.M. Giebultowicz, J.J. Rhyne and J.K. Furdyna, *J. Appl. Phys.* **61**, 3537 (1987); **61**, 3540 (1987).
- ¹⁶ Such a value provides a similar T_1 -level splitting as reported (Ref. 5) for CdS:Fe. We should stress, however, that the exchange integral J_{NN} is not very sensitive for C_p : increasing C_p 5 times to 150 cm^{-1} results only in a 3% increase of J_{NN} .
- ¹⁷ K. Matho, *J. Low. Temp. Physics* **35**, 165 (1979).

Chapter III, paragraph 4

Magnetization steps in iron - based diluted magnetic semiconductors

[published in Phys. Rev. B 41, 7330 (1990)]

I. INTRODUCTION

Diluted magnetic semiconductors (DMS) generally consist of a nonmagnetic semiconducting host in which a controlled fraction of cations are replaced by isovalent magnetic ions. Up till recently the investigations were almost exclusively restricted to DMS containing Mn^{2+} as the magnetic ion¹. An increasing number of papers at the moment, however, deal with DMS containing other transition elements, such as Co^{2+} or Fe^{2+} . Magnetically the latter ions represent a more general, though more complex, case since, in addition to the spin, also orbital momenta are involved².

Notwithstanding the increasing number of investigations devoted to these compounds, the experimental status is still somewhat poor. In contrast to Mn DMS, for instance, no experimental data have been reported yet which enable one to determine the nearest-neighbor (NN) interaction strength J_{NN} in a straightforward way. The strength and sign of J_{NN} are of great fundamental interest and are intimately related to the band structure and the location of the electronic levels within the *s* and *p* bands of the anions³. In Fe DMS, to which we will restrict ourselves in this paper, the antiferromagnetic *d-d* interactions have only been estimated experimentally from the high-temperature susceptibility, which includes model-dependent parameters⁴.

For Mn DMS the location of steps in the magnetization, among others, has been used

as a direct probe of the determination of J_{NN} ⁵. In this report we will show that, despite the complexity of the Fe^{2+} energy-level scheme, in this case magnetization steps should also be detectable and could be used to determine J_{NN} , provided that $|J_{NN}|$ exceeds a certain critical interaction. Moreover, we will show that the position of the first magnetization step is almost independent of sample orientation and crystal-field parameters. These results therefore offer experimentalists the opportunity to establish the Fe^{2+} - Fe^{2+} exchange interaction from the high-field magnetization.

II. THE Fe-Fe PAIR

The quantum-mechanical treatment of the isolated Fe^{2+} ion, substituted in a semiconducting host, has been elaborately evaluated by Slack, Roberts, and Vallin and others⁶. In addition to their treatment for Fe-doped crystals, a Heisenberg-type Fe^{2+} - Fe^{2+} interaction has been included for DMS (see our previous paper⁷):

$$\mathcal{H} = \mathcal{H}_{CF} + \mathcal{H}_{SO} + \mathcal{H}_{EXCH} + \mathcal{H}_B \quad (1)$$

$$\mathcal{H}_{i,EXCH} + \mathcal{H}_{i,B} = -2JS_i \cdot S_j + \mu_B B \cdot (L_i + gS_i) \quad (2)$$

The basis for (2) is formed by a ${}^5E \times {}^5E$ subspace, where 5E represents the ten low-lying eigenfunctions of the cubic crystal-field Hamiltonian including spin-orbit interaction

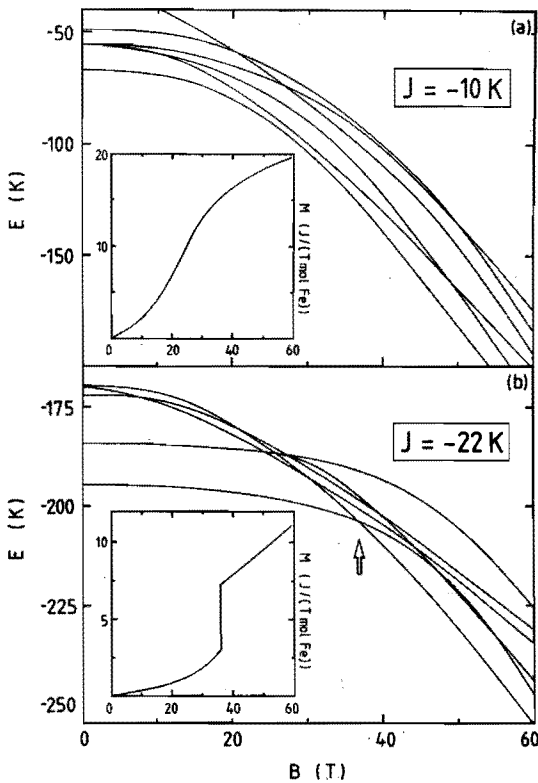


FIG. 1. Low-lying energy levels and magnetization, at $T = 0$ (see insets), of the Fe^{2+} pair for B along the crystallographic $[111]$ axis; (a) $J = -10$ K, (b) $J = -22$ K, the arrow indicates the position of the magnetization step.

$(H_{CF} + H_{SO})$ ^{6,7}. From the field dependence of the eigenvalues the magnetization for one-mole Fe^{2+} ions can be calculated by

$$\mathbf{M} = -\frac{1}{2}R \sum_i \left[\frac{\partial E_i}{\partial B} \right] \frac{e^{-E_i/k_B T}}{\sum_j e^{-E_j/k_B T}} B/|B| \quad (3)$$

with i and j running from 1 to 100.

For uncoupled pairs ($J = 0$) the situation is relatively simple. For $B = 0$ we recall that the low-lying A_1 , T_1 , E , T_2 and A_2

are separated roughly by $6\lambda^2/\Delta$, where λ represents the spin-orbit parameter and Δ (or $10Dq$) the crystal-field splitting. For the calculations we used the parameters for $\text{Zn}_{1-x}\text{Fe}_x\text{Se}$: $\lambda = -95 \text{ cm}^{-1}$, $\Delta = 2940 \text{ cm}^{-1}$; see Sec. III. In the presence of the external field, mixing with higher states repulses the magnetically inactive ground state, thereby inducing a net magnetic moment. For small fields the ground state varies with $-B^2$, yielding at low temperatures the so-called Van Vleck-type of paramagnetism.

For antiferromagnetically coupled pairs ($J < 0$) the energy schemes become very complicated and it follows, somewhat remarkable, that a critical interaction strength $|J_{\text{crit}}|$ ($J_{\text{crit}} \approx -13/-17$ K depending on the

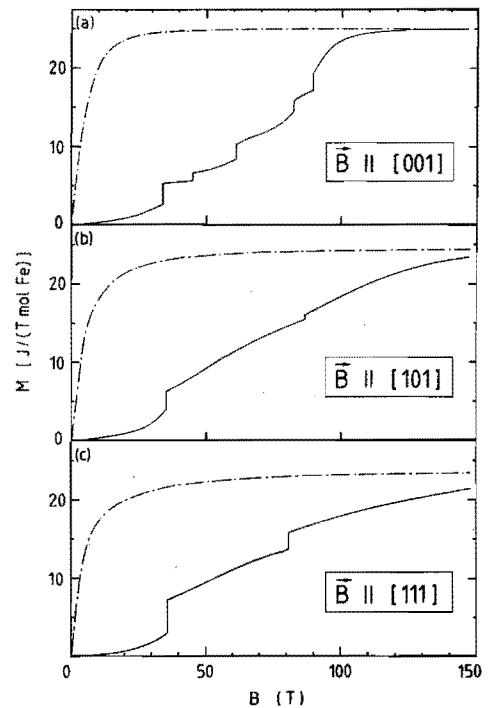


FIG. 2. Magnetization, at $T = 0$, of an Fe^{2+} single ion ($J = 0$, $-\cdot-$), and an Fe^{2+} pair ($J = -22$ K, $—$), for B along three crystallographic axes: (a) $[001]$, (b) $[101]$, (c) $[111]$.

field-direction) is present, above which steps in the magnetization are visible. The occurrence of such a critical interaction results from the interplay of the terms in the full Hamiltonian (1): crystal field including spin-orbit coupling, exchange, and magnetic field. For $|J| < |J_{\text{crit}}|$ the relatively large degree of mixing repulses the ground state in that amount that excited states cannot intersect. The downward bending of the ground state is quantified by the zero-temperature susceptibility χ which depends on the crystal-field parameters λ^2/Δ and the interaction J . For increasing J the susceptibility of the pair decreases and in the limit of large J (with an antiferromagnetic ground state) χ becomes zero. This reduction of χ with increasing J creates the crossing phenomenon. As an illustration, energy levels and magnetization for $J = -10$ K and $J = -22$ K are plotted in Fig. 1. We will return to this subject in the Discussion.

In general, the position of the steps depend strongly on the field direction as illus-

trated in Fig. 2 for B along the [001], [101], and [111] axes. We want to emphasize that, as far as the first step is concerned (see Figs. 2 and 3) the field direction does not influence its position significantly (always within 10%), but only the size of the step. Quite surprisingly, it also appears that, despite the complex energy scheme of the Fe^{2+} pair, a close resemblance with the spin only situation ($g\mu_B B_{\text{step1}} = 2k_B |J|$) is obtained, even for J closely approaching J_{crit} . Furthermore, we checked the sensitivity of the first-step position on the crystal-field parameter λ . An increase from -95 to -105 cm^{-1} , which actually increases the single-ion splitting with 22%, induces a step shift of roughly 5%.

III. THE ACTUAL CRYSTAL

Using the results of Sec. II one is now able to describe the magnetization of an actual DMS crystal. We will confine ourselves to $\text{Zn}_{1-x}\text{Fe}_x\text{Se}$, which, from the magnetic point of view, is representative for several Fe-containing DMS originating from the II-VI group [e.g., $\text{Cd}_{1-x}\text{Fe}_x\text{Te}$ (Ref. 8)]. Moreover, the crystal-field parameters are quite well established^{6,7,9} and in addition, from the high- T susceptibility J_{NN} [-22 K (Ref. 4)] has been estimated.

To calculate the magnetization of such a random array of Fe ions, one usually⁵ decomposes the array in singles (no nearest neighbors), nearest-neighbor pairs, triples and higher-order arrays as determined by statistics (cluster approximation). This approach, however, is valid in case the exchange interaction is restricted to nearest neighbors only. In principle the long-range character of J should be taken into account, which couples every spin with others. In such a case the system can be described within the so-called extended nearest-neighbor pair approximation (ENNPA)¹⁰. For $\text{Zn}_{1-x}\text{Fe}_x\text{Se}$ it has been suggested⁷ that $J \sim R^{-6,8}$. The evidence, however, is rather weak and a sharper decrease with distant, which reduces J to J_{NN} only, cannot be excluded⁷.

In Fig. 4 the results for both cases, i.e.,

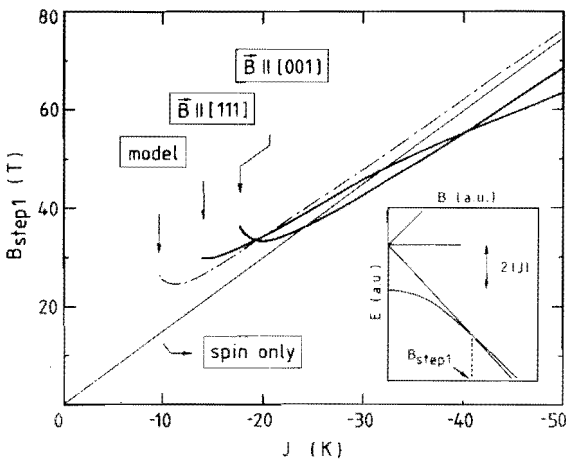


FIG. 3. Position of the first magnetization step as a function of interaction strength, for B along the crystallographic [001] and [111] axis; the spin-only case ($g\mu_B B_{\text{step1}} = 2k_B |J|$) and the results within the introduced model [see the inset and Eq. (4)] are also shown.

the ENNPA and cluster approximation (restricted to singles and pairs), are drawn for $x = 0.05$, showing the characteristic step in the [111] magnetization. Only minor differences between the two approximations can be distinguished due to the energetically close resemblance between isolated and weakly coupled ions. Since in fact these differences are restricted to small fields, where $g\mu_B B \approx k_B |J|$ for J beyond the NN, we may conclude that the steps are insensitive to the tail of J . Neglect of internal fields so far, however, can possibly affect the position of the steps seriously¹¹. The influence of a nonzero temperature is also depicted in Fig. 4. It is clear that due to thermal population of excited states, which is relatively important at fields in the vicinity of B_{step} , a broadening of the steps will be induced.

The actual change in the magnetization at B_{step} , brought about by the nearest-neighbor pairs, is independent of any approxima-

tion. In contrast to the Mn case the step size is not completely determined by statistics only, but also depends on parameters such as J , λ^2/Δ , and field orientation. As an illustration, for $J_{\text{NN}} = -22$ K and $B \parallel [111]$ it follows that $\delta M \approx 30xP_{\text{pair}}(x)$ emu/g, $P_{\text{pair}}(x)$ based on randomly distributed Fe ions [$= 12x(1-x)^{18}$]. For $x = 0.05$ this results in a step size of ≈ 0.35 emu/g. As a consequence, δM can serve as a probe for the randomness of the magnetic system, which, by this means, has been verified for Mn-containing DMS⁵.

To our knowledge no experimental data exist on the magnetization in the regime where, on the basis of the present calculations, steps should occur. For $B < 15$ T data are reported for $\text{Cd}_{1-x}\text{Fe}_x\text{Te}$ (Ref. 8) and $\text{Zn}_{1-x}\text{Fe}_x\text{Se}$ (Ref. 7), and a reasonable description within the pair approximation can be obtained; see the supplementary data in Fig. 4. However, since these data do not extend to the magnetization step, which is the subject of this report, we will not attempt any further interpretation.

IV. DISCUSSION

The calculations revealed the existence of a critical value $|J_{\text{crit}}|$ below which no steps in the magnetization can be observed. In addition to the comments made before, we will introduce a simple model which explains the observed phenomena in a more transparent way. The part of the complicated energy scheme of the Fe pair, which intuitively is responsible for the occurrence of magnetization steps, can be approximated by the following assumptions: (i) the singlet ground state varies quadratically with field: $E_0 = -\chi_{\text{pair}}(T=0)B^2$, obeying Van Vleck-type of paramagnetism; (ii) the first intersection with E_0 will be brought about by states closely following the spin-only eigenfunctions of a pair: $E_1 = m_{s,\text{pair}}g\mu_B B$, $m_{s,\text{pair}} = -1$; and (iii) for $B = 0$, E_0 and E_1 are separated by $2|J|$, which is in principle only valid for spin-only eigenfunctions of a pair ($J \gg \lambda^2/\Delta$). The difference between the ground and the first excited state can be written as:

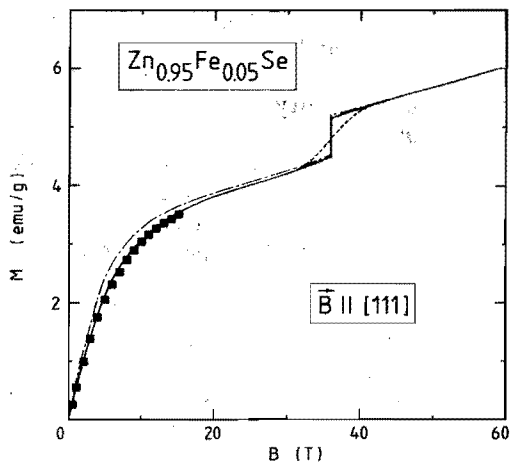


FIG. 4. Magnetization of $\text{Zn}_{0.95}\text{Fe}_{0.05}\text{Se}$ for B along the crystallographic [111] axis, using the ENNPA with $J = -22R^{-6.8}$ K ($T = 0$, —, $T = 1.5$ K, - - -) and the cluster approximation with $J = -22$ K ($T = 0$, - · - ·); the squares represent data from Ref. 7.

$$E_0 - E_1 = -\chi_{\text{pair}}(T=0)B^2 + g\mu_B B - 2k_B |J| \quad , \quad (4)$$

where the pair susceptibility can be obtained by treating \mathcal{H} for vanishing small fields. Figure 3 is supplemented with the first positive root of Eq. (4); the second root is unphysically large. The existence of a critical interaction strength ($J_{\text{crit}} = -10$ K), though somewhat smaller in magnitude than observed in the exact treatment ($J_{\text{crit}} = -13/-17$ K), is indeed predicted. It is clear from Fig. 3 that this simple model apparently contains the essential elements from both the crystal-field part and the spin-only part of \mathcal{H} , thereby inducing the phenomena observed by treatment of the full Hamiltonian.

Experimentally, the existence of the step magnetization in Fe-based DMS is not as evident as suggested by the present calculations since obviously, if $|J_{\text{NN}}| < |J_{\text{crit}}|$, which is not excluded¹², no characteristic steps will be observed. For $|J_{\text{NN}}| > |J_{\text{crit}}|$, we already discussed the close relation between randomness and the height of the magnetization step. Apart from that we should also consider the width of the step as a limiting factor. The influence of the temperature can be reduced by performing the experiments well below 4.2 K. Additional broadening of the step could be induced by any extra matrix element in the Hamiltonian. As an example, it has been shown very recently for Mn¹³, that a DM anisotropy, though very small, would lift the degeneracy of the ground state at B_{step} , thereby widening the step. Further, also internal fields¹¹ and even the experimental conditions (static versus pulsed field)¹³ are believed to affect the structure of the magnetization step.

Despite the complicating factors listed above, we feel encouraged by our present numerical treatment of the Fe²⁺-Fe²⁺ pair, that steps in the magnetization of Fe-containing DMS should be detectable, thereby offering the unique possibility to establish the exchange interaction between adjacent Fe²⁺ ions in a rather straightforward way. The experimental conditions the high-field mag-

netization should be subject to can be summarized as follows: (a) temperature should be kept well below 4.2 K for an optimal population of the ground state; (b) observation of at least the first magnetization step would require fields of the order of 50 T; (c) the use of oriented single crystals is preferable, though not essential, for the position of the first step; fields parallel to the [111] axis should produce maximal step sizes; and (d) an Fe-concentration $x \approx 0.052$ should be chosen to maximize the NN pairs.

-
- 1 J.K. Furdyna, J. Appl. Phys. **64**, R29 (1988)
 - 2 A. Mycielski, J. Appl. Phys. **63**, 3279 (1988)
 - 3 B.E. Larson, K.C. Hass, H. Ehrenreich and A.E. Carlsson, Phys. Rev. B **37**, 4137 (1988)
 - 4 A. Twardowski, A. Lewicki, M. Arciszewska, W.J.M. de Jonge, H.J.M. Swagten and M. Demianiuk, Phys. Rev. B **38**, 10749 (1988)
 - 5 See for instance, S. Foner, Y. Shapira, D. Heiman, P. Becla, R. Kershaw, K. Dwight and A. Wold, Phys. Rev. B **39**, 11793 (1989)
 - 6 W. Low and M. Weger, Phys. Rev. **118**, 1119 (1960); G.A. Slack, S. Roberts and J.T. Valin, *ibid.* **187**, 511 (1969); J.P. Mahoney, C.C. Lin, W.H. Brumage and F. Dorman, J. Chem. Phys. **53**, 4286 (1970)
 - 7 H.J.M. Swagten, A. Twardowski, W.J.M. de Jonge and M. Demianiuk, Phys. Rev. B **39**, 2568 (1989)
 - 8 C. Testelin, A. Mauger, C. Rigaux, M. Guillot and A. Mycielski, Solid State Commun. **71**, 923 (1989)
 - 9 M. Hausenblas, L.M. Claessen, A. Wittlin, A. Twardowski, M. von Ortenberg, W.J.M. de Jonge and P. Wyder, Solid State Commun. **72**, 27 (1989).
 - 10 C.J.M. Denissen, H. Nishihara, J.C. van Gool and W.J.M. de Jonge, Phys. Rev. B **33**, 7637 (1986); A. Twardowski, H.J.M. Swagten, W.J.M. de Jonge and M. Demianiuk, *ibid.* **36**, 7013 (1987)
 - 11 B.E. Larson, K.C. Hass and R.L. Aggarwal, Phys. Rev. B **33**, 1789 (1986)
 - 12 We already argued that the expression which determines J_{NN} from the high-temperature

expansion of χ includes numerical model-dependent expressions which could obscure this approximation; further, in compounds other than $\text{Zn}_{1-x}\text{Fe}_x\text{Se}$, having slightly different crystal-field parameters, the value of J_{crit} itself will be somewhat different apart from the fact that also J_{NN} is *a priori* different from that in $\text{Zn}_{1-x}\text{Fe}_x\text{Se}$ (Ref. 4).

- 13 Y. Shapira, S. Foner, D. Heiman, P.A. Wolff and C.R. McIntyre, *Solid State Commun.* **70**, 355 (1989)

CHAPTER FOUR

Carrier - concentration - dependent magnetic behavior in IV-VI group diluted magnetic semiconductors

In paragraph 1 of this chapter we will describe the preparation of the IV–VI group compounds $\text{Pb}_{1-x-y}\text{Sn}_y\text{Mn}_x\text{Te}$ and $\text{Sn}_{1-x}\text{Mn}_x\text{Te}$, used for the investigations presented in paragraphs 2 and 3. The systems are synthesized using the Bridgman technique, yielding good–quality crystals, consisting of monocrystals with dimensions up to 1 cm^3 . The effects of nonzero segregation on the composition is analyzed. Secondly, we will pay attention to the manipulation of the carrier density in these materials, by applying isothermal annealing processes in a proper environment.

The influence of the concentration of charge carriers on the ferromagnetic phase transition of the diluted magnetic semiconductor $\text{Pb}_{1-x-y}\text{Sn}_y\text{Mn}_x\text{Te}$ for various compositions is reported in paragraph 2. A critical density of carriers above which a ferromagnetic transition can take place, is observed. A simple modified RKKY mechanism for semiconductors is proposed in which carriers from two valence bands located in different regions of the Brillouin zone contribute and a finite mean free path is implemented. An excellent quantitative agreement with the data is obtained.

In paragraph 3 it is shown that for the diluted magnetic semiconductor $\text{Sn}_{1-x}\text{Mn}_x\text{Te}$ also a critical carrier density ($p_c \approx 3 \cdot 10^{20}\text{ cm}^{-3}$) can be found above which ferromagnetic behavior is displayed. This behavior can be explained within the two–band RKKY model. Preliminary experiments on the nature of the low–temperature phase are presented.

Chapter IV, paragraph 1

Preparation and carrier concentrations of $\text{Pb}_{1-x-y}\text{Sn}_y\text{Mn}_x\text{Te}$ and $\text{Sn}_{1-x}\text{Mn}_x\text{Te}$

For the research on IV-VI group alloys¹ the preparation of high-quality crystalline structures, if possible large monocrystals, is necessary. From the point of view of semi-conducting effects, it is, for instance, often desirable to synthesize crystals with extreme purity, in order to obtain mobilities as high as possible. Also from the magnetic point of view, it is desirable to investigate large single crystals, where additional effects from grain boundaries, crystal imperfections or impurities are, tentatively, reduced to a minimum. Moreover, for some magnetic techniques, such as neutron scattering, it is often necessary to have mono-crystals of considerable size. For this purpose several crystal-growing techniques², such as Czochralski, Kyropoulos,

and vapor growth, can be employed. Nevertheless, the vast majority of IV-VI compounds can be conveniently synthesized by applying Bridgman single-crystal growth³. Very recently also thin films and layered structures containing IV-VI group semiconductors and/or DMS have been prepared by means of MBE⁴.

As for the bulk systems used in the present investigation (see Chapter I and the following paragraphs) they were all prepared by the conventional Bridgman technique. In this process the melt is contained in a growth ampoule and is solidified by lowering the ampoule through the negative temperature gradient of the furnace. In our vertical furnace this gradient is supplied by the natural

TABLE I. Materials grown with the Bridgman single-crystal growth apparatus; the purity of the constituents is given in between brackets (e.g., 6N \approx 99.9999%); m is the mass of the constituents; f is the metal/nonmetal fraction, which for $\text{Sn}_{1-x}\text{Mn}_x\text{Te}$ has been chosen according to existing phase diagrams on SnTe ⁴; *shaking* denotes the time interval the melt has been shaken before Bridgman growth; V is growth rate.

Material	Constituents	m (g)	f	<i>shaking</i> (h)	V (mm/h)
$(\text{Pb}_{0.25}\text{Sn}_{0.72}\text{Mn}_{0.03})_f\text{Te}$	Pb(6N), Sn(5N) Te(5N), MnTe ₂ (3N)	20	1	6	1.4
$(\text{Pb}_{0.52}\text{Sn}_{0.45}\text{Mn}_{0.03})_f\text{Te}$	Pb(6N), Sn(5N) Te(5N), MnTe ₂ (3N)	20	1	6	1.4
$(\text{Sn}_{0.97}\text{Mn}_{0.03})_f\text{Te}$	Sn(5N), Te(5N) MnTe ₂ (3N)	20	0.984	5	1.4
$(\text{Sn}_{0.94}\text{Mn}_{0.06})_f\text{Te}$	Sn(5N), Te(5N) MnTe ₂ (3N)	40	0.984	5	1.4

drop in temperature from the middle section to the bottom of the furnace; see Fig. 1. The shape of the crucible is such that single-crystal growth can start at a conical tip without the need of a crystal seed, and, if appropriate conditions are satisfied, see below, the mono-crystal can extend steadily throughout the crucible. There exist two alternative Bridgman techniques, one where the furnace is pulled over the ampoule and one where both the ampoule and furnace are fixed whereas the temperature is slowly being decreased. For completeness, we would also like to mention the Bridgman-Stockbarger variant⁵ where instead of a slowly varying temperature a steplike gradient is used, provided by a two-zone furnace.

The Bridgman technique has several disadvantages which are primarily induced by the contact between the melt and the crucible. First, impurities can be picked up from the wall, and, in the case of the quartz ampoules⁶ we used, it is known that chemical reactions with the melt can take place. To prevent this, the ampoules are, after careful cleaning and etching, carbon-coated by pyrolysis with acetone. Secondly, the wall can act as a undesirable nucleation site of the solid state, and, finally, during the cooling process after the growth, the contraction of the ampoule wall can seriously damage the crystal or create dislocations and other crystal imperfections. In our equipment, a cooling rate less than $0.5\text{ }^\circ\text{C}/\text{min}$ seems to be sufficiently low to prevent the ampoule or crystal from cracking.

The quality of the crystals is governed by a delicate balance between the speed of the solidification interface and the steepness of the temperature gradient normal the interface. It is well-known that a shallow gradient can cause so-called constitutional supercooling, this is a breakdown of the sharp solid-liquid interface yielding uncorrelated solidification throughout the melt. According to a macroscopic transport model² where convection and radial concentration gradients are neglected, the temperature gradient dT/dx and the growth rate V should, in or-

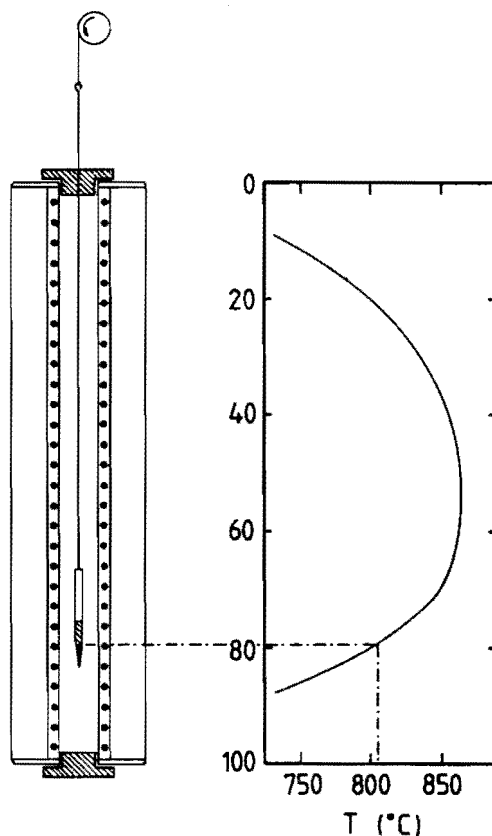


FIG. 1. Bridgman single-crystal growth equipment. The constituents are sealed under 10^{-6} Torr in a carbon-coated quartz ampoule. After heating the crucible up to approximately $50\text{ }^\circ\text{C}$ above the melting point, the melt is shaken for several hours in order to stir it and to prevent vapor inclusions. Subsequently, the actual Bridgman growth starts by moving the ampoule slowly downward through the negative temperature gradient of the furnace (see the right-hand side of the figure). Solidification takes place at an interface where $T_{\text{furnace}} = T_{\text{melt}}$, exemplified for $\text{Sn}_{1-x}\text{Mn}_x\text{Te}$. The temperature is controlled by using a computer based on a 68000 microprocessor. This system also activates two stepping motors, one for shaking the melt, and one, together with a retardation device, for lowering the ampoule at any rate below 15 mm/h .

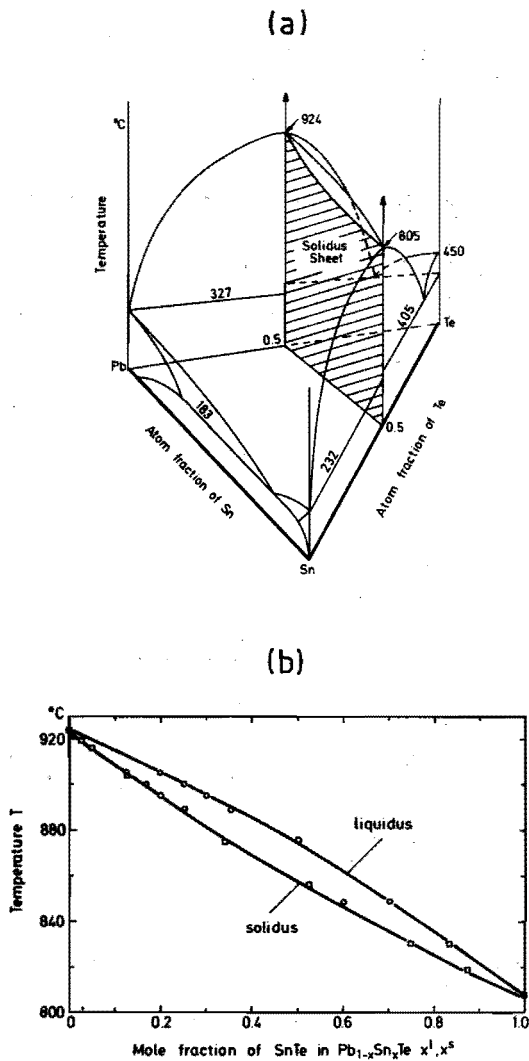


FIG. 2. (a) Temperature - composition phase diagram for the Pb-Sn-Te ternary system. (b) Temperature - composition phase diagram for Pb_{1-x}Sn_xTe; after Ref. 1.

der to avoid supercooling in a compound A_yB_{1-y}, be chosen such that the following condition is satisfied:

$$\frac{dT/dx}{V} > \frac{mC_0}{D} \frac{1-k}{k}, \quad (1)$$

- with m : absolute value of the liquidus slope
 C_0 : starting melt concentration (y)
 k : segregation coefficient ($\equiv C_s/C_l$) between A and B at $C_1 = y$
 D : diffusion coefficient of liquid A in liquid A_yB_{1-y}.

The left-hand side of Eq. 1 can be controlled by a proper choice of experimental conditions, whereas the right-hand part comprises intrinsic properties of the alloy. As an example for Pb_{0.28}Sn_{0.72}Te, the parameters k and m can be inferred from the phase diagram of Pb_{1-y}Sn_yTe¹ depicted in Fig. 2, yielding $k \approx 0.88$ and $m \approx 130^\circ\text{C}$ per mole fraction solute. By inserting $D = 7 \cdot 10^{-5} \text{ cm}^2/\text{s}$ (reported for SnTe in Pb_{0.8}Sn_{0.2}Te⁷) and $dT/dx = 5^\circ\text{C}/\text{cm}$ for the furnace in Fig. 1, we find for that V should not exceed 2.5 mm/h. Depending on the specific system and available equipment, Bridgman growth usually takes place at rates between 0.1 and 10 mm/h. In our growing apparatus these velocities are realized by a stepping motor together with a retardation device, resulting in discrete steps always smaller than 1 μm . Any arbitrary velocity below roughly 15 mm/h can be chosen. Before Bridgman growth starts, a second stepping motor shakes the melt ($f = 50 \text{ Hz}$, $\text{ampl.} = 1.6 \text{ mm}$) for homogenization and for the removal of vapor included in the melt (mostly near the ampoule wall).

Unfortunately, for the Mn-containing Pb_{1-x-y}Sn_yMn_xTe systems, no information is yet available on the solubility properties of Mn. We are therefore not able to estimate the growth rate necessary to exclude supercooling and we were forced to adapt growth rates reported⁸ for Pb_{1-x-y}Sn_yMn_xTe and Sn_{1-x}Mn_xTe, which usually resulted in good-

quality large monocrystals. The growth parameters used to synthesize our systems, as well as other preparatory details, are gathered in Table I. The crystal structure of these systems have been investigated by x-ray techniques. No noticeable deviations from the reported rocksalt structure (see Chapter I) could be detected, and, in some cases, it was checked that the ingot consists of monocrystals with dimensions up to 1 cm^3 . The composition of the crystals (Pb, Sn, Mn and Te) is determined by electron probe micro analysis (EPMA). In the radial direc-

tion no fluctuations in composition have been found. Along the longitudinal direction though, we found a smooth variation of the composition as depicted in Fig. 3 for $Pb_{0.52}Sn_{0.45}Mn_{0.03}Te$, which we will consider in some more detail.

The variation in Sn (and Pb) content is a common feature for these compounds¹ and can be ascribed to the nonzero segregation between solidus and liquidus line, which we saw in Fig. 2. By assuming a constant segregation factor k , a large diffusion compared to the growth rate, no diffusion in the solid part of the crystal, and no convection in the liquid, the concentration profile for a conical ampoule (see Fig. 3) follows²

$$C_s(x) = kC_0(1-g)^{k-1}, \quad (2)$$

with g the fraction of material solidified:

$$g = \frac{x^3/[L_1^2(L_1+3L_2)]}{(3x-2L_1)/(L_1+3L_2)} \quad \begin{array}{l} 0 < x < L_1 \\ L_1 < x < L_1+L_2. \end{array}$$

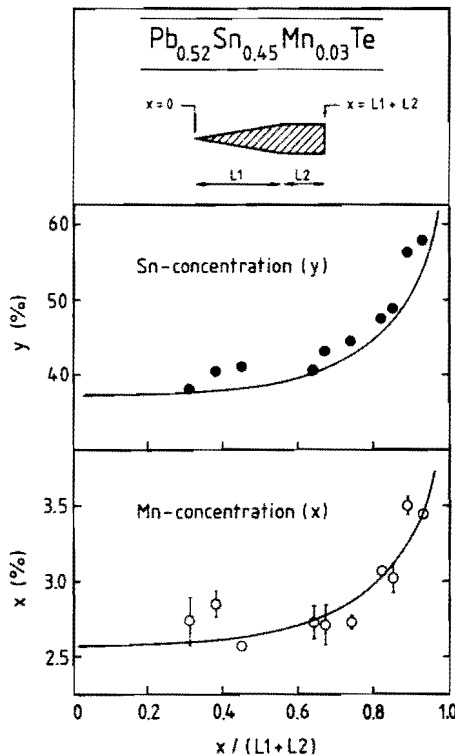


FIG. 3. Compositional profiles for $Pb_{0.52}Sn_{0.45}Mn_{0.03}Te$ obtained by EPMA analysis. The data have been fitted to Eq. 2 (the solid lines), yielding for the best overall agreement with the data, $k = 0.83$ for the Sn and $k = 0.86$ for the Mn concentration.

The Sn profile in $Pb_{0.52}Sn_{0.45}Mn_{0.03}Te$ shown in Fig. 3 has been fitted to this expression, yielding for the best overall agreement with the data $k = 0.83$, which is surprisingly close to the value deduced from the PbTe - SnTe phase diagram in Fig. 2 (approximately 0.78 for $Pb_{0.55}Sn_{0.45}Te$). This implies that apparently the growth conditions were satisfactorily and supercooling did not occur, but also that the role of the substitutional Mn ions on the phase relations in the $Pb_{1-y}Sn_yTe$ systems can be neglected. From the compositional profile of the Mn [Fig. 3(c)] we have to conclude that segregation of MnTe in $Pb_{1-y}Sn_yTe$, similar to SnTe in PbTe, cannot be neglected too. The segregation coefficient for the MnTe solubility, obtained from fitting the data in Fig. 3(c) with Eq. 2, is practically equal to that for SnTe in PbTe, being 0.86. From the concentration profiles in Fig. 3 we may deduce that for a sample taken from the part of the ingot where $x/(L_1+L_2) < 0.8$, the Sn and Mn variation over a typical directional sample size ($\leq 2\text{ mm}$) will never exceed 4%. As a conclusion from this, we may

state that though the most profitable situation occurs when k is very close to unit and concentrations are constant, the segregation of the substituents in our systems is small enough to prevent undesirable compositional profiles over the length of the crystals. Moreover, from the magnetic point of view, it is not only advantageous to know exactly what Mn concentration is in the system but the concentration should also be as constant as possible throughout the sample dimensions.

We have checked that in both $Pb_{1-y}Sn_yTe$ and $SnTe$, Mn concentrations of at least 10% can be substituted in the semiconducting host, without clear signs of a reduction of the crystal quality. Nonsupercooling conditions are apparently satisfied and no drastic changes in the segregation coefficient (between $MnTe$ and $Pb_{1-y}Sn_yTe$) may therefore be expected. Nevertheless, due to the lack of any detailed phase diagrams of the $SnTe - MnTe$ or $PbTe - SnTe - MnTe$ system, the crystal growing processes in IV-VI group DMS are still far from controllable and prevent the crystal grower from manipulation of the growth parameters by pure physical arguments.

The carrier concentration in IV-VI group semiconductors^{1,9} is, in general, relatively high ($10^{18} - 10^{22} \text{ cm}^{-3}$). By appropriate annealing procedures it is possible to control the density of carriers, which, as we will see, is rather crucial in our studies of magnetic properties. For $PbTe$, $SnTe$ and $Pb_{1-y}Sn_yTe$ it is well established¹ that these high densities originate from a natural abundance of metal- or nonmetal vacancies, which create holes and electrons, respectively.

The density of defects is governed by the formation enthalpy (H_v) of the vacancies, which, in a very simplified model, is determined by¹:

$$N = N_0 \exp(-H_v/k_B T) , \quad (3)$$

where N is the density of defects and N_0 is the concentration of lattice cells. In IV-VI compounds these enthalpies are small with respect to other semiconductors due to the

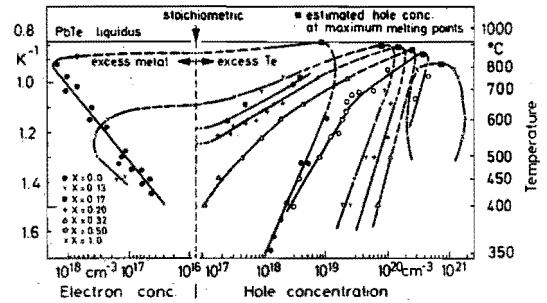


FIG. 4. Apparent carrier concentrations at 77 K (300 K for $SnTe$) versus isothermal annealing temperature for $Pb_{1-x}Sn_xTe$ from various authors; after Ref. 1.

ionic nature of the chemical bond in these compounds. This also explains why carrier concentrations in the more covalent semiconductors (e.g., $CdTe$, $ZnSe$; see Fig. 14 in Chapter I) are considerably smaller.

One of the consequences of the high number of vacancies is the fact that $PbTe$ and $SnTe$ will never exist in pure metal and nonmetal stoichiometry. In $PbTe$ ¹ both n - and p -type conductivity is observed and this implies that the solidus area extends to both the nonmetal and metal-rich side, from $Pb_{0.9998}Te$ to $Pb_{1.00008}Te$, respectively. In $SnTe$ on the other hand¹, the solidus area is completely shifted to the Te -rich side, due to the relatively small formation enthalpy for Sn vacancies in comparison with Te vacancies⁹, and, consequently, only p -type conductivity is observed with carrier concentrations roughly between 10^{20} ($Sn_{0.9996}Te$) and 10^{21} cm^{-3} ($Sn_{0.953}Te$). These phase boundaries are drawn in Fig. 4, together with supplementary data for the ternary $Pb_{1-y}Sn_yTe$, showing that for increasing Sn concentration the carrier densities gradually transform from $PbTe$ to $SnTe$.

By isothermal annealing of $Pb_{1-y}Sn_yTe$ one is able to control the number of vacancies. At a constant temperature the crystal is kept under metal or nonmetal vapor for several days (depending on temperature and

sample size) and afterwards, when an equilibrium has been reached, a rapid quench to room-temperature will freeze in the achieved defect structure. For instance, annealing of as-grown SnTe (apparent carrier concentration $p_{300\text{K}} \approx 8 \cdot 10^{20} \text{ cm}^{-3}$) at $T = 650 \text{ }^\circ\text{C}$ under a Sn-rich atmosphere will yield $p_{300\text{K}} \approx 2 \cdot 10^{20} \text{ cm}^{-3}$, as can be deduced from Fig. 4. The annealing procedures we applied for several magnetic samples listed in Table I are basically performed according to the recipes given by Brebrick¹⁰ and Hewes *et al.*¹¹ for nonmagnetic systems. The presence of Mn^{2+} had no visible effect on the phase boundary depicted in Fig. 4, though in some cases a small reduction of the number of Mn^{2+} ions was observed after annealing.

In order to obtain very small carrier concentrations in SnTe, even smaller than $p_{300\text{K}} \approx 2 \cdot 10^{20} \text{ cm}^{-3}$ (Fig. 4), we had to apply an alternative procedure developed by Inoue *et al.*¹². They were able to reduce the carrier density to below $1 \cdot 10^{20} \text{ cm}^{-3}$ by isothermal annealing under Zn vapor, at $T = 650 \text{ }^\circ\text{C}$. Tentatively, this is due to the more covalent Zn-Te bond with respect to Sn-Te, and consequently, a great number of additional Sn vacancies can be occupied by Zn atoms. In contrast to the narrow solidus area in SnTe, the $\text{Pb}_{1-y}\text{Sn}_y\text{Te}$ solid phase boundaries (Fig. 4) are such that a very wide range of densities can be achieved without the use of doping with other elements. Nevertheless, in future research on IV-VI group DMS it might be necessary to extend the current carrier-density regime, for instance, to concentrations exceeding 10^{21} cm^{-3} . In that case, more effort should be employed on the effects of doping, since besides the manipulation of the vacancy density by (isovalent) doping with Zn, and also $\text{Cd}^{1,9}$, it is possible to add nondivalent foreign ions, e.g. Na^{13} , to the system. The donor or acceptor levels these dopants might create within the band structure can supply the additional charge carriers.

- 1 *Physics of IV-VI compounds and alloys*, edited by S. Rabii (Gordon and Breach, London, 1974); D.R. Lovett, *Semimetals and narrow-bandgap semiconductors*, (Pion, London, 1977); G. Nimtz, B. Schlicht and R. Dornhaus, *Narrow-gap semiconductors*, (Springer, Berlin, 1983); *Narrow-gap semiconductors and related materials*, edited by D.G. Seiler and C.L. Littler (Hilger, Bristol, 1990).
- 2 See for instance, J.C. Brice, *Selected topics in solid state physics: The growth of crystals from liquids*, (North Holland, Amsterdam, 1973), Vol. XII; A.W. Vere, *Crystal growth, principles and progress*, (Plenum Press, New York, 1987).
- 3 P.W. Bridgman, Proc. Amer. Acad. Arts Sci. **60**, 305 (1925).
- 4 See for instance, G. Bauer and H. Clemens in *Narrow-gap semiconductors and related materials*, edited by D.G. Seiler and C.L. Littler (Hilger, Bristol, 1990), p. S122.
- 5 D.C. Stockbarger, Rev. Sci. Instr. **7**, 133 (1936).
- 6 The melting point of the IV-VI compounds is sufficiently low to permit the use of quartz ampoules; at approximately $1500 \text{ }^\circ\text{C}$ quartz becomes soft and can no longer serve as crucible for Bridgman growth.
- 7 A.L. Fripp, R.K. Crouch, W.J. Debnam Jr, I.O. Clark and J.B. Wagner, J. Cryst. Growth **73**, 304 (1985).
- 8 See references in Chapter I of this thesis, and references in G. Bauer, in *Diluted Magnetic Semiconductors*, edited by R.L. Aggarwal, J.K. Furdyna and S. von Molnar (Materials Research Society, Pittsburgh, 1987), Vol. 89, p. 107.
- 9 F.F. Sizov and S.V. Plyatsko, J. Cryst. Growth **92**, 571 (1988); O.A. Pankratov and P.P. Povarov, Solid State Commun. **66**, 847 (1988); H.M. Polatoglou, Physica Scripta **39**, 251 (1989).
- 10 R.F. Brebrick, J. Phys. Chem. Solids **24**, 27 (1963).
- 11 C.R. Hewes, M.S. Adler and D. Senturia, J. Appl. Phys. **44**, 1327 (1973).
- 12 M. Inoue, M. Tanabe, H. Yagi and T. Tatsuoka, J. Phys. Soc. Jpn. **47**, 1879 (1979).
- 13 M. Ocio, Phys. Rev. B **10**, 4274 (1974).

Chapter IV, paragraph 2

Hole density and composition dependence of ferromagnetic ordering in $\text{Pb}_{1-x}\text{Sn}_y\text{Mn}_x\text{Te}$

[published in Phys. Rev. B 37, 9907 (1988)]

I. INTRODUCTION

Diluted magnetic or semimagnetic semiconductors — i.e., semiconducting alloys with substituted magnetic ions — exhibit a variety of interesting transport, magneto-optical, and magnetic properties¹. Recently Story, Gałazka, Frankel and Wolff² reported the observation of a carrier-concentration induced ferromagnetic transition in $\text{Pb}_{0.25}\text{Sn}_{0.72}\text{Mn}_{0.03}\text{Te}$ above a critical carrier concentration p_{crit} . This can be considered as a demonstration of the strong effect of carrier concentration on the magnetic properties of diluted magnetic semiconductors, resulting in a magnetic phase diagram which includes the carrier concentration as a parameter.

Application of pressure on the system in the ferromagnetic regime yielded a shift in the transition temperature (T_c) which, according to Suski, Igalson and Story³, could be *qualitatively* understood on the basis of the Ruderman-Kittel-Kasuya-Yosida (RKKY) interaction mechanism⁴. It was pointed out, however, that a redistribution of carriers due to the pressure dependence of the specific band structure should be taken into account. A RKKY interaction between localized moments, resulting from intraband scattering of the charge carriers by the magnetic moments, seems to be the only interaction that is strong enough and sufficiently long ranged to explain the magnitude of the observed critical temperature well above the critical carrier concentration. The abrupt change in T_c at the critical hole density p_{crit} , however,

cannot be understood by the RKKY model, originally modeled for free (parabolic) electrons.

In this paper, we will present new experimental data on the phase diagram of $\text{Pb}_{1-x}\text{Sn}_y\text{Mn}_x\text{Te}$ (PSMT). A model will be presented which explains *quantitatively* the typical carrier concentration dependence of the Curie-Weiss temperature Θ and T_c . In particular, we will show that the steplike increase of Θ at a critical hole density can be understood on the basis of the modified RKKY interaction mechanism extended with a more realistic two-valence-band approximation and a finite mean free path for the carriers. With this modification, a new extension for the applicability of the RKKY interaction in the diluted magnetic semiconductors is suggested.

$\text{Pb}_{1-x}\text{Sn}_y\text{Mn}_x\text{Te}$ is a quaternary alloy with a rocksalt fcc lattice in which the Mn ions are randomly distributed. The samples were grown by a Bridgman method. The composition and homogeneity were characterized by x-ray diffraction and microprobe measurements. All investigated samples were single phased ($0.005 < x < 0.09$ and $0.47 < y < 0.72$). The carrier concentration of PSMT can be controlled by isothermal annealing in a Te- or Sn-rich atmosphere from below 10^{20} cm^{-3} to above 10^{21} cm^{-3} . Such carrier densities are much larger than those found in $\text{Pb}_{1-x}\text{Mn}_x\text{Te}$ and vary over a much wider range than in $\text{Sn}_{1-x}\text{Mn}_x\text{Te}$ and $\text{Ge}_{1-x}\text{Mn}_x\text{Te}$. The carrier density in PSMT is almost temperature independent below 100 K

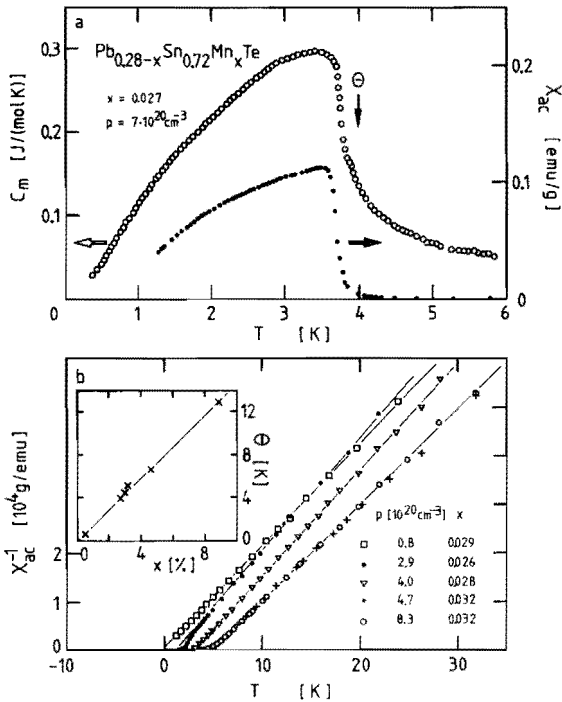


FIG. 1. (a) Low-temperature magnetic specific heat (C_m) and ac susceptibility (χ_{ac}) of $\text{Pb}_{0.28-x}\text{Sn}_{0.72}\text{Mn}_x\text{Te}$, $x = 0.027$ and $p = 7 \cdot 10^{20} \text{ cm}^{-3}$, showing the transition to a ferromagnetic state. (b) Inverse ac susceptibility (χ_{ac}^{-1}) for $x \approx 0.03$ and several carrier concentrations (p); the Curie-Weiss temperature (Θ) as a function of the Mn concentration (x), in the ferromagnetic regime, is shown in the inset.

and the values for the carrier concentration quoted here were measured at $T = 79$ K.

ac susceptibility and specific-heat measurements have been performed in the temperature range 0.4–50 K. Above the critical carrier concentration $p_{\text{crit}} \approx 3 \cdot 10^{20} \text{ cm}^{-3}$ a magnetic phase transition was observed. An illustration of the low-temperature behavior is shown in Fig. 1(a). Magnetization and dc susceptibility confirmed the ferromagnetic nature of the transition. The high-temperature part of χ_{ac} , corrected for the diamagnetic contribution of the host ma-

terial, obeys a Curie-Weiss law at temperatures above roughly 10 K, as shown in Fig. 1(b). The Curie-Weiss temperature Θ , which is proportional to the average exchange interaction between the Mn ions, matches T_c within a few tenths of a degree and is proportional to x as expected for a random system with long-range interactions [see inset in Fig. 1(b)]. Figure 2 shows the carrier concentration dependence of Θ for several compositions, supplemented with the earlier results of Story *et al.*² Above p_{crit} an abrupt, almost steplike increase of Θ from approximately zero to large positive values is observed, indicating a net ferromagnetic interaction. The data in Fig. 2 suggest a rather universal dependence on the composition, only slightly dependent on the composition. However, we like to note that in $\text{Pb}_{0.50}\text{Sn}_{0.47}\text{Mn}_{0.03}\text{Te}$ a reduction of p_{crit} ($\approx 1 \cdot 10^{20} \text{ cm}^{-3}$), with respect to the systems with $y = 0.72$ is suggested, although a larger set of samples is necessary to obtain more pertinent conclusions.

To explain the abrupt transition to a ferromagnetic phase as the hole density exceeds a critical density, we will introduce a simple model. We consider a system of local

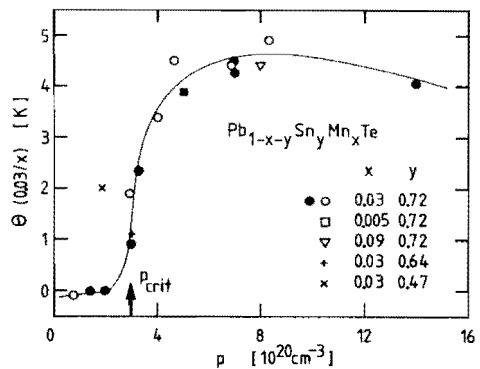


FIG. 2. Curie-Weiss temperature, scaled on $x = 0.03$ [$\Theta(0.03/x)$] of $\text{Pb}_{1-x-y}\text{Sn}_y\text{Mn}_x\text{Te}$ as a function of the carrier concentration (p). The dark circles are data obtained from Story *et al.* (Ref. 2). The solid line is a guide to the eye.

ized magnetic moments, the Mn ions in the $\text{Pb}_{1-y}\text{Sn}_y\text{Te}$ matrix, interacting with the free holes. The following assumptions will be made: (i) intraband RKKY interaction between the magnetic moments; (ii) mean-field approximation for the spin system; (iii) a finite mean free path for the free holes; and (iv) representation of the complicated band structure of PSMT by a set of two parabolic valence bands with different effective masses, as shown in Fig. 3. The first assumption includes the use of second-order perturbation theory, although for PSMT the exchange constant J might well be of the same order of magnitude as the Fermi energy (E_F) of the free holes (see, however, the discussion of Mauger and Godart in Ref. 5). The mean-field approximation completely neglects the dynamics of the spin system. The RKKY interaction was originally modeled for metals, i.e., for free electrons with parabolic bands. The application to semiconductors requires at least two essential modifications, which are expressed in the third and fourth assumption. First, the mean free path of free carriers cannot be taken to be infinite. Secondly, the detailed band structure of a semiconductor might play a decisive role. We used the band structure of $\text{Pb}_{1-y}\text{Sn}_y\text{Te}$ as a reference model for the band structure of PSMT. It is assumed that the presence of Mn ions does not significantly alter the band

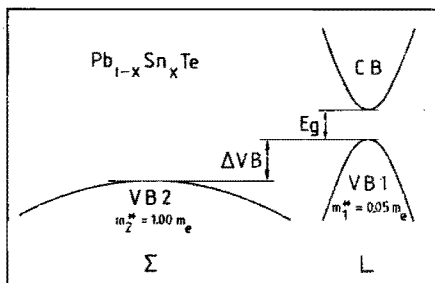


FIG. 3. Schematic illustration of the band structure of $\text{Pb}_{1-x}\text{Sn}_x\text{Te}$ used in the model calculations as described in the text.

structure (see Ref. 1). We take into account only the highest two valence bands according to different band structure calculations⁶⁻⁹ for SnTe and $\text{Pb}_{1-y}\text{Sn}_y\text{Te}$ with $y > 0.4$.

Although the assumptions listed above are rather crude, we believe that this simple model contains the relevant characteristics of the magnetic subsystem as well as the hole subsystem. Within this model, the Curie-Weiss temperature is given by

$$\Theta = \frac{2S(S+1)x}{3k_B} \sum_{i=1}^2 \sum_{j \geq 1} J_i^{\text{eff}}(R_j), \quad (1a)$$

where $J_i^{\text{eff}}(R_j)$ is the exchange integral

$$J_i^{\text{eff}}(R_j) = \left[\frac{m_i^*}{m_e} J_i^2 \right] \frac{m_e}{128 \pi^3 \hbar^2} \left[\frac{a_0^2}{j^2} \right] e^{-R_j/\lambda} F(z_j^i), \quad (1b)$$

with

$$F(z_j^i) = [\sin(z_j^i) - z_j^i \cos(z_j^i)], \quad (1c)$$

and with $z_j^i = 2k_F^i R_j$, where k_F^i is the Fermi wave number for the i th band. R_j is the distance between two lattice points in the fcc lattice ($R_0 = 0$ and R_1 is the nearest-neighbor distance). S is the magnitude of the spin ($S = 5/2$ for Mn^{2+}), J_i the exchange constant for VB i , and a_0 is the lattice parameter. The effect of a finite mean free path (λ) is incorporated along the lines proposed by de Gennes¹⁰, by inclusion of an exponential term in $J_i^{\text{eff}}(R_j)$.

Next, some results of our model calculation for $\text{Pb}_{0.25}\text{Sn}_{0.72}\text{Mn}_{0.03}\text{Te}$ will be presented. We would like to stress that the parameters are not obtained from a fit to the experimental data. The lattice parameter $a_0 = 6.347 \text{ \AA}$ was estimated from the $\text{Pb}_{1-x}\text{Mn}_x\text{Te}$ and $\text{Sn}_{1-x}\text{Mn}_x\text{Te}$ data^{11,12} by linear Vegard-type interpolation. For the exchange constants, it was assumed that $J_1 = J_2 = 0.3 \text{ eV}$, from a linear interpolation between the experimental values¹³ for $\text{Pb}_{1-x}\text{Mn}_x\text{Te}$ (0.07 eV) and for $\text{Sn}_{1-x}\text{Mn}_x\text{Te}$ (0.40 eV).

However, it is *a priori* not excluded that the exchange integrals differ for both valence bands¹⁴. For the effective masses we take the values from Ocio¹⁵ for $\text{Pb}_{0.53}\text{Sn}_{0.47}\text{Te}$: $m_1^* = 0.05m_e$ and $m_2^* = 1.00m_e$. Figure 4(a) shows the Curie-Weiss temperature as a function of hole density, as calculated from Eq. (1) with

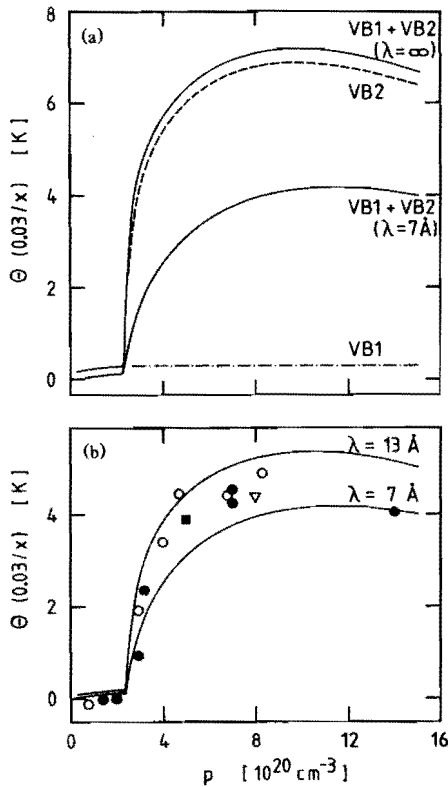


FIG. 4. (a) Curie-Weiss temperature scaled on $x = 0.03$ [$\Theta(0.03/x)$] as a function of the carrier concentration (p), as calculated from Eq. (1). The full lines correspond to contribution from both valence bands, for $\lambda = \infty$ and $\lambda = 7 \text{ \AA}$, whereas the dashed-dotted and dashed line represent the contribution of VB1 and VB2, respectively, for $\lambda = \infty$. (b) $\Theta(0.03/x)$ as a function of p , for $\lambda = 7 \text{ \AA}$ and $\lambda = 13 \text{ \AA}$, in combination with the experimental data for $\text{Pb}_{1-x-y}\text{Sn}_y\text{Mn}_x\text{Te}$; see Fig. 2 for the description of the symbols.

contributions from both valence bands. Also, the theoretical curves corresponding to the case that only VB1 or VB2 is filled are inserted, for an infinite mean free path. The difference between these contributions is mainly caused by the considerable difference between the effective masses m_1^* and m_2^* , see Eq. 1(b). In Fig. 4(b) the model calculations are compared with the experimental data. The different curves correspond to different values of the mean free path λ of the holes. It is clear from this plot that the effect of λ can be large. We used realistic values for λ , i.e., 7 and 13 \AA , corresponding to the experimental observed mobilities in the range 15–50 cm^2/Vs . The critical hole concentration in Figs. 4(a) and 4(b), $p_{\text{crit}} \approx 2.4 \times 10^{20} \text{ cm}^{-3}$, has been determined from a two-band Kane model¹⁵, with as additional parameters¹⁶ $E_g = 0.15 \text{ eV}$ and $\Delta E_{\text{VB}} = 0.6 \text{ eV}$ (see Fig. 3). Experimental values for the critical carrier concentration p_{crit} ^{15,17}, deduced from the temperature dependence of the Hall factor, vary roughly between 2 and $3 \cdot 10^{20} \text{ cm}^{-3}$, which is consistent with the Kane-approximation.

The excellent agreement between the calculations and the data shown in Fig. 4(b) is obvious. The observed steplike increase of Θ to positive (ferromagnetic) values at a critical carrier density as well as the magnitude of Θ above and below that critical concentration are correctly predicted. At this point, however, it should be noted that the *quantitative* agreement may be somewhat fortuitous since it depends also on the value for J_1 and J_2 , the p - d exchange constants, which in a first approximation we have assumed to be equal to 0.3 eV by linear interpolation. A further verification of the validity of the model can possibly be found in an extension of the composition range (Pb-Sn) which would yield a slight shift in p_{crit} brought about by the variation in ΔE_{VB} . The observed quasi-universal behavior of $\Theta(p)$ in the restricted composition range studied so far, is in accordance with the existing data on ΔE_{VB} in that range^{15,17}.

It is worthwhile to note that on the basis

of the present model the contrasting magnetic behavior of $\text{Sn}_{1-x}\text{Mn}_x\text{Te}$ and $\text{Pb}_{1-x}\text{Mn}_x\text{Te}$ can be explained by the difference in carrier concentration. Ferromagnetism was found in $\text{Sn}_{1-x}\text{Mn}_x\text{Te}$ ¹⁸ (with $p \approx 5 \cdot 10^{20} \text{ cm}^{-3}$) while $\text{Pb}_{1-x}\text{Mn}_x\text{Te}$ ($p < 10^{20} \text{ cm}^{-3}$) is paramagnetic down to very low temperatures where recently a spin-glass transition was observed¹⁹. The reported antiferromagnetic (AF) sign of the interactions in $\text{Pb}_{1-x}\text{Mn}_x\text{Te}$ is probably due to the increasing relevance of other than intraband mechanisms which might be AF for low carrier concentrations. In fact, one might conjecture that also in PSMT for low concentrations a spin-glass transition at very low temperatures would occur.

Finally, we would like to add that one of the essential results of the present study, i.e., the first indication of separate contributions from carriers in different regions of the Brillouin zone might also be relevant for calculations of interband interaction mechanisms which have been proposed for diluted magnetic semiconductors.

Note: the calculations we presented include the assumption of an isotropic RKKY interaction between the Mn ions, yielding a correct prediction of $\Theta(p)$; however, some recent results point to the relevance of the Σ -band symmetry, which, possibly, can alter the calculations performed in this paragraph of the thesis.

- 1 N.B. Brandt and V.V. Moshchalkov, *Adv. Phys.* **33**, 193 (1984); J.K. Furdyna and N. Samarth, *J. of Appl. Phys.* **61**, 3526 (1987); R.R. Galazka, in *Proceedings of the 3rd Conference on the Physics of Magnetic Materials, Szczyrk-Bila, Poland, 1986*, edited by W. Gorzkowski, H.K. Lachowicz and H. Szymczak (World Scientific, Singapore, 1987), p. 26.
- 2 T. Story, R.R. Galazka, R.B. Frankel and P.A. Wolff, *Phys. Rev. Lett.* **56**, 777 (1986).

- 3 T. Suski, J. Igalson and T. Story, in *Proceedings of the 18th International Conference on the Physics of Semiconductors, Stockholm, 1986*, (World Scientific, Singapore, 1987), p. 1747; *J. Magn. Magn. Mat.* **66**, 325 (1987).
- 4 M. Rudermann and C. Kittel, *Phys. Rev.* **96**, 99 (1954); T. Kasuya, *Progr. Theor. Phys.* **16**, 45 (1956); K. Yoshida, *Phys. Rev.* **106**, 893 (1957).
- 5 A. Mauger and C. Godart, *Phys. Reports* **141**, 51 (1986).
- 6 Y. Ota and S. Rabii, in *The Physics of Semimetals and Narrow Gap Semiconductors*, edited by D.L. Carter and R.T. Bate (Pergamon, New York, 1971) p. 343.
- 7 J.O. Dimmock, in *The Physics of Semimetals and Narrow Gap Semiconductors*, edited by D.L. Carter and R.T. Bate (Pergamon, New York, 1971) p. 319.
- 8 G. Martinez, M. Schluter and M.L. Cohen, *Phys. Rev. B* **11**, 651 (1976).
- 9 Tung and M.L. Cohen, *Phys. Rev.* **180**, 823 (1969).
- 10 P.J. de Gennes, *J. Phys. Radium* **23**, 630 (1962).
- 11 V.G. Vanyarkho, V.P. Zlomanov and A.V. Novoselova, *Izv. Akad. Nauk. SSSR Neorg. Mater.* **6**, 1534 (1970).
- 12 U. Sondermann, *J. Magn. Magn. Mat.* **2**, 216 (1976).
- 13 *Landolt-Bornstein: Physics of II-VI and I-VII compounds, semimagnetic semiconductors*, edited by O. Madelung (Springer, Berlin, 1982), Vol. 17, Pt. b.
- 14 J. Ginter, J.A. Gaj and Le Si Dang, *Solid State Commun.* **48**, 849 (1983).
- 15 M. Ocio, *Phys. Rev. B* **10**, 4274 (1974).
- 16 G. Nimtz, B. Schlicht and R. Dornhaus, *Narrow Gap Semiconductors*, (Springer, Berlin, 1983).
- 17 A. Aladgadgyan and A. Toneva, *Phys. Status Solidi (b)* **85**, K131 (1978).
- 18 A. Mauger and M. Escorne, *Phys. Rev. B* **35**, 1902 (1987).
- 19 M. Escorne, A. Mauger, J.L. Tholence and R. Triboulet, *Phys. Rev. B* **29**, 6306 (1984).

Chapter IV, paragraph 3

Carrier - concentration dependence of the magnetic interactions in $\text{Sn}_{1-x}\text{Mn}_x\text{Te}$

[published in Semicond. Sci. Technol. 5, S131 (1990)]

I. INTRODUCTION

The IV-VI group compounds $\text{Pb}_{1-x-y}\text{Sn}_y\text{Mn}_x\text{Te}$ represent up till now a rather unique class of materials since the density of carriers (p) is included in the magnetic phase diagram, demonstrating a strong coupling between the magnetic and electronic structure. As was shown by Story, Gałazka, Frankel and Wolff¹, strong ferromagnetic interactions between the Mn^{2+} ions are developed when the density of carriers exceeds a critical value p_c ($\approx 3 \cdot 10^{20} \text{ cm}^{-3}$).

Recently we have shown² that this intriguing behavior can be explained by taking into account the contributions to the RKKY interaction mediated by carriers located in different regions of the Brillouin zone. The dramatic increase of the interactions at p_c is then brought about by the entrance of the Fermi level into a set of heavy-hole valence bands, located along the Σ axis, which strongly enhances the long-range RKKY interaction.

On the basis of this model one could speculate about the contrasting magnetic behavior of $\text{Pb}_{1-x}\text{Mn}_x\text{Te}$ and $\text{Sn}_{1-x}\text{Mn}_x\text{Te}$. Although both materials have a similar band structure and have been studied rather thoroughly³, their entirely different low-temperature magnetic properties (antiferromagnetic for $\text{Pb}_{1-x}\text{Mn}_x\text{Te}$ and ferromagnetic for $\text{Sn}_{1-x}\text{Mn}_x\text{Te}$) seem somewhat puzzling. From the basic result of the modified two-band RKKY model one might conjecture that this behavior is caused by the considerable difference in

carrier density. $\text{Sn}_{1-x}\text{Mn}_x\text{Te}$ is, in that respect, an extreme case since it commonly possesses such high densities of carriers that the second set of valence bands is populated, yielding strong ferromagnetic interactions. Reduction of the carrier density below p_c would transform the system into a paramagnet, if our model applies.

So far, no strong effect of the carrier density in $\text{Sn}_{1-x}\text{Mn}_x\text{Te}$ has been reported and we therefore thought it worthwhile to study the influence of p on the low-temperature magnetic properties of $\text{Sn}_{1-x}\text{Mn}_x\text{Te}$ in order to corroborate our conjecture and observe the expected breakdown of the ferromagnetic interactions. Furthermore, we will focus our attention on the low-temperature phase for $p > p_c$, in order to characterize this phase, which in earlier reports has been denoted as ferromagnetic, spin-glass, as well as reentrant spin-glass³⁻⁶.

II. RESULTS

A. Influence of carrier concentration

The experiments were performed on $\text{Sn}_{0.97}\text{Mn}_{0.03}\text{Te}$ and $\text{Sn}_{0.94}\text{Mn}_{0.06}\text{Te}$ samples grown by a Bridgman method. The as-grown carrier concentration varies between 5 and 10 times 10^{20} cm^{-3} , due to slight deviations from stoichiometry. Lower carrier concentrations can be obtained by isothermal annealing in Zn atmosphere⁶.

Figure 1 shows the ac susceptibility, the magnetization, and specific heat of a sample

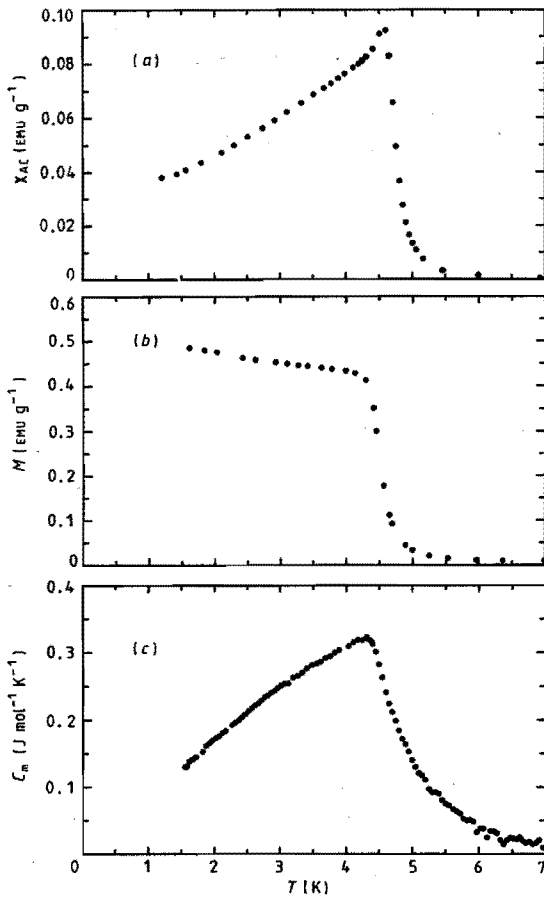


FIG. 1. $\text{Sn}_{0.97}\text{Mn}_{0.03}\text{Te}$, $p = 7\text{--}10 \cdot 10^{20} \text{ cm}^{-3}$
 (a) ac susceptibility, (b) magnetization for $H_{\text{DC}} = 5 \text{ G}$, and, (c) magnetic specific heat.

with carrier concentrations in the range $7\text{--}10 \cdot 10^{20} \text{ cm}^{-3}$, the range to which earlier investigations were restricted. In this range, a transition to a "ferromagnetic"-like ordered state is observed. When the carrier concentration is reduced (notably below $5 \cdot 10^{20} \text{ cm}^{-3}$), the transition shifts considerably to lower temperatures (see Fig. 2) and changes its shape till, at the lowest density $p \approx 3 \cdot 10^{20} \text{ cm}^{-3}$, a second transition in the susceptibility seems to appear at $T = 100 \text{ mK}$. These data clearly demonstrate the carrier-concen-

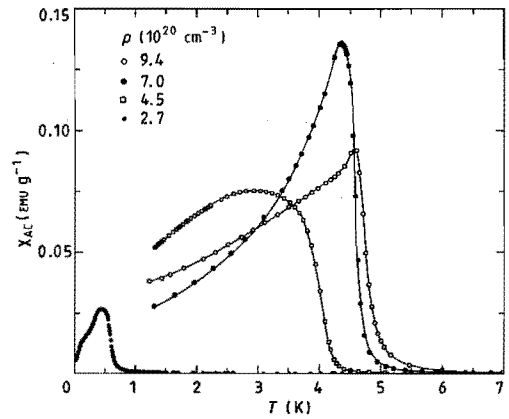


FIG. 2. ac susceptibility of $\text{Sn}_{0.97}\text{Mn}_{0.03}\text{Te}$ for several carrier concentrations; driving ac field: 0.016 G , 920 Hz .

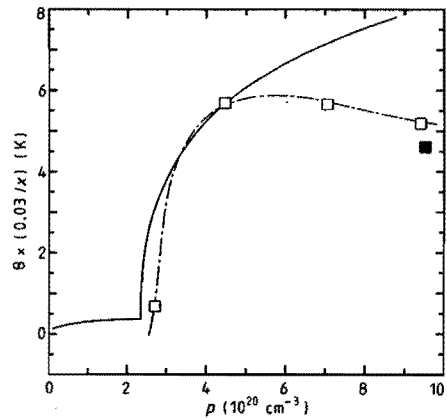


FIG. 3. Curie-Weiss temperature (scaled on $x = 0.03$) as a function of the carrier concentration; the open squares are the data for $\text{Sn}_{0.97}\text{Mn}_{0.03}\text{Te}$, whereas the dashed-solid line only represents a guide to the eye. A preliminary data point for $x = 0.06$ has also been inserted (full square). Calculations within the modified RKKY model are given by the solid line.

tration dependence of the phase transition.

In order to obtain more quantitative results on the interaction strength, the high-temperature susceptibility was measured. A clear Curie-Weiss behavior was observed above 10 K. The Curie-Weiss constant Θ , which monitors the total interaction strength, is plotted in Fig. 3 and a dramatic, almost steplike decrease of Θ from positive (ferromagnetic) values to zero is observed near $p_c \approx 3 \cdot 10^{20} \text{ cm}^{-3}$. The same figure contains the results of a calculation of Θ (or $\sum J_{ij}$) based on the two-band RKKY model mentioned before². The steplike behavior is reproduced rather well, although the magnitude of Θ in the ferromagnetic regime is somewhat arbitrary since it contains the effective mass m^* of the second valence band, which is not known accurately⁷.

In summary, we conclude that the present results corroborate our conjecture that the carrier-induced ferromagnetism may be a rather universal effect as a consequence of the specific band structure.

B. Low-temperature magnetic behavior

Several studies have been devoted to the magnetic properties of $\text{Sn}_{1-x}\text{Mn}_x\text{Te}$ at high carrier densities ($p > p_c$)³⁻⁵. Generally, a ferromagnetic phase is assumed in accordance with the experimentally observed positive Curie-Weiss temperature (Θ). However, also a spin-glass transition and reentrant spin-glass behavior have been reported depending on the Mn^{2+} concentration³. In order to investigate the nature of the phase transition, we performed zero-field-cooled (ZFC) and field-cooled (FC) magnetization measurements, as well as ac susceptibility experiments in the presence of a dc field.

The ZFC and FC magnetization results for $\text{Sn}_{0.97}\text{Mn}_{0.03}\text{Te}$ are shown in Fig. 4. Samples with $x = 0.06$ show similar behavior in various applied fields. The difference between ZFC and FC decreases with increasing external fields. Above roughly 50 G the two curves coincide. Saturation magnetization is not reached until fields in the kG range are

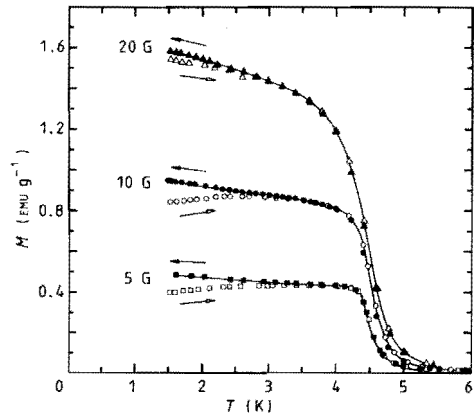


FIG. 4. ZFC and FC magnetization of $\text{Sn}_{0.97}\text{Mn}_{0.03}\text{Te}$, $p = 9.4 \cdot 10^{20} \text{ cm}^{-3}$, for three dc fields; ZFC, open symbols; FC, closed symbols. The saturation magnetization amounts $M_{\text{sat}} = 3.65 \text{ emu/g}$.

applied. The irreversible behavior is also reflected in hysteresis loops (not shown here) which show an increase in coercitive force with decreasing T .

In low external fields ($< 100 \text{ G}$) the ac susceptibility splits into two distinguished contributions, shifting apart with increasing field (Fig. 5). The high-temperature maximum may be correlated to critical fluctuations near T_c and thus marks the onset of long-range order⁸. The maximum varies approximately as $H^{-\alpha}$ with $\alpha = 0.96 \pm 0.02$, which is somewhat larger than for a 3D-Heisenberg ferromagnet⁸.

The interpretation of the low-temperature maximum in the susceptibility is somewhat dubious. It could be attributed to a reentrant spin-glass boundary, which is supported by the close resemblance of the data with the Sherrington Kirkpatrick reentrant spin-glass model⁹, shown in Fig. 5(b). However, it could also be associated with a Hopkinson maximum, which shape strongly depends on the domain structure and anisotropy in both random and homogeneous ferromagnetic systems⁸.

On the basis of the available evidence it

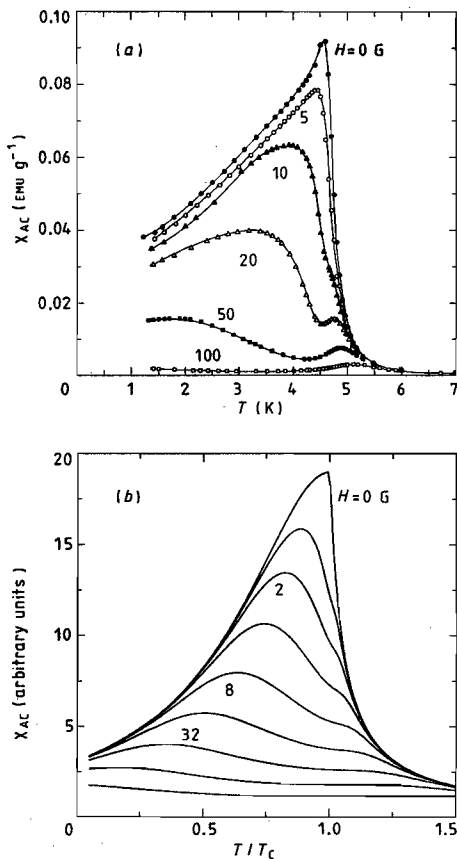


FIG. 5. ac susceptibility in the presence of external dc fields; (a) $\text{Sn}_{0.97}\text{Mn}_{0.03}\text{Te}$, $p = 9.4 \cdot 10^{20} \text{ cm}^{-3}$; (b) model calculations with the SK model, using $\eta = 0.95$; dc fields are in units $10^{-3} H_{DC}/T_C$.

is hard to decide about the specific mechanism. The behavior of the ZFC and FC magnetization in low fields and the field dependence of the dynamic susceptibility could be considered as characteristic features related

to a (reentrant) spin-glass. However, if domains are taken into account, a ferromagnetic transition cannot be ruled out on the basis of the available evidence. Moreover, the Mn concentrations used in the present study ($x = 0.03$ and 0.06) imply average Mn-Mn distances rather close to the first ferromagnetic-antiferromagnetic oscillation in the RKKY-interaction (for carrier concentrations around 10^{21} cm^{-3}), which might obscure the general tendencies. Further, exploration of the effect of both Mn concentration and carrier concentration on the (T, x, p) magnetic phase diagram of $\text{Sn}_{1-x}\text{Mn}_x\text{Te}$ seems therefore necessary.

- 1 T. Story, R.R. Galazka, R.B. Frankel and P.A. Wolff, *Phys. Rev. Lett.* **56**, 777 (1986).
- 2 H.J.M. Swagten, W.J.M. de Jonge, R.R. Galazka, P. Warmenbol and J.T. Devreese, *Phys. Rev. B* **37**, 9907 (1988).
- 3 For some recent reports see, A. Mauger and M. Escorne, *Phys. Rev. B* **35**, 1902 (1987); M. Escorne, A. Mauger, J.L. Tholence and R. Triboulet, *ibid.* **29**, 6306 (1984).
- 4 U. Sondermann, *J. Magn. Magn. Mater.* **2**, 216 (1976).
- 5 M.P. Mathur, D.W. Deis, C.K. Jones, A. Patterson, W.J. Carr and R.C. Miller, *J. Appl. Phys.* **41**, 1005 (1970).
- 6 M. Inoue, M. Tanabe, H. Yagi and T. Tatsuoka, *J. Phys. Soc. Jpn.* **47**, 1879 (1979).
- 7 G. Nimtz, B. Schlicht and R. Dornhaus, *Narrow gap Semiconductors* (Springer, Berlin, 1983).
- 8 I. Maartense and G. Williams *J. Phys. F* **6**, L121 (1976).
- 9 D. Sherrington and S. Kirkpatrick, *Phys. Rev. Lett.* **35**, 1792 (1975).

SAMENVATTING

Dit proefschrift beschrijft een experimenteel onderzoek naar het magnetische gedrag van verdunde magnetische halfgeleiders. Dit zijn nieuwe verbindingen van conventionele halfgeleiders zoals CdTe of ZnSe, waarin een bekend gedeelte van de cation-roosterplaatsen (x) is vervangen door random gesubstitueerde magnetische ionen, zoals het divalente Mn^{2+} . In Hoofdstuk I wordt een overzicht gegeven van de fysische eigenschappen van verdunde magnetische halfgeleiders, waarbij de nadruk ligt op het magnetische gedrag in relatie met de overige delen van het proefschrift.

In Hoofdstuk II wordt de lage-temperatuur soortelijke warmte en susceptibiliteit van de II-VI groep verdunde magnetische halfgeleiders $Zn_{1-x}Mn_xSe$ en $Zn_{1-x}Mn_xS$ gerapporteerd, voor Mn concentraties tussen 0.01 en 0.53. Voor alle systemen wordt een spinglas overgang waargenomen (bij de zogenaamde *freezing* temperatuur T_f) die op grond van schalingsanalyse compatibel is met een antiferromagnetische (AF) lange-dracht interactie tussen Mn^{2+} ionen van het type $J(R) \sim R^{-n}$, met $n = 6.8$ voor $Zn_{1-x}Mn_xSe$ en 7.6 voor $Zn_{1-x}Mn_xS$. Hierop gebaseerd zijn de thermodynamische grootheden beschreven met de extended nearest-neighbor pair approximation (ENNPA), die in een bevredigende simultane beschrijving voorziet van alle beschikbare experimentele gegevens. In de vergelijking met overige verdunde magnetische halfgeleiders wordt er onder meer aandacht geschonken aan het universele gedrag van $T_f(x)$ in systemen met een brede bandafstand, en wordt de relatie gelegd met theoretische exchange modellen die aan de Mn^{2+} - Mn^{2+} interactie ten grondslag liggen.

Hoofdstuk III beschrijft de magnetische eigenschappen van een nieuwe klasse verdunde magnetische halfgeleiders, op basis van Fe^{2+} in plaats van Mn^{2+} . De soortelijke warmte en susceptibiliteit van $Zn_{1-x}Fe_xSe$ en $Hg_{1-x-y}Cd_yFe_xSe$, met Fe concentraties tus-

sen 0.01 en 0.25, zijn experimenteel bepaald. Ook in deze systemen bestaat er een AF interactie, tezamen met indicaties voor spinglas overgangen bij lage temperaturen, en kunnen de thermodynamische grootheden simultaan beschreven worden met de ENNPA. Met betrekking tot het mechanisme van de interactie zijn er geen aanwijzingen gevonden voor de invloed van Fe toestanden die gelegen zijn boven de valentieband en die voortkomen uit de specifieke $3d^6$ configuratie van Fe^{2+} . Door de invloed van kristalveld en spin-baan koppeling is de sterkte en dracht van de Fe^{2+} - Fe^{2+} interactie moeizaam te achterhalen. Via uitdrukkingen voor de Curie-Weiss temperatuur voor deze systemen kan een schatting gemaakt worden voor de interactie tussen naburige Fe ionen: $J_{NN} = -22$ K voor $Zn_{1-x}Fe_xSe$, -18.8 K voor $Cd_{1-x}Fe_xSe$, en -18 K voor $Hg_{1-x}Fe_xSe$. Berekeningen van de hogere magnetisatie van Fe-houdende verdunde magnetische halfgeleiders tonen aan dat J_{NN} wellicht *direct* geëxtraheerd kan worden uit de positie van stapvormige veranderingen bij lage temperaturen.

De invloed van de concentratie van ladingsdragers op de ferromagnetische fase van de verdunde magnetische halfgeleiders $Pb_{1-x-y}Sn_yMn_xTe$ en $Sn_{1-x}Mn_xTe$ ($x < 0.10$) wordt gerapporteerd in Hoofdstuk IV. In deze systemen is er een kritische gatendichtheid waarneembaar, waarboven de aanvankelijk geringe interacties getransformeerd worden naar een sterke ferromagnetische koppeling. Met behulp van een simpel Ruderman-Kittel-Kasuya-Yosida model, dat gemodificeerd is voor de bijdrage van ladingsdragers vanuit verschillende gebieden uit de Brillouin zone, is het gedrag van de Curie-Weiss temperatuur te beschrijven, zowel wat betreft het bestaan van p_{crit} als de sterkte van de ferromagnetische koppeling boven p_{crit} . Er is bovendien een aanvang gemaakt met de karakterisering van de geobserveerde magnetische fasen.

LIST OF PUBLICATIONS

Magnetic properties of $Zn_{1-x}Mn_xS$.

H.J.M. Swagten, A. Twardowski, W.J.M. de Jonge, M. Demianiuk and J.K. Furdyna, *Solid State Comm.* **66**, 791 (1988).

Hole density and composition dependence of ferromagnetic ordering in $Pb-Sn-Mn-Te$.

H.J.M. Swagten, W.J.M. de Jonge, R.R. Gałazka, P. Warmenbol and J.T. Devreese, *Phys. Rev. (Rapid Communication)* **B 37**, 9907 (1988).

The magnetic properties of II-VI group Fe-type diluted magnetic semiconductors.

H.J.M. Swagten, A. Twardowski, F.A. Arnouts, W.J.M. de Jonge and M. Demianiuk, in "Proceedings of the International Conference on Magnetism", edited by D. Givord (France, 1988); *J. de Physique C* **8**, 873 (1988).

Hole density and composition dependence of the diluted magnetic semiconductor $PbSn-MnTe$.

H.J.M. Swagten, H. v.d. Hoek, W.J.M. de Jonge, R.R. Gałazka, P. Warmenbol and J.T. Devreese, in "Proceedings of the 19th International Conference on Physics of Semiconductors", edited by W. Zawadski, (Warsaw, 1988), p. 1559.

Carrier-concentration-dependent magnetic properties of the diluted magnetic semiconductor $Sn(Mn)Te$.

H.J.M. Swagten, S.J.E.A. Eltink and W.J.M. de Jonge, in "Growth, characterization and properties of ultrathin magnetic films and multilayers", edited by B.T. Jonker, J.P. Heremans and E.L. Marinaro (Materials Research Society, Pittsburgh, 1989), Vol. 151, p. 171.

Magnetic specific heat of the diluted magnetic semiconductor $Hg_{1-x}Fe_xSe$.

H.J.M. Swagten, F.A. Arnouts, A. Twardowski, W.J.M. de Jonge and A. Mycielski, *Solid State Comm.* **69**, 1047 (1989).

Magnetic properties of the diluted magnetic semiconductor $Zn_{1-x}Fe_xSe$.

H.J.M. Swagten, A. Twardowski, W.J.M. de Jonge and M. Demianiuk, *Phys. Rev. B* **39**, 2568 (1989).

Magnetization steps in Fe-based diluted magnetic semiconductors.

H.J.M. Swagten, C.E.P. Gerrits, A. Twardowski and W.J.M. de Jonge, *Phys. Rev. (Rapid Communication)* **B 41**, 7330 (1990).

Low-temperature specific heat of Fe-based DMS.

H.J.M. Swagten, A. Twardowski, E.H.H. Brentjens, W.J.M. de Jonge, M. Demianiuk and J.A. Gaj, in "Proceedings of the 20th International Conference on the Physics of Semiconductors", Thessaloniki, 1990, to be published.

Magnetic behavior of the diluted magnetic semiconductor $Zn_{1-x}Mn_xSe$.

A. Twardowski, H.J.M. Swagten, W.J.M. de Jonge, and M. Demianiuk, *Phys. Rev. B* **36**, 7013 (1987).

Thermodynamic properties of iron-based II-VI semimagnetic semiconductors.

A. Twardowski, H.J.M. Swagten, T.F.H. v.d. Wetering, W.J.M. de Jonge, *Solid State Comm.* **65**, 235 (1988).

Magnetic susceptibility of iron-based semimagnetic semiconductors: high-temperature regime.

A. Twardowski, A. Lewicki, M. Arciszewska, W.J.M. de Jonge, H.J.M. Swagten and M. Demianiuk, *Phys. Rev. B* **38**, 10749 (1988).

Carrier induced magnetic interaction in the diluted magnetic semiconductor $PbSnMnTe$.

W.J.M. de Jonge, H.J.M. Swagten, R.R. Gałazka, P. Warmenbol and J.T. Devreese, *IEEE transactions on Magnetics* **24**, 2542 (1988).

The d-d exchange interaction in the semi-magnetic semiconductor ZnFeSe.

A. Twardowski, H.J.M. Swagten and W.J.M. de Jonge, in "Proceedings of the 19th International Conference on Physics of Semiconductors", edited by W. Zawadski (Warsaw, 1988), p. 1543.

Correlation between electronic and magnetic properties in the IV-VI group diluted magnetic semiconductors.

S.J.E.A. Eltink, H.J.M. Swagten, N.M.J. Stoffels and W.J.M. de Jonge, J. Magn. Mater. **83**, 483 (1990).

Specific heat study of Fe-based narrow and wide gap diluted magnetic semiconductors.

W.J.M. de Jonge, H.J.M. Swagten, C.E.P. Gerrits and A. Twardowski, in "Narrow-gap semiconductors and related materials", edited by D.G. Seiler and C.L. Littler (Hilger, Bristol, 1990); Semicond. Sci. Technol. **5**, S270 (1990).

Carrier concentration dependence of the magnetic interactions in Sn(Mn)Te.

W.J.M. de Jonge, H.J.M. Swagten, S.J.E.A. Eltink and N.M.J. Stoffels, in "Narrow-gap semiconductors and related materials", edited by D.G. Seiler and C.L. Littler (Hilger, Bristol, 1990); Semicond. Sci. Technol. **5**, S131 (1990).

Specific heat of Zn_{1-x}Co_xSe semimagnetic semiconductors.

A. Twardowski, H.J.M. Swagten, W.J.M. de Jonge and M. Demianiuk, Acta Phys. Polon. A **77**, 167 (1990).

Magnetization study of Fe-based II-VI group diluted magnetic semiconductors.

W.J.M. de Jonge, H.J.M. Swagten and A. Twardowski, in "Properties of II-VI semiconductors: bulk crystals, epitaxial films, quantum well structures, and dilute magnetic systems", edited by F.J. Bartoli Jr., H.F. Schaake and J.F. Schetzina (Materials Research Society, Pittsburgh, 1990), Vol. 161, p. 485.

Low-temperature specific heat of the diluted magnetic semiconductor Hg_{1-x-y}Cd_yFe_xSe.

A. Twardowski, H.J.M. Swagten and W.J.M. de Jonge, Phys. Rev. B **42**, 2455 (1990).

Neutron diffraction on the diluted magnetic semiconductor Sn_{1-x}Mn_xTe.

C.W.H.M. Vennix, E. Frikkee, H.J.M. Swagten, K. Kopinga and W.J.M. de Jonge, in "35th Annual Conference on Magnetism and Magnetic Materials", San Diego, 1990, to be published.

EPR study of s-d exchange in PbSnMnTe.

T. Story, C.H.W. Swuste, H.J.M. Swagten, R.J.T. van Kempen and W.J.M. de Jonge, in "35th Annual Conference on Magnetism and Magnetic Materials", San Diego, 1990, to be published.

Diluted magnetic semiconductors.

W.J.M. de Jonge and H.J.M. Swagten, in "Proceedings of the NATO Institute on the Science and Technology of Nanostructured Materials", Greece, 1990, to be published.

DANK

voor de waardevolle bijdrage aan dit proefschrift,

Jos v. Amelsvoort
Frank Arnouts
Gerrie Baselmans
Pascal Bloemen
Paul Boomkamp
Rob Braun
Eric Brentjens
Joop v.d. Broek
Rinus Broekmans
Hans Dalderop
Wil Delissen
Cees Denissen
J. Devreese
Jerome Dubois
Noucha Duncker
Paul Eggenkamp
Menno Eisenga
Stephan Eltink
J. Flokstra
R. Galazka
Gerard v. Gastel
Karel Gerrits
Bob Groeneveld
Ruth Gruyters
Frank Haarman

Hans Heijligers
Hans v.d. Hoek
Erik Janse
Wim de Jonge
Rob v. Kempen
Klaas Kopinga
Edward Maesen
Jef Noijen
Peter Nouwens
Marc v. Opstal
A. v.d. Pasch
Marco Poorts
Helga Pouwels
Cees v.d. Steen
Nico Stoffels
Tomasz Story
Coen Swuste
Andrzej Twardowski
Suzanne te Velthuis
Kees Vennix
Rianne van Vinken
Peter Warmenbol
Eric v.d. Wetering
Marc Willekens
Jos Zeegers

faculteitswerkplaats Natuurkunde
faculteit Natuurkunde, Universiteit van Antwerpen
faculteit Scheikundige Technologie, vakgroep Fysische Chemie
faculteit Technische Natuurkunde, Universiteit Twente
glastechnische groep CTD
groep Cooperatieve Verschijnselen, vakgroep Vaste Stof
groep Halfgeleiderfysica, vakgroep Vaste Stof
groep Lage Temperaturen, vakgroep Vaste Stof
heliumbedrijf faculteit Natuurkunde
Institute of Experimental Physics, University of Warsaw
Institute of Physics, Polish Academy of Sciences, Warsaw
Institute of Technical Physics, Warsaw
secretariaat vakgroep Vaste Stof
Shell Nederland B.V.
stichting FOM

DE AUTEUR

H.J.M. Swagten,
gehuwd met J.M.C. Swagten-Mestrom.

- 1962 Geboren op 26 juli te Roermond,
zoon van W.J.M. Swagten en A.M. Swagten-Pulles.
- 1974 – 1980 Middelbaar onderwijs aan het Bisschoppelijk College "Broekhin"
te Roermond.
30 mei 1980: examen Atheneum – B.
- 1980 – 1987 Universitair onderwijs aan de Technische Universiteit
Eindhoven, Faculteit der Technische Natuurkunde.
Afstudeeronderzoek in de Vakgroep der Vaste Stof,
groep Cooperatieve Verschijnselen.
11 februari 1987: ingenieursexamen (met lof).
Titel: "Het magnetische gedrag van $Pb_{1-x}Sn_yMn_xTe$ ".
- 1987 – 1990 Promovendus (als Onderzoeker In Opleiding, stichting
Fundamenteel Onderzoek der Materie) aan de Technische
Universiteit Eindhoven, Faculteit der Technische Natuurkunde,
in de Vakgroep der Vaste Stof, groep Cooperatieve Verschijnselen.
20 november 1990: promotie.
Titel: "The magnetic behavior of diluted magnetic
semiconductors".
-

STELLINGEN

behorende bij het proefschrift

THE MAGNETIC BEHAVIOR OF DILUTED MAGNETIC SEMICONDUCTORS

door H.J.M. Swagten

1. Bij de interpretatie van de lage-temperatuur soortelijke warmte van verdunde magnetische halfgeleiders moet men terdege rekening houden met de modificatie van de rooster soortelijke warmte in vergelijking met die van het halfgeleidende gastmateriaal[†]. In enkele gevallen, en met name $\text{Hg}_{1-x}\text{Mn}_x\text{Se}$ en $\text{Hg}_{1-x}\text{Fe}_x\text{Se}$, kan de veronachtzaming van dit effect[‡] leiden tot apert onjuiste conclusies.

[†] dit proefschrift, Hoofdstuk III, paragraaf 2

[‡] R.R. Galazka, S. Nagata and P.H. Keesom, Phys. Rev. B **22**, 3344 (1980); A. Lewicki, J. Spalek and A. Mycielski, J. Phys. C **20**, 2005 (1987).

2. Het "three-level-superexchange" model van Larson, Hass, Ehrenreich en Carlsson[†], en met name de voorspelling omtrent het lange-dracht karakter van de magnetische interactie in II-VI groep verdunde magnetische halfgeleiders met een grote bandafstand, wordt bevestigd door het geobserveerde universele gedrag van de spinglas overgangstemperatuur[†] in deze materialen.

[†] B.E. Larson, K.C. Hass, H. Ehrenreich en A.E. Carlsson, Phys. Rev. B **37**, 4137 (1988)

[‡] dit proefschrift, Hoofdstuk I en Hoofdstuk II, paragraaf 1.

3. Escorne, Godinho, Tholence en Mauger[†] relateren het gedrag van de dynamische susceptibiliteit van $\text{Sn}_{1-x}\text{Mn}_x\text{Te}$, met Mn concentraties variërend tussen 0.03 en 0.06, aan een zogenaamde re-entrant spinglasfase. Deze interpretatie is onjuist, omdat in hun experimenten niet voldaan is aan de laag-veld limiet voor de magnetisatie.

[†] M. Escorne, M. Godinho, J.L. Tholence en A. Mauger, J. Appl. Phys. **57**, 3424 (1985).

4. Bij de berekeningen van de Curie-Weiss temperatuur in IV-VI groep verdunde magnetische halfgeleiders, op basis van het twee valentiebanden RKKY-model[†], dient rekening gehouden te worden met de symmetrie-eigenschappen van de Σ -band.

[†] dit proefschrift, Hoofdstuk I en IV

5. Het door Hagen en Griessen[†] opgestelde inversieschema om de verdelingsfunctie voor thermisch geactiveerde fluxbeweging in supergeleiders te bepalen uit de relaxatie van de magnetisatie is in principe alleen juist in de limiet van een kleine spreiding in de activeringsenergie.

[†] C.W. Hagen en R. Griessen, *Phys. Rev. Lett.* **62**, 2857 (1989).

6. Aan de basis van elk fysisch onderzoek aan de vaste stof staat de synthese van geschikte kristalstructuren. Dit strookt niet met de ondergeschikte aandacht voor preparatieve details in veel wetenschappelijke publicaties.

7. Het verdient aanbeveling de benaming "verdunde magnetische halfgeleiders" te hanteren in plaats van "semimagnetische halfgeleiders", omdat laatstgenoemde de suggestie wekt dat de magnetische verschijnselen die geobserveerd worden in deze materialen, slechts ten dele of zelfs quasi-magnetisch zouden zijn, hetgeen niet juist is.

8. Bij de vaststelling van snelheidslimieten voor motorboten op stromende vaarwegen[†], is de toevoeging van het coördinatenstelsel, stilstaand of meebewegend ten opzichte van het water, op zijn plaats.

[†] zie bijvoorbeeld, Bijzonder reglement snelle motorboten Maas, *Stb.* **564**, 1345 (1971).

9. De beweegredenen van de onderzoeker om wetenschappelijke resultaten te publiceren en de mate waarin de onderzoeker publiceert[†], hangen niet noodzakelijkerwijze samen met de kwaliteit en de relevantie van de publicatie. Bij de beoordeling daarvan doen deze beweegredenen zelfs niet ter zake.

[†] P.A.J. Ackermans, proefschrift TUE 1990 (stellingen).

10. Het inzicht in de arbeids- en inkomensverhoudingen op universiteiten kan verrijkt worden door het besef dat, weliswaar op basis van een structureel draagvlak van wetenschappelijke stafleden, de daadwerkelijke uitvoering van het wetenschappelijke onderzoek in handen ligt van promovendi.

11. Middelen tegen kaalhoofdigheid gaan voorbij aan de esthetische verrukking die er van het kalende mannenhoofd uit kan gaan.